Durham E-Theses

Some aspects of inelastic neutron scattering from inorganic compounds

John Tomkinson

How to cite:

Use policy

SOME ASPECTS OF INELASTIC NEUTRON

SCATTERING FROM INORGANIC

COMPOUNDS.

by

John TOMKINSON   B.Sc. (Dunelm)

Grey College.

A thesis submitted in part fulfilment of the requirements
for the degree of Doctor of Philosophy in the University
of Durham.

December 1974

Without the support of
my whole family this work
could not have been
attempted, and I should
like to express my thanks
to my parents for providing
active encouragement to all
I have done.

The fear of the Lord is wisdom
and to turn from evil is understanding

JOB 28:28

PREFACE

The work described in this thesis is original, except in those
portions where it is specifically stated to the contrary. It
has not been submitted, either wholly, or in part, for a degree
at this, or at any other university.

John Tomkinson

19 xii 1974

ACKNOWLEDGEMENTS

SUMMARY

The alkali metal borohydride salts were studied through their inelastic neutron scattering, and infrared, spectra. The main librational transition was observed in all of these salts and reorientational barriers have been calculated. The two librational transitions predicted for lithium borohydride, and the low temperature phase of sodium borohydride, were also observed.

The molecular borohydrides of aluminium and zirconium were studied, by a comparison of their inelastic neutron scattering spectra and their published Raman and infrared spectra. The low energy molecular vibrations were observed and assigned. Intermediate energy vibrations, about $800cm^{-1}$, were difficult to observe in $Al(BH_4)_3$, but suggest that previous infrared assignments may be suspect. The octohydrotriborate ion was also studied. The barriers to internal reorientation have been calculated and the nature of reorientation in these fluxional compounds is discussed.

Solid solutions of ammonium ions incorporated into the alkali halide salts were prepared, and studied by their inelastic neutron scattering spectra. The gross outlines of these neutron spectra were in agreement with predictions, and the main librational transitions have been observed. A low temperature spectrum of potassium (ammonium) bromide is interpreted in terms of the "single approach" model used by previous authors. Barriers to reorientation of the defect ions within these crystals have been calculated.

The electrostatic and repulsive interactions occuring in the solid solutions were calculated, to determine which was the more important in fixing molecular orientation in these systems. Absolute values of the

potential energies are presented and indicate that repulsion is the more dominant. However the results obtained from the study of the solid solutions have shown that a strong attractive potential must be present. This has been attributed to hydrogen bonding.

CONTENTS

INTRODUCTORY THEORY

In this chapter it is intended to introduce the theory which

forms the basis of the interpretation of the measurements presented

later.   These measurements were taken by inelastic scattering of

thermal neutrons and absorption of infrared radiation.   Whilst the

former requires a detailed mathematical treatment, the latter has been

extensively covered.   Some consideration must be given to the

infra red absorption spectrum since it is measured indirectly, through

its Fourier transform.   The theory of Fourier transform spectroscopy,

as applied to infrared absorption, will be presented first;   and the

theory of neutron scattering later.   The comments which are made

about Fourier spectroscopy in the first section, especially in regard

to limitations, apply equally well to all transform techniques.   The

limitations imposed on an $I(\omega)$ as obtained from $F(x)$ (discussed in the

first section) are exactly those imposed on a $G(\underline{r},t)$ obtained from

$S(\underline{Q},\omega)$ (discussed in the second section).

1. **The theory of infrared absorbsion spectra obtained by Fourier**
   transform techniques.

   1.1   The spectrometer actually used is fully described in

section II.   However as can be seen it essentially consists of three

parts, firstly two coherent light beams, a method of measuring the

displacement of the two beams with respect to each other, and finally

a total incident energy detector.   In the simple case of both light

beams being of equal intensity and composed of only one frequency,

the intensity at the detector is given by equation (1). (27).

$$E(x) = I(1 + \cos 2\pi\omega x) \qquad\qquad (i)$$

I, intensity of light beam.

ω, frequency of light.

x, relative displacement of the beams.

E(x), detected intensity as a function of x.

In a more realistic case the source has a frequency spectrum $I(\omega)$, and the two coherent beams are not necessarily of equal intensity but of $I_1(\omega)$ and $I_2(\omega)$. Then the detected intensity becomes. (27)

$$E(x) = \int_{-\infty}^{\infty} I_D(\omega)d\omega + \int_{-\infty}^{\infty} I(\omega)(1 + \cos 2\pi\omega x)\,d\omega \qquad\qquad (ii)$$

where

$$I_1(\omega) = I(\omega)$$
$$I_2(\omega) = I(\omega) + I_D(\omega) \qquad\qquad (iii)$$
$$I_D(\omega) = c.I(\omega)$$

$I_1(\omega)$, intensity of beam 1

$I_2(\omega)$, " " 2

c, constant.

Substituting (iii) at x = 0 into (ii)

$$E(0) = 2 + c \int_{-\infty}^{\infty} I(\omega)d\omega \qquad\qquad (iv)$$

Using (iii) and (iv)

$$E(x) = \left(\frac{1+c}{2+c}\right) E(0) + \int_{-\infty}^{\infty} I(\omega)\cos 2\pi\omega x\,d\omega \qquad\qquad (v)$$

The integral in eq. (v) represents a variation in intensity, which superimposes on a steady intensity given by E(0).   At large values of x this variation is negligible, unless the beams are monochromatic, and the integral can be set equal to zero.

$$E(x) \simeq \left(\frac{1+c}{2+c} \right) E(0) \qquad\qquad (vi)$$

for $x \to \infty$

Therefore eq.(v) may be written.

$$E(x) - E(D) = \int_{-\infty}^{\infty} I(\omega) \, \text{Cos } 2\pi\omega x \, d\omega \qquad\qquad (vii)$$

where D is a large value of x.

let

$$F(x) = E(x) - E(D) \qquad\qquad (viii)$$

thus the function F(x) has been transformed into a function in the variable ω, $I(\omega)$.

$$F(x) = \int_{-\infty}^{\infty} I(\omega) \, \text{Cos } 2\pi\omega x \quad d\omega \qquad\qquad (ix)$$

This is equivalent to a Fourier transformation and by the inversion theorem for Fourier transforms. (4)

$$I(\omega) = \int_{-\infty}^{\infty} F(x) \, \text{Cos } 2\pi\omega x \quad dx \qquad\qquad (x)$$

In this, $I(\omega)$ represents the spectrum of the source, if there are any absorptions due to the instrument or any samples introduced then the total intensity spectrum $I_T(\omega)$ is obtained.

$$I_T(\omega) = I(\omega) - I_s(\omega) \qquad (xi)$$

$I_s(\omega)$, frequency spectrum of sample.

Then by a property of Fourier transforms

$$I(\omega) - I_s(\omega) = \int_{-\infty}^{\infty} (F(x) - F_s(x)) \; Cos \; 2\pi\omega x \; dx \qquad (xii)$$

It is not necessary to know the function $F(x)$ continuously, it is possible to measure $F(x)$ only at specific intervals of x and still retain a complete description of $F(x)$. (23). (This applies only if $I(\omega)$ has a value ω_a above which $I(\omega)$ is zero, and the measurements $F(x)$ are taken over $x = \mp\infty$, see later). By this sampling theorem x is now a discrete variable. Unfortunately it cannot be guaranteed that a sample of $F(x)$ will be taken when $x = 0$. The function $F(x)$ thus becomes in general non symmetric about $x = 0$, and the simple transform of eq. (x) no longer applies. If the function $F(x)$ is auto correlated, self convolved, then a new function $A(h)$ is produced.

$$A(h) = \int_{-\infty}^{\infty} F(x) \cdot F(x-h) \; dh \qquad (xiii)$$

or

$$A(h) = F(x) * F(x) \qquad (xiv)$$

The function A(h) is completely symmetric about h = 0 and contains all the information from F(x) which is needed to obtain I(ω). From the well known property of Fourier transforms

$$\int_{-\infty}^{\infty} F(x) * F(x) \cos 2\pi\omega x \ dx = I(\omega)^2 \qquad \text{(xv)}$$

The Fourier transform conducted in eq. (x) is the transform of the real part of F(x). The function F($\bar{x}$) actually carries more information than just the power spectrum I(ω). This extra information, the phase spectrum, can be obtained by conducting the total Fourier transform of F(x), which involves the imaginary and real parts. When the function F(x) is auto correlated this extra information is lost. Enough information is retained, however, to construct the power spectrum I(ω) as in eq. (xv); there is a slight loss of resolution in I(ω) caused by the loss of the imaginary part of F(x).

As was indicated earlier, in the sampling theorem, certain things are assumed about the extent of the spectrum I(ω) and the measurements F(x). In practice there is no frequency above which I(ω) is zero, and the measurement of F(x) cannot be continued over infinity in x.

These two experimental difficulties impose restrictions upon the frequency distribution obtained.

(a) There is a minimum wavelength below which the techniques used can yield no information on I(ω). This is because wavelengths shorter than the sampling interval, Δx, are undefined.

$$\lambda_{min} = 2\Delta x \qquad\qquad\text{(xvi)}$$

$$\therefore \quad \bar{v}_{max} = \frac{1}{2\Delta x}$$

Δx, sampling internal, cm.

λ_{min}, minimum wavelength, cm.

$\bar{v}_{max}$, maximum frequency, cm.$^{-1}$

(b) There is a limit to the resolution which can be achieved by the techniques. Perfect matching between the real $I(\omega)$ and that obtained by the transform is only possible for an infinite number of readings of $F(x)$. If readings are not taken over $x = \mp\infty$ the matching becomes less perfect, this can be considered as a resolution effect. Since this is a diffraction function, $F(x)$, the Rayleigh criterion is used to give the resolution limit. (27)

The Rayleigh criterion is an arbitary convention which has been adopted for simplicity. Two equally intense lines are regarded as being just resolved when the intensity at the midpoint between them is $8/\pi^2$ their maximum intensity.

$$\Delta\bar{v}_R \simeq \frac{1}{2N\Delta x} \qquad\qquad\text{(xvii)}$$

$\Delta\bar{v}_R$, resolution limit.

$N\Delta x$, maximum path difference between the two beams.

N, number of points used to define $F(x)$.

Just as light interacts with a sample, to produce an absorption spectrum, other forms of radiation may also interact. Specifically neutrons; by scattering off the nuclii neutrons provide similar, but complimentary, information about a sample.

2. The Scattering of Neutrons by a target.

2.1 Particles may be regarded as having wave like properties, and they become describable by wavefunctions. These are the solutions to the dynamical differential equations which represent the particle and the system it is interacting with. Most commonly these equations are of the Schrodinger type, e.g. eq. (i)

$$\left(\frac{-\hbar^2 \nabla^2}{2m} + V(\underline{r}) \right) \psi = E\psi \tag{i}$$

where

$$\nabla^2 = \frac{\partial^2}{\partial x^2} + \frac{\partial^2}{\partial y^2} + \frac{\partial^2}{\partial z^2}$$

$\hbar$, Plancks constant divided by 2π.

m, neutron mass.

ψ, solutions of equation. 'wave functions'

$V(\underline{r})$, potential function describing the potential in which the neutron moves.

$\underline{r}$, position vector of the neutron

E, a constant, the eigen value of the equation.

The Schrodinger equation for the motion of a neutron through free space is.

$$\frac{-\hbar^2 \nabla^2}{2m} \psi_i = E\psi_i \tag{ii}$$

Introducing a weak potential field, $V(\underline{r})$, can be regarded as a
perturbation of the solutions to the free space equation

$$\frac{-\hbar^2 \nabla^2}{2m} \psi_g + V(\underline{r}) \psi_g = E' \psi_g \qquad \text{(iii)}$$

$$\psi_g = \psi_i + \psi_f$$

ψ_i, wave function solutions to eq.(ii)

ψ_g, " " eq.(iii)

ψ_f, " representing a scattered wave

The form of the wave function which represents the effects of
the perturbation, shows how the target scatters the incident neutrons.
Simplification of eq. (iii) can be achieved by approximation.

$$\frac{-\hbar^2 \nabla^2}{2m} \psi_f + V(\underline{r}) \psi_i = E \psi_f \qquad \text{(iv)}$$

since

$$E \sim E'$$

$$\text{for } \underline{r} \to \infty \qquad \text{(v)}$$

and

$$\psi_g \sim \psi_i$$

$$\text{for } \underline{r} \to \infty$$

This is the Born approximation, and has been used with success to
describe the scattering of neutrons from atoms.   Strictly speaking
the application of this approximation to neutron-nucleon interaction
is not valid.   The interaction of the neutron and nucleus is a
'strong' interaction, this type of interaction is extremely intense

but of very short range. The Born approximation is usually applied to cases of weaker interactions, such as Coulombic fields. However sufficiently good predictions have been obtained by the use of this approximation to merit its application. (1). On introducing the neutron momentum eq. (iv) rearranges.

$$(\nabla^2 + \underline{k}^2) \, \psi_f \;=\; \frac{2m}{\hbar^2} \; V(\underline{r}) \psi_i \qquad\qquad \text{(vi)}$$

where

$$\frac{\hbar}{\lambda} \;=\; m\underline{v}$$

$\underline{v}$, neutron velocity

$\underline{k}$, wave vector of the neutron,
            its momentum

and

$$\underline{k} \;=\; \frac{1}{\lambda}$$

λ, De Broglie wavelength associated
with the neutron of energy E.

The wave functions assume the form of the simplest description of a plane wave. Except for the very weak scattered wave which must be a spherical wave, thus

$$\psi \;=\; \exp\{-i \, \underline{r} \cdot \underline{k}\}$$

$$\qquad\qquad\qquad\qquad \text{(viii)}$$

$$\psi_f \;=\; f(\theta). \; \frac{\exp\{-i \, \underline{r}.\underline{k}\}}{|\underline{r}|}$$

$f(\theta)$, scattering amplitude

θ, scattering angle.

The spherical wave, ψ_f, is weighted by the factor $f(\theta)$. This factor relates the extent of the perturbation to the amount of scattering it produces. The intensity of the scattering is proportioned to the spatial Fourier transform of the perturbation. Where the initial state of the neutron is known and its final state is described by the element of solid angle into which it is scattered; then the scattering amplitude plays the role of a transition probability between the two states.

$$f(\theta) \propto T_{i,f} = \int \psi_f^* V(\underline{r}) \psi_i \ d\sigma \qquad \text{(ix)}$$

$\qquad$ *, indicates the complex conjugate.

$\qquad$ $T_{i,f}$; transition probability.

$\qquad$ $\int d\sigma$; integral over all space.

$\qquad$ subscript i, indicates initial state property

$\qquad$ " f, indicates final state property.

and

$$f(\theta) = \left(\frac{m}{2\pi\hbar^2} \right) T_{i,f} \qquad \text{(x)} \quad \text{(19)}$$

In Dirac notation (ix) is simply

$$T_{i,f} = <f \mid V(\underline{r}) \mid i> \qquad \text{(xi)}$$

Here

$\qquad$ $\mid a>$, represents ψ_a

and

$\qquad$ $<a\mid$, represents ψ_a^*

$\qquad$ Where a is a quantum number which defines the wave function. Integration over all space is implicit in the use of these symbols.

For experimental reasons it is usual to express the interaction
of the neutron and target by a differential scattering cross section.

$$\frac{ds}{d\Omega} = \frac{N^{\underline{o}} \text{ of neutrons scattered into solid angle } \Omega \text{ per unit time}}{N^{\underline{o}} \text{ of neutrons incident upon target per unit time}}$$

(xii)

s, scattering cross section experimentally
determined

Ω , solid angle.

which is the flux of neutrons through Ω in unit time

from (viii) $\qquad \left(\frac{ds}{d\Omega} \right)_{i,f} = \left| f(\theta) \right|^2 \qquad$ (xiii) (19)

then from (xiii) and (x)

$$\left(\frac{ds}{d\Omega} \right)_{i,f} = \left(\frac{m}{2\pi\hbar^2} \right)^2 \left| < f \left| V(\underline{r}) \right| i > \right|^2 \qquad \text{(xiv)}$$

However not all scattering events are elastic, the scattering cross
section thus becomes energy dependent.   Since energy must be
conserved the final energy of the neutron must be simply related to
the energy states of the target system.   Total energy conservation
is provided for in the delta relationship due to Dirac (33).

$$\delta(E_f - E_i \mp \hbar\omega) \qquad \text{(xv)}$$

E, an energy state of the target system

$\hbar\omega$, energy change of the neutron.

(Integration of this symbol is implied)

$$\int dA \; \delta(A) = 1 \quad \text{for } \delta(A) \neq 0$$

$$\text{and } \delta(A) \neq 0 \text{ where } A = 0$$

Thus equations of the type (xv) can be expressed in a different form through the delta integral

$$\delta(A) = \frac{1}{2\hbar} \int_{-\infty}^{\infty} \exp\{iAt\} \, dt$$

where in eq. (xv)

$E_f > E_i$ defines down scattering, and neutron energy loss.

$E_f < E_i$ defines up scattering, and neutron energy gain.

The scattering equation must be weighted over the initial states of the system and summed over all the initial and final states. This provides the total double differential scattering cross-section.

$$\frac{d^2 s}{dEd\Omega} = \frac{|k_f|}{|k_i|} \left(\frac{m}{2\pi\hbar^2}\right)^2 \sum_{i,f} g_i \; |<f|V(\underline{r})|i>|^2 \; \delta(E_f - E_i \mp \hbar\omega)$$

$$(\text{xvi})$$

where
$$\sum_i g_i = 1$$

g_i, weighting factor over initial states

(Considerations concerning the spin states of the neutron are omitted in (xvi)).

Fermi (1936) has suggested a suitable pseudo-potential to represent $V(\underline{r})$ in eq. (xvi).

$$V(\underline{r}) = \frac{2\pi\hbar^2}{m} \cdot b \cdot \delta(\underline{r} - \underline{R}) \qquad \text{(xvii)}$$

$\underline{R}$, position vector of target.

This is the only form for $V(\underline{r})$ which will provide for isotropic scattering from independent bound nuclii, in the Born approximation (29). This is a reflection of the difficulty of applying the Born approximation to strong interactions. Several scattering centers are represented by the summation.

$$V(\underline{r}) = \left(\frac{2\pi\hbar^2}{m} \right) \sum_{1} b_1 \, \delta(\underline{r} - \underline{R}_1) \qquad \text{(xviii)}$$

b_1, scattering length of 1th nucleous

$\underline{R}_1$, position vector of 1th nucleous

Using equations (xviii), (ix), (viii), (xvi) and the delta integral yields in the original, integral, notation

$$\frac{d^2 s}{d\Omega dE} = \frac{k_f}{k_i} \sum_{i,f} g_1 \Big| \sum_{1} b_1 \int_{-\infty}^{\infty} e^{-i \cdot \underline{k}_f \cdot \underline{r}} \cdot e^{\frac{i r t}{\hbar}} \cdot e^{\frac{-i \underline{R}_1 t}{\hbar}} \cdot e^{i \underline{k}_i \underline{r}} \cdot$$

$$\cdot d\sigma \Big|^2 \delta(E_f - E_i \mp \hbar\omega) \qquad \text{(xix)}$$

and in Dirac notation

$$\frac{d^2 s}{dE d\Omega} = \frac{k_f}{k_i} \sum_{i,f} g_1 \Big| < f \Big| \sum_{1} b_1 \cdot \exp\{i\underline{Q} \cdot \underline{R}_1\} \Big| i > \Big|^2 \delta(E_f - E_i \mp \hbar\omega) \qquad \text{(xx)}$$

where

$$k = |\underline{k}|$$

and $\underline{Q} = \underline{k}_i - \underline{k}_f$

$\underline{Q}$, the momentum change of the neutron.

This equation is important and forms the basis of subsequent treatment, here and in many other texts. However the connection between the experimentally observed spectrum, measured as $\dfrac{d^2 s}{dE d_\omega}$, and the properties of the target system is not immediately obvious. It is usual to express the differential scattering cross-section as a 'scattering law', and to develop the dynamics of the target system in correlation functions. A very simple connection exists between the two concepts.

2.2 The scattering law and the correlation functions.

In order to develop the ideas of a scattering law and correlation functions it is necessary to expand $eq.$ 2.1(xx) and transform it into the Heisenberg representation. Using the delta integral, 2.1(xx) becomes

$$\frac{d^2 s}{d\Omega dE} = \frac{k_f}{k_i} \quad \frac{1}{2\pi\hbar} \int_{-\infty}^{\infty} dt \, \exp[-i\omega t] \sum_{i,f} g_i < i| \sum_l b_l^* \exp\{-i\underline{Q}.\underline{R}_l\}$$

$$. |f> . <f| \exp\left\{\frac{itE_f}{\hbar}\right\} . \sum_{l'} b_{l'} \exp(i\underline{Q}.\underline{R}_{l'}). \exp\left(\frac{-it\,E_i}{\hbar}\right) \, | i>$$

(i)

t, time

b_l^*, spin scattering length of lth atom

$b_{l'}$, isotope scattering length of l'^{th} atom.

Where (i) is restricted to the case of neutron energy gain,
a similar expression applies for neutron energy loss, and
substituting the Hamitonian operator for the target system, $\hat{H}$, into (i)

$$\frac{d^2s}{d\Omega dE} = \frac{k_f}{k_i} \frac{1}{2\pi\hbar} \int_{-\infty}^{\infty} dt \; \exp[-i\omega t] \sum_{i,f} g_i < i| \sum_{1} b_1^* \exp\{-i\underline{Q}.\underline{R}_1\}|f> .$$

$$. < f| \sum_{1'} b_{1'} \exp\left\{\frac{i\hat{H}t}{\hbar}\right\} \exp\{i\underline{Q}.R_{1'}\}.\exp\left\{\frac{-i\hat{H}t}{\hbar}\right\}| i > \qquad (ii)$$

The Heisenberg representation of the dynamical system is in terms
of the equation.

$$\frac{i d\hat{R}_{1'}(t)}{dt} = \hat{R}_{1'}(t)\hat{H} - \hat{H}\hat{R}_{1'}(t) \qquad (iii)$$

$$= [\hat{R}_{1'}(t),\hat{H}]$$

[,],   the comulator relationship.

$\hat{R}_{1'}(t)$,   time dependent operator which is
      the solution to (iii).

$\hat{}$,   indicates an operator, which is in
      a matrix form.

Now

$$\exp(i\underline{Q}.\hat{R}_{1'}(t)) = \exp\left(\frac{i\hat{H}t}{\hbar}\right).\exp(i\underline{Q}.\underline{R}_{1'}).\exp\left(\frac{-i\hat{H}t}{\hbar}\right) \qquad (iv)$$

and at t = 0.

$$\exp(i\underline{Q}.\hat{R}_1(0)) = \exp\left(\frac{i\hat{H}.0}{\hbar}\right).\exp(i\underline{Q}.\underline{R}_1)\exp\left(\frac{-i\hat{H}.0}{\hbar}\right) \qquad (v)$$

Substituting (iv) and (v) into (ii) yields

$$\frac{d^2s}{dEd\Omega} = \frac{k_f}{k_i} \frac{1}{2\pi\hbar} \int_{-\infty}^{\infty} dt \exp[-i\omega t] \sum_{1'1} b_1^* b_{1'} < \exp(-i\underline{Q}.\hat{R}_1(0)).$$

$$. \exp(i\underline{Q}.\hat{R}_{1'}(t)) > \qquad\qquad (vi)$$

Where the termal average is written in a simplified manner

$$\sum_i g_i < i| \quad |f> \quad = \quad < \quad > \qquad\qquad (vii)$$

In this thesis only incoherent scattering from independent bound hydrogen atoms will be considered. The large incoherent scattering cross section of hydrogen, 79.7 barns (32), allows the simplification of (vi) to include only these effects (all subsequent formulae will pertain primarily to the incoherent scattering process), and equation (vi) becomes.

$$\frac{d^2s}{dEd\Omega} = N \frac{k_f}{k_i} . B . S(\underline{Q}, \omega) \qquad\qquad (viii)$$

where

$$B = |b - \overline{b}|^2, \quad \text{using the notation of Allen (1973).}$$

$$B, \quad \text{is the incoherent scattering cross section for the target system.}$$

also

$$S(\underline{Q}, \omega) = \frac{1}{2\pi\hbar} N \int_{-\infty}^{\infty} dt \exp[-i\omega t] \sum_1 < \exp(-i\underline{Q}.\hat{R}_1(0)).\exp(i\underline{Q}.\hat{R}_1(t)) >$$

$$\qquad\qquad (ix)$$

S($\underline{Q}$, ω) is the scattering law and is a summary of the dynamics of the target in terms of the measurable parameters of the experiment. These parameters are the energy and momentum change of the neutron. This scattering law can be transformed from the momentum, energy space into the position, time realm.

$$S(\underline{Q}, \omega) = \frac{1}{2\pi\hbar} N \iint \exp(-i(\omega t - \underline{Q}.\underline{r})).G_s(\underline{r}, t)d\underline{r}\ dt \qquad (x)$$

$G_s(\underline{r}, t)$, the self correlation function.

This scattering law, derived specifically for neutron energy gain, is related to the corresponding scattering law for neutron energy loss. All things being equal, the chance of an up scattering event is the same as for a down scattering event. If this were not so the target would be systematically drained of, or loaded with, energy. However the population of target states capable of undergoing neutron up scattering events is greater; this is the condition of detailed balance.

K, Boltzmans Constant

T, Absolute temperature

$$S(\underline{Q}, \omega) = S(-\underline{Q}, -\omega). \exp\left(\frac{\hbar\omega}{KT}\right)$$

Alternatively this can be seen as a property of the correlation functions. These are complex time functions, their Fourier transforms (S($\underline{Q}$, ω))would be expected to be unsymmetrical functions of ω.

The self correlation function is the double Fourier transform of S($\underline{Q}$, ω) and is a representation of the variation with time of the

position of the independent hydrogen atoms.   Classically $G_s(\underline{r}, t)$ can

be regarded as a probability function;   the probability that a

proton at $\underline{r} = 0$, when $t = 0$, will be at $\underline{r}$ when time $= t$.   This

formalisation shews clearly the connection between the observed

spectrum and the target dynamics, and is due to Van Hove (1954).

2.3 Scattering Law applied to molecules and crystals.

The scattering law has been derived for independent atoms,

specifically hydrogen atoms.   In the case of neutron scattering from

molecules the description of atoms in terms of the simple position

vectors loses significance.   A description involving a molecular

concept of the atomic positions would be more useful.   After this

the scattering can be separated into contributions arrising from the

molecular motions.   These are translational, rotational and

vibrational in nature.

The position vector of an atom can be expanded as

$$\underline{R}_1 = \underline{c}_1 + \underline{b}_1 + \underline{u}_1 \tag{i}$$

$\underline{R}_1$,   general position vector of the 1th nucleus

$\underline{c}_1$,   centre of mass position vector of the
molecule of the 1th atom.

b_1,   position vector of the mean position of
the 1th atom.

u_1,   displacement vector of the 1th atom.

It is obvious that $\underline{c}_1$, $\underline{b}_1$, and $\underline{u}_1$ will be time dependent and also $\underline{b}_1$

and $\underline{u}_1$ will be orientationally dependent.   The thermal average part

of eq. 2.2(ix) becomes.

$$< \exp\{-i\underline{Q}.(\hat{c}_1(0) + \hat{b}_1(0) + \hat{u}_1(0))\}.\exp\{i\underline{Q}.(\hat{c}_1(t) + \hat{b}_1(t) + \hat{u}_1(t))\} >$$

(ii)

$\hat{c}_1, \hat{b}_1, \hat{u}_1,$ are Heisenberg operators which express the time dependence of the relevant vectors.

If the Heisenberg operators commute with each other then they are essentially independent. The scattering law can be separated immediately into the relevant contributing parts.

The operator $\hat{c}_1$ is only time dependent and describes the translational movements of the molecule. The operator $\hat{b}_1$, because of its dependence on the molecular orientation, can be used for the rotational description.

$$\underline{b}_1 = b_1 . \underline{1}_1(W)$$

(iii)

$$b_1 = |\underline{b}_1|$$

$\underline{1}_1$, a unit vector

W, the set of Euler angles fixing orientation of the molecule.

The operator $\hat{u}_1$ can be expressed as a function of the normal modes of vibration of the molecule where

$$\underline{u}_1 = \sum_e \underline{h}_1^e j_1^e q_e(t)$$

(iv)

$\underline{h}_1$, a unit vector

j_1, an amplitude

$q(t)$, a normal coordinate

e, index signifying a normal mode.

Unfortunately $\underline{u}_1$ is also dependant upon W (through the unit vector $\underline{h}_1(W)$.) This demands that the vibrational and rotational contributions to the scattering are coupled. This coupling is usually ignored (!), which facilitates interpretation and calculation. Only small errors are assumed to result from this approximation. The scattering law of eq. 2.2(ix) becomes.

$$S(\underline{Q},\omega) = \frac{1}{2\pi\hbar N} \int_{-\infty}^{\infty} dt \, \exp[-i\omega t] \sum_1 < \exp(-i\underline{Q}.\hat{c}_1(0)).\exp(i\underline{Q}.\hat{c}_1(t))> .$$

$$. < \exp(-i\underline{Q}.\hat{b}_1(0)).\exp(i\underline{Q}.\hat{b}_1(t))> .$$

$$. < \exp(-i\underline{Q}.\hat{u}_1(0)).\exp(i\underline{Q}.\hat{u}_1(t))>$$

$$(v)$$

which can be written

$$S(\underline{Q},\omega) = \frac{1}{2\pi\hbar N} . S_T(\underline{Q},\omega) * S_R(\underline{Q},\omega) * S_V(\underline{Q},\omega) \qquad (vi)$$

Subscript T, a translational property

" R, a rotational property

" V, a vibrational property

(The symbol * stands for convolution, c.f. 1.1(xiii) and 1.1(xiv)) with the separation of the scattering law into its component parts it becomes possible to discuss these independently.

2.3.1 Molecular vibrational contribution

This topic has been thoroughly discussed by Zemach (1956), and the calculations presented here follow this early paper. It is necessary to calculate the thermal average of the contributions made to the total scattering law eq. 2.3(v) by the displacement vectors, this is.

$$< \exp(-i\underline{Q}.\hat{\underline{u}}_1(0)).\exp(i\underline{Q}.\hat{\underline{u}}_1(t)) >$$

where   (i)

$$\underline{u}_1 = \sum_e \underline{C}_1^e \, q_e(t)$$

$$\underline{C}_1^e, \quad \text{amplitude vector of the } 1^{th} \text{ atom} \\ \text{in the } e^{th} \text{ mode.}$$

thus

$$\exp(i\underline{Q}.\hat{\underline{u}}(t)) = \exp(i\underline{Q}.\sum_e \underline{C}_1^e.q_e(t))$$

$$\text{for} \quad e = 1,2,3 \ldots$$

$$= \exp\{i(\underline{Q}.\underline{C}_1^l q_l(t) + \ldots)\}$$

$$= \prod_e \exp\{i\underline{Q}.\underline{C}_1^e.q_e(t)\}$$ (ii)

The normal modes of a molecule are by definition dynamically independent and eq. (i) becomes

$$\prod_e < \exp(-i\underline{Q}.\underline{C}_1^e.q_e(0)).\exp(i\underline{Q}.\underline{C}_1^e.q_e(t)) >$$ (iii)

using $\quad [x.\hat{A}, x.\hat{B}] = x^2[\hat{A},\hat{B}]$

and $\quad \exp\hat{A}. \exp\hat{B} = \exp\{\hat{A} + \hat{B} + \tfrac{1}{2}[\hat{A},\hat{B}]\}$

Equation (iii) can be expanded for a particular mode; the index, e, is temporarily dropped.

$$< \exp\{i.\underline{Q}.\underline{C}_1(q(t)-q(0)) + \tfrac{1}{2}(\underline{Q}.\underline{C}_1)^2[q(0),q(t)]\} > \qquad (iv)$$

A modified form of a theorem after Block (1932) is used

$$< \exp.A > = \exp(\tfrac{1}{2} < A^2 >)$$

$$A, \quad \text{a coordinate}$$

thus (iv) is

$$\exp(-(\underline{Q}.\underline{C}_1)^2 < q^2(0) > + (\underline{Q}.\underline{C}_1)^2. < q(t).q(0) > \qquad (v)$$

It is assumed that q(t) behaves as the coordinate of a one dimensional oscillator thus

$$q(t) = \left(\frac{\hbar}{2m\omega} \right)^{\tfrac{1}{2}}.\{ \hat{a}.\exp(-i\omega t) + \hat{a}^+. \exp(i\omega t)\}$$

where $\qquad [\hat{a},\hat{a}^+] = 1 \qquad\qquad (vi)$

$$[\hat{a},\hat{a}] = [\hat{a}^+, \hat{a}^+] = 0$$

$\hat{a}^+, \hat{a};$ are the creation, anihilation, operators which operate on the oscillator eigen functions to give the eigen function of the next highest, lowest, oscillator state.

m, mass of scattering atom; index 1 temporarily omitted.

From there it can be seen that

$$< q(t).q(0)> = \frac{1}{2m\omega} \{< \hat{a}\hat{a}^+> \exp(-i\omega t) + < \hat{a}^+\hat{a} > \exp(i\omega t)\}$$

(vii)

since

$$< \hat{a}\hat{a}^+> = <n>+1$$

$$< \hat{a}^+\hat{a} > = <n>$$

(3)

where

$$<n> = \sum_i g_i . <i|n|f> = \sum_i g_i . n$$

and

$$\sum_i n.g_i = \left(\frac{1}{z-1}\right)$$

n, quantum state of the oscillator

$$= \frac{1}{2m\omega} \left\{ \left(\frac{1}{z-1} +1\right) \exp(-i\omega t) + \left(\frac{1}{z-1}\right) \exp(i\omega t)\right\}$$

where $z = \exp\left\{\frac{\hbar\omega}{KT}\right\}$

(viii)

K, Boltzmans constant

T, absolute temperature

The function $(z - 1)^{-1}$ represents the occupancy number of the energy level considered, thus.

$$< q(t).q(0) > = \frac{1}{2m\omega(z-1)} \{z.\exp(-i\omega t) + \exp(i\omega t)\}$$

(ix)

and

$$< q^2(0) > = <q(0).q(0)> = \frac{1}{2m\omega(z-1)} \{z + 1\} \qquad \text{(x)}$$

Substituting equations (ix) and (x) into (v) gives the thermal average required.

$$\exp\left[\frac{-(Q.\underline{C}_1)^2}{2m\omega} \cdot \left(\frac{z+1}{z-1} \right) + \frac{(Q.\underline{C}_1)^2}{2m\omega} \left(\frac{1}{z-1} \right) \left(z.\exp(-i\omega t) + \exp(i\omega t) \right) \right] \qquad \text{(xi)}$$

However the second part of this exponent may be expressed in the form of modified Bessel function since (3)

$$\exp\{ \frac{x}{2} . (y + \frac{1}{y})\} = \sum_{n=-\infty}^{\infty} y^n I_n(x) \qquad \text{(xii)}$$

$I_n(x)$, the nth order modified Bessel function of the first kind; argument, x.

The Bessel function of the first kind is given by

$$I_n(x) = \sum_{m=0}^{\infty} \frac{(-1)^m (\frac{x}{2})^{n+2m}}{m! \ (n+m)!} \qquad \text{(12)}$$

substituting $y = \exp(i\omega t).z^{-\frac{1}{2}}$

Equation (xi) becomes; expanding z from eq.(viii)

$$\exp\left[\frac{-(Q.\underline{C}_1)^2}{2m\omega} \cdot \text{Coth} \left(\frac{\hbar\omega}{2KT} \right) \times \sum_{-\infty}^{\infty} \exp(in\omega t).\exp\left(\frac{-n\hbar\omega}{2KT}\right). I_n \left\{ \frac{(Q.\underline{C}_1)^2}{2m\omega \ \sinh\left(\frac{\hbar\omega}{2KT}\right)} \right\} \right.$$

$$\text{(xiii)}$$

This is for one specific mode, when the product is taken over all the modes, e, these each contribute a delta function to the cross-section. This delta function is an energy delta function and appears at their characteristic normal frequency. The double differential scattering cross-section for vibration is easily found from (xiii) by substituting into 2.3 (v) and performing the Fourier transform.

$$\frac{d^2s}{d\Omega dE} = \frac{k_f}{k_i} \cdot \frac{1}{N} \sum_1 B_1{}^2 \exp(-2D_1) \exp(\frac{-n\hbar\omega_e}{2KT}).$$

$$\cdot I_1\left\{\frac{(Q \cdot \underline{C}_1^e)^2}{2m\omega_e \sinh\left(\frac{\hbar\omega_e}{2KT}\right)}\right\} \delta(\hbar\omega \pm \hbar\omega_e) \quad \text{(xiv)}$$

where

$$D_1 = \frac{m_1}{4} \sum_e \frac{Q \cdot \underline{C}_1^e}{(\omega_e/\hbar)^{\frac{1}{2}}} \cdot \coth\left(\frac{\hbar\omega_e}{2KT}\right) \quad \text{(xv)}$$

ω_e, the normal frequency of vibration of the normal mode e.

D_1, the Debye-waller factor

In practice the terms in the argument of the Bessel function are small and it is realistic to approximate this function by the first term in its power series expansion.

$$I_n(x) \sim (\tfrac{1}{2} x)^{|n|} \cdot (|n|)^{-1} \quad \text{(xvi)}$$

The use of the first order only is valid where the scattering cross-section reflects the one phonon process. Here the vibrationary oscillator undergoes the exchange of one quantum with the neutron. In the cases of higher quantum exchanges, the two or three phonon processes, the appropriate order of the Bessel function must be used. It is for this reason that the scattering cross-section of a two phonon event is lower than the one phonon event. The argument of the Bessel function controlls the intensity of the scattering from a mode. When reasonable values of the parameters are substituted for the terms of the argument, eq. (xiv) and eq. (xvi), the ratio of the first phonon cross-section to the second phonon cross-section can be obtained. Such a calculation indicates that for a fundamental frequency of $200cm^{-1}$, whose intensity is defined as 100%, the first overtone should have an intensity of about 20% and the third overtone of about 9%. Using this and developing the differential cross-section for up scattering equation (xiv) becomes, for the one phonon process.

$$\frac{d^2s}{d\Omega dE} = \sum_{e,1} \frac{k_f}{k_i} \cdot \frac{1}{2\pi\hbar} \quad B^2 \exp(-2D_1) - (\frac{1}{z-1}) \cdot \frac{|\underline{Q} \cdot \underline{c}_1^e|^2}{2m\left(\frac{\omega_e}{\hbar}\right)} \cdot \delta(\hbar\omega + \hbar\omega_e)$$

$$(xvii)$$

(where a similar cross-section results for down scattering)
Equation (xvii) shows several aspects of molecular spectroscopy which are peculiar to neutron inelastic studies. The intensity of the scattering event is dependent on the magnitude of the displacement

of the scattering atom from its mean position, $\underline{c}_1^e$. This intensity
is also governed by the size of the momentum transfer $\underline{Q}$. There is
thus an intensity variation for various scattering angles, predicted.
Overall there would be expected to be a decrease of intensity with
angle, which is shown by the Debye-Waller factor, eq. (xv). Since
the argument of the hyperbolic contangent, eq. (xv), decreases with
any increase in temperature, then the Debye-Waller factor increases.
Thus, for any one vibrational mode, the intensity of the scattering
will decrease as temperature increases. The combined effects of the
displacement term and the Debye-Waller factor is to produce spectral
shifts with scattering angle; in low resolution spectra. (31).
A further consequence of the intensity being governed by the Bessel
function, eq. (xiv) and eq. (xvi), is that the intensity is a function
of $\underline{Q}^2$ for a one phonon event and $\underline{Q}^4$ for the two phonon (first
overtone) event. Although sharp delta features are expected in
the energy transfer, associated with the normal modes of the molecule,
this may not be observed. The scattering from the vibrations must
be convolved with the rotational and translational motion and this
will broaden the bands significantly (see equation 2.2 (vi)), apart
from experimental resolution effects.

2.3.2 Molecular translational contribution.

In a gas or a liquid molecules are translated through space by
colliding off neighbours, diffusion. However in solids the molecules
are constrained to remain on a lattice point. The molecule still
moves, by small displacements from the mean position. These

displacements can be regarded as the frustrated translational motions of the centre of mass of the molecule, they become larger as the temperature increases. As with a molecule the total dynamical state of a crystal can be described in terms of a series of independent coordinates, the normal coordinates, which is the description of each atom as an independent oscillator, performing a normal mode vibration. If the crystal as a whole were treated strictly in this fashion the number of normal coordinates to be found would be very large, 3N-6. (Where N is the number of molecules in the crystal). The symmetry of the lattice allows considerable simplification (6). This simplification is obtained by the inclusion of an extra index to mark the dynamical equations of the system and their solutions. This index g is the reciprocal lattice vector defined by eq. (i) and reflects the translational symmetry of the lattice.

$$g = \frac{n}{L} \cdot \underline{s}_1 + \frac{n_2}{L_2} \cdot \underline{s}_2 + \frac{n_3}{L_3} \cdot \underline{s}_3 \qquad (i)$$

where
$$n_i = 0, \pm 1, \pm 2, \ldots\ldots$$

$$\text{for } i = 1, 2, 3$$

$$\underline{s}_i \cdot \underline{t}_j = 2\pi \delta_{ij}$$

$$\text{for } i,j = 1, 2, 3$$

$\underline{t}_j$, the basis vectors of a unit cell of the crystal.

L_j, number of unit cells in the crystal, along direction j.

In a molecular lattice the motions of the individual atoms can be separated into low frequency and high frequency displacements. The high frequency motions are the vibrations resulting from the large force constants associated with molecular bonds. The low frequency motions are the vibrations resulting from the weak intermolecular forces. These low frequency modes can be described in terms of the displacements of the centre of mass of the molecule, or the molecular ion. Thus although the centre of mass of a molecule may not scatter neutrons strongly, the low frequency motions of the tightly bound atoms show its motions. A similar vector description to equation 2.3 (i) is given for the low frequency vibrations

$$\underline{R}_1 = \underline{c}_1 + \underline{b}_1 + \underline{v}(\underline{g})_y \qquad\qquad (ii)$$

$\underline{v}(\underline{g})_y$, displacement vector of the centre of mass of the molecule y, to which atom 1 is attached.

$\underline{v}(\underline{g})_y$ is a function of the direction which the displacement takes in the crystal ($\underline{g}$). The contribution to the scattering law made by these vibrations will be given by the thermal average

$$< \exp(-i\underline{Q}.\ \hat{v}_y(\underline{g})).\ \exp(i\underline{Q}.\ \hat{v}_y(\underline{g})) > \qquad\qquad (iii)$$

$\hat{v}_y(\underline{g})$, the Heisenberg operator which reflects the time dependence of the displacement $\underline{v}_y(\underline{g})$

where

$$\hat{v}_y(g) \;=\; \sum_e \underline{U}_{-y}^e(g) \cdot q_e(t) \qquad\qquad \text{(iv)}$$

$\underline{U}_{-y}^e(g)$, polarisation vector of the centre of mass y, in the mode. e.

(Compare with equation 2.3.1 (i)).

Similar methods to those used in the molecular vibrational case, 2.3.1, may be applied here. This is because both systems are describing the motions of the atoms as independent harmonic oscillators. A double differential scattering cross-section is obtained. The single phonon process for the incoherent up scattering is then given by (v)

$$\frac{d^2s}{dEd\Omega} \;=\; \sum_{g,e,y} \frac{k_f}{k_i} \frac{1}{2\pi\hbar} \; B^2 \cdot \exp(-2D_y)\left(\frac{1}{z-1}\right) \cdot$$

$$\cdot\; \frac{\left|\underline{Q} \cdot \underline{U}_y^e(g)\right|^2}{2m_y\left(\frac{\omega^e(g)}{\hbar}\right)} \cdot \delta(\hbar\omega + \hbar\omega^e(g\nu) \qquad \text{(v)}$$

$\omega^e(g)$, the frequency of the eth normal lattice mode, with the lattice vector g.

m_y, mass of the yth ion.

D_y, Debye-Waller factor of the yth ion.

where the summation now runs over y instead of 1.

(compare to equation 2.3.1 (xvii)).

Because the scattering indicated by (v) is incoherent the scattering will occur over all values of g for which solutions ($\omega^e(g)$) to

the dynamical equations exist. The scattering is likely therefore to be broad in nature. There is no restriction concerning conservation of momentum, which is present for the double differential cross-section for coherent scattering. Under these circumstances alignment of the crystal with respect to the neutron vectors loses significance, and it is usual to employ poly crystalline samples. (33).

Equation (v) may be taken further. $|\underline{Q}.\underline{U}_y^e(g)|^2$ can be replaced by an average taken over a constant frequency surface represented by $\overline{|\underline{Q}.\underline{U}_y^e(g)|^2}$. When this is done the summation over all values of g can be replaced by an integration over the density of phonon states, thus (v) becomes. (17).

$$\frac{d^2s}{dEd\Omega} = 3N\ B^2 \int_{-\infty}^{\infty} d\omega\ Z(\omega)\ \frac{k_f}{k_i}\ \frac{\overline{|\underline{Q}.U_y^e(g)|^2}}{2m_y\ (\frac{\omega}{\hbar})}\ .$$

$$\cdot\ (\frac{1}{z-1}).exp(-2D).\delta(\hbar\omega + \hbar\omega_e)\qquad (vi)$$

In the case of a monatomic cubic crystal the value of $\overline{|\underline{Q}.\underline{U}_y^e(g)|^2}$ can be evaluated analytically, and gives. (14).

$$\overline{|\underline{Q}.\underline{U}_y^e(g)|^2}\ =\ \tfrac{1}{3}\ Q^2$$

for cubic crystal only

where

$$Q = |\underline{Q}|$$

and therefor eq.(vi) becomes.

$$\frac{d^2s}{dEd\Omega}\ =^?\ N\ \frac{k_f}{k_i}\ B^2.exp(-2D)\ (\frac{1}{z-1}).\ \frac{Q^2}{2m\omega}\ .\ Z(\omega)\qquad (vii)$$

where

$$Z(\omega), \quad \text{frequency distribution spectrum of the crystal phonons; the phonon density of states.}$$

$$\int_0^\infty Z(\omega) \ d\omega \equiv 1 \qquad\qquad (viii)$$

2.3.3 Molecular Rotational Contribution

The rotational aspects of neutron scattering cover two important areas which are closely related. These are the scattering in an unhindered system, free rotation, and the scattering in a strongly hindered system, libration. Between these two extremes are systems whose rotational motions cannot be described by these approximations. Amongst these compounds are many molecular crystals (25), the plastic crystals (28), and, significantly, the ionic ammonium salts (18,13). It is only possible to work from the thermal average toward a scattering law (as was previously done) in the case of libration or free rotation. The intermediate cases are usually treated by modelling. A mathematical model is constructed for the correlation function and this is transformed into the scattering law. The models used to describe this intermediate stage are usually combinations of the two extreme cases. Two models will be discussed here, the first applies to situations involving fixed geometry and rapid reorientation. The second is more general and can treat cases where libration and reorientation are equally important. Further, the latter model can be transformed into the description of the two extreme cases, above.

The jump diffusion model was originally used by Chudley (1961) to explain diffusion in a liquid. This was applied to solids by Skold (1968). The centre of mass of the molecule is fixed, and about this the molecule is considered to execute instantaneous jumps. After any such jump the molecule remains fixed in orientation, apart from libration motions, for a given length of time. This period of librational motion is followed by another instantaneous jump. From the geometry of the molecule and its lattice it is possible to define the starting and finishing positions of the scattering atom. These can be used to obtain the necessary scattering law, thus.

$$S_R(\underline{Q}, \omega) = \frac{N}{2\pi} \int G_R(\underline{r}, t) . \exp(i(\underline{Q}.\underline{r} - \omega t)) d\underline{r} dt \qquad (i)$$

(compare equations 2.3(vi) and 2.2(x)).

When the rotational motion is treated classically in terms of the above model only the starting and finishing positions of the scattering atom are required. The self-correlation function can be written as (9).

$$G_R(\underline{r}, \underline{t}) = \sum_i P_i(t) . \delta(\underline{r} - \underline{r}_i) \qquad (ii)$$

i,   available number of sites for scattering atom to be in.

$P_i(t)$,   probability that the proton is at $\underline{r}_i$, when time $= t$, given it was at $\underline{r}$ at time $= 0$.

The $P_i(t)$ are the solutions to a simultaneous differential rate equation (5), eq (iii), this is the case because the jumps are completely uncorrelated.

$$\frac{\partial P_i(t)}{\partial t} = \frac{1}{\tau} \left\{ \frac{1}{n} \sum_{j=1}^{n} P_j(t) - P_i(t) \right\} \tag{iii}$$

$j,$ summation index over all the n' sites from which the jump can be made to the ith site.

$\frac{1}{\tau},$ the jump probability for all such equivalent sites.

Because of the known geometry of the system the boundary conditions relating to eq.(iii) are known and it can be solved to obtain $P_i(t)$. (5, 24, 25). Substitution into eq. (ii) and its Fourier transform yields the scattering law $S_R(Q,\omega)$. In the case of polycrystalline samples the results must be averaged over all $\underline{Q}$, (24). The model predicts an elastic peak (which reflects the fact that even over large periods of time the scattering atom is localised close to the lattice point). Further it predicts scattering at very low energy transfer, in the quasi elastic region.

If instrumental resolution is not good the separation of these two effects id difficult. The relative contributions to the total scattering in this region in dependent upon the neutron momentum transfer $\underline{Q}$. In this model the $\underline{Q}$ dependence of each component tends to be simple. Calculations can lead to an estimate of the full width at half height of the elastic and Quasi elastic peaks combined; at a

given $\underline{Q}$.   Thus although the full width at half height of the quasi

elastic peak is constant the value for the combination should show

variation in $\underline{Q}$ (25).   This variation is oscillatory in nature and

appears to be in accord with observation (13).   It is obvious that the

model is non physical, since it allows instantaneous reorientation,

without regard to a finite molecular inertia.   A slightly more '

sophisticated model was used by Lassier (1969) to calculate optical

properties for some systems.   In his model the finite nature of

molecular inertia is taken into account.

The rotor, with a given inertia, is in a state of libration or

rotation dependent upon its energy and the depth of the potential well

in which it moves.   When the rotational energy is greater than the

well depth the rotor rotates.   The rotor is kept in equilibrium

with the surrounding lattice by randomly receiving different rotational

energies.   The new rotational energies are chosen according to a

Boltzman distribution.   The random periods of time after which the

rotor is given a new energy are generated by the poisson distribution.

(The Poisson distribution is the distribution usually found for

uncorrelated events.   The chance of an event happening, $P(t)$, at

that time, t, is governed by a characteristic time, τ. Such that

$$P(t) = \frac{(t/\tau)^{m}.\exp(-t/\tau)}{m!} \qquad \text{m is the mean number of events.})$$

From these calculations the time correlation functions can be

obtained and used to give the scattering law.   This model would be

expected to be more realistic than that proposed by Chudley (1961), but

it still retains the non physical feature of instantaneous rotational

energy changes.

A similar model was used by Larsson (1973) specifically for
neutron scattering, and is based upon orientational correlation functions.
A simple physical model proposed.   On the average a molecule in a
crystal will be surrounded by a mean density of neighbours.   During
short periods of time t_o the neighbours will be more densly packed
about it, the molecule may librate but may not reorientate.   Again
for short periods of time t_1 the neighbours will be less densly packed,
and reorientation is free.   The extent of the reorientation will be
governed by the molecular inertia and its energy, as well as the length
of t_1 .(the direction and extent of reorientation may also be governed
by local geometry of the lattice).   The steps used by Larsson to
expand the scattering law in terms of functions representing libration
and rotation will be outlined.   The double differential scattering
cross-section may be written (21).

$$\frac{d^2 s}{d\Omega dE} = \frac{k_f}{k_i} \frac{1}{2\pi} \int_{-\infty}^{\infty} \exp(-i\omega t)\, I(\underline{Q}, t)\, dt \qquad (iv)$$

where

$$I(\underline{Q},t) = \sum_{l=1}^{N} < \exp(-i\underline{Q}.\underline{R}(0)).\exp(i\underline{Q}.\underline{R}(t))> G(W_o, W, t) \qquad (v)$$

> $G(W_o, W, t)$,   angular correlation
> function, the probability
> that the molecular reorientation
> is in dW, centred at W for
> time = t if the orientation
> was W_o at time = 0.

The angular correlation function can be expanded as a series of steps,
described by the functions $f_n(W_o, W, t)$. (14).   Each step describes the

smearing out of the scattering atom in time and space, so,

$$G(W_o, W, t) = \sum_{n=o}^{\infty} f_n(W_o, W, t) \qquad (vi)$$

The $f_n(W_o, W, t)$ are composed of partial correlation functions. These partial correlation functions describe how the scattering atom spreads during libration, $g(W_o, W, t)$, and during rotation $h(W_o, W, t)$. These new functions are active during the time periods t_o and t_i respectively. In order that each $f_n(W_o, W, t)$ should be composed of the correct amount of these partial correlation functions they must be weighted according to the probability of finding a molecule in that particular state. Thus the $f_n(W_o, W, t)$ become.

$$f_o(W_o, W, t) = p(t).g(W_o, W, t)$$

$$f(W_o, W, t) = -\int_o^t dt \int dW \ q(t-t)h(W_o, W, t-t,).p'(t)g(W_o, W, t)$$

$$f_2(W_o, W, t) =$$

$$\text{etc.} \qquad (vii)$$

$p(t)$, probability of finding a molecule in a librational state.

$q(t)$, probability of finding a molecule in a rotational state.

Larsson has limited his study to the isotropic case where, in the limit of long times, the scattering atom must describe the surface of a sphere. (The radius of the sphere is the magnitude of the position vector of the scattering atom, with respect to the molecular centre of mass. This is b, compare with equation 2.3(i)). This is the only case when $g(W_o, W, t)$ and $h(W_o, W, t)$ can be expanded in terms of

spherical harmonics since then they are dependent on W_o and W only through the difference $W-W_o$. (11)

$$g(W_o,W,t) = \sum_{l,m} g_l(t) \; Y_{l,m}(W) \; Y_{l,m}^*(W_o)$$

$$h(W_o,W,t) = \sum_{l,m} h_l(t) \; Y_{l,m}(W) \; Y_{l,m}^*(W_o) \qquad\qquad (viii)$$

$Y_{l,m}(x)$, are the spherical harmonics of argument x.

(see Section III appendix I)

By substitution from (viii), (vii) and (vi) into (v) it can be shewn that

$$S_R(Q,\omega) = \sum_{l=o}^{\infty} (2l+l) \; j_l^2(Q.b) \; S_l(\omega) \qquad\qquad (ix)$$

$j_l(x)$, spherical Bessel function of order. l, and argument x.

where

$$S_l(\omega) = \frac{l}{t_o+t_l} \cdot \frac{l}{\pi} \cdot Real\left\{ \frac{t_o a_l(\omega)+t\; b_l(\omega)+2a_l(\omega)b_l(\omega)}{l-a_l(\omega)b_l(\omega) \; / \; t_o t_l} \right\}$$

$$a_l(\omega) \equiv \int_{-\infty}^{\infty} \exp(-i\omega t).p(t).g_l(t).dt$$

$$b_l(\omega) \equiv \int_{-\infty}^{\infty} \exp(-i\omega t).q(t).h_l(t).dt$$

The chance that the molecule is found in a librational state is given by $t_o \; / \; (t_l + t_o)$. (For the rotational case this is $t_l \; /(t_l + t_o)$.). After time, t, the probability that the molecule is

still in this state is given by the functions $p(t)$ and $q(t)$.   Thus.

$$p(t) = \exp(-t/t_o)$$
$$q(t) = \exp(-t/t_1) \qquad (x)$$

The functions $p(t)$ and $q(t)$ describe the decrease in the population of librators, and rotators, with time.   The motions of the individual members of the population are damped out in time by the relaxation functions.   Given by

$$g_1(t) = F_1^{lib}(t)$$
$$h_1(t) = F_1^{rot}(t) \qquad (xi)$$

$F_1^{lib}(t)$,   the librational relaxation function.

$F_1^{rot}(t)$,   the rotational relaxation function.

These relaxation functions can be stated in terms of two parts, which reflect their short time and long time behaviour, thus (15)

$$F_1^{lib}(t) = F_{11}^{lib} + F_{21}^{lib}(t)$$

$$F_1^{lib}(t) = F_{11}^{lib}$$

for $t \to \infty$ $\qquad (xii)$

The relaxation functions are decomposed in this manner to facilitate computation later.

(and similarly for $F_1^{rot}(t)$) Thus (xi) becomes.

$$g_1(t) = F_{|1}^{lib} + F_{21}^{lib}(t)$$

$$h_1(t) = F_{|1}^{rot} + F_{21}^{rot}(t) \qquad\qquad (xiii)$$

Larsson has indicated four limiting cases about which some general comments can be made; these four cases occur upon the substitution of (xiii) back into the relevent equations.

Case (a)

$$t_o \gg t_{|} \; ; \quad t_o \rightarrow \infty$$

An elastic peak is generated which is caused by special inelastic scattering with $h_\omega = 0$. Its intensity is governed by a factor $j_1^2(Q.b)$, for values of $Q.b < |$ this is similar to a Debye-Waller factor. Under other circumstances the intensity of the elastic peak should show complicated variation (shown in Fig. Li).

Case (b)

$$t_o \gg t_{|} \; ; \quad t_o \text{ short}$$

A sharp elastic peak is obtained whose intensity varies as $j_o^2(Q.b)$. The quasi elastic peak width is controlled by the librational time, the full width at half height being $2/t_o$. (Shewn in Fig. Li).

41.

Case (c)

$$t_o \ll t_1 \quad ; \quad t_1 \quad \text{short}$$

Again an elastic peak whose intensity goes as $j_o^2(Qb)$. The quasielastic peak is now controlled by the rotational period, the full width at half height being $2/t_1$. (Shown in Fig. Ii)

Case (d)

$$t_o \ll t_1 \quad ; \quad t_1 \to \infty$$

The scattering law reduces to the well known form for free rotation (15,10). Thus for $S_1(\omega)$ in eq.(ix)

$$S_1^{rot}(\omega) = \frac{1}{2I+1} \left[\delta(\omega) + \frac{4}{\sqrt{\pi}} \sum_{m=1}^{1} \left(\frac{I}{2mKT} \right)^{3/2} \cdot \omega^2 \cdot \exp\left(\frac{-I\omega^2}{2m^2KT} \right) \right]$$

(Shown in Fig. Ii).

In order to proceed further with the model it is necessary to assume specific forms for the librational and rotational relaxation functions. The choice of functions used to represent these relaxations should depend on the system under consideration. Calculations have been conducted for the methane molecule (15). Whilst the results are not quantitatively applicable to the compounds studied here, they should be qualitatively useful. The rotational relaxation function for a spherical top molecule has been previously derived (22) and may be substituted immediately.

Fig. I.1   42.
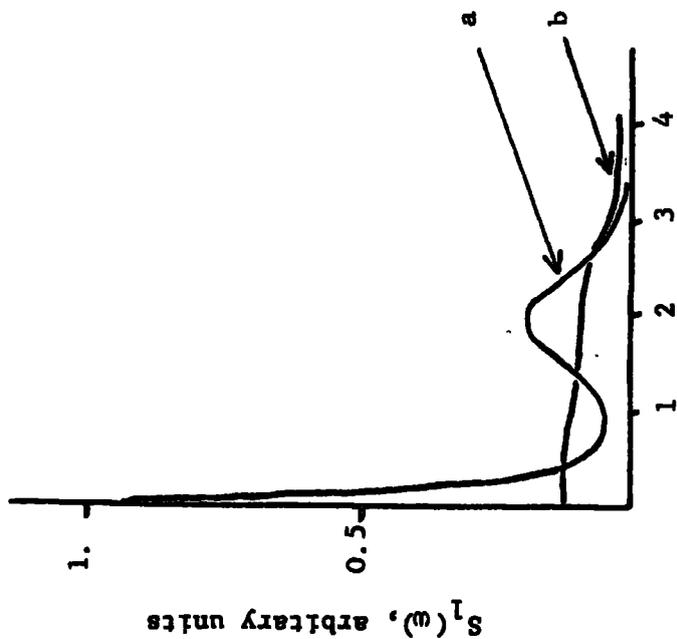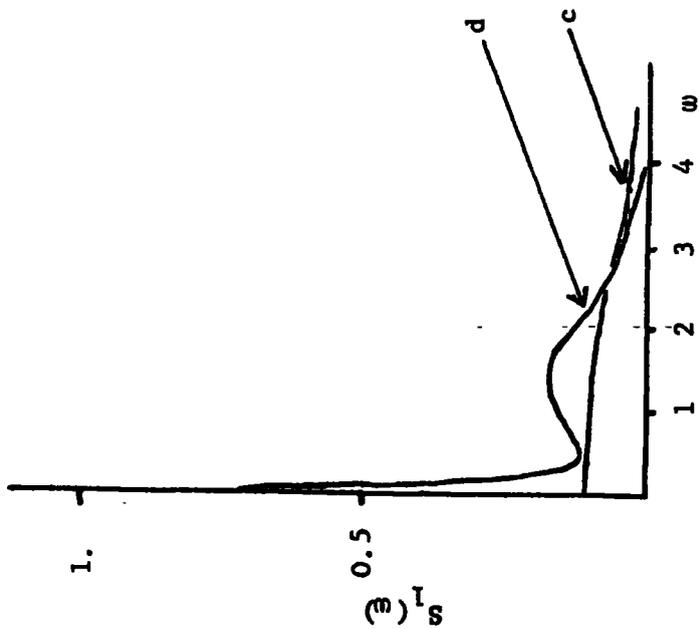
The scattering function $S_1(\omega)$

Illustrating Larrson's predictions for;

a,	$t_o \gg t_1$,	$t_o \to \infty$	(14)
b,	$t_o \gg t_1$,	t_o short	
c,	$t_o \ll t_1$,	t_1 short	
d,	$t_o \ll t_1$,	$t_1 \to \infty$	

$$F_1^{rot}(t) = \frac{1}{2I+1} \cdot \left(1 + 2 \sum_{u=1}^{1} \frac{(1-u^2 t^{*2})\exp(-u^2 t^{*2})}{2} \right) \qquad \text{(xiv)}$$

where

$$t^* = t \left(\frac{KT}{I} \right)^{1/2}$$

I, inertial value of spherical top.

The functions which might be used to represent the librational relaxation function have not been studied. However, a function which is consistent with expected properties, and gives the correct form to the final scattering law can be constructed. Allow

$$F_1^{lib}(t) = F_{11}^{lib} + (1 - F_{11}^{lib}) \exp\left(- \frac{s^2 t^2 1(1+1)}{2} \right) \cdot$$

$$\cdot \cos(W_o t(1(1+1))^{1/2}) \qquad \text{(xv)}$$

W_o, characteristic librational frequency.

s, relaxation constant controlling the decay of the libration amplitude

The scattering law $S_R(Q, \omega)$ obtained from these librational and rotational relaxation functions must show the correct form for its second moment in ω. This can be approached through the functions $f_1(t)$ defined by equations (vi), (vii) and (viii)

$$\left(\frac{df_1(t)}{dt}\right)_{t\,=\,0} = 0$$

and

$$\left(\frac{d^2f_1(t)}{dt^2}\right)_{t=0} = \frac{t_0}{t_0+t_1}\left(\frac{\partial^2 g_1}{\partial t^2}\right)_{t=0} + \frac{t_1}{t_1+t_0}\left(\frac{\partial^2 h_1}{\partial t^2}\right)_{t=0}$$

If the specific forms used for the relaxation functions are expanded for small times then (xiv) and (xv) become.

$$F_1^{lib}(t) = g_1(t) = 1 - 1(1+1)[s^2 + \omega_0^2)\cdot\tfrac{1}{2}] (1 - F_{11}^{lib})t^2$$

$$+ \quad \ldots\ldots\ldots \qquad \text{(xvi)}$$

for $t = 0$

$$F_1^{rot}(t) = h_1(t) = 1 - [\tfrac{1}{2}(1(1+1))] (\tfrac{KT}{I})t^2 + \ldots\ldots$$

for $t = 0$ (xvii)

The second time derivative is

$$\frac{d^2f_1(t)}{dt^2} = -\lfloor \frac{t_0}{t_0+t_1}\cdot 1(1+1)(s^2+\omega_0^2)(1 - F_{11}^{lib}) +$$

$$+ \frac{t_1}{t_0+t_1}\cdot (1(1+1)\cdot \tfrac{KT}{I})\rfloor \qquad \text{(xviii)}$$

The second frequency moment of the scattering law can be produced from eq.(ix) and is (for $F_{11} = F_{11}$ assumed).

$$\int_{-\infty}^{\infty} \omega^2 \, S_R(Q, \omega) d\omega = \frac{2}{3} Q^2 . b^2 . \frac{KT}{I} \qquad \text{(xix)}$$

therefore, $(1 = \mathbf{I})$

$$\frac{d^2 f_{\mathbf{I}}(t)}{dt^2} = \frac{2KT}{I} \qquad \text{(xx)}$$

If equations (xviii) and (xx) are to be consistant then

$$(s^2 + \omega_o^2)(\mathbf{I} - F_{\mathbf{II}}^{\text{lib}}) = \frac{KT}{I}$$

or

$$F_{\mathbf{II}}^{\text{lib}} = \mathbf{I} - \left(\frac{KT}{I(s^2 + \omega_o^2)} \right) \qquad \text{(xxi)}$$

The spectrum predicted from (ix) with the specific substitutions of (xiv) and (xv), and the conditions of (xxi) can be described. It is dominated by an elastic peak, and shows inelastic features. The features are gaussian, centred at neutron energy change of $\omega_o \sqrt{2}$, with a full width at half height of $s\sqrt{2}$. Equation (xxi) shows that ω_o will move into the elastic region as $F_{\mathbf{II}}^{\text{lib}}$ decreases. The limits of $F_{\mathbf{II}}^{\text{lib}}$ are o and $\mathbf{I}$, these extremes may be associated with the height of the barrier to rotation, V_o. Such that

$$F_{\mathbf{II}}^{\text{lib}} \sim o$$
$$\text{for } V_o < KT$$

$$F_{\mathbf{II}}^{\text{lib}} \sim \mathbf{I}$$
$$\text{for } V_o \gg KT \qquad \text{(xxii)}$$

There are other important aspects of this model, in particular its reference to the quasi elastic region.   It is predicted that there will be contributions to the quasi elastic width from both the rotational and the librational components of motion.   It is also obvious that the intensity of the elastic peak, which sits upon the quasi elastic peak, will not necessarily show a simple Q variation. It was suggested (14) that most of the experiments conducted on the quasi elastic region, to date, were probably of too poor a resolution.   Such that they were unable to study the detailed structure of the relaxation functions which might be used to predict $S_R(Q, \omega)$ through eq. (ix).

2.4 Comparison of optical and neutron scattering spectra

In order to make useful comparisons of the results from two different techniques it is essential to make the measurements under similar conditions.   Optical spectra represent the zero momentum transfer condition (this is because the wavelength, frequency relationship for photons is linear and is determined by a large constant, the speed of light).   Whereas neutron scattering spectra are collected at many different momentum transfers, but never zero. (This is because of the experimental difficulties with the transmitted neutrons which represent 90% of the incident flux).   However Egelstaff (1961) has shown that a function of the incoherent scattering law can be extrapolated back to provide a frequency distribution function at zero momentum transfer.   Thus.

$$\left[\frac{S(Q, \omega)}{Q^2} \right]_{\substack{limit \\ Q \to o}} . \ 2mh\omega \sinh\left(\frac{\hbar\omega}{2KT} \right) \ = \ Z(\omega) \qquad (1)$$

It was shown that $\left[\dfrac{S(Q, \omega)}{Q^2} \right]$ is linear in Q^2, analytically for small values of Q^2. In this case $Z(\omega)$ is the frequency distribution function of all the contributing parts, at zero momentum transfer.

In the case of neutron down scattering the ability to extrapolate back is lost. The neutrons are collected over a large region of momentum transfer. However this machine collects data over the molecular vibrational region (see Section II). Molecular vibrations produce equivalent energy transfer over large sections of momentum transfer (i.e. these modes are non dispersive). Down scattered neutron spectra are thus directly comparable with infrared absorption spectra.

References

1. Allen, G. Rep. Prog. Phys. $\underline{36}$, 1073, (1973).

2. Bloch, F. Z. Physik. $\underline{74}$, 294, (1932).

3. Boutin, H. "Molecular Spectroscopy with Neutrons". M.I.T.
    Press (1968).

4. Bracewell, R. "The Fourier Transform and its applications".
    McGraw-Hill (1965).

5. Chudley, C.T. Proc. Phys. Soc., $\underline{77}$, 353, (1961).

6. Donovan, B. "Lattice Vibrations" Chapman-Hall (1971).

7. Egelstaff, P.A. Proc. I.N.S. (Vienna), 25, (1961).

8. Fermi, E. Ricerca Scientifica, $\underline{1}$, 13, (1936).

9. de Graaf, L.A. Proc. I.N.S. (Grenoble), 247, (1972).

10. Griffin, G.W. Proc. I.N.S. (Chalk River), $\underline{1}$, 435, (1963).

11. Jackson, "Classical Electrodynamics" Wiley, N.Y. (1967).

12. Jones, D.S. "The Theory of Electromagnetism" Pergamon (1964).

13. Kim, H.J. Solid State Comm. $\underline{8}$, 889, (1970).

14. Larsson, K.E. Phys. Rev. $\underline{A3}$, 1006, (1971).

15. Larsson, K.E. J. Chem. Phys., $\underline{59}$, 4612, (1973).

16. Lassier, B. J. Phys. (Paris) $\underline{34}$, 473, (1973).

17. Lomer, W.M.; see ref. 7.

18. Palevsky, L. J. Phys. Chem. Solids. $\underline{24}$, 617, (1963).

19. Pauli, W. "Lectures on Physics" M.I.T. Press (1973).

20. Sears, V.F., Can. J. Physics. $\underline{44}$, 1279, (1966).

21. Sears, V.F. Can. J. Physics. $\underline{44}$, 1299, (1966).

22. Sears, V.F. Can. J. Physics. 45, 237, (1967).

23. Shannon, C.E. Proc. I.R.E. 37, 10, (1949).

24. Skold, K. J. Chem. Phys. 49, 2443, (1968).

25. Springer, T. "Springer tracts in Modern Physics". 64, (1972).

26. Stockmeyer, R. Phys. Stat. Solidi. 27, 269, (1968).

27. Strong, J. J. Opt. Soc. Amer. 49, 844, (1959).

28. Timmermans, J.J. Phys. Chem. Solids 18, 1, (1961).

29. Turchin, V.E. "Slow Neutrons" Jerusalem (1965).

30. Van Hove, L. Phys. Rev. 95, 249, (1954).

31. White, J.W.; as ref. 32.

32. Willis, B.T.M. "Chemical applications of Thermal Neutron
         Scattering" Oxford (1973).

33. Windsor, C.; as ref. 32.

34. Zemach, A.C. Phys. Rev. 101, 118, (1956).

CHAPTER II

THE SPECTROMETERS

The spectrometers used in this study are of two types. The spectrophotometer which covers the far infra-red region, and the neutron spectrometers. The neutron machines cover the same region, and a little above, as does the infrared machine but are entirely different in construction and operation.

The infrared spectrometer will be discussed first and then the neutron up scattering and down scattering spectrometers. The limitations of each machine will be indicated. The neutron machines will be compared and contrasted. Finally the factors which govern the resolution of the neutron spectrometers will also be discussed.

1. Spectrophotometer for the Far-Infrared region.

The instrument used for the far-infrared absorption studies was a Beckman-RIIC, FS720, spectrophotometer. This consists of a heavy, evacuable, metal shell containing the elements of a Michelson interferometer. These are a high pressure mercury source, a beam splitter, a fixed and a moving mirror, and a detector (see Fig. IIi).

The light source is a high pressure mercury arc lamp, which is water cooled. The infra-red radiation is obtained from the heating effect of the arc on the silica sleeve of the lamp. It is important that the arc remain stable in the centre of the lamp. The beam splitter, of which there are several types, is made of mylar. (Mylar is a transparent plastic with a high dielectric constant). The thinnest

beam splitter is 0.0006cm, and was the one used to obtain the
spectra presented in this thesis.   Other thicknesses of beam splitter
can be used to improve transmission in specific regions of the spectrum.

Although the spectrometer is an all reflectance instrument using
front silvered mirrors the two most important mirrors are those used
in the interferometry.   The mirrors are 8cm. in aperture, one is fixed
to the metal casing, and the other is translated along a path at right
angles to it.   The moving mirror is moved toward or away from the
beam splitter at a slow speed.   This is achieved by a gear reduction
train and a screw drive, from a synchronous motor.   The alignment
of the moving mirror is constant.   When the two mirrors are equidistant
from the beam splitter (this is the condition of 'zero path difference'),
the fixed mirror may be aligned to optimise transmission.   The moving
mirror traverses a maximum of 10cm; 5cm. each side of zero path difference.
At any one time the position of the moving mirror is determined by
a Moire fringe system, to within 8 microns.   After passing through the
sample the light is condensed, by a plastic lens, into a light guide
and falls upon a detector.   A Golay cell detector is used, it has a
3mm diamond window, and responds to changes in the total incident
energy.

The radiation is chopped, at the source, this results in a
rough alternating signal from the detector.   The electronics of the
spectrophotometer take the raw signal amplify and smoothe it into a
good sine wave.   This sine wave is converted into a D.C. level, which
is then digitised and punched out onto eight track paper tape.

Fig. II.i

52.

Far Infrared Spectrophotometer

Fig. II.ii

53.
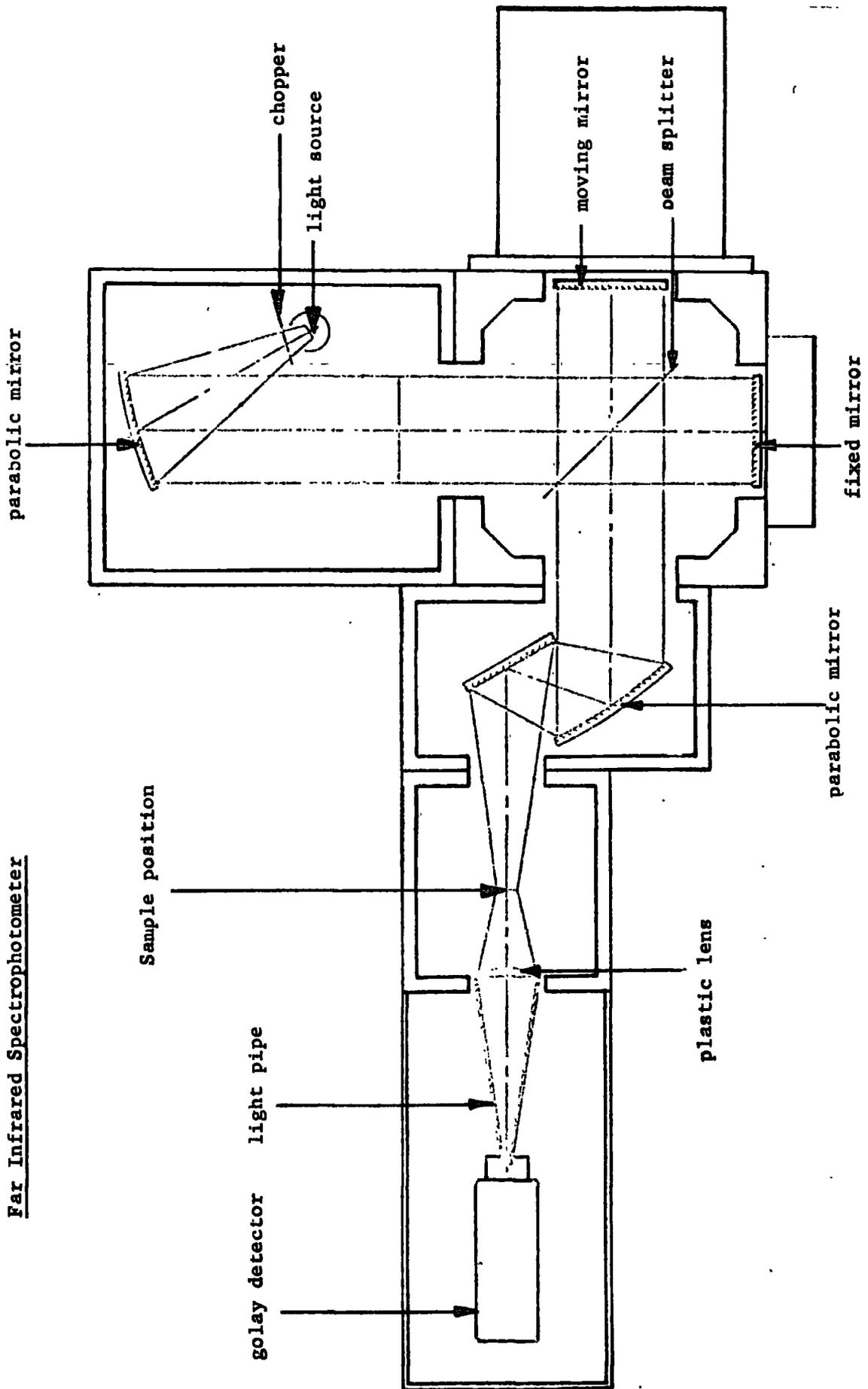
Sample Dewar for the Far Infrared Spectrophotometer

Vacuum jacket

coolant
reservoir

copper
bar
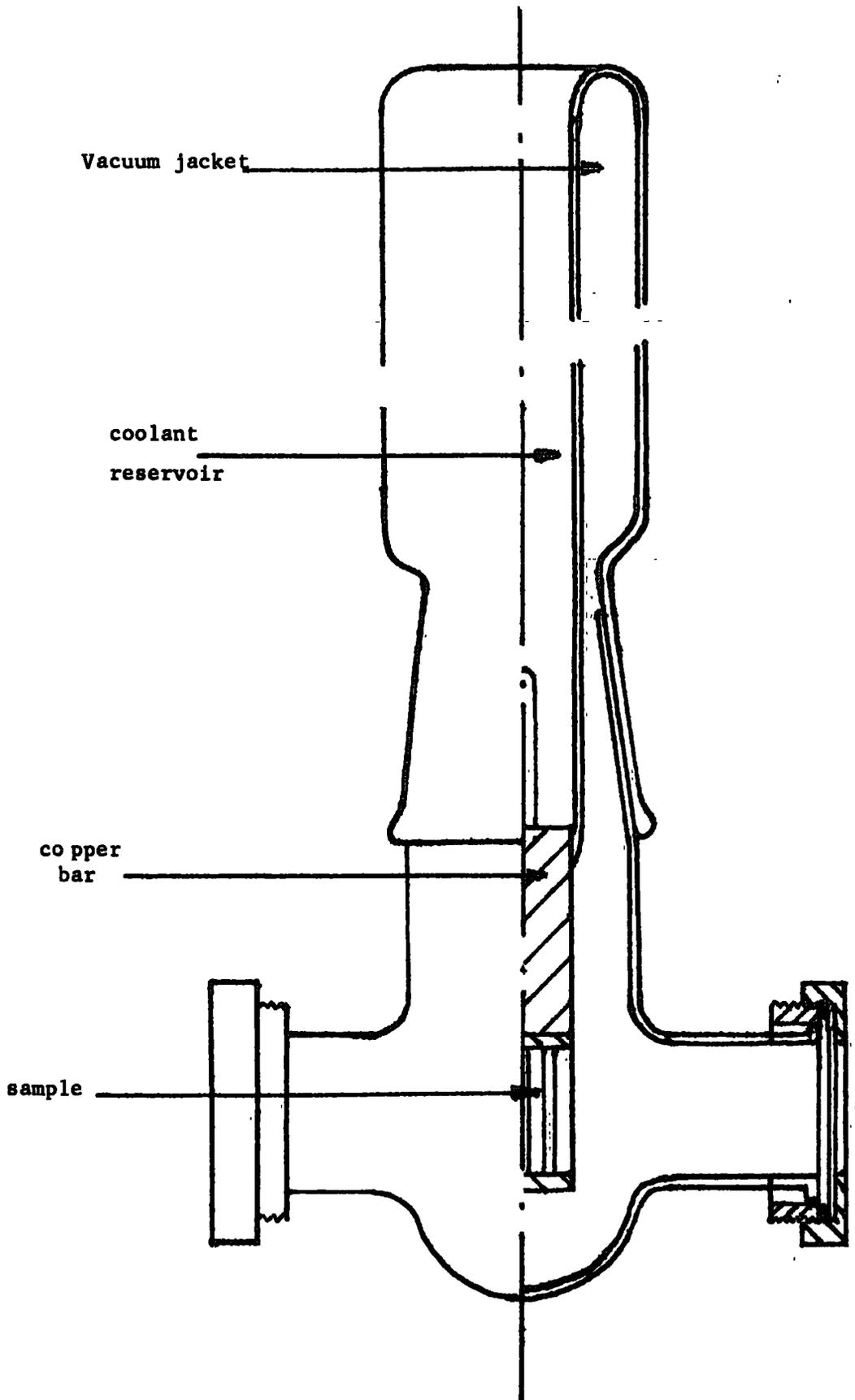
sample

During the period when a spectrum is being recorded the spectrometer

is under vacuum.   At a pressure of about 0.2torr. the absorptions

due to water in the atmosphere are removed.   The sample compartment

is not under vacuum but is flushed out continuously with dry nitrogen.

This arrangement enables spectra of samples at low temperatures to be

obtained easily.   The sample is maintained at the low temperature,

usually 77°K of liquid nitrogen, in a simple dewar (see Fig. IIii).

The sample is in good thermal contact with the coolant, through a

copper bar.   The dewar is fitted with polythene windows and is

continuously evacuated, by a mercury diffusion pump backed by a rotary

oil pump.   The whole of the base of the dewar fits into the sample

compartment and is surrounded by dry nitrogen gas.   Unfortunately this

type of cryostat is limited in the temperatures which it can reach.

All of the interferograms recorded for this thesis took about

40 minutes to run and contained over a thousand points.   Usually the

spectrum is obtained by transforming 1024 data sets, each one

representing an 8 micron advance of the moving mirror.   Using equations

given in   I,   estimates of the resolution and maximum frequency can

be obtained.   Since data are collected at 8×10^{-4}cm. intervals the

maximum frequency, about which information can be obtained, is 625cm^{-1}

(eq.(I.xvi)).   The resolution, given by eq.(I.xvii is about 0.61cm.$^{-1}$.

(This is a highly optimistic value.   The results are normally transformed

with a frequency increment of about 2cm.$^{-1}$).   The transformations are

accomplished on the N.U.M.A.C. computer, an I.B.M. 360-67.   The computer

program used is based on the Cooley (1965) algorithm, which is fully

described by Symon (1972).   Computations take about 130 secs (central

processing time) and require about 150K bytes of store.

2. Spectrometers for the neutron scattering spectra.

The spectrometers used to obtain the neutron inelastic scattering spectra will be preceeded by a description of the neutron source. The up scattering and the down scattering machines will then be described. The limitations of these spectrometers and the factors affecting resolution will also be discussed. Finally the resolutions of the machines, in the different spectral regions, will be compared.

2.1 Sources

There are the two thermal research reactors at Harwell, DIDO and PLUTO; and also the smaller reactor at Aldermaston, Herald. These reactors are fuelled by Uranium, enriched in the naturally fissile isotope $U_{,}^{235}$ and develop about 22m.watts each. (Herald is less powerful and only develops 5m.watts). In these reactors a stable fission chain reaction is established, and many products are generated (11). The product of greatest significance are the large numbers of neutrons (generation of large numbers of neutrons is a necessary condition for a chain reaction to occur). In thermal reactors these energetic neutrons are brought into thermal equilibrium with the reactor, by a moderator. The moderator is a large mass of non-absorbing material, deuterium oxide fulfils this role at Harwell. Any neutron excess is allowed to leak out of the reactor core along beam holes. The moderated neutron spectrum has a Boltzman distribution of energies, with a high energy tail (see Fig. IIiii).

Fig. II.iii

56.

Wavelength spectrum of neutrons

, for a typical moderator temperature (13)

peak flux

Neutron Flux, n(λ)

Neutron wavelength, λ

1 2 3 4 Å
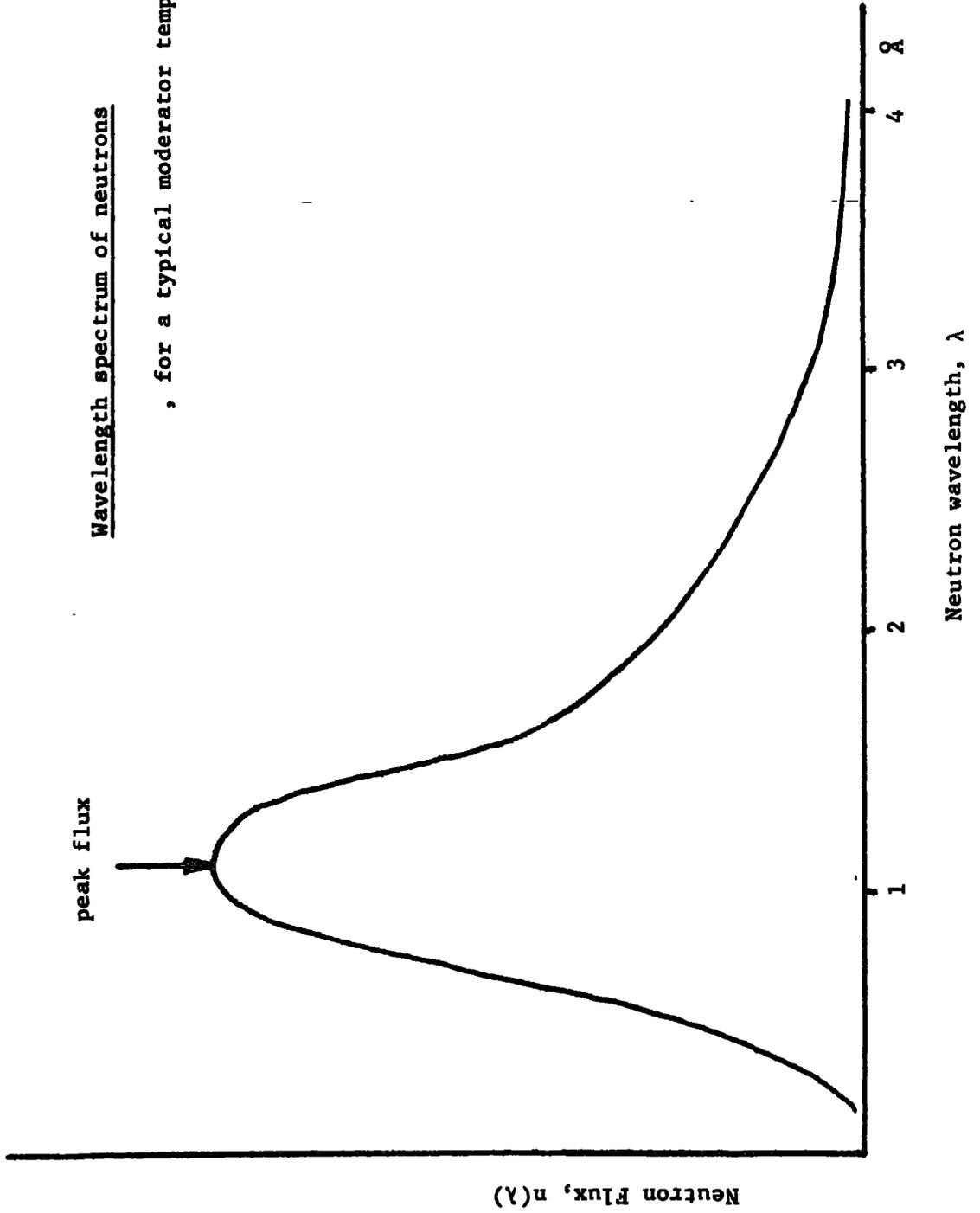
2.2 The up scattering spectrometer.

The machine used for the up scattering experiments is the time-of-flight (t.o.f.) spectrometer mounted on the 6" beam tube in DIDO. This is the 6H machine and is shown in Fig. IIiv. The background of fast, unmoderated, neutrons is reduced by a cooled polycrystalline Beryllium filter (see later) and gamma rays are reduced by a Bismuth filter. At the reactor face a spectrum of neutron energies is available, with wavelengths greater than 3.96Å. In the experiments conducted for this thesis the incident energy with maximum flux was chosen. This is selected by two phased rotors and is 4.2Å (37cm^{-1}, 1062 μs.m^{-1}, 4.6 meV).

The two rotors act as beam choppers, they are mounted on a vertical axis and have curved slots cut into their body. Only those neutrons travelling at the correct speed can pass along these slots. Neutrons which are faster or slower will be scattered or absorbed by the body of the rotor, which is a magnesium-cadmium alloy. The narrow group of velocities passed by the first rotor traverse the short distance to the second rotor, and the neutrons disperse in space according to their relative speeds. The second rotor passes a narrow band from within the group previously selected. For the majority of the time the rotors effectively close off the beam of neutrons, releasing them in short time bursts. This pulses the neutrons and allows the neutron energy to be analysed by determining its time of arrival at the detectors. The time of arrival is measured with respect to the start time of the pulse, and is later for slower neutrons. The neutrons are pulsed about 500 times a second. The essentially monochromatic neutrons are incident upon the sample, which is contained in the sample changer.

Fig. II.iv

A cross section through the 6H, upscattering, time of flight spectrometer (3)
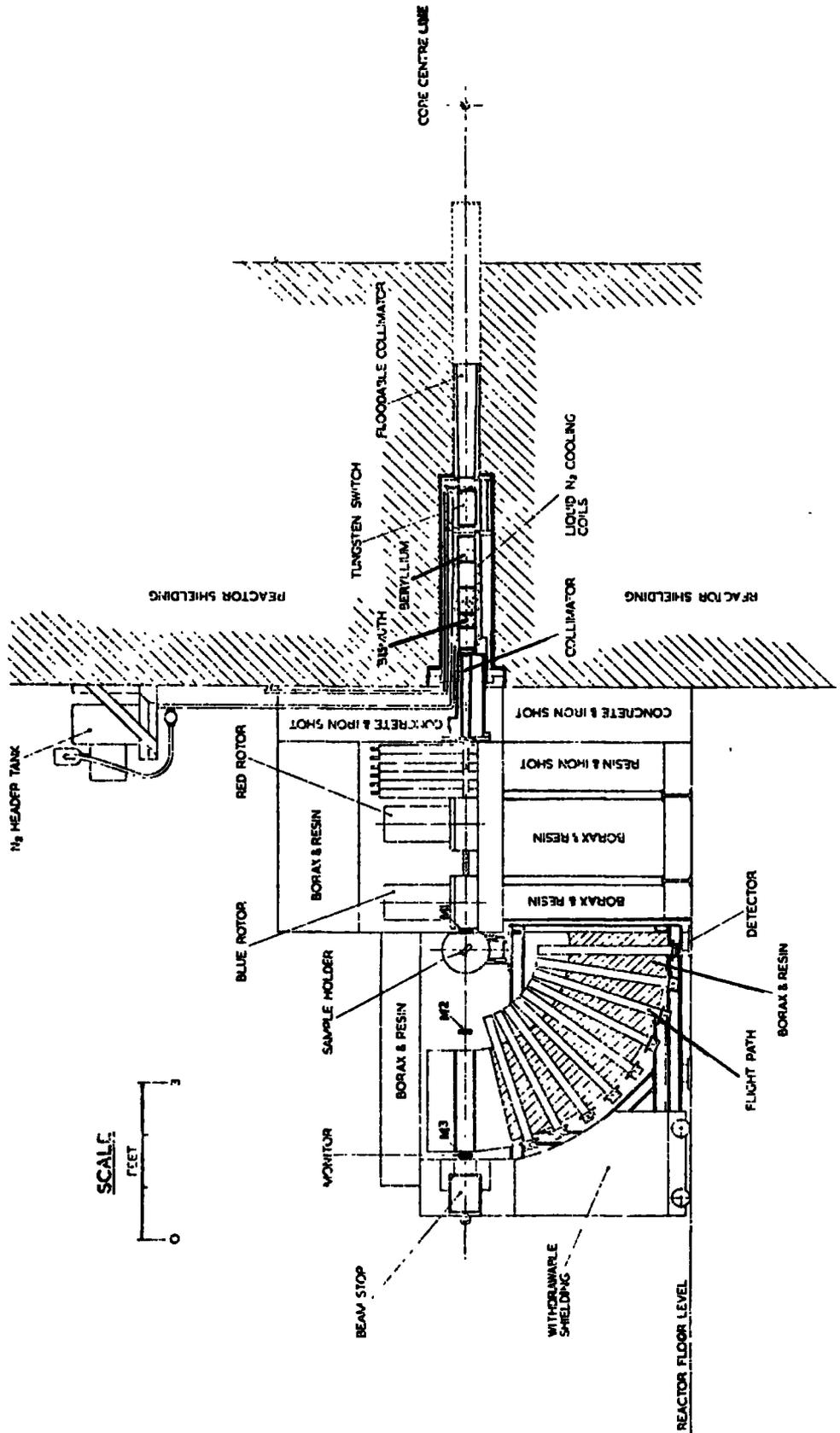
The sample changer places the sample at 45° to the incident beam
and maintains the required experimental environment. To prevent the
gross effects of atmospheric scattering the sample is surrounded by
either helium gas, or a vacuum. The sample may be heated, electrically,
or cooled. (Cooling is achieved by passing a regulated flow of liquid
nitrogen through a cooling loop within the sample changer). The
temperature of the sample is monitored and controlled by thermocouples.
The sample changer puts the sample, a background, and a sheet of
vanadium, into the beam consecutively; on a medium time period cycle.
In this manner a sample spectrum and background spectrum is obtained
concurrently, and a check on the counter efficiencies is maintained
throughout the run (3).

Upon interacting with the sample the neutrons may be scattered
toward any one of nine detector banks. These are arranged at 9°
intervals from 18° to 90° scattering angle. The detectors lie at
the end of cadmium lined flight tubes, which will tend to collimate
the scattered beam. All of the detectors are equidistant from the
sample, 1.35 m. Neutrons which are not scattered, about 90% of
those incident upon the sample, are monitored by three fission chambers.
These are placed, one 13cm. before, and two after the sample, at 55 and
118cm. away. The t.o.f. distribution of energies obtained from
these monitors is used to provide the value for the incident neutron
energy.

The scattered neutrons are detected in helium proportional counters,
these use the He^3 isotope. The neutrons interaction with the helium
atom may be written (4)

$$He^3 + n' \rightarrow H' + T^3$$

T, tritium.

The gas ionises, due to the large applied potential, and a discharge is recorded. The intensity of the discharge is proportional to the number of neutrons causing the discharge. The detected neutrons are sorted according to their time of arrival after the start of the neutron pulse. They are usually placed together in time groups about six micro seconds wide. It usually requires twenty-four hours to accumulate enough spectral data for analysis.

The data is held on a magnetic drum for display purposes during the experiment and is transferred to a magnetic tape for analysis. This analysis is conducted in two parts. The first stage analysis corrects for counter efficiencies, and analyses the monitor results and the vanadium scattering data. The second part obtains the scattering law from the measured double differential scattering cross-section. These computations are conducted on the I.B.M. 370-195 at the S.R.C. Rutherford Laboratory. The programs have been fully described previously (2), they require about 80 secs of the central processor time and about 300 Kbytes of store.

2.3 The Down scattering spectrometer.

The instrument used for the down scattering inelastic neutron spectra is mounted on the PLUTO research reactor at Harwell. It is a standard triple axis spectrometer modified to operate with a Beryllium filter detector system. This is shown in Fig. IIv. The PLUTO reactor provides a thermal neutron flux similar to that described earlier. The whole spectrum of neutron energies is used, none are filtered off before selecting the incident neutron energy. After leaving the reactor the neutrons are incident upon an aluminium crystal.

(Copper and germanium are also available but aluminium was used for
all the spectra presented in this thesis). Using the Bragg condition,

$$2d. \sin \theta = n\lambda \tag{i}$$

where n = 1, 2, ...

$\qquad$ n, $\quad$ order (usually unity)

$\qquad$ d, $\quad$ separation of the atomic planes.

$\qquad$ λ, $\quad$ chosen wavelength

$\qquad$ θ, $\quad$ Bragg angle.

an incident neutron energy is chosen. Specific planes in the
aluminium crystal are used to optimise the resolution and flux. These
planes are the 3.1.1. and the 5.1.1., to cover the region of the spectrum
from 200 to 700cm^{-1} and 600 to 1000cm^{-1} respectively (occasionally the
1.1.1. plane is used to go below 200cm^{-1}). Surrounding the
monochromator crystal is a rotating drum which carries heavy shielding.
Other neutron velocities which satisfy the Bragg condition, but at
different angles are thus absorbed. The beam of neutrons selected
is monitored by a fission chamber. In this manner a check is kept
on the number of neutrons incident on the sample for a given wavelength.
When spectra are taken with a constant number of monitor counts for each
incident energy then the spectra obtained are directly proportional to
the density of states (discussed in section I) (10). Above 1000cm^{-1}
the flux available from the monochromator falls away.

The monochromatic neutron beam is incident upon the sample. This
is held at 45° to the beam, to increase the number of neutrons scattered
towards the detectors. The sample is contained within a dewar which

Fig. II.v

62.

Beryllium Filter up scattering spectrometer: plan (7)

(detail of Beryllium Filter)

Paired $^{10}BF_3$ detectors

Liquid nitrogen filling port

Liquid nitrogen bin

Vacuum pumping port

Thermocouple connection

Beryllium blocks

Cooling coils

Collimator cone

Beam size selector

Shielding

Soller slits

Cadmium slits

Vacuum pump

Counter electronics

Sectors

Monochromator

Monitor

Sample table

Cryostat and Beryllium filter

Dance floor
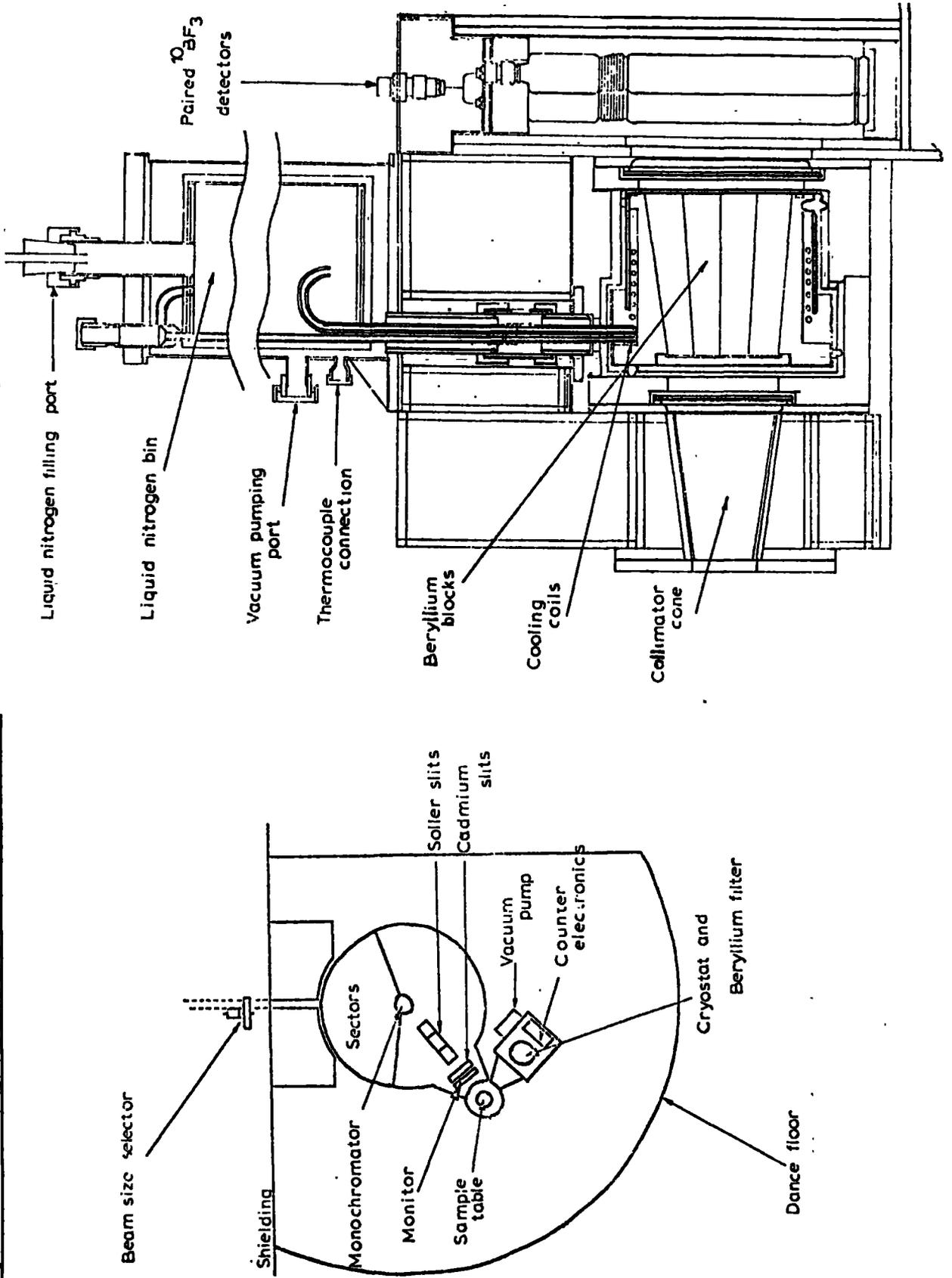
maintains it at a low temperature, usually liquid nitrogen is the coolant. (Helium is used as the exchange gas). It is not necessary to interchange the sample, a background, and vanadium; as is the case with the up scattering spectrometer. This is because the reproducibility of the incident neutron energy is better and the efficiency of the detectors is constant (see later). Neutrons scattered by the sample may pass on toward the detector system.

The detector assembly, which is nominally at 90° to the incident beam, has large acceptance angles, 17.5°, 17.5°. Before reaching the detectors the neutrons pass through a Beryllium filter, cooled to liquid nitrogen temperatures. Thus only neutrons with a wavelength greater than 3.96Å, i.e. those that have lost most of their energy to the sample, are transmitted. All other neutrons are scattered off toward cadmium shielding. Since only a narrow band of neutron energies is passed by the filter (0 to 5 meV) the efficiency of the detectors is, to a good approximation, the same for all of them. It is usual to cover specific regions of the spectrum with this instrument, and data collection for any one sample would be of the order of twelve hours.

The instrument is controlled by a small computer, a P.D.P.8. Input parameters which determine the region of the spectrum to be covered, the number of points to be taken, and the time spent collecting data are specified. These are written onto a magnetic tape, with other information regarding the monochromator. From this information the Bragg condition is used to obtain the correct angle which gives the required incident energy. The machine proceeds automatically, the results obtained for anyone incident energy are printed out and written

onto a magnetic tape. At appropriate points sections of the spectrum
are plotted out for easy reference. The result obtained is a list
of the incident neutron energies and the number of detected neutrons
at that energy.

These results are not analysed in the same way as those obtained
from the t.o.f. instrument. However there is an uncertainty in
the energy transfer which the neutrons have undergone. This is due
to the finite band pass width of the filter, the values are uncertain
by 42 cm^{-1} (5meV). Thus the energy transfer can be up to 42cm^{-1}
less than the incident energy recorded. To overcome this difficulty a
response curve for the instrument has been prepared (7). This is
based upon the fact that the filter is not equally transparent to all
neutron wavelengths. Provided that the wavelength is greater than the
cut-off wavelength (see later) the filter transmits those neutrons of
shorter wavelength better. Also the neutrons are detected with
greater efficiency as their energy increases. The detection function
of the system is thus more like a right angle triangle, than a simple
broad band response (10). If the incident energy of the neutrons is
known this curve provides the best estimate of the energy transfer,
this is shown in Fig. IIvi. The energy transfer finally recorded for a
transition will also depend upon the separation between consecutive
data points.

2.4 Polycrystalline Filters.

Polycrystalline filters are used on both up scattering and down
scattering machines to remove unwanted neutron components. They
consist of a polycrystalline mass of an element, usually Beryllium.

Fig. II.vi

Calculated correction curves for the Aluminium 3.1.1. plane (7)
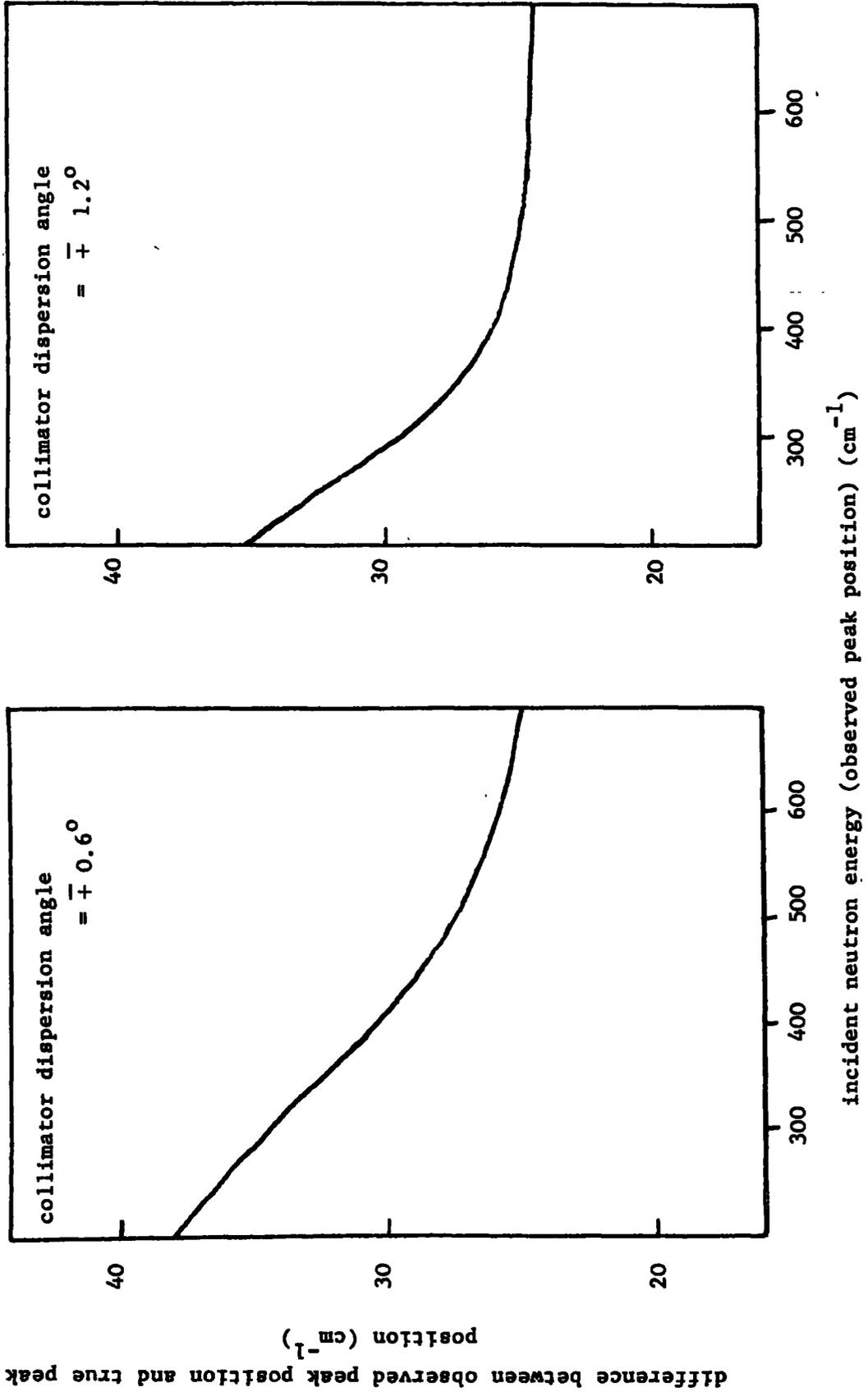
In a polycrystalline sample all possible crystal orientations are represented. Thus all neutron wavelengths from zero, up to some maximum wavelength must interact with some crystalites for which the Bragg condition holds, eq. (i). These neutrons are scattered. The maximum wavelength above which the Bragg condition cannot be satisfied is for a 90° Bragg angle, thus eq. (i) becomes;

$$2d = \lambda_{max.} \qquad (ii)$$

where $n = 1$

λ_{max}, that wavelength which is just scattered.

d, is the largest planar spacing.

Beryllium has a cut off at λ_{max} of 3.96Å (15). This element is used in preference to others because of the high λ_{max} and also because at liquid nitrogen temperatures the filter is very efficient. Wavelengths longer than λ_{max} are readily transmitted but the filter is almost opaque to shorter wavelengths (15). The cut-off is also a very sharply defined edge for beryllium (15).

2.5 A comparison of the up scattering and down scattering spectrometers

Although the two spectrometers are limited to different extents in many aspects, they suffer a common disadvantage compared to other spectroscopic techniques. This is the limitation imposed by the neutron source. The total flux available at the core of a reactor is of the order of 10^{14} neutrons per cm^2 per sec. However the flux

incident on the sample is only about 10^5 neutrons per cm^2 per sec. Compared to the flux available to Raman vibrational spectroscopists (about 10^{18} photons per cm^2 per sec) this flux is very poor.

The up scattering spectrometer has the advantage that it can collect data with good resolution at low energy transfer, and it has a good signal to noise ratio (17). On this machine it is possible to collect data at several scattering angles simultaneously. Unfortunately the resolution falls away rapidly as the neutron energy transfer increases. This results in an effective limit of $400cm^{-1}$ on the energy transfer, above this value little useful information is gained. Although resolution could be improved in this region, the population of these energy states is low. This population is given by the Boltzman distribution, and the sample must be maintained at a reasonable temperature to ensure the population of the excited states. It is usual to maintain the sample within 60° of the ambient temperature, (ca. 294^oK).

The Beryllium filter down scattering spectrometer is in many ways complimentary to the upscattering machine. It is most useful when energy transfers of $200cm^{-1}$ and above are to be studied. The down scattering spectrometer has better resolution in these regions, and no complex analysis is required, if constant monitor counts are taken. In order to reduce the background noise high scattering angles are used (about 90°), simultaneous data collection at several angles is not feasable in the present experimental conditions. Background noise is a serious limitation to this technique, the down scattering spectrometer has a higher ratio of background to signal counts than the up scattering machine. Above $1200cm^{-1}$ the signal to noise ratio

is so bad as to restrict the use of the machine. It is usual to

maintain the sample at about liquid nitrogen temperatures, $77^{o}K$.

This reduces the effect of the Debye-Waller factor and also multiphonon

scattering (see Section I). The high scattering angle leads

to a large Debye-Waller factor which tends to suppress the intensity

of observed bands. Multiphonon events, at high scattering angles,

lead to broad bands. Cooling the sample should lead to sharp bands

of larger intensity, and this is observed.

2.6 Effects governing the resolution of the neutron spectrometers.

One of the most significant differences between the up scattering

and down scattering spectrometers is in their resolution. Resolution

is a measure of the variance of the distribution of the population of

neutrons which are scattered by the same process. In practical

terms the best estimate of the resolution is probably that used by

Harryman (1972). The resolution is the full energy width at half

height of the spectrometers response to a delta function. It is

useful to note that for an analytical population distribution there is

a simple connection between the half height and the variance. (Neutrons

are normally regarded as being distributed in energy according to a

Gausian function). In the elastic region of the spectrum the

resolution can be determined experimentally, the incoherent scattering

from vanadium will provide this. However in the inelastic region this

direct measurement is not possible, since there are no suitable standards.

The resolution of the down scattering spectrometer will be governed

by three factors. Firstly the resolution uncertainty in the

monochromated neutron beam. This is introduced by the mosaic spread

of the monochromator. Secondly there is the uncertainty in the

scattering angles, introduced by the dispersion of the collimator.

This angular spread of neutrons allowed by the collimator is usually

quite large and it is usual to make the mosaic spread of the crystal

of a similar order. This has the advantage of increasing scattered

flux whilst retaining the best resolution given by the collimator,(1).

Finally there is the variance of the transmission function of the

beryllium filter window. This is dependent upon the incident neutron

energy (17). The resolution becomes better as higher order planes

in the monochromater are used. Higher order planes, e.g. 3.1.1., have

a larger plane spacing than the lower orders, e.g. 0.0.1. It can be

seen from the Bragg condition, eq. (i), that to coherently scatter a

given wavelength neutron from a set of widely spaced planes requires

a larger Bragg angle than from a set of narrowly spaced planes.

That this is advantageous can be appreciated by differentiating

eq. (i) thus.

$$\frac{d\lambda}{d\theta} = 2d. \cos\theta \qquad\qquad (iii)$$

thus $\qquad d\lambda = 2d.\cos\theta. \, d\theta$ $\qquad\qquad\qquad$ (iv)

$d\lambda$, is associated with the uncertainty in the wavelength.

$d\theta$, is associated with the dispersion angle of the collimator.

The effects of a large value of dθ can be reduced by having a small value of Cosθ, i.e. θ is large. As indicated above this requires the use of high order planes. Unfortunately the scattered intensity falls off as Sinθ, such that considerations of flux may become more urgent than resolution.

The factors affecting the resolution of the up scattering spectrometer have been fully discussed by Harryman (1972). As with the down scattering spectrometer there are three main effects. Firstly the resolution uncertainty due to the rotor selection of neutrons. This has been studied by Royston (1964). There are contributions from several sources, including the intrinsic spread of neutrons which can pass through the rotor slots, the divergence of the collimated beam, and the effects of wobble in the rotors. The next major factor in determining resolution is the angle of the sample to the incident beam. The sample is normally at 45° to the beam. Scattering from its leading edge will take place about 26×10^{-6}sec. prior to that from the trailing edge of the sample (this calculation assumes an incident t.o.f. of 1062 μs.m^{-1}). Finally there is an uncertainty due to the finite thickness of the detectors. The probability of detection is proportional to the counter thickness, the detectors are cylindrical. These effects must be convolved to produce the final resolution. Extensive tables covering the possible experimental configurations have been prepared (8). Typical values for the experiments conducted in this thesis are reproduced in Fig. IIvii.

It is obvious from Fig. IIvii that the upscattering spectrometer has the best resolution at lower energy transfer. This resolution,

Fig. II.vii

71.
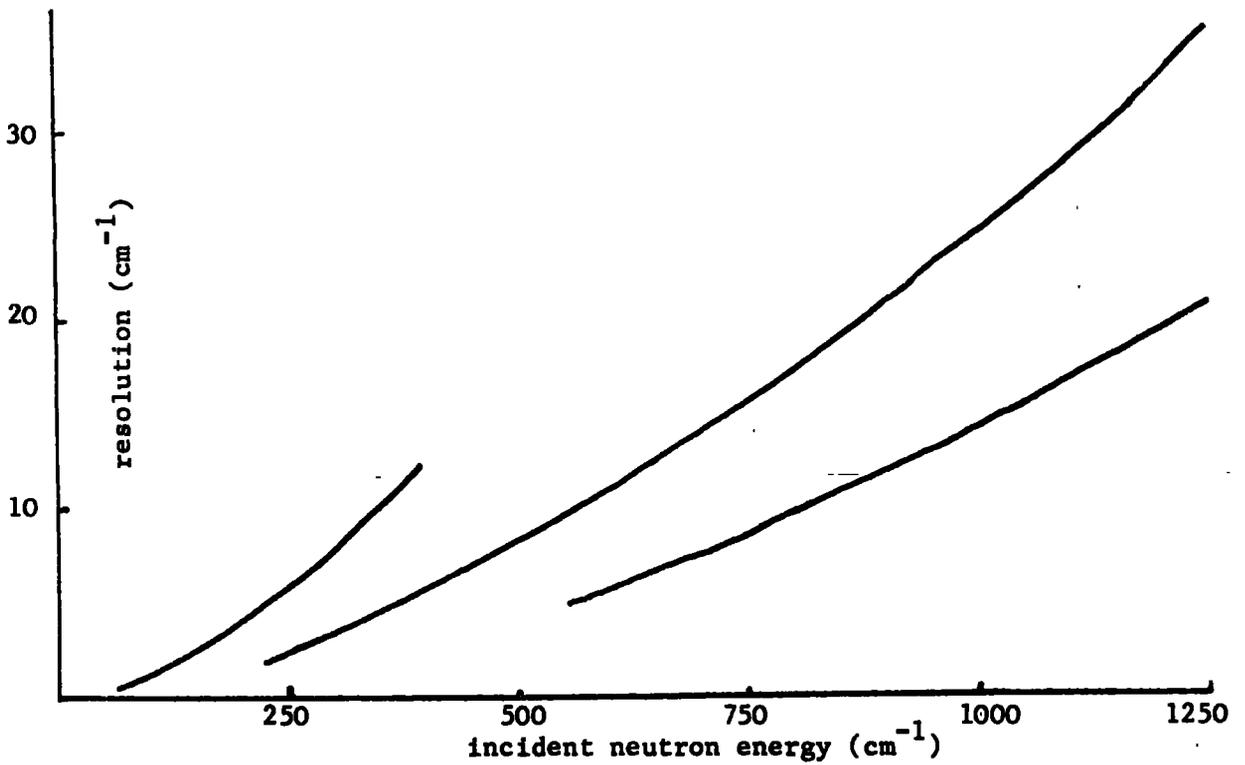
Resolution of the down scattering spectrometer at various incident
energies. (Aluminium monochromator, and a collimator dispersion angle
of 0.6⁰).
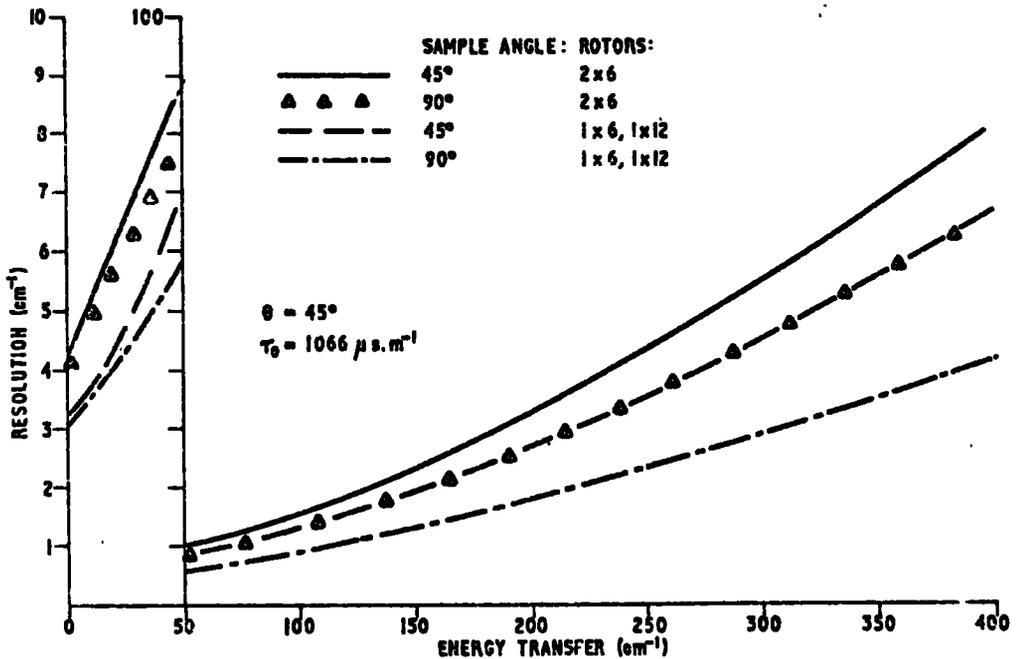
Resolution of the up scattering spectrometer at various energy
transfers. (comparing 6 slot and 12 slot rotors). (8)

however, falls off rapidly with increasing energy transfer. In the region of $200cm^{-1}$ the resolution of the upscattering spectrometer is about the same as that of the down scattering machine. Above $250cm^{-1}$ the down scattering spectrometer has the better resolution. When obtaining a spectrum in the region of $200cm^{-1}$ the higher counting rate of the down scattering machine is important. Such that as much useful data would be obtained from an 8 hour run on the down scattering machine as from a 24 hour run on the up scattering spectrometer (except that data over a range of momentum transfer is lost).

3. The Graphite Monochromator Chopper spectrometer.

The high resolution graphite monochromator chopper (G.M.C.) up scattering spectrometer, at Aldermaston, was also used for some studies in the quasielastic region (see Section IV.). In this spectrometer the incident neutron wavelength is defined by Bragg scattering from pyrolytic graphite crystals. Two crystals of graphite are aligned, such that neutrons, Bragg scattered off the first crystal, travel back toward the second crystal. These neutrons are scattered by the second crystal onto the sample (see Fig. IIviii). In this manner the incident neutron energy is well defined and the beam should carry no other radiation, except for the normal background. The incident beam is pulsed, by interrupting it with a single rotor. The sample conditions, neutron detection, and spectral analysis are essentially the same as those on 6H at Harwell. In this machine however the detector to sample distance is longer, 1.6m; and the scattering angles are from $20°$ to $90°$ in $10°$ increments.

This machine suffers from the disadvantage of being attached to a relatively low flux reactor (Herald). Samples which take about 24 hours to obtain sufficient data on 6H require several days of running time on G.M.C.

Fig. II.viii

74.

Plan of the G.M.C. neutron spectrometer (9)
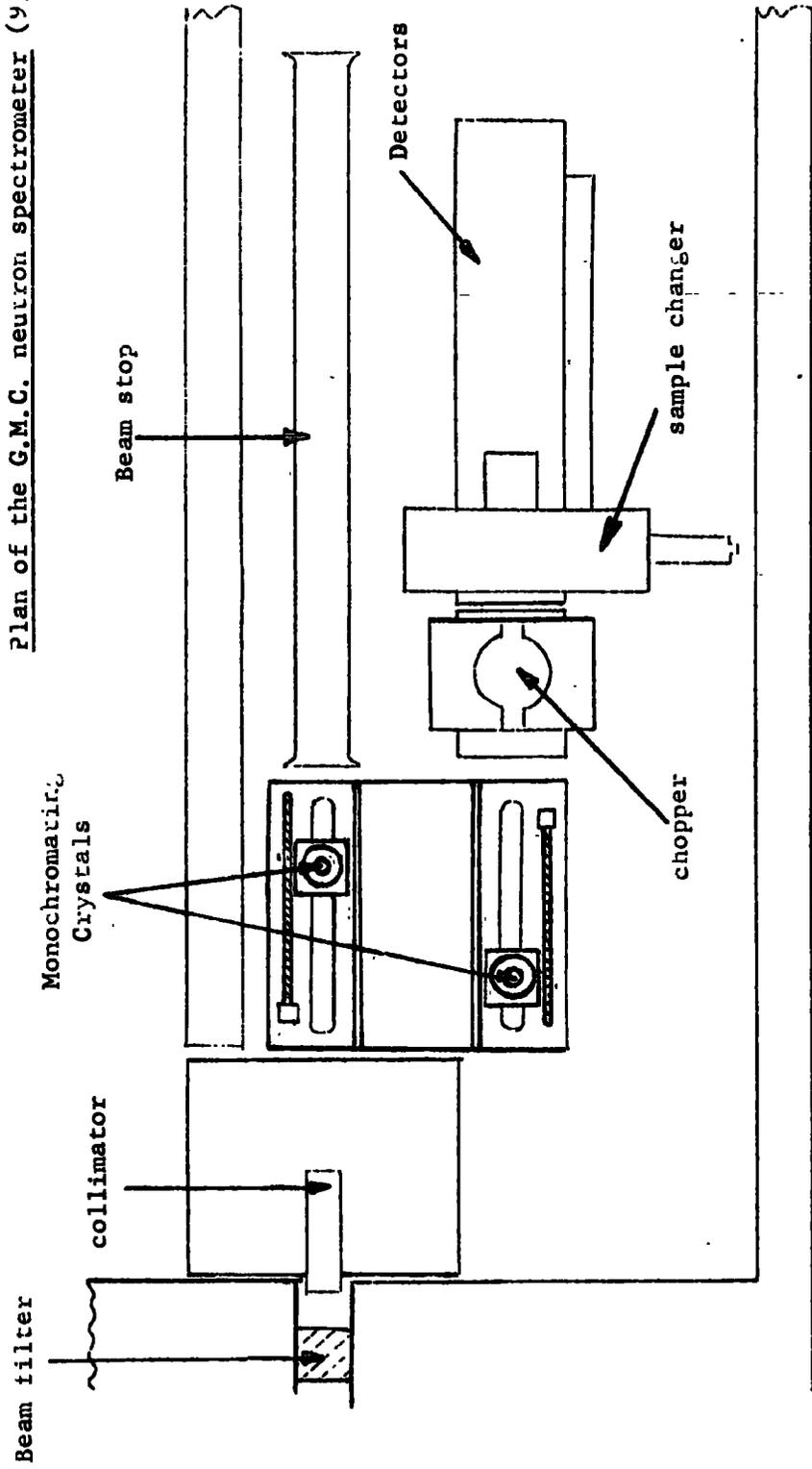
References

1. Arndt, U.W. "Single Crystal Diffractometry" Cambridge (1966).

2. Baston, A.H. "The Collection and Processing of data from three

    t.o.f. Neutron Spectrometers", H.M.S.O. (1972) Harwell

    report M. 2570.

3. Bunce, L.J. "The DIDO(6H) long wavelength Inelastic Neutron

    Spectrometer" H.M.S.O. (1970) Harwell report R.6246.

4. Cocking, S.J. see ref. 6.

5. Cooley, J.W. Math. of Computation $\underline{19}$, 195, (1965).

6. Egelstaff, P.A. "Thermal Neutron Scattering" Academic Press (1965).

7. Gamlen, P.H. Harwell A.E.R.E. report - unpublished (1974).

8. Harryman, M.B.M.   "   "   (1972).

9. Heffer, P.H.J. "A neutron scattering study of hydrogen in

    certain metals, and improved instrumentation for such work".

    Thesis (1974), Birmingham University.

10. Iyengar, P.K. see ref. 6.

11. Jakeman, D. "Physics of Nuclear reactors" English Univ. Press

    (1966).

12. Royston, R.J. Nuc. Inst. and Methods $\underline{30}$, 184, (1964).

13. Stirling, G.C. see ref. 16.

14. Symon, D.A. "A Study of Transition Metal Compounds in liquid

    HCl". Thesis (1972), Durham University.

15. Turchin, V.F. "Slow Neutrons". Jerusalem (1965).

16. Willis, B.T.M. "Chemical Applications of Thermal Neutron

    Scattering". Oxford (1973).

17. Wright, C.J. "Applications of Inelastic Neutron Scattering to

    Transition Metal Chemistry". Thesis (1971) Oxford University.

CHAPTER III

LIBRATIONAL POTENTIAL ENERGY FUNCTIONS

The description of dynamical systems is dependent upon the availability of mathematical models to represent them adequately. The differential equations which represent the system contain both kinetic and potential energy terms, and have solutions which are related to the experimental observables. In the case of molecular librations the kinetic energy term is well known and the object is to obtain an adequate parametric description of the potential term. There are two ways of obtaining this potential energy function. Either, the dynamics are observed through the transitions of the system between its static states. Then, assuming a dynamical model, a description of the potential is obtained. Alternatively, the potential field is modelled itself directly, to obtain the same quantitative data. In the first section of this chapter the dynamical models of the system are described. Approximations made in this treatment are discussed and solutions, in terms of the relevant observables are obtained. In the next section the alternative is presented. Approximations involved in this model are discussed, and solutions obtained.

Both of these methods of obtaining parameters of the potential field will be based upon a common assumption. This is that the potential is not a function of time. It is known, for the case of intramolecular dynamics, that the variation of the potential with time is unimportant (17). This is a consequence of the fact that

deformations of the molecular frame are very much more rapid than librations. This results in a time average value of the potential field being experienced by the librator. However, where the potential is determined by a crystal lattice, time averaging cannot occur. This is because the lattice is also a dynamical system, the vibrational frequencies of which range from zero to values close to that of libration. Larrson (1973) has used this fact to explain the gross features of the inelastic scattering spectra from some solids (see Section I). Thus whilst the results may represent the best values obtained in the static field approximation, they are not complete descriptions of potential fields in crystal lattices. The assumption is necessary to both simplify the equations describing the dynamics and also to enable the potential model in the second section to provide reasonable results for a short computational time.

1. <u>Solutions to the Equations of motion for a hindered rotor.</u>

1.1 <u>The rotor problem in one dimension.</u>

The equation used is a three dimensional Schrodinger equation, see Section I. Its solutions are the eigen states of the system. A cartesian coordinate system would be inappropriate to rotational problems and Euler angles are used (see Appendix II). In highly symmetric systems it is usually possible to choose a set of coordinates which are independent. The three dimensional problem is thus separable into three one dimensional problems. Only the solutions to these equations will be discussed. The one dimensional Schrodinger equation for the hindered rotor may be written (8)

$$\frac{d^2 m(\theta)}{d\theta^2} = \frac{2I}{\hbar^2} \{E - V(\theta)\} m(\theta) = 0 \qquad \text{(i)}$$

m(θ), eigen functions of equation (i)

θ, dimension

E, eigenstates of the equation

I, rotator's inertia

$\hbar$, Planck's constant divided by 2π

V(θ), potential energy function.

The potential energy function V(θ) should be expressed as a Fourier series in θ (28).

$$V(\theta) = \sum_r a_r \, Cos \, (nr\theta) + b_r \, Sin \, (nr\theta) \qquad \text{(ii)}$$

r = 0, 1, 2 ....

a_r, b_r, the Fourier coefficients

n, the number of equivalent minima experienced by the rotor as θ goes from 0 to 2π radians.

It has been found that the general formulation for V(θ) given in eq. (ii) may be simplified. It is usually replaced by (9)

$$V(\theta) = \frac{Vo}{2} \{1 - Cos \, n\theta\} \qquad \text{(iii)}$$

Vo, height of the barrier to reorientation between minima, for the coordinate θ.

The removal of the sine expansion is a reflection of the symmetry of the potential well; and contributions involving the higher orders of the cosine expansion are usually found to be insignificant (9). The next cosine term contributes about 4% to the determination of the eigen value. However under the appropriate conditions these higher orders become significant (discussed later). Substitution of eq. (ii) into eq. (ii) obtains, for eq. (i)

$$\frac{d^2 M(x)}{dx^2} + (a + 16.b.\cos 2x).M(x) = 0 \qquad (iv)$$

where

$$x = \frac{n\theta}{2}$$

$$b = \frac{1}{4} \left(\frac{IV_0}{n^2 \hbar^2} \right)$$

$$a = \frac{8I}{n^2 \hbar^2} \left(E - \frac{V_0}{2} \right)$$

This is the usual form of the Mathieu differential equation (20). The solutions to eq. (iv) must be periodic in x to give physically meaningful results. In general this is not the case, and restrictions are placed on a to give this periodicity.(a becomes a complicated function of b (20)). The solutions to the Mathieu equation have been extensively tabulated only for the cases of two and three-fold wells (4,13). These solutions are not easily obtained and it is usual to make approximations to solve eq. (iv) for the many-fold potential.

1.2 Approximations to the Mathieu equation.

1.2.1. a weakly hindered rotor.

In a weakly hindered rotor the value of Vo must be low, and consequently b is approximately zero. Eq. (iv) becomes

$$\frac{d^2 M(x)}{dx^2} + aM(x) = 0 \qquad\qquad (v)$$

which has the simple solutions

$$M(x) = \exp(irx) \qquad\qquad (vi)$$

$$r = 0, \mp 1, \mp 2 \ldots ..$$

However, $M(\theta) \equiv M(\theta + \frac{2\pi}{n})$

which follows from symmetry, thus from eq. (vi) and (iv)

$$\exp(\mp ir\theta \cdot \frac{n}{2}) = \exp(\mp ir\theta \cdot \frac{n}{2}) \cdot \exp(\mp ir \frac{n}{2} \cdot \frac{2\pi}{n})$$

and

$$\exp(\mp ir\pi) = 1 \qquad\qquad (vii)$$

which is only true for r = 0, 2, 4, ...

Substitution of eq. (vi) into (v) yields

$$r^2 = a = \frac{8I}{n^2 \hbar^2} \ (E - \frac{Vo}{2})$$

or

$$E - \frac{Vo}{2} = \frac{n^2 \hbar^2}{2I} \cdot (\frac{r}{2})^2 \qquad\qquad (viii)$$

$$r = 0, 2, 4, \ldots ..$$

(For n = 1 and the value of Vo = 0; eq. (viii) reduces to the solutions of a rigid rotor confined to a plane (8), as would be expected). This case is inappropriate to the interpretation of solid state studies. Molecules in solids may reorientate but they are not free rotors in the sense of a gaseous molecule.

1.2.2 Strongly hindered rotor.

1.2.2.1 The deep well approximation.

For a strongly hindered rotor the value of Vo in eq. (iv) is large, i.e. the potential well is deep. In these circumstances the molecule will only be slightly displaced from its mean position in the well. The cosine term of eq. (iii) is expanded as a series.

$$\text{Cos } (y) = 1 - \frac{y^2}{2!} + \frac{y^4}{4!} \qquad \text{(ix)}$$

All terms higher than the quadratic are dropped (this is the harmonic approximation). Thus in eq. (iv)

$$\text{Cos } 2x = (1 - 2x^2) \qquad \text{(x)}$$

and

$$\frac{d^2 M(x)}{dx^2} + (a + 16b.(1-2x^2)).M(x) = 0$$

which gives

$$\frac{d^2 M(x)}{dx^2} + (a + 16b - 32b \, x^2)M(x) = 0 \qquad \text{(xi)}$$

Comparing eq. (xi) with the harmonic oscillator equation

$$\frac{d^2 \Psi(x)}{dx^2} + (\alpha - \beta^2 x^2)\Psi(x) = 0$$

yields

$$\alpha = a + 16b$$

$$\beta^2 = 32b$$

The solutions to the harmonic oscillator problem are well known (8).

$$\alpha = \beta.(2r + 1)$$

$$r = 0, 1, 2 \ldots$$

thus

$$a = 2(2r + 1)\sqrt{8b} - 16b$$

which gives

$$E = (r + \tfrac{1}{2})n\hbar \quad \frac{Vo}{2I} \tag{xii}$$

$$r = 0, 1, 2 \ldots$$

This set of solutions is suitable for librators with deep potential wells. A deep well, it has been suggested (4), is applicable when

$$\sqrt{\frac{\dfrac{nr}{8I \ Vo}}{n^2}} < 0.4 \tag{xiii}$$

From eq. (xii) it can be seen that the fundamental librational frequency is given by

$$E_1 - E_0 = \Delta E = n\hbar \; \frac{Vo}{2I}$$

$$Vo = \frac{8\pi^2 I}{n^2} \; v^2 \qquad\qquad\qquad\qquad (xiv)$$

v, fundamental transition frequency (Hz).

and

$$v_r = \frac{r.n}{2\pi} \; \sqrt{\frac{Vo}{2I}}$$

$r = 1, 2, 3 \ldots..$

v_1, fundamental transition

v_2, first overtone

v_3, etc.

The same final equation is obtained from a classical description of the dynamics of the oscillator. In this case Schrodinger's equation is replaced by Lagrange's equation and the same approximations are made.

1.2.2.2 The formulation of Das.

Das (1956) has given a method of obtaining approximate solutions to the Mathieu equation (eq. (iv)). These involve the expression of the solutions as series, and further empirical correction terms. This can be used to treat the case of an intermediate barrier.

The Mathieu equation is assumed to have a periodic solution which can be expressed as a power series. Correspondingly the characteristic roots of the equation can be expanded by an analogous series (16) from eq. (iv)

$$a \sim \{-\frac{k^2}{2} + (2r + 1)k - \frac{1}{4}(r^2 + (r + 1)^2) - \frac{1}{16}(r^3 + (r+1)^3)\frac{1}{k}\ldots\}$$

(xv)

where

$$k = \left(\frac{8IVo}{n^2\hbar^2}\right)^{\frac{1}{2}}$$

$r = 0, 1, 2 \ldots$

(If the series is terminated after the second term then

$a = ((2r + 1)k - k^2/2)$; which corresponds with the deep well,

harmonic, approximation). In a deep well eq. (xv) can be expanded

to give arbitrary accuracy. In a shallow well the possibility of quantum

mechanical tunnelling occurs. This produces t sublevels for every

librational level which occurred in the deep well case. These

sub levels are separated by small amounts, A_r^t. The series now

becomes

$$a_r^t \sim \{-\frac{k^2}{2} + (2r + 1)k - \frac{1}{4}(r^2 + (r + 1)^2)\ldots\} + A_r^t$$

(xvi)

subscript r, the rth librational state

superscript t, the tth tunnelling sublevel

where the number of sublevels is
$$\begin{cases} (n + 1)/2 \; ; \; n = odd \\ (n + 2)/2 \; ; \; n = even \end{cases}$$

and t = 0 always occurs.

The form which A_r^t takes was determined by Das from a method after

Goldstein (1929); it is:

$$A_r^t = \cos(\frac{2\pi t}{n}) \cdot \frac{2^{3r} \cdot n^2 \cdot k^{r+3/2}}{\pi^{\frac{1}{2}} r!} \cdot \exp(-2k)$$

(xvii)

By substitution from (iv) for a_r^t a value of the relevent energy, E_r^t, is obtained.

$$E_r^t = V_o\{(2r + 1)k^{-1} - \frac{1}{4}(r^2 + (r+1)^2)k^{-2} - \frac{1}{16}(r^3 + (r+1)^3)k^{-3} + 2A_r^t\}$$

(xviii)

(For very low barriers it is necessary to correct the form which A_r^t takes, a suitable method is given by Das (1956)). Assuming that no tunnelling occurs, i.e. ignoring A_r^t, eq. (xv) can be developed in terms of the fundamental librational transition frequency; for different values of n (25). (The series in eq. (xv) is terminated after the third term). Then

$$\underline{n = 2} \quad V_o = \frac{1}{4}\left(\frac{\hbar^2}{2I}\right)\left(\frac{4\pi I \nu}{\hbar} + 1\right)^2$$

(xix)

$$\underline{n = 3} \quad V_o = \frac{9}{16}\left(\frac{\hbar^2}{2I}\right)\left(\frac{4}{9}\cdot\frac{4\pi I \nu}{\hbar} + 1\right)^2$$

(xx)

$$\underline{n = 4} \quad V_o = \left(\frac{\hbar^2}{2I}\right)\left(\frac{1}{4}\cdot\frac{4\pi I \nu}{\hbar} + 1\right)^2$$

(xxi)

1.3 Coupled rotors in the deep well approximation.

The previous sections have dealt with single, or independent, one dimensional rotors; the total potential being the sum of the individual barriers. If a compound contains several rotors in a molecular framework then there are two possibilities. Either the rotors are well separated by distance and rotate in a potential

determined by the fixed frame of the molecule (this is the

internal-top case ,the rotors are essentially independent); or

alternatively the rotors are closely associated with each other and

the potential of any one of them is related to the relative

orientations of the others.   This is a coupled oscillator problem,

and the rotors are not independent.   The internal-top problem is

essentially similar to the single rotor problem previously covered.

Studies have been mainly confined to threefold wells (tops with C_3

symmetry) because of the tabulated Mathieu functions (13).   Although

for the coupled oscillators problem it is possible to solve the

Mathieu equation numerically (11) it can be treated more simply.

In these systems it is useful to make the classical approximation,

and to describe the dynamics of the system by Lagrange's equation.

$$\frac{d}{dt} \cdot \frac{\partial L}{\partial \dot{\theta}_r} - \frac{\partial L}{\partial \theta_r} = 0 \qquad\qquad (i)$$

where

$\dot{\theta}_r = \frac{d}{dt} \theta_r$

$L = V - T$

$r = 0, 1, 2 \ldots. N$

subscript r, the rth rotor

L, the Lagrangian

V, potential energy of the
        system, a function of θ

θ, angular coordinate

T, kinetic energy of the system

N, total No. of rotors

Here only the solution for the simplest case is required.   This is

where the potential energy of any rotor is dependent upon the

orientation of all the other rotors.   (i.e. all of the rotors are

coupled).   Specifically the solutions for aluminium and zirconium

borohydrides will be required. (The molecular geometries of these two molecules are shown in Fig. Vi and Fig Vii).

In such a system of rotors the potential energy arises from two interactions. Just as in the single rotor problem there is a basic potential as the rotor moves with respect to the fixed frame of the molecule. Superimposed upon this is a second, which is a function of the different orientation of the neighbouring rotors. This potential involves a term, V_1, which might be regarded as a coupling constant (19). For the rotation of a borohydride unit about the metal boron axis, in the two molecules, the respective potential energies may be written. (V(θ)Al, total potential for aluminium borohydride; V(θ)Zr, for zirconium borohydride).

$$V(\theta)Al = \frac{VAl}{2}(3-\cos 2\theta_1 - \cos 2\theta_2 - \cos 2\theta_3)$$

$$+ \frac{V_1Al}{2}(3-\cos2(\theta_1-\theta_2)-\cos 2(\theta_2-\theta_3)- \cos 2(\theta_3-\theta_1))$$

V_1, coupling potential   (ii)

$$V(\theta)Zr = \frac{VZr}{2} (4 - \cos 3\theta_1 - \cos 3\theta_2 - \cos 3\theta_3 - \cos 3\theta_4)$$

$$+ \frac{V_1Zr}{2} (4 - \cos 3(\theta_1-\theta_2) - \cos 3(\theta_2-\theta_3)-\cos 3(\theta_3-\theta_4) -$$

$$\cos 3(\theta_4-\theta_1))$$

(iii)

The terms in 2θ arise because in aluminium borohydride there are two potential minima; and in zirconium borohydride, since there are

three minima, terms in 3θ appear. In all cases the kinetic energy is simply given as

$$T = \sqrt{\frac{I}{2}} \, \dot{\theta}^2_r$$ (iv)

The terms in equations (ii) and (iii) are simplified by the introduction of the deep well approximation. The cosine terms are then given by eq. (1.2 (x)) and equation (ii) and (iii) become, on rearranging

$$V(\theta)Al = \left(\frac{8V_1Al}{2} + \frac{4VAl}{2} \right) \left(\frac{\theta_1^2}{2} + \frac{\theta_2^2}{2} + \frac{\theta_3^2}{2} \right)$$

$$- \frac{4V_1Al}{2} \left(\theta_1\theta_2 + \theta_2\theta_3 + \theta_3\theta_1 \right)$$ (v)

$$V(\theta)Zr = \left(\frac{18V_1Zr}{2} + \frac{9VZr}{2} \right) \left(\frac{\theta_1^2}{2} + \frac{\theta_2^2}{2} + \frac{\theta_3^2}{2} + \frac{\theta_4^2}{2} \right)$$

$$- \frac{9V_1Zr}{2} \left(\theta_1\theta_2 + \theta_2\theta_3 + \theta_3\theta_4 + \theta_4\theta_1 \right)$$

(vi)

Combining eq. (v) and (vi) with eq. (iv) produces the Lagrangians for the two systems. Then making the substitutions

$$kAl = \left(\frac{8V_1Al}{2} + \frac{4VAl}{2} \right); \quad P_{AL} = \frac{-4 \, V_1Al}{2}$$ (vii)

$$k r = \left(\frac{18 \, V_1 Zr}{2} + \frac{9 \, vZr}{2} \right); \quad P_{Zr} = - \frac{9V_1 Zr}{2} \qquad \text{(viii)}$$

and knowing

$$\frac{dT_1}{d\theta_1} = 0 ; \qquad \frac{dV(\theta)}{dt} = 0$$

gives, for aluminium borohydride (which is used as an example)

$$I \theta_1 + k_{Al} \theta_1 + P_{Al} (\theta_2 + \theta_3) = 0$$

$$I \theta_2 + k_{Al} \theta_2 + P_{Al} (\theta_1 + \theta_3) = 0$$

$$I \theta^2 + k_{Al} \theta_3 + P_{Al} (\theta_1 + \theta_2) = 0 \qquad \text{(ix)}$$

(A similar set of equations obtains for zirconium borohydride).

Using as solutions to these equations

$$\theta_1 = A \exp (i_\omega t)$$

$$\theta_2 = B \exp(i_\omega t) \qquad \text{(x)}$$

$$\theta_3 = C \exp(i_\omega t)$$

A,B,C; constants.

i, $(-1)^{\frac{1}{2}}$

t, time

ω angular frequency

This leads directly to the secular determinant

$$\begin{vmatrix} -I_{\omega}^2 + k_{Al} & P_{Al} & P_{Al} \\ P_{Al} & -I\omega^2 + k_{Al} & P_{Al} \\ P_{Al} & P_{Al} & -I\omega^2 + k_{Al} \end{vmatrix} = 0$$

(xi)

for zirconium borohydride the determinant would be

$$\begin{vmatrix} -I\omega^2 + k_{zr} & P_{zr} & P_{zr} & P_{zr} \\ P_{zr} & -I\omega^2 + k_{zr} & P_{zr} & P_{zr} \\ P_{zr} & P_{zr} & -I\omega^2 + k_{zr} & P_{zr} \\ P_{zr} & P_{zr} & P_{zr} & -I\omega^2 + k_{zr} \end{vmatrix} = 0$$

Where the solutions to this type of determinant are

$$((-I\omega^2+k) - P)^{N-1}.((-I\omega^2+k) + (N-1)P) = 0 \qquad \text{(xii)}$$

N, the number of rotors, the order of the determinant.

For the case of aluminium borohydride there are three solutions, two degenerate out of phase motions of all the borohydride units, and one singly degenerate in phase motion of the units. These correspond to

$$k_{Al} + 2P_{Al} = I\omega^2$$

and

$$k_{Al} - P_{Al} = I\omega^2$$

substituting from eq. (vii) and rearranging gives

$$V_{A1} = 2\pi^2 I \nu_A^2 \qquad\qquad (xiii)$$

$$3V_{A1} + V_{1A1} = 2\pi^2 I \nu_E^2$$

where

$$2\pi\omega = \nu$$

ν_A, frequency of the in phase motion (Hz)
(an A mode)

ν_E, frequency of the out of phase modes (Hz) (an E mode).

Similarly for the case of zirconium borohydride. There are four energy states of the system: three degenerate out of phase modes and one singly degenerate in phase mode.

$$k_{zr} - P_{zr} = I \omega^2$$

$$k_{zr} + 3P_{zr} = I \omega'^2$$

Substituting from eq. (viii) and rearranging yields

$$V_{Zr} + 3V_{1Zr} = \frac{8}{9}\pi^2 I \nu_F^2$$

$$V_{Zr} - V_{1Zr} = \frac{8}{9}\pi^2 I \nu_A^2$$

ν_A, frequency of the in phase mode (an A mode)

ν_F, frequency of the out of phase modes (an F mode)

These equations can be used to interpret the experimental results
of Section V.

The molecules, aluminium and zirconium borohydride, have formal
analogues in trimethyl amine and neopentane. These compounds contain
three and four coupled rotors respectively. (Although the point
group symmetry of trimethyl amine is different from that of aluminium
borohydride, C_{3v} as compared to D_{3h}) trimethyl amine and neopentane
have both been studied previously. The coupling of the methyl rotors
in trimethyl amine was treated by Lide (1958). The problem was
expressed in quantum mechanical terms and two librational modes were
predicted, an A mode and an E mode. The observed microwave spectrum
was interpreted to give a barrier to rotation of 4.4 Kcal mole^{-1}.
The coupling of the methyl rotors in neopentane was treated slightly
differently by Grant (1968). The simple potential function of eq. (1.1
(iii) was not used, higher order interactions were considered as well.
Two main transitions were predicted, involving the two librational
modes A and F. These were observed in the inelastic neutron spectrum
and the barrier to rotation was 5.03 Kcal mole^{-1}.

2. **The calculation of the potential energy function directly.** ;

The total potential of a molecular ion, at different orientations,
in a crystal is composed of the contributions from several interactions.
These interactions include monopole electrostatic attraction, multipole
electrostatic attraction, London (dispersive or Van der Waals) attractive
forces, and steric repulsive forces. The London forces are quantum
mechanical in nature, they are weak and play an important part only in

the formation of crystals of uncharged molecules. The monopole
electrostatic forces are the main attractive forces in crystals like
sodium chloride (3). Multipolar contributions are only important
when the crystal is composed of molecular ions. The steric
repulsive forces are the forces which prevent the collapse of the
crystal. The simplest description of the total potential experienced
by a non spherical ion within an alkali halide lattice must be
in terms of the major contributing forces. These are the monopolar
electrostatic attraction and the steric repulsion. The two forces
will be considered separately, the total potential will be the
computed summation. The methods used to obtain the relevent potentials
are very general, but will be applied specifically to the orientational
potential of a tetrahedral ion incorporated within an alkali halide
lattice.

2.1 Determination of the monopolar electrostatic potential function.

The electrostatic lattice attraction has been studied by many
authors (21, 15, 3, 30). The methods of De Wett (1959) are used
to obtain the angular potential variation. His work is reproduced here,
using his nomenclature. The electrostatic potential energy at a
test point, due to a unit charge, can be written as eq. (i). (This
is illustrated in Fig. IIIi.)

$$V(\underline{R}) = \frac{-1}{|\underline{R}_p|} = \frac{-1}{|\underline{R} - \underline{r}_p|} \tag{i}$$

where

$\underline{R}_p$, vector from charge to test position.

$\underline{R}_p = f(R_p, \theta, \phi)$
etc.

$\underline{R}$, vector position of the test from the arbitrary origin.

$R_p = |\underline{R}_p|$

$\underline{r}_p$, vector position of the charge from the arbitrary origin.

Fig. III.i

93.

The vector relationship between the positive arbitary origin the point of interest, q, and the negative charge, P, in a simple lattice.

$$\underline{R}_p = \underline{R} - \underline{r}_p$$
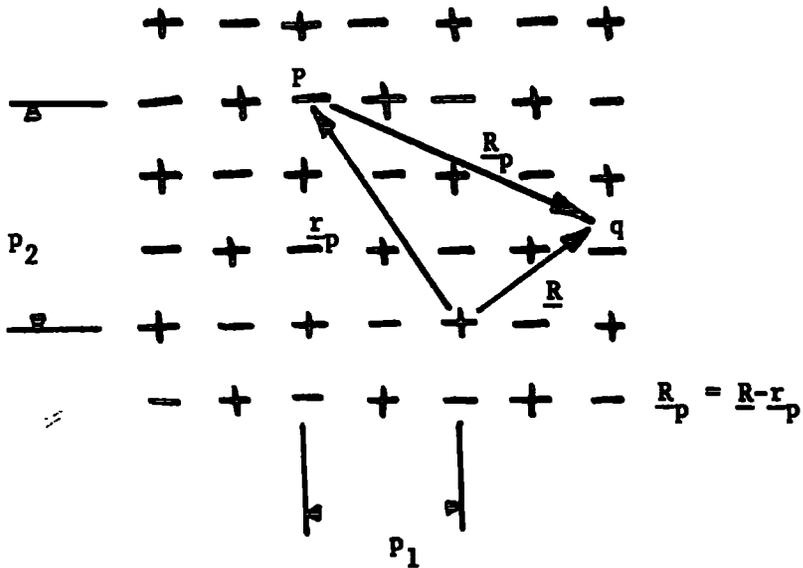
Fig. III.ii

The polar coordinate system (R, θ, ϕ) and its relationship to the cartesian coordinates (x, y, z)
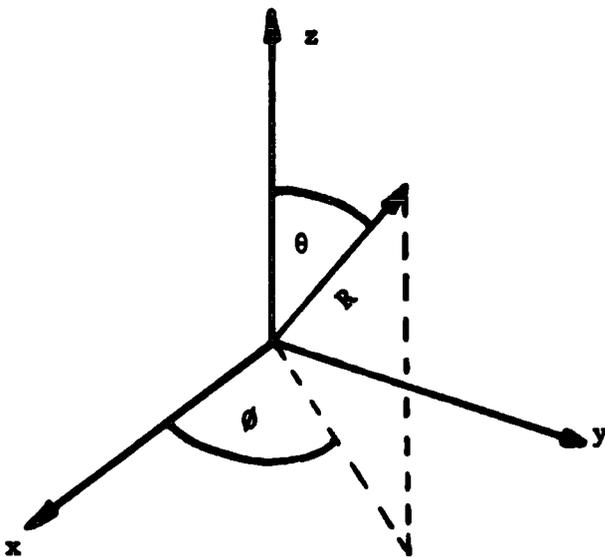
Standard polar coordinates are used in this description. (These

are defined in Fig. IIIii).

In a lattice of point charges the potential is the summation

over all the ions.

$$V(\underline{R}) = \sum_{P} \frac{(-1)^{P}}{|\underline{R}-\underline{r}_p|} \tag{ii}$$

$P = p_1 + p_2 + p_3$ $\underline{r}_p$, are now vectors describing the lattice points.

$\underline{r}_p = p_1\underline{d}_1 + p_2\underline{d}_2 + p_3\underline{d}_3$ $\underline{d}_i$ basis vectors of the unit cell.

p_i, integers.

(This is illustrated in Fig. IIIi). The origin is arbitrarily

chosen as a positive charge, and the contribution of this charge

to the potential at $\underline{R}$ is specifically omitted. Since the ions are

either positive or negative their position in the lattice effectively

defines their charge.

Just as any continuous function in one dimension can be approximated

by a linear combination of sines and cosines, (the Fourier series) so

a three dimensional angular function can be represented by a linear

combination of spherical harmonics. The definition of spherical

harmonics and some useful properties are given in Appendix I.

The vectors $\underline{R}$ and $\underline{r}_p$ are three dimensional functions and may be

expanded individually. Further, from the addition theorum of

spherical harmonics the denominator of eq. (ii) can be written

$$|\underline{R}-\underline{r}_p|^{-1} = \sum_{l=0}^{\infty} \sum_{m=-1}^{+1} \left(\frac{4\pi}{2l+1}\right) R^l \cdot r_p^{-1-l} \cdot Y_{l,m}^* (\theta_p, \phi_p)$$

(iii)

where $R < r_p$ (see appendix I)

Equation (ii) $\therefore$ becomes

$$V(\underline{R}) = \sum a_{l,m} R^l Y_{l,m}^* (\theta, \phi)$$

(iv)

where

$$a_{l,m} = \left(\frac{4\pi}{2l+}\right) \sum_p r_p^{-1-l} Y_{l,m}(\theta_p, \phi_p) \cdot (-1)^P$$

It is obvious that the potential is determined by two factors. The first concerns the positioning of the point of interest, the test point at $\underline{R}$. The second is the contribution made by the whole crystal to the potential at the test point, this is contained in the $a_{l,m}$ term. De Wett has developed a method of evaluating the $a_{l,m}$, and specifically evaluated them for the two simple cubic lattices, sodium chloride type and caesium chloride type. (These are reproduced in Table IIIi). These cubic lattices are particularly suitable for treatment in this manner because of their high symmetry. Equation (iv) is simplified, l must have even values and m is fourfold or zero. Another aspect of the symmetry is that the linear combinations of the spherical harmonics must be invariant under the operations of the cubic group (Oh). Then from eq. (iv)

$$V(\underline{R}) = a_{0,0} + a_{4,0} \cdot R^4 \cdot \underline{Y}_4 + a_{6,0} \cdot R^6 \cdot \underline{Y}_6$$
$$+ a_{8,0} \cdot R^8 \cdot \underline{Y}_8 + a_{10,0} \cdot R^{10} \cdot \underline{Y}_{10} + \dots$$

(v)

Table III.i

<u>The values of $a_{1,m}$ used in the computations.</u>

Crystal lattice type	for $m = 0$ 1	$a_{1,m}$ (*)
NaCl	0	-1.74756
	4	-4.2290
	6	-0.9729
	8	-2.5216
	10	-0.7824
CsCl	0	-1.76267
	4	+5.3670
	6	-1.5456
	8	-0.2634
	10	-

(*) taken from ref (32)

where

$$\underline{Y}_4 = (\tfrac{5}{14})^{\frac{1}{2}} (Y^*_{4,4} + Y^*_{4,-4}) + Y^*_{4,0}$$

$$\underline{Y}_6 = (\tfrac{-7}{2})^{\frac{1}{2}} (Y^*_{6,4} + Y^*_{6,-4}) + Y^*_{6,0}$$

$$\underline{Y}_8 = (\tfrac{5}{3})(\tfrac{13}{110})^{\frac{1}{2}} (Y^*_{8,8} + Y^*_{8,-8}) + (\tfrac{1}{3})(\tfrac{14}{11})^{\frac{1}{2}}(Y^*_{8,4} + Y^*_{8,-4}) + Y^*_{8,0}$$

$$\underline{Y}_{10} = -(\tfrac{187}{130})^{\frac{1}{2}}(Y^*_{10,8} + Y^*_{10,-8}) - 6(\tfrac{11}{390})^{\frac{1}{2}}(Y^*_{10,4} + Y^*_{10,-4}) + Y^*_{10,0}$$

The potential of a tetrahedron at different orientations in the
crystal is thus easily obtained. It is the sum of the four
potentials perceived by the corners of the tetrahedron. The
tetrahedron carries a set of cartesian coordinates fixed to it, the
body set. These coordinates are related to the crystal's coordinates,
the space set, by the Euler angles. (This is discussed in
Appendix II). The space set of coordinates, are aligned along the
main symmetry axes of the crystal. At each orientation of the
tetrahedron the total electrostatic potential is obtained through
a computer program, this is discussed and a listing given in Appendix
III. The results of these computations are discussed later.

2.2 Determination of the steric repulsive potential function.

Compared with the Coulombic attraction the steric repulsive
forces in a crystal are of very short range. Several mathematical
forms have been used to represent this potential (30). The most
commonly used expression is that presented by Born (1932). It has
an exponential form which stems from the quantum mechanical prediction

that the electron distribution about an atom falls off exponentially.
Then the repulsion between two atoms is.

$$V(s) = B.\exp(-(s - (r_a + r_b))/\rho) \qquad (i)$$

ρ, range parameter

s, separation of the atomic nucleii.

r_a, radius of the atom a

r_b,   "   "   " b

B, strength parameter of the interaction.

Because of the short range of these interactions (ρ is low, about
0.4Å) and the quite large separations of the ions in an alkali
halide lattice (lattice parameter of about 5Å) the forces are
effectively zero for separations greater than one unit cell. This
is fundamentally different from the case of electrostatic attraction
and its computation can be treated more simply. In this case it is
practicable, without loss of accuracy, to calculate the repulsion of
a corner of the tetrahedron from a small section of the whole crystal.
Where contributions to the energy from ions in uhit cells greater than
one away from the origin may be ignored. The repulsion against each
ion is calculated independently, and they are all summed. As with
the electrostatic case the tetrahedron carries a body set of coordinates.
These are related to the space set of coordinates by the Euler angles
(discussed in Appendix II). At each orientation the total repulsion
energy is calculated through a computer program, this is discussed

and a listing given in Appendix III.   The results of these
computations will now be discussed.

2.3 The calculated variation of potential energy with molecular orientation.

When an ammonium ion reorientates between potential minima it
will tend to take the path of minimum energy (unless the ion has
received a large amount of energy, when it will reorientate to 'another
well by any route). Such a minimum energy route could be expressed
as a coordinate describing the reorientation.   The potential would
then be a function of this single coordinate.   This coordinate is
not easily determined, and would be a complicated function of all
three Euler angles used to describe molecular orientation in space.
It would not reflect the symmetry of the system in any obvious manner.
In these calculations the Euler angles (see Appendix II) are used as
the reorientation coordinates they retain the symmetry of the system
and enable the relative contributions of electrostatic attraction and
steric repulsion to be easily compared.   Such coordinates will tend
to over-estimate the barriers to reorientation, which are calculated.

The variation of the electrostatic and steric potentials were
obtained directly from the computer programs discussed in Appendix III.
These results are presented separately.   Firstly electrostatic
calculations for sodium chloride lattices are considered.

It can be seen from Tables IIIii, IIIiii, and vii that the calculated
electrostatic potentials, for both the pure host lattice and the
incorporated ammonium salts, are in reasonable agreement with
literature values for the pure host lattices.   The ammonium ion can
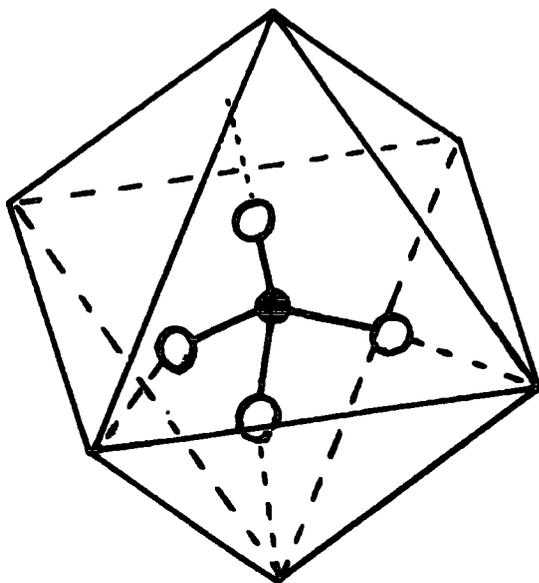
Fig. III.iii

Closest approach of three protons.

Fig. III.iv

Single approach model in an
electrostatic potential minimum.
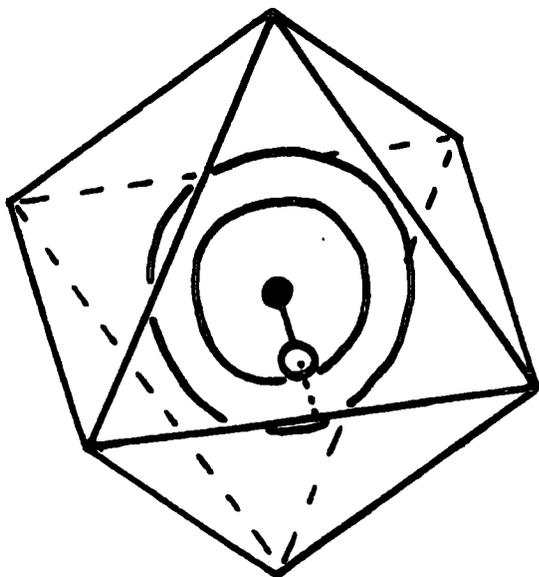
Fig. III.v

Single approach model in an
electrostatic potential maximum.

Orientations of the ammonium ion in the sodium chloride type lattice.

repulsion potential minimum
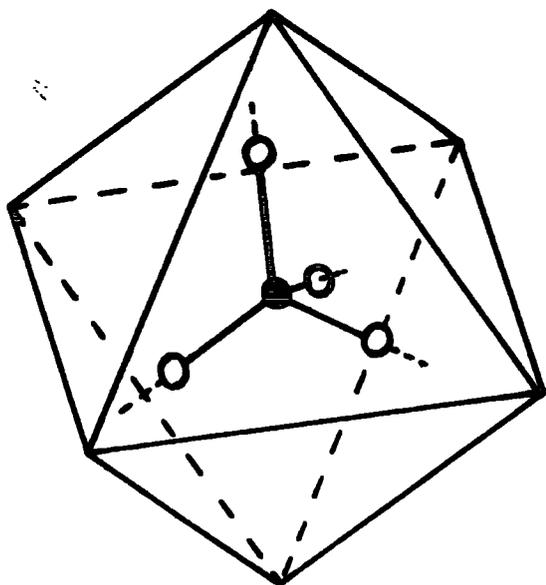
Fig. III.vi

repulsion potential maximum
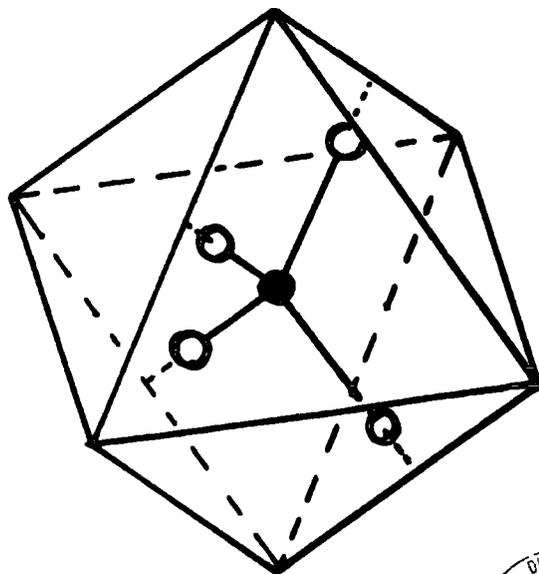
Fig. III.vii

orientate itself quite specifically in the sodium chloride type

lattice. This orientation is where the corners of the

tetrahedron approach, as closely as possible, three nearest neighbours.

Direct alignment along bonds is impossible as is illustrated by

Fig. IIIiii. There are many equivalent orientations of this type,

but it is unlikely that the molecule will remain in any of them.

This is because of the very small difference between the value of this

potential minimum and the value of the next lowest potential minimum

(about 10 cal mole^{-1}, sic.) This next lowest potential is where

one corner of the tetrahedron points directly at an opposite ion,

nearest neighbour. This is the single approach model of Plum (1953)

see Fig. IIIiv. There is no change in potential as the tetrahedron

rotates about this C_3 symmetry axis (within the limits of the

calculation). It may be said that for temperatures above about 10°K

the single approach model is the one which would normally be assumed,

on electrostatic grounds. It is energetically difficult to

reorientate the single approach corner to another nearest neighbour.

The values of these potential wells are given in Table IIIii. This

is still a low barrier to reorientation. If $\frac{1}{2}$KT is assumed for each

rotational degree of freedom, the ammonium ion should be capable of

reorientating the C_3, single approach axis, at about 30°K. The

rotational motion of the ammonium ion, at 294°K, will be essentially

unrestricted. These wells will be significant only at low

temperatures. This is because the value of $\frac{1}{2}$KT becomes less and

also because the host lattice contracts, increasing the reorientational

barrier. (The present calculations are based on ambient temperature

unit cell data).

In the caesium chloride type lattice it is possible to have all the corners of the tetrahedron directly aligned with nearest neighbours. This configuration is electrostatically the most stable, and is shown in Fig. IIIviii.   Reorientations between symmetrically equivalent potential minima are hindered.   The rotation about any C_3 symmetry axis of the tetrahedron is more difficult than that about any S_4 symmetry axis.   The two barriers are shown in Fig. IIIxi. The ratio of the two barriers is 1.7117 (within the limitations of the calculation).

The problem of the electrostatic barrier to reorientation of ammonium ions in caesium chloride lattice types has been treated in the literature (21, 12, 15, 29).   The approach chosen is usually that of Nagamiya (1942), which is exactly analogous to that of De Wett presented here (32).   The electrostatic potential field was expanded as a summation of spherical harmonics.   However in order to reduce the computational problem a simplifying assumption was introduced. Only the first non-trivial term in the potential expansion was taken. (This is equivalent to using only the term $a_{4,0}.R^4.\underline{Y}_4$ in eq. (2.1(v)). Although this transaction has never been justified the accuracy lost appears to be minimal.   The truncated sequence predicts that reorientation about a C_3 axis of the ammonium is 1.777 times more difficult than about an S_4 axis.   (This compares very favourably with the value presented above, and introduces an error of no more than about 4%)

Stated in terms of Cartesian coordinates the potential of the

Orientations of the ammonium ion in caesium chloride type lattices.
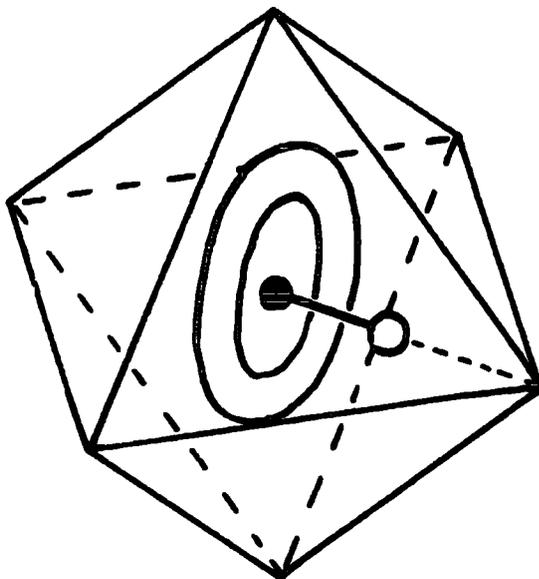
Fig. III.viii

The four approach model in an Electrostatic
potential minimum.
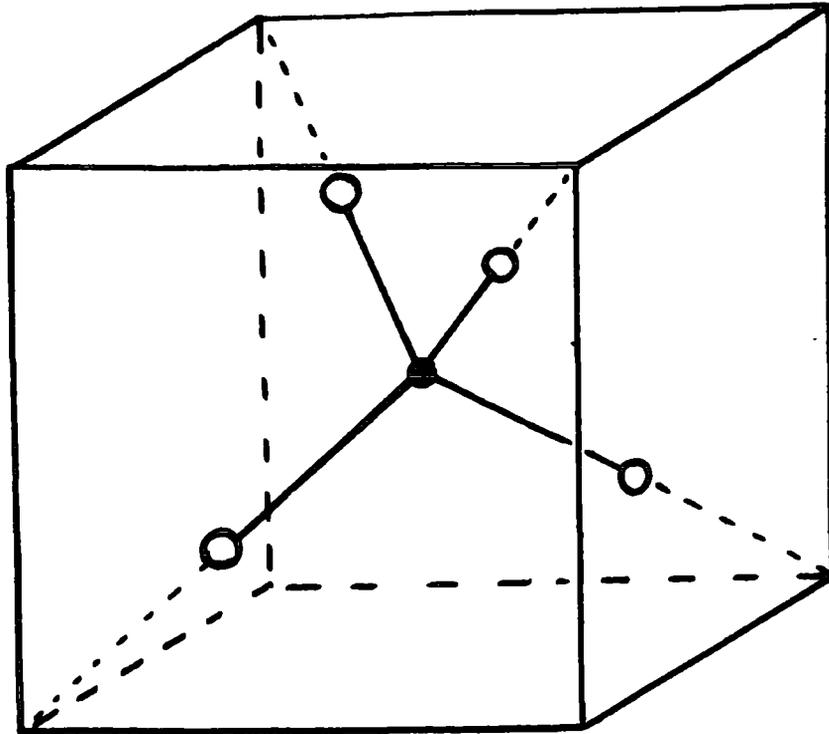
Fig. III.ix

The four approach model in Electrostatic
potential maximum.
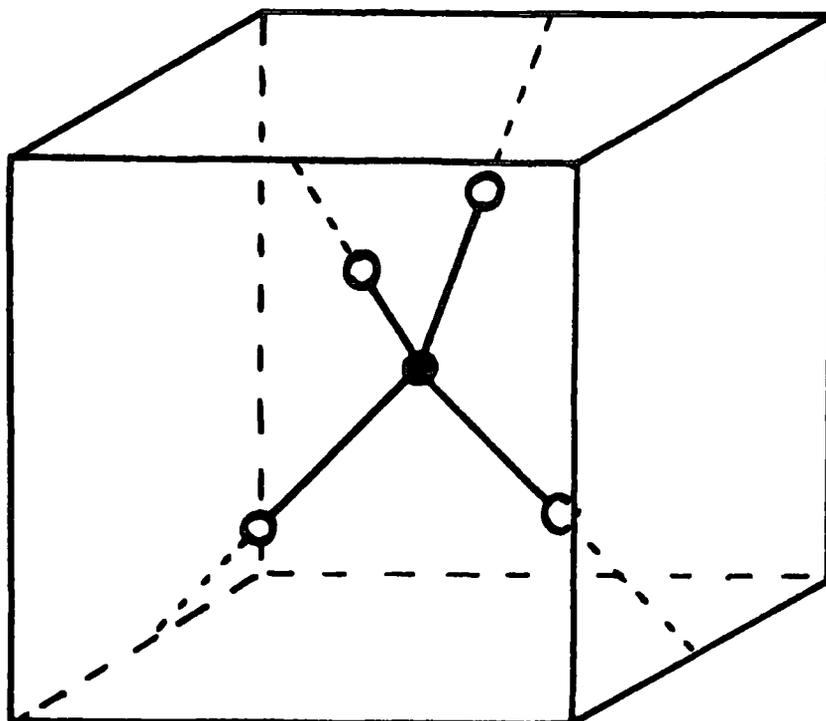
tetrahedron was

$$V = \frac{V_0}{2} \sum_{i=1}^{4} \left(\frac{x_i^4 + y_i^4 + z_i^4}{\rho^4} - \frac{3}{5} \right)$$ (i)

ρ, NH bond length

At the equilibrium position, direct approach of all hydrogens to nearest neighbours, a value of V can be calculated

$$V = \frac{14V_0}{5}$$ (ii)

Here the V_0 term is related to the absoluted barrier height.
No absolute values for the electrostatic potential were presented but the potential function was used to solve Schrodinger's equation for the system.

The potential function cannot be substituted immediately into Schrodinger's equation, since the resulting differential equation is too complex to solve. Two methods of approximation have been used. In the first, due to Gutowsky (1954), a new set of coordinates is chosen; x', y', z'. These are related to the old set; x, y, z. The set x', y', z' are attached to the tetrahedral ion and the set x, y, z are the axes of the ceasium ion cube; the axes x, y, z projected out of the cubes' faces. Then the angles θ, and ϕ are the polar coordinates of z' in terms of x, y, z; and the angle ψ is the measure of displacement about the z' axis. At equilibrium, direct approach of the four hydrogen atoms toward the nearest neighbours, the z and z' axis are alligned and the x', y' axis are

displaced by $^\pi/4^c$ from the x, y axes.   Equation (i) becomes by transformation

$$V = \frac{Vo}{2}\{-(\frac{49}{8})\cos^4\theta + (\frac{21}{4})\cos^2\theta - (\frac{21}{40})$$

$$+ (\frac{7}{8}).\sin^4\theta.(\cos 4\ \psi - \cos 4\ \phi)$$

$$+ (\cos^2\theta + \frac{1}{8}\sin^4\theta)\cos 4\ \phi.\cos 4\ \psi$$

$$- \frac{1}{2}.(\cos\ \theta + \cos^3\theta).\sin 4\ \phi.\sin 4\ \psi\} \qquad \text{(iii)}$$

In the limit of small oscillations three independent coordinates can be chosen, those used by Gutowsky were

$$\xi = \theta.\cos\phi$$
$$\eta = \theta.\sin\phi \qquad\qquad\qquad \text{(iv)}$$
$$\zeta = \phi + \psi + \frac{\pi}{4}$$

which are displacements about the cubic set of axes x, y, z. This leads to

$$V = \frac{Vo}{2}\{-\frac{12}{5} + 8(\xi^2 + \eta^2 + \zeta^2) - \frac{32}{3}(\xi^4 + \eta^4 + \zeta^4)...\} \qquad \text{(v)}$$

Again a value for V at equilibrium can be determined; $\xi = \eta = 0$, and $\zeta = {}^\pi/4^c$.

$$V = -0.762\ Vo \qquad\qquad\qquad \text{(vi)}$$

Gutowsky applied first order perturbation theory to obtain the energy levels of this anharmonic isotropic oscillator

$$E_{r_1 r_2 r_3} = -\frac{6}{5}Vo + (r_1 + r_2 + r_3 + \frac{3}{2}).\hbar w - \frac{1}{16}\left[\sum_{i=1}^{3}(2r_i^2 + 3r_i + \frac{5}{4}) + \right.$$

$$\left. + r_1.r_2 + r_1.r_3 + r_2.r_3 \right] \frac{(\hbar w)^2}{Vo} \qquad \text{(vii)}$$

where

$$w = 16Vo/2T$$

and

$$r = 0, 1, 2 \ldots$$

The fundamental transition, ν, $(\Delta E = E_{1,0,0} - E_{0,0,0} = h\nu)$ yields:

$$Vo = \frac{1}{16}\left\{ \frac{(h\nu + \frac{5\hbar^2}{2I})}{\hbar^2/2I} \right\} \qquad \text{(viii)}$$

ν, observed librational harmonic.

This equation has seen extensive use in the study of ammonium salts by infrared absorption (6). This method has been criticised by Venkataraman (1966), who provided an alternative. Since the potential function used by Gutowsky in the Schrodinger equation fails to give the correct equilibrium potential (compare eqs. (ii) and (vi)), Venkataraman used the one dimensional approximation. The Schrodinger equation becomes the Mathieu equation, as discussed previously. For the case of the double potential well, tables are available for the solution of this equation (2). The results obtained by Venkataraman are only applicable to the ordered caesium chloride phase of ammonium halide salts; they should be used with circumspection elsewhere.

Very recently (15) work has been reported on the electrostatic potential barrier in the pure ammonium halides. Huller (1974) has obtained a potential function which is based upon eq. (2.1(ii)) but has been taken further. The charge distribution on the ammonium ions was expanded in terms of spherical harmonics. Thus he was not confined to the simple case of one ammonium ion in an infinite host lattice; which is the limitation of the calculations presented here. Account was also taken of the polarisabilities of the ions. It was assumed that the potential well of the crystal was represented by the calculated potential well. The model was fitted, successfully, to experimental data; no absolute values of the potential in specific orientations were given. Two important interactions were completely omitted, the variation of the repulsion potential, and calculation of a hydrogen bonding interaction. Ebisuzaki (1974) has shown that these interactions are important in the ammonium halides.

The variation of steric repulsive energy reflects the inversion symmetry which connects both attraction and repulsion and also the caesium chloride and sodium chloride lattice types (shown in Fig. IIIx). The calculated repulsion energies of Tables IIIiv, v, and vi compare favourably with the literature values for the pure hosts, Table IIIvii. In the sodium chloride type lattice the corners of the tetrahedron are directed away from the nearest neighbours. They point out of the faces of the octahedron of surrounding neighbours (toward the next nearest neighbours). Again reorientation about an S_4 symmetry axis of the tetrahedron is easier than its C_3 axis. Whilst in the caesium chloride type structure the tetrahedron, again, arranges itself in a

Fig. III.x

109.

Symmetry relationships of a cube and an

octohedron

Fig.III.xi 110.
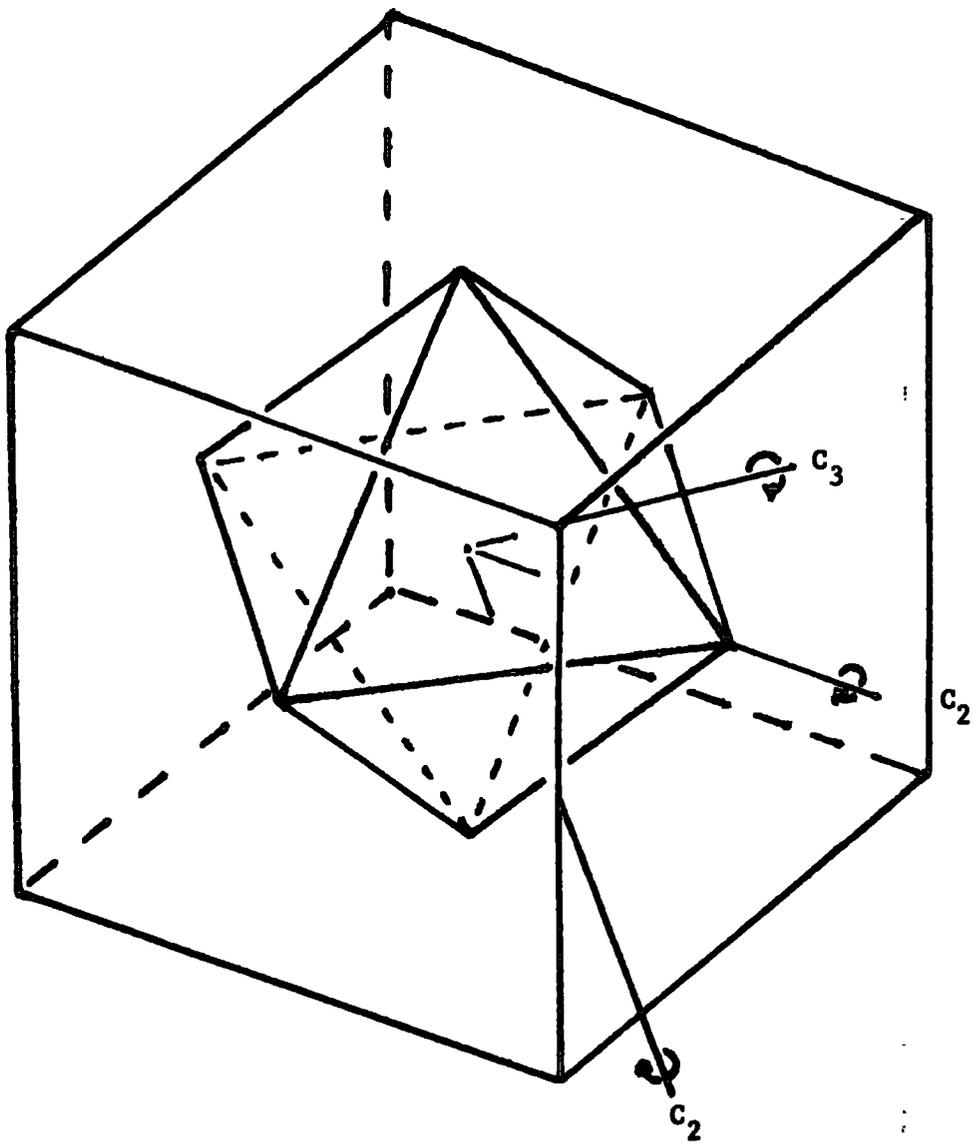
Variation in electrostatic potential as the ammonium ion, in a caesium chloride type lattice reorientates about in C_3, or S_4 symmetry axis.
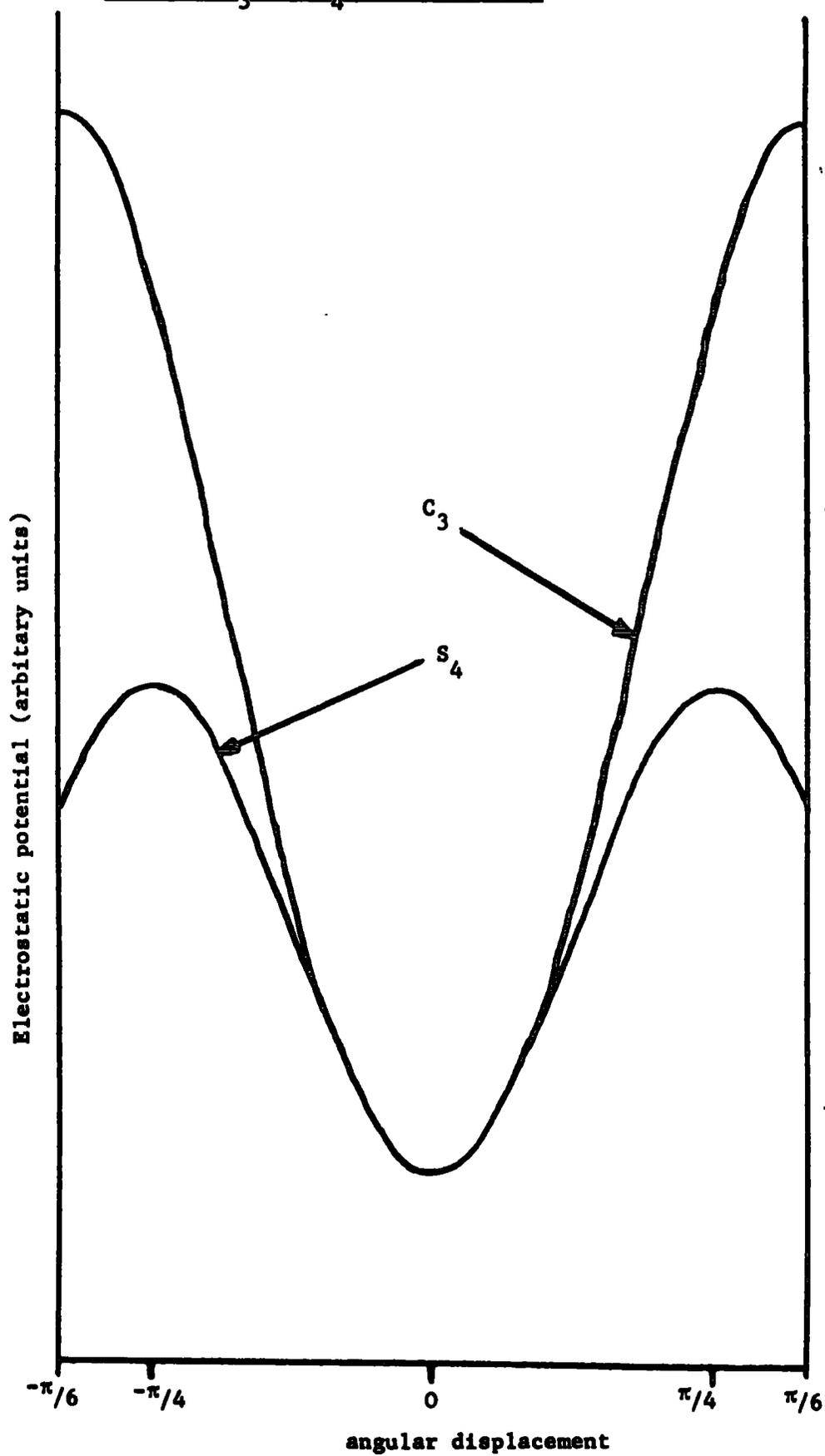
very shallow well, when three corners are equidistant from nearest neighbours. But a single approach model is also quite stable, the corner now points out through the face of a surrounding cube of ions toward a next nearest neighbour. There is no variation as the molecule rotater about this C_3 axis (within limitations of the calculation). It should also be noticed that if a single approach in the sodium chloride lattice is studied, where one corner points directly at a nearest neighbour, then although the repulsive energy is high, compared to the potential minimum discussed above, it shows no variation for rotation about this C_3 axis.

These calculations are the first attempt to directly estimate the reorientational barrier of an incorporated ion in a cubic crystal. Absolute values for the electrostatic and repulsive potentials, such as those presented here, show immediately which potential is the more important in any one system. They indicate that the assumption of a predominantly electrostatic potential well is probably wrong. It is unlikely that the electrostatic potential well in the pure ammonium halides is any deeper than that in the incorporated salts. Whilst the repulsive potential well will be increased because of the polyatomic ammonium ion neighbours. The fortuitous success of the calculations conducted by Gutowsky (1954), Venkataraman (1966) and Huller (1974) stems from the presence of another attractive potential in the crystal. (This is most likely to be hydrogen bonding, and is discussed later). A similarity in general forms would be all that is required to fit an electrostatic model to a different attractive potential.

The calculated repulsion potential wells are deeper than the electrostatic potential wells by up to an order of magnitude. Thus, although the electrostatic potential energy of the final lattice dictates the formation of these mixed crystals, the orientation of the ammonium ions in the lattice is not governed by the electrostatic potential. The main reason for this is the large variation of the repulsion potential with orientation, compared with the small variation from the electrostatic potential. It may be that the protons carry all of the charge of the ammonium ion, but this would make a difference of only 25% in a very small number. However at lower temperatures the contraction of the lattice could favour much deeper electrostatic potential wells. Alternatively it may be that the repulsion potentials calculated here are fortuitously in line with the literature. The radius of a proton, used in the repulsion calculation (see Appendix III), was estimated; and it may not accurately reflect the characteristics of a hydrogen atom. It should be noted that the repulsion potential due to the nitrogen atom in the ammonium ion was omitted from the calculations. Also that no attempt was made to estimate the deformation of the pure host lattice about the ammonium ion. Since the ammonium ion is a defect introduced into the lattice, the immediate environment about it may be significantly different from a pure host lattice.

A more serious ommission from these calculations may be the neglect of hydrogen bond formation. Hydrogen bonding plays a significant role in many systems, especially those involving the highly electro negative elements, such as oxygen, nitrogen and chloride. Hydrogen bond strengths can be quite significant and may approach values similar to the

repulsion energy barrier (7). Unfortunately no simple, and successful, formulation for the calculation of hydrogen bond strengths is known. Piela (1973) has attempted to use ab initio molecular orbital calculations to obtain estimates of hydrogen bond strengths. For one case in particular the result is interesting, the bond strength in the HOH ----Cl $^-$ complex was ca. 19 Kcal mole^{-1}. If the formation of such strong bonds were possible in the incorporated salts they would tend to out-weigh the repulsive forces in the crystal. Hydrogen bond formation is equivalent to another attractive force in the crystal. It will have the same general characteristics as the electrostatic potential. Only the detailed shape of the potential well would be modified by the nature of hydrogen bonding. The importance of hydrogen bonding would probably be more apparent in the caesium chloride type lattices, where alignment of the tetrahedral ammonium ion within the cube allows the simultaneous formation of four hydrogen bonds. Recent observations indicate that hydrogen bonding is important in the ammonium halide salts (7).

2.3.1 Calculations on sodium borohydride

The steric repulsion energy program was used to calculate the reorientational barriers in the ordered phase of sodium borohydride. This salt has a tetragonal structure below its λ point (see Section IV), which is only slightly distorted from cubic symmetry. The steric repulsion program can be very easily applied to such a structure. Since the electrostatic potential is not expected to have a large variation, with reorientation, the steric repulsion should be the most

important factor in determining the ordering and the reorientational barrier. In the program the whole crystal is ordered, and only the central borohydride unit is allowed to reorientate; about the crystalographic axes. (Concerted motions of several borohydride ions could not be treated).

The results clearly show that the central borohydride ion occupies an ordered position when in a steric potential minimum. That the steric potential well is not well represented by a simple sinusoid shape, and that reorientation about the a or b crystal axes is slightly more hindered than that about the c axis. The absolute values of the potential wells was unrealistically high, and probably stems from the large hydrogen atom radius. (In the borohydride ion the hydrogen atoms carry negative charge. Their size can be estimated in a way similar to the method used for the ammonium ion, see Appendix III).

Table III.ii   The calculated Electrostat.c Potential of an ammonium ion incorporated in a sodium chloride type lattice; for the specific orientations shown in Figs IIIiii,iv,v.

Host lattice		(5) lattice parameter 10^{-8}cm	Calculated Electrostatic Lattice Energy K. cals mole^{-1}				Potential Barriers Kcal mole^{-1} Differences of columns		
			Pure Host Lattice	Incorporated salts ammonium ion oriented as shown in			2,3	3,4	2,4
				Fig. IIIiii	Fig.IIIiv	Fig.IIIv			
Na	Cl	5.4602	212.4757	212.6187	212.5963	212.4424	0.0224	0.1539	0.1763
	Br	5.974	194.2015	194.2924	194.2784	194.1809	0.0139	0.0976	0.1116
	I	6.475	179.1753	179.2358	179.2266	179.1618	0.0092	0.0648	0.0740
K	Cl	6.2929	184.3602	184.4302	184.4192	184.3443	0.0109	0.0749	0.0858
	Br	6.599	175.8085	175.8336	175.8549	175.7962	0.0087	0.0588	0.0674
	I	7.0655	164.2007	164.2398	164.2338	164.1919	0.0060	0.0419	0.0479
Rb	Cl	6.590	176.0486	176.1040	176.0955	176.0361	0.0085	0.0594	0.0679
	Br	6.863	169.0456	169.0907	169.0837	169.0355	0.0070	0.0482	0.0551
	I	7.340	158.0599	158.0921	158.0873	158.0527	0.0049	0.0346	0.0394

Madelung constant for NaCl type lattice = 1.74756

Table III.iii   The calculated Electrostatic Potential of an ammonium ion incorporated in a caesium chloride type lattice;   for the specific orientations shown in Figs. IIIviii,ix

| Pure Host lattice | Lattice parameters Å (5) | Calculated Electrostatic Lattice Energy Kcal mole^{-1} | | | Barrier to reorientation Kcal mole^{-1} |
		Pure Host lattice	Incorporated ammonium ion oriented as Fig.IIIviii	oriented as Fig.IIIix	
Cs Cl	4.121	163.9436	164.8796	164.0528	0.827
Br	4.296	157.2652	158.0247	157.3586	0.666
I	4.5667	147.9430	148.4974	148.0121	0.485

madelung constant for the CsCl type structure is 1.76267

Table III.iv   The calculated steric potential of an ammonium ion (*) incorporated in a sodium chloride type lattice:

for the specific orientations shown in Figs. IIIiii, iv, v.

Pure Host lattice	Calculated Repulsion Energy (*) Kcals mole⁻¹ ammonium ion oriented as shown in			Potential Barrier Difference of columns		
	Fig. IIIiii	Fig.IIIiv	Fig. IIIv	1,2	2,3	1,3
Na Cl	64.64	63.22	53.79	1.42	9.43	10.84
Br	45.26	44.31	38.03	.94	7.22	8.17
I	38.40	37.63	32.63	.78	4.99	5.77
K Cl	20.05	19.65	17.02	.40	2.63	3.03
Br	18.73	18.36	15.95	.37	2.41	2.78
I	16.61	16.30	14.25	.32	2.04	2.36
Rb Cl	13.21	12.96	11.33	.25	1.63	1.88
Br	12.91	12.67	11.04	.24	1.63	1.87
I	11.24	11.04	9.73	.20	1.31	1.51

(*) The radii of the ions used in this calculation are given in appendix III. The repulsion due to the central nitrogen atom is omitted.

The results presented are the absolute repulsion energies on four protons in Kcals mole⁻¹ and are discussed in appendix III.

117.

Table III.v

The calculated steric potential of an ammonium ion(*)
incorporated into a caesium chloride type lattice for the
specific orientations shown in Fig. IIIviii,ix.

Pure Host lattice	Calculated Repulsion Energy (*) Kcals mole^{-1}		Barrier to reorientation Kcal. mole^{-1}
	ammonium ion Fig.IIIviii	oriented arm Fig. IIIix	
CsCl	9.0375	7.5888	1.44
Br	8.3444	6.9776	1.36
I	7.2462	6.0561	1.19

(*) The radii of the ions used here are presented in
     Appendix III, and the repulsion energy of the central
     nitrogen atom is omitted.

Table III.vi

**The calculated steric potential of an ammonium ion (*)
incorporated into a sodium chloride type lattice, for the
specific orientations shown in Figs. IIIvi, vii.**

Pure Host lattice		Calculated Repulsion Energy(*) Kcal mole^{-1} ammonium ion as in		Potential Barrier Kcal mole^{-1}
		Fig. IIIvi	Fig. IIIvii	
Na	Cl	41.57	51.77	10.20
	Br	31.39	38.80	7.41
	I	25.69	31.53	5.84
K	Cl	13.44	16.48	3.04
	Br	12.99	15.90	2.90
	I	11.35	14.87	3.52
Rb	Cl	8.99	10.95	1.97
	Br	8.81	10.73	1.91
	I	7.73	9.37	1.64

(*) The radii of the ions used in this calculation are given in
    Appendix III.   Repulsion due to the central nitrogen atom
    is omitted.

<u>Table III.vii</u>

<u>The Electrostatic and repulsion energies of the</u>
<u>alkali metal halides.</u>

Alkali Halide		Electrostatic Energy Kcal mole^{-1}	Repulsion energy Kcal mole^{-1}
Na	Cl	205.6	22.5
	Br	194.0	20.1
	I	179.2	17.0
K	Cl	184.3	20.7
	Br	175.8	19.4
	I	164.1	17.2
Rb	Cl	176.2	19.8
	Br	168.4	18.5
	I	158.0	17.0
Cs	Cl	163.8	17.0
	Br	157.2	16.4
	I	147.8	14.5

reproduced from Cubicciotti (1959), (1960)

REFERENCES

1. Born, M. Z. Physik. 75, 1, (1932).

2. "Tables relating to the Mathieu Function" Columbia Univ. (1951).

3. Cubicciotti, D. J. Chem. Phys., 31, 1646, (1959).
   : erratum J. Chem. Phys. 33, 1579, (1961).

4. Das, T.P. J. Chem. Phys., 25, 896 (1956).

5. Donnay, J.D.H. "Crystal Data" Am. Cryst. Associ. (1963).

6. Durig, J.R. J. Chem. Phys., 52, 5542, (1970).

7. Ebisuzaki, Y. J. Chem. Phys., 61, 3170, (1974).

8. Eyring, H. "Quantum Chemistry" Wiley (1944).

9. Finch, A. "Chemical Applications of Far Infrared Spectroscopy"
   Achademic Press (1970).

10. Goldstein, S. Proc. Roy. Soc. Edinburg. 49, 210 (1929).

11. Grant, D.M. Phys. Rev. Letters. 20, 983, (1968).

12. Gutowsky, H.S. J. Chem. Phys., 22, 643, (1954).

13. Herschbach, D.R. "Tables for the internal Rotation problem"
    Harvard Univ. (1957).

14. Huggins, M.L. J. Chem. Phys., 5, 143, (1937).

15. Huller, A. J. Chem. Phys., 61, 3599 (1974).

16. Ince, E.L. Proc. Roy. Soc. Edinburg. 46, 316, (1925).

17. Kochler, J.S. Phys. Rev., 57, 1006 (1940).

18. Levy, H.A. J. Am. Chem. Soc. 75, 1536, (1952).

19. Lide, D.R. J. Chem. Phys., 28, 572 (1958).

20. Margenan, H. "The mathematics of Physics and Chemistry"
    Van Nostrand (1943).

21. Nagamiya, T. Proc. Phy-Math. Soc. Japan., 24, 136 (1942).

22. Pauling, L. Phys. Rev., $\underline{36}$, 430 (1930).

23. Piela, L. Chem. Phys. Letters. $\underline{19}$, 134 (1973).

24. Plum, R.C. J. Chem. Phys., $\underline{21}$, 366 (1953).

25. Temme, F.P. J. Chem. Soc. Faraday., $\underline{69}$, 783 (1973).

26. Tosi, M.P. Solid State Physics, $\underline{16}$, 1, (1963).

27. Tosi, M.P. J. Phys. Chem. Solids, $\underline{25}$, 45, (1964).

28. Townes, C.H. "Microwave spectroscopy" McGraw-Hill (1955).

29. Venkataraman, G. J. Phys. Chem. Solids. $\underline{27}$, 1103, (1966).

30. Waddington, T.C. Adv. Inorg. and Radiochem. $\underline{1}$, 157, (1959).

31. Waddington, T.C. Molecular Physics., $\underline{21}$, 761 (1971).

32. De Wett, F.W. "Electrostatic Fields in Ionic Crystals"
    Utrecht Univ. Thesis (1959).

APPENDIX I

Spherical Harmonics

Spherical Harmonics are a set of functions which can be used to expand any two dimensional function in polar coordinates. Thus

$$g(\theta,\phi) = \sum_{l=0}^{\infty} \sum_{m=1}^{l} A_{l,m} Y_{l,m}(\theta,\phi)$$

$\theta,\phi;$ coordinates

$A_{lm},$ coefficients

$l,m;$ indices

$Y_{l,m}(\theta,\phi),$ spherical harmonic

$g(\theta,\phi),$ any arbitary function in θ and ϕ.

A suitably normalised spherical harmonic is given by

$$Y_{l,m}(\theta,\phi) = \left[\frac{(2l + 1)}{4\pi} \cdot \frac{(l - m)}{(l + m)} \right]^{\frac{1}{2}} \cdot P_l^m(\cos\theta) \cdot \exp(im\phi)$$

$$(i)$$

where

$P_l^m(x),$ the associated Legendre function.

$$l, (-l)^{\frac{l}{2}}$$

$$P_l^m(x) = (1 - x^2)^{m/2} \cdot \frac{d^m}{dx^m} \cdot P_l(x)$$

where

$$P_l(x) = \frac{(2l)!}{2^l \cdot l!^2} \cdot \left\{ x^l - \frac{l(l-1)}{2(2l-1)} \cdot x^{l-2} + \ldots \right\}$$

(the legendre function, or polynomial).

Two useful properties of spherical harmonics are

$$Y_{1,m}^{*}(\theta,\phi) = (-1)^{-m} \cdot Y_{1,-m}(\theta,\phi)$$

where Y^{*} denotes the complex conjugate of Y and

$$G(r,\theta,\phi) = \sum_{1=0}^{\infty} \sum_{m=-1}^{1} (A_{1m}r^{1} + B_{1m}r^{-(1+l)}) \, Y_{1,m}(\theta,\phi) \qquad (iii)$$

The addition theorem for spherical harmonics is (I)

$$\frac{1}{|\underline{x} - \underline{x}'|} = \sum_{1=0}^{\infty} \sum_{m=-1}^{1} \left(\frac{4\pi}{21+}\right) \frac{r^{1}}{r'^{1+1}} \cdot Y_{1,m}^{*}(\theta',\phi') \cdot Y_{1,m}(\theta,\phi) \qquad (iv)$$

$\underline{x} = (r, \theta, \phi)$ ref (I) Jackson, J.D.

$\underline{x}' = (r',\theta',\phi')$ "Classical Electrodynamics" Wiley
N.Y. (1967).

APPENDIX II

Euler Angles

The orientation of any molecule in space requires the specification of three angular coordinates. These three angles are the Euler angles (1). Definitions of these angles are not all equally useful, and the literature is inconsistent in their definition. In this study a set of Euler angles involving rotation about each of the cartesian coordinate axes in turn is adopted. The definitions correspond to the concepts of yaw, pitch and roll used in aerodynamics.

The orientation of a molecule in space must be with respect to some fixed coordinate system representing the orientation of space. Such an arbitrary set of axes is shown in Fig. IIIix, they are the right handed set X,Y,Z; this is the space set. Rigidly attached to the molecule, and with the same origin as X,Y,Z, is another set of cartesians x,y,z; the body set. The Euler angles will define the orientation of x,y,z with respect to X,Y,Z. Rotation about axis x is the Euler angle alpha (α), rotation about y is angle beta (β) and about the z axis is the angle gamma (γ). All of these rotations are in an anticlockwise sense, when looking down the positive body axis toward the origin. A series of equations will be derived which will allow coordinates, originally stated in the body set, to be expressed in terms of the space set; for any given set of Euler angles.

The following order of operations is defined. When the two sets of coordinates are aligned the body set are displaced from the

Fig. III.xii

126.

The Euler Angles

Rotation α about x.

$R(\alpha)$

Rotation β about y

$R(\beta)$
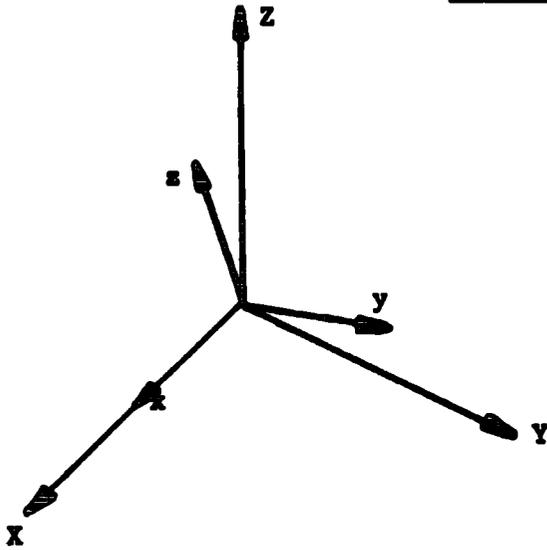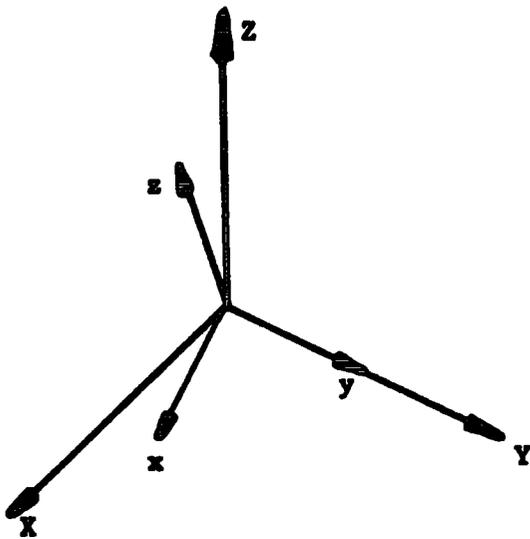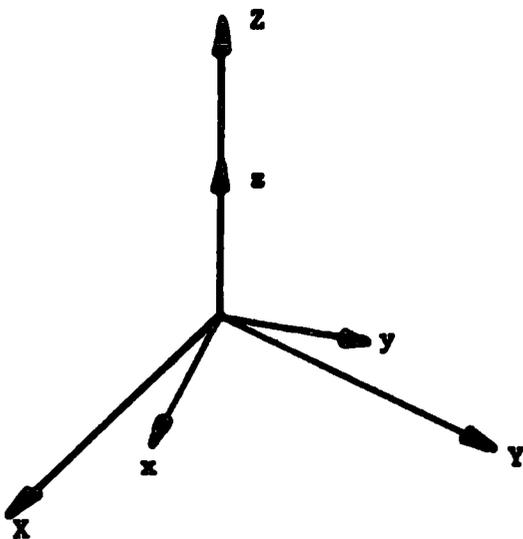
Rotation γ about z

$R(\gamma)$

space set by firstly a rotation, gamma, then beta and finally alpha.
Thus

$$\hat{R} = R_x(\alpha) \cdot R_y(\beta) \cdot R_z(\gamma) \qquad \text{(i)}$$

$\hat{R}$, displacement operator

$R_i(\theta)$, operator displacing the body
set by θ degrees about the ith
axis.

(The operators operate to the right in sequence from the right). Where
the body set is already displaced from the space set the two are
realigned by the inverse operation).

$$\hat{R}^{-1} = R_z(-\gamma) \cdot R_y(-\beta) \cdot R_x(-\alpha) \qquad \text{(ii)}$$

where the negative sign means
clockwise rotation.

The operators are simply given in matrix form. (2)

$$R_z(-\gamma) = \begin{vmatrix} \text{Cos } \gamma & -\text{Sin } \gamma & 0 \\ \text{Sin } \gamma & \text{Cos } \gamma & 0 \\ 0 & 0 & 1 \end{vmatrix} \qquad \text{(iii)}$$

$$R_y(-\beta) = \begin{vmatrix} \text{Cos } \beta & 0 & \text{Sin } \beta \\ 0 & 1 & 0 \\ -\text{Sin } \beta & 0 & \text{Cos } \beta \end{vmatrix} \qquad \text{(iv)}$$

$$R_x(-\alpha) = \begin{vmatrix} 1 & 0 & 0 \\ 0 & \cos\alpha & -\sin\alpha \\ 0 & \sin\alpha & \cos\alpha \end{vmatrix} \quad \text{(iv)}$$

which leads immediately to a matrix representation of $\hat{R}^{-1}$. However the matrix only operates on the column matrix of coordinates.

$$\hat{R}^{-1} \begin{vmatrix} x \\ y \\ z \end{vmatrix} = \begin{vmatrix} X \\ Y \\ Z \end{vmatrix} \quad \text{(vi)}$$

So that eq. (vi) can be written as three equations.

$X = (\cos\beta.\cos\gamma)x + (\sin\alpha.\sin\beta.\cos\gamma - \cos\alpha.\sin\gamma)y$

$\quad + (\cos\alpha.\sin\beta.\cos\gamma + \sin\alpha.\sin\gamma)z$

$Y = (\cos\beta.\sin\gamma)x + (\sin\alpha.\sin\beta.\sin\gamma + \cos\alpha.\cos\gamma)y$

$\quad + (\cos\alpha.\sin\beta.\sin\gamma - \sin\alpha.\cos\gamma)z$

$Z = (-\sin\beta)x + (\sin\alpha.\cos\beta)y + (\cos\alpha.\cos\beta)z \quad \text{(vii)}$

The equations were used to obtain the space coordinates from the body coordinates knowing the Euler angles.

ref.

(1) Margenan, H.
"The mathematics of Physics and Chemistry"
Van Nostrand (1943).

(2) Schutte, C.J.H.

"The wave mechanics of atoms molecules and ions"
Edward Arnold (1968).

APPENDIX III

The Programs and manipulation of results

Two computer programs were written to facilitate the
calculation of the electrostatic and steric potential of an ion
incorporated into an alkali metal halide. The mathematical basis
for these two sets of calculations are discussed in the text and
appendices I and II.

The programs are written in Fortran and were compiled and run
on the Cambridge University computer, an I.B.M. 370/155. The
electrostatic potential program compiles within 3 sec. and uses
between 45 sec. and 28 min. of central processor time for execution.
The more orientations of the incorporated ion, which are required
the longer the program takes. This program uses 100 K bytes of
storrage. The steric potential program compiles within 3 sec.
and uses between 3 min 53 sec. and 144 min. of central processor time
for execution. The larger number of steps in the steric potential
program makes its execution slower than that of the electrostatic
program. This program also uses 100 K bytes of store.
Acknowledgements are due to the computing staff of U.K.A.E.A. Harwell
for permission to use their Legendre function generating sub routine,
PNM.

The electrostatic potential of an ion in a binary crystal can
always be expressed in the form (2)

$$U = \frac{\alpha \cdot z^+q \cdot z^-q}{1} \qquad (1)$$

U, electrostatic potential of
the ion.

α, a constant characteristic of
the lattice, the Madelung
constant.

z^+q, the charge on the positive ion.

z^-q, the charge on the negative ion.

l, a characteristic length of the
crystal.

For the alkali metal halides this can be expressed as

$$U = 2.\frac{\alpha}{a}.q^+_{\cdot}q^- \qquad \qquad (ii)$$

q, electronic charge

a, the unit cell parameter

$$z^+ = z^- = 1$$

The Madelung constant for the case of sodium chloride lattice type
is 1.74756 (2). The charge on the ions is 4.803×10^{-10} Franklin
(absolute e.s.u.) and the nearest neighbour distance, for sodium
chloride itself is 2.7301×10^{-8} cm. This gives a calculated
electrostatic lattice energy from eq. (ii) of 212.47 Kcal mole^{-1}.
The incorporated ammonium ion is polyatomic and the simple Madelung
constant can no longer be used. The electrostatic program
calculates that part of the modified Madelung constant due to the
four protons. This is substituted into eq. (ii) and used along
with the fractional charge carried by each proton. (The value used
was, 0.2 of the electronic charge (3)). Such a calculation omits
the extra electrostatic energy gained by the presence of the central,

charged nitrogen atom.   Since this atom is on a lattice point the simple Madelung constant is used, along with the fractional charge carried by the nitrogen, in eq. (ii).   When the results are added this gives a value very close to the electrostatic energy of the pure host lattice.   The discrepancies between the two are caused by the ammonium ions orientation in the lattice.

The steric repulsion energy program requires more than the fundamental constants which were used in the electrostatic calculations.   Each type of ion has associated with it a characteristic radius which can be used to calculate the repulsion energy using eq. (2.2i).   These are Huggins basic radii and several compilations of them are known (2, 1).   Such radii are not strictly applicable to these calculations, since they were obtained from the pure salts.   However they should provide good relative values for the repulsion energies.   The list of basic radii given by Tosi (1964) were used for the alkali metal halide ions (see Table IIIviii).   The basic radius of the ammonium ion protons was calculated, after Waddington (1971).   The crystallographic data of the ordered ammonium halides was used with the known nitrogen-hydrogen bond length in the ammonium, 1.03Å (3).   The ionic radius of the halides in these salts was taken from Tosi (1963).   A contact radius was thus obtained, this was taken to be the ionic radius of the protons. Assuming a linear relationship between the ionic and basic radii a basic radius for the proton was interpolated from known data.   (This radius is also given in Table IIIviii).   The value of B, used in eq. (2.2(i)), was 0.338×10^{-12} erg molecule^{-1}.   The repulsion energy

Table III.viii

**The basic radii of the ions used in the repulsion
energy calculation program.**

Ion	Basic radius, Å
Na	1.170
K	1.463
Rb	1.587
Cl	1.585
Br	1.716
I	1.907
H	0.57

ref. Tosi (1964)

of the central nitrogen atom was omitted.

References

1. Tosi, M.P.   J. Phys. Chem. Solids., 25, 45 (1964).

2. Waddington, T.C.   Adv. Inorg. and Radiochem.   1, 157 (1959).

3. Waddington, T.C.   Molecular Physics   21, 761 (1971).

```
C THIS PROGRAM IS INTENDED TO DETERMINE THE POTENTIAL SURFACE SEEN BY
C A MOLECULAR ION ROTATING WITHIN AN IONIC CRYSTAL
C
C  THE PROGRAM ASSUMES
C                1: POINT CHARGES AND MASSES
C   ·    ·       2: UNHINDERED ROTATION ON ALL AXIES
C                3: FIXED CENTER OF MASS
C
C
C  THE PROGRAM USES EULER ANGLES TO DETERMINE THE GEOMETRY OF THE ION
C  WITHIN THE CRYSTAL, THUS GREAT CARE MUST BE TAKEN IN ENTERING THE
C  INITIAL POSITIONS  OF ATOMS.
       IMPLICIT REAL*8(A-H,O-Z)
       COMMON VPT
       DIMENSION VPT(37,37)
       REWIND 7
C      SET UP THE B-H BOND ANGLES.
       READ(5,10) R
   10 FORMAT(F8.4)
       READ(5,40) BH1THE,BH1THI
       READ(5,40) BH2THE,BH2THI
       READ(5,40) BH3THE,BH3THI
       READ(5,40) BH4THE,BH4THI
   40 FORMAT(2F8.4)
       WRITE(6,170)
  170 FORMAT(10X,' POLAR COORDINATES OF THE PROTONS ',//
      X,15X,' THETA ',8X,' THI ',/)
       WRITE(6,160) BH1THE,BH1THI,BH2THE,BH2THI,BH3THE,BH3THI
      X, BH4THE,BH4THI
  160 FORMAT(4(14X,F8.4,5X,F8.4,/))
       WRITE(6,165) R
  165 FORMAT(15X,' RADIUS ',2X,F6.4,/)
C      SET UP THE INITIAL ANGLE VALUES FOR
C      ALPHA
C      BETA ·
C      GAMMA
       ALPHA = 0.0
       BETA = 0.0
       GAMMA=0.0
   20 VPTSUM=0.0
       CALL POLAR(BH1THE,BH1THI,ALPHA,BETA,GAMMA,THETA,THI,R)
       VPTSUM=VPTSUM+VPTR(THETA,THI,R)
       CALL POLAR(BH2THE,BH2THI,ALPHA,BETA,GAMMA,THETA,THI,R)
       VPTSUM=VPTSUM+VPTR(THETA,THI,R)
       CALL POLAR(BH3THE,BH3THI,ALPHA,BETA,GAMMA,THETA,THI,R)
       VPTSUM=VPTSUM+VPTR(THETA,THI,R)
       CALL POLAR(BH4THE,BH4THI,ALPHA,BETA,GAMMA,THETA,THI,R)
       VPTSUM=VPTSUM+VPTR(THETA,THI,R)
       I = IFIX(SNGL(BETA)) / 5 + 1
       J = IFIX(SNGL(ALPHA)) /5 + 1
       VPT(I,J) = VPTSUM
       ALPHA= ALPHA + 5.0
       IF(ALPHA.LT.182.0) GO TO 20
       ALPHA = 0.0
       IF(BETA.GT.35.2.AND.BETA.LT.35.4)BETA=35.0
       BETA = BETA + 5.0
       IF(BETA.GT.34.9.AND.BETA.LT.35.1)BETA=35.275
       IF(BETA.LT.182.0) GO TO 20
       CALL PRNI(GAMMA,R)
       STOP
       END
```

```fortran
      SUBROUTINE POLAR(BHT,BHTH,ALPH,BET,GAMM,THETA,THI,R)
      IMPLICIT REAL*8(A-H,O-Z)
C     THIS SUBROUTINE WORKS OUT THE ANGLES THETA AND THI FOR THE SPECIFI
C     BOND POSITION USING CARTESIAN CO-ORDINATES THEN POLAR CO-URDINATES
C     CONVERT RH BOND ANGLES TO RADIANS.
      BHTHE=BHT*1.745D-2
      BHTHI=BHTH*1.745D-2
C     CALCULATE THE INDEPENDAT CO-ORDINATES .
C
      XI= R * DSIN(BHTHE) * DCOS(BHTHI)
      YI= R * DSIN(BHTHE) * DSIN(BHTHI)
      ZI= R * DCOS(BHTHE)
C
C     CONVERT THE SPACE ANGLES IN TO RADIANS.
      ALPHA=ALPH*1.745D-2
      BETA=BET*1.745D-2
      GAMMA=GAMM*1.745D-2
C
C
C     CALCULATE THE DEPENDANT CO-ORDINATES X,Y, Z
C
C
C
      X1=DCOS(BETA)*DCOS(GAMMA)
      Y1=DSIN(ALPHA)*DSIN(BETA)*DCOS(GAMMA) - DCOS(ALPHA)*DSIN(GAMMA)
      Z1=DCOS(ALPHA)*DSIN(BETA)*DCOS(GAMMA) + DSIN(ALPHA)*DSIN(GAMMA)
      X=X1*XI +Y1*YI +Z1*ZI
C
C
      X2=DCOS(BETA)*DSIN(GAMMA)
      Y2=DSIN(ALPHA)*DSIN(BETA)*DSIN(GAMMA) + DCOS(ALPHA)*DCOS(GAMMA)
      Z2=DCOS(ALPHA)*DSIN(BETA)*DSIN(GAMMA) - DSIN(ALPHA)*DCOS(GAMMA)
      Y=X2*XI +Y2*YI +Z2*ZI
C
C
      X3= - DSIN(BETA)
      Y3= DSIN(ALPHA)*DCOS(BETA)
      Z3= DCOS(ALPHA)*DCOS(BETA)
      Z=X3*XI +Y3*YI +Z3*ZI
C
C     CALCULATE THE POLAR CO-ORDINATES THETA THI
      ARG1 = Z / R
      ARG2=Y/X
      ARG1=DABS(ARG1)
      ARG2=DABS(ARG2)
   73 THETA=DARCOS(ARG1)
      THI=DATAN(ARG2)
C     CONVERT THETA AND THI INTO DEGREES.
      THETA=THETA/1.745D-2
      THI=THI/1.745D-2
      IF(Y.LT.0.0) GO TO 100
      GO TO 400
  100 IF(X.LT.0.0) GO TO 200
      GO TO 300
  200 THI=THI+180.00
      GO TO 600
  300 THI=360.00-THI
      GO TO 600
  400 IF(X.LT.0.0) GO TO 500
      GO TO 600
  500 THI=180.00-THI
  600 CONTINUE
      IF(Z.LT.0.0) GO TO 700
      GO TO 800
  700 THETA=180.0-THETA
  800 CONTINUE
C
   75 CONTINUE
      RETURN
      END
```

```
      FUNCTICN VPTR(THETA,THI,R)
      IMPLICIT REAL*8(A-H,O-Z)
      PI=3.14159
C     SET UP THE CCNSTANTS SO,S4,S4,S8,S10
      VPTR=0.0
      S0=-1.76267
      S4=+4.542 *DSQRT((4.0*PI)/9.0)
      S6=-1.572 *DSQRT((4.0*PI)/13.0)
      S8=-0.3063 *DSQRT((4.0*PI)/17.0)
      S10=0.0
   20 CONTINUE
C     CALCULATE Y4 TERM
      YSM4=0.0
      N=4
      M=4
    1 YSM4=YSM4+YLM(THETA,THI,N,M)
    2 YSM4=YSM4+YLM(THETA,THI,N,M)
      M=0
    3 Y4=(5.0/14.0)**0.5*YSM4+YLM(THETA,THI,N,M)
C     CALCULATE Y6 TERM
      YSM6=0.0
      N=6
      M=4
    4 YSM6=YSM6+YLM(THETA,THI,N,M)
    5 YSM6=YSM6+YLM(THETA,THI,N,M)
      M=0
    6 Y6=-(7.0/2.0)**0.5*YSM6+YLM(THETA,THI,N,M)
C     CALCULATE THE FIRST PART OF THE Y8 TERM
      YSM8I=0.0
      N=8
      M=8
    7 YSM8I=YSM8I+YLM(THETA,THI,N,M)
    8 YSM8I=YSM8I+YLM(THETA,THI,N,M)
C     CALCULATE THE SECOND PART OF THE Y8 TERM
      YSM8J=0.0
      M=4
    9 YSM8J=YSM8J+YLM(THETA,THI,N,M)
   11 YSM8J=YSM8J+YLM(THETA,THI,N,M)
C     CALCULATE THE FINAL Y8 TERM
      M=0
   12 Y8=(5.0/3.0)*(13.0/110.0)**0.5*YSM8I+
     1    (1.0/3.0)*(14.0/11.0)**0.5*YSM8J+YLM(THETA,THI,N,M)
C     CALCULATE THE FRST PART OF THE Y10 TERM
      YSM10I=0.0
      N=10
      M=8
   13 YSM10I=YSM10I+YLM(THETA,THI,N,M)
   14 YSM10I=YSM10I+YLM(THETA,THI,N,M)
C   . CALCULATE THE SECOND PAT OF THE Y10 TERM
    . YSM10J=0.0
      M=4
   16 YSM10J=YSM10J+YLM(THETA,THI,N,M)
   17 YSM10J=YSM10J+YLM(THETA,THI,N,M)
C     CALCULATE THE FINAL Y10 TERM
      M=0
   18 Y10=-(187.0/130.0)**0.5*YSM10I-
     1      6.0*(11.0/390.0)**0.5*YSM10J+YLM(THETA,THI,N,M)
C     CALCULATE THE FINAL TERM VPTR
  100 VPTR = S0 + S4*R**4*Y4 + S6*R**6*Y6 + S8*R**8*Y8 + S10*R**10*Y10
      RETURN
      END
```

```
      FUNCTION YLM(THETA,THI,N,M)
C     FUNCTION CALCULATES SPHERICAL HARMONIC Y(L,M(THETA,THI))
C     FOR FIXED VALUES OF THETA & THI.WHERE L=( AND USES THE R.H.E.L.
C     FUNCTION PNM FOR CALCULATING ASSOCIATED LEGENDRE POLYNOMIAL.
     ·IMPLICIT REAL*8(A-H,O-Z)
C     · N= THE ORDER AND M = THE DEGREE ,THFT= THE BOND ANGLE AND
C     THI THE ROTATIONAL ANGLE
      PI=3.14159
      XTHETA=DCOS(THETA*1.745D-2)
      K=N-M
      J=N+M
C     K AND J ARE THE ARGUMENTS OF THE FACTORIAL FUNCTION NFACT
      A=DFLOAT(2*N+1)/(4.0*PI)
      B=FACT(K)/FACT(J)
      YLM=DSQRT(A*B)*PNM(XTHETA,N,M,IER)*CSTHIM(M,THI)
   1  CONTINUE
      RETURN
      END




      FUNCTION CSTHIM(M,THI)
      IMPLICIT REAL*8(A-H,O-Z)
      THIM=THI*1.745D-2*DFLOAT(M)
      CSTHIM=DCOS(THIM)
      RETURN
      END




      FUNCTION FACT(N)
      IMPLICIT REAL*8(A-H,O-Z)
      A=DFLOAT(N)
      FACT=1.0    .
      IF (A.GT.0.0) GO TO 10
      RETURN
   10 FACT=FACT*A
      A=A-1.0
      IF(A.GT.0.0) GO TO 10
      RETURN
      END
```

```
C      FUNCTION PNM
       FUNCTION PNM(X,N,M,IER)
       IMPLICIT REAL*8 (A-H,O-Z)
C
C
C      WHERE M=0, OR ANY POSITIVE NUMBER.    M=ABS(M) IS USED.
C      TO CALCULATE LEGENDRE POLYNOMIAL OF ORDER N & DEGREE M,
C      FOR COS(THETA)=X.        IER IS ERROR FLAG.
C      AT FIRST PMM ( M TH ORDER & M TH DEGREE) IS EVALUATED FROM
C      RECURSION RELATION
C      P(N,M) = P(N-2,M)+(2*N-1)*P(N-1,M-1)*SIN(THETA)
C      P(N,M)=0, IF N IS LESS THAN M.
C      PNM IS THEN OBTAINED FROM A SECOND RECURSION RELATION
C      PNM = ((2*N-1)*X*P(N-1,M) - (N+M-1)*P(N-2,M))/(N-M)
C
C      REF :  SPECIAL FUNCTIONS .. .. BY W.W.BELL (VAN NOSTRAND, 1968)
C
C
       IER=0
       IF( M.LT.0) M=-M
       IF(N.LT.0.OR.M.GT.N) GO TO 180
       IF(X*X.GT.1.0) GO TO 150
       PNM=1.0
       IF(M.GT.0) GO TO 10
       IF(N.EQ.0) GO TO 100
       PNM=X
       IF(N.EQ.1) GO TO 100
       NL=2
       PHIGH=1.0
       GO TO 30
C
   10 SINE= DSQRT( 1.0 - X*X)
       DO 20 K=1,M
       PNM= DFLOAT(K+K-1)*SINE*PNM
   20 CONTINUE
       IF(N.EQ.M) GO TO 100
       PHIGH=0.0
       NL=M+1
C
   30 CONTINUE
       XM=DFLOAT(M)
       DO 50 L=NL,N
       XN=DFLOAT(L)
       PLOW=PHIGH
       PHIGH=PNM
       PNM= ((XN+XN-1.0)*X*PHIGH - (XN+XM-1.0)*PLOW)/(XN-XM)
   50 CONTINUE
  100 RETURN
C
  150 CONTINUE
       IER=1
       PRINT 160
  160 FORMAT( / ' COS(THETA) FOR LEGENDRE POLYNOMIAL EXCEEDS UNITY AND
      1THEREFORE IER SET TO ONE & PNM TO ZERO. ' / )
  180 PNM=0.0
       RETURN
       END
```

```
            SUBROUTINE PRNT(GAMMA,R)
      IMPLICIT REAL*8(A-H,O-Z)
      COMMON /PREP/ VPT
      DIMENSION VPT(37,37)
      WRITE(6,10) R, GAMMA
10 FORMAT('1',35X,'TABLE OF VPT ENERGIES FOR'/13X,'R = ',F8.4/
   19X,'GAMMA=',F6.2)
      WRITE(6,20)
20 FORMAT(/2X,'BETA',55X,'ALPHA'/)
      WRITE(6,30)
30 FORMAT(14X,'0.00',6X,'5.00',5X,'10.00',5X,'15.00',5X,'20.00',5X,
   1'25.00',5X,
   2'30.00',5X,'35.00',5X,'40.00',5X,'45.00',5X,'50.00',5X,'55.00')
      BETA= 0.0
      DO 50 I=1,37
      WRITE(6,40) BETA,(VPT(I,J),J=1,12)
      IF(BETA.EQ.35.28)BETA=35.0
      BETA = BETA + 5.0
      IF(BETA.EQ.35.0)BETA=35.28
40 FORMAT(1X,F6.2,5X,12(F8.5,2X))
50 CONTINUE
      WRITE(6,10) R,GAMMA
      WRITE(6,20)
      WRITE(6,60)
60 FORMAT(12X,'60.00',5X,'65.00',5X,'70.00',5X,'75.00',5X,'80.00',5X,
   1'85.00',5X,'90.00',5X,'95.00',4X,'100.00',4X,'105.00',4X,'110.00',
   24X,'115.00')
      BETA = 0.0
      DO 70 I=1,37
      WRITE(6,40) BETA,(VPT(I,J),J=13,24)
      IF(BETA.EQ.35.28)BETA=35.0
      BETA = BETA + 5.0
      IF(BETA.EQ.35.0)BETA=35.28
70 CONTINUE
      WRITE(6,10) R,GAMMA
      WRITE(6,20)
      WRITE(6,80)
80 FORMAT(12X,'120.00',4X,'125.00',4X,'130.00',4X,'135.00',4X,
   1'140.00',4X,'145.00',4X,'150.00',4X,'155.00',
   2'X,'160.00',4X,'165.00',4X,'170.00',4X,'175.00')
      BETA = 0.0
      DO 90 I=1,37
      WRITE(6,40) BETA,(VPT(I,J),J=25,36)
      IF(BETA.EQ.35.28)BETA=35.0
      BETA = BETA + 5.0
      IF(BETA.EQ.35.0)BETA=35.28
90 CONTINUE
      WRITE(6,100)
100 FORMAT(/40X,'-----------*********-----------*********----------')
      WRITE(6,110)
110 FORMAT(/30X,'TABLE OF VALUES FOR VPT, ALPHA=180.0,BETA=0.0 -180.0
   1'/)
      WRITE(6,120)
120 FORMAT(20X,'ALPHA',36X,'BETA')
      WRITE(6,130)
```

```
130  FORMAT (31X,'0.00',6X,'10.00',5X,'15.00',5X,'20.00',5X,'25.00',5X,
    1'30.00',5X,'35.00',5X,'40.00')
     ALPHA=180.0
     J=37
     WRITE(6,140) ALPHA,(VPT(I,J),I=1,9)
140  FORMAT(20X,F6.2,4X,10(F8.5,2X))
     WRITE(6,150)
150  FORMAT(30X,'45.00',5X,'50.00',5X,'55.00',5X,'60.00',5X,'65.00',5X,
    1'70.00',5X,'75.00',5X,'80.00',5X,'85.00')
     WRITE(6,140) ALPHA,(VPT(I,J),I=10,18)
     WRITE(6,160)
160  FORMAT(/30X,'90.00',5X,'95.00',4X,'100.00',4X,'105.00',4X,'110.00'
    1,4X,'115.00',4X,'120.00',4X,'125.00',4X,'130.00')
     WRITE(6,140) ALPHA,(VPT(I,J),I=19,27)
     WRITE(6,170)
170  FORMAT(/29X,'135.00',4X,'140.00',4X,'145.00',4X,'150.00',4X,
    1'155.00',4X,'160.00',4X,'165.00',4X,'170.00',4X,'175.00',4X,
    2'180.00')
     WRITE(6,140) ALPHA,(VPT(I,J),I=28,36)
     RETURN
     END
```

```
            IMPLICIT REAL*8(A-H,O-Z)
            COMMON /PEP1/ X,Y,Z,RAD,UCA,UCB,UCC
            COMMON /KEP2/ NEACH,NIONS
            COMMON /PPLP/ VREP
            DIMENSION X(20,50),Y(20,50),Z(20,50),RAD(20),NEACH(20)
            DIMENSION VREP(37,37)
C.
C.
C.      THIS PROGRAM IS INTENDED TO CALCULATE THE TOTAL REPULSION
C.      OF A MOLECULE IN ITS DIFFERENT ORIENTATIONS IN A HOST
C.      LATTICE.
C.
C.      ANY GUEST MOLECULE GEOMETRY OF FOUR PROTONS CAN BE USED.
C.
C.      ONLY HOST LATTICES OF CUBIC SYMMETRY CAN BE TREATED.
C.
C.
C.      READ IN SAMPLE ION DATA
C.      NIONS = THE NUMBER OF DIFFERENT TYPES OF IONS PRESENT IN THE UNIT CEL
C.      NEACH(I) = THE NUMBER OF TYPE I IONS PRESENT
C.      RAD(I) = THE BASIC RADIUS OF THE TYPE I ION
C.
            READ(5,10) NIONS
            READ(5,10)(NEACH(I),I=1,NIONS)
            READ(5,15)(RAD(I),I=1,NIONS)
C.
C.      READ IN THE LATTICE CO-ORDINATES OF THE SAMPLE IONS
C.
            DO 20 I=1,NIONS
            N=NEACH(I)
            READ(5,25)(X(I,J),Y(I,J),Z(I,J),J=1,N)
         20 CONTINUE
C.
C.
C.      READ IN THE CENTRAL ATOM CO-ORDINATES AND THE BASIC RADIUS
C.      OF THE PROTON.
C.
            READ(5,30) BX,BY,BZ,PRAD
            READ(5,40) BH1THE,BH1THI
            READ(5,40) BH2THE,BH2THI
            READ(5,40) BH3THE,BH3THI
            READ(5,40) BH4THE,BH4THI
         40 FORMAT(2F8.4)
            READ(5,45) R
         45 FORMAT(F6.4)
C.
C.      READ IN THE UNIT CELL DIMENSIONS
C.
            READ(5,35) UCA,UCB,UCC
C.
C.      WRITE OUT UNIT CELL INFORMATION.
C.
            WRITE(6,100)
        100 FORMAT('1',10X,'BASIC UNIT CELL INFORMATION'/
           110X,'ION TYPE',3X,'NUMBER',3X,'RADIUS',3X,'COORDINATES'/
           23 X,'X',7X,'Y',7X,'Z')
            DO 110 I=1,NIONS
            N=NEACH(I)
```

```
      WRITE(6,130) I,N,RAD(I),(X(I,J),Y(I,J),Z(I,J),J=1,N)
130 FORMAT(12X,I3,6X,I3,6X,F5.4,3F8.4/(36X,3F8.4))
110 CONTINUE
      WRITE(6,140) BX,BY,BZ,PRAD
140 FORMAT(//,10X,' CENTRAL ATOM CO-ORDINATE ',3(2X,F6.4)/
     1  10X,' PROTON BASIC RADIUS ',5X,F6.4//)
      WRITE(6,150) UCA,UCB,UCC
150 FORMAT(10X,'A=',F8.4/10X,'B=',F8.4/10X,'C=',F8.4)
      WRITE(6,170)
170 FORMAT(10X,' POLAR COORDINATES OF THE PROTONS ',//
     X,15X,' THETA ',6X,' THI ',/)
      WRITE(6,160) BH1THE,BH1THI,BH2THE,BH2THI,BH3THE,BH3THI
     X,BH4THE,BH4THI
160 FORMAT(4(14X,F8.4,5X,F8.4,/))
      WRITE(6,165) R
165 FORMAT(15X,' RADIUS ',2X,F6.4,/)
C.
C.    SET UP THE INITIAL ANGLE VALUES FOR ALPHA , BETA , AND GAMMA.
C.
      ALPHA=0.0
      BETA = 0.0
      GAMMA=0.0
      SUMREP= 0.0
50 SREPEN = 0.0
      CALL POLAR2(BH1THE,BH1THI,ALPHA,BETA,GAMMA,BX,BY,BZ,R,PX,PY,PZ)
      CALL REPULS(PX,PY,PZ,PRAD,SUMREP,R)
      SREPEN =SREPEN + SUMREP
      CALL POLAR2(BH2THE,BH2THI,ALPHA,BETA,GAMMA,BX,BY,BZ,R,PX,PY,PZ)
      CALL REPULS(PX,PY,PZ,PRAD,SUMREP,R)
      SREPEN = SREPEN + SUMREP
      CALL POLAR2(BH3THE,BH3THI,ALPHA,BETA,GAMMA,BX,BY,BZ,R,PX,PY,PZ)
      CALL REPULS(PX,PY,PZ,PRAD,SUMREP,R)
      SREPEN = SREPEN + SUMREP
      CALL POLAR2(BH4THE,BH4THI,ALPHA,BETA,GAMMA,BX,BY,BZ,R,PX,PY,PZ)
      CALL REPULS(PX,PY,PZ,PRAD,SUMREP,R)
      SREPEN = SREPEN + SUMREP
      I = IDINT(BETA) /5 + 1
      J =IDINT(ALPHA)/5 +1
      VREP(I,J)=SREPEN
      IF(I.EQ.1.AND.J.EQ.1) GO TO 60
      GO TO 70
60 WRITE(6,46) SREPEN
46 FORMAT( ' FIRST ELEMENT ',E14.6)
70 CONTINUE
      ALPHA = ALPHA + 5.0
      IF(ALPHA.LE.180.0) GO TO 50
      ALPHA = 0.0
      IF(BETA.GT.35.2.AND.BETA.LT.35.4)BETA=35.00
      BETA = BETA + 5.0
      IF(BETA.GT.34.9.AND.BETA.LT.35.1)BETA=35.275
      IF(BETA.LE.90.0)GO TO 50
      CALL PRNT(GAMMA,R)
      STOP
10 FORMAT(2013)
15 FORMAT(10F6.4)
25 FORMAT(12F6.4)
30 FORMAT(4F6.4)
35 FORMAT(3F8.4)

      END
```

```
            SUBROUTINE REPULS (PX,PY,PZ,PRAD,SUMREP,R)
           .IMPLICIT REAL*8(A-H,O-Z)
            COMMON /REP1/ X,Y,Z,RAD,UCA,UCB,UCC
            COMMON /REP2/NEACH,NIONS
            DIMENSION X(20,50),Y(20,50),Z(20,50),RAD(20),NEACH(20)
C.          SUBROUTINE TO CALCULATE THE TOTAL REPULSION OF THE UNIT-CELL
C.          AGAINST A REFINED PROTON.
C.          THE SUMMATION IS CARRIED OUT IN PARTS WITH NUMBER OF PARTS BEING
C.          EQUAL TO THE NUMBER OF DIFFERENT IONS.
C.          THE IDEAS WERE SIMPLIFIED AND DEVELOPED FROM DON JENKINS
C.          REPULSION ENERGY PROGRAM
C.
C.          SET UP THE CONSTANTS REQUIRED FOR A CUBIC UNIT CELL.
C.
            RHO= 0.345
            B=1.0
            AA=UCA*PX
            BB=UCB*PY
            CC=UCC*PZ
            SUMREP = 0.0
C.
C.          BEGIN INITIAL LOOP OF CALCULATION.
C.
            DO 15 I=1,NIONS
            N =NEACH(I)
            SUMR =0.0
            DO 17 J=1,N
C.
C.          BEGIN THE LOOP TO CALCULATE THE REPULSION ENERGY OF THE REFERENCE
C.          PROTON AGAINST THE TARGET ION.
C.
            SUM=0.0
            DO 20 LH=1,5
            LHI=LH-3
            FLAGD=0.0
            DD1=X(I,J)+LHI
            IF(DD1.GT.0.49.AND.DD1.LT.0.51)FLAGD=1.0
            DD=UCA*DD1
            DO 20 LK=1,5
            LKI=LK-3
            FLAGE=0.0
            EE1=Y(I,J)+LKI
            IF(EE1.GT.0.49.AND.EE1.LT.0.51)FLAGE=1.0
            EE=EE1*UCB
            DO 20 LL=1,5
            LLI=LL-3
            FLAGF=0.0
            FF1=Z(I,J)+LLI
            IF(FF1.GT.0.49.AND.FF1.LT.0.51)FLAGF=1.0
            FF=FF1*UCC
            FLAGS=FLAGE+FLAGF+FLAGD
            IF(FLAGS.GT.2.9.AND.FLAGS.LT.3.1)GO TO 20
C.
C.          CALCULATE THE PERPENDICULAR DISTANCE S.
C.
            S=DSQRT'(AA-DD)**2+(BB-EE)**2+(CC-FF)**2)
            SRHO=S/RHO
            IF(SRHO.GT.170.0)GO TO 20
          3 CONTINUE
```

```
C.
C.      SUM FOR THE RECIPRECAL SPACE.
C.
        .SUM=SUM+DEXP(-SPHO)
   20 CONTINUE
C.
C.      SUM FOR ALL LIKE IONS IN THE UNIT-CELL AND MULTIPLY BY THE BASIC
C.      RADDI
C.
        SUMR=SUMR + B*DEXP((RAD(I)+PRAO)/RHO) *SUM
   17 CONTINUE
C.
C.      SUM FOR ALL IONS IN THE UNIT-CELL TO GIVE TOTAL REPULSION.
C.
        SUMREP =SUMREP + SUMR
   15 CONTINUE
        RETURN
        END
```

```fortran
      SUBROUTINE POLAR2(BHTH,BHT,ALPH,BET,GAMM,BX,BY,BZ,R,PX,PY,PZ)
      IMPLICIT REAL*8(A-H,O-Z)
C.
C.    THIS SUBROUTINE WORKS OUT THE CARTESIAN CO-ORDINATES X,Y,Z FOR THE
C.    POSITION OF THE PROTON ON THE SURFACE OF THE SPHERE. THE SUBROUTINE
C.    IS A MODIFY VERSION OF POLAR USED IN THE  ELECTROSTATIC PROGRAM.
C.
      BHTHE=BHTH*1.745D-2
      BHTHI=BHT*1.745D-2
C     CALCULATE THE INDEPENDAT CO-ORDINATES
C
   10 CONTINUE
      XI= R * DSIN(BHTHE) * DCOS(BHTHI)
      YI= R * DSIN(BHTHE) * DSIN(BHTHI)
      ZI= R * DCOS(BHTHE)
C
C     CONVERT THE SPACE ANGLES IN TO RADIANS.
   20 CONTINUE
      ALPHA=ALPH*1.745D-2
      BETA=BET*1.745D-2
      GAMMA=GAMM*1.745D-2
C
C     CALCULATE THE DEPENDANT CO-ORDINATES X,Y, Z
C
   40 CONTINUE
      X1=DCOS(BETA)*DCOS(GAMMA)
      Y1=DSIN(ALPHA)*DSIN(BETA)*DCOS(GAMMA) - DCOS(ALPHA)*DSIN(GAMMA)
      Z1=DCOS(ALPHA)*DSIN(BETA)*DCOS(GAMMA) + DSIN(ALPHA)*DSIN(GAMMA)
      X=X1*XI +Y1*YI +Z1*ZI
C
C
      X2=DCOS(BETA)*DSIN(GAMMA)
      Y2=DSIN(ALPHA)*DSIN(BETA)*DSIN(GAMMA) + DCOS(ALPHA)*DCOS(GAMMA)
      Z2=DCOS(ALPHA)*DSIN(BETA)*DSIN(GAMMA) - DSIN(ALPHA)*DCOS(GAMMA)
      Y=X2*XI +Y2*YI +Z2*ZI
C
C
      X3= - DSIN(BETA)
      Y3= DSIN(ALPHA)*DCOS(BETA)
      Z3= DCOS(ALPHA)*DCOS(BETA)
      Z=X3*XI +Y3*YI +Z3*ZI
C.
C.    CALCULATE THE PROTON LATTICE CO-ORDINATES.
C.
      PX = BX + X
      PY = BY + Y
      PZ = BZ + Z
C.
      RETURN
      END
```

CHAPTER IV

THE ALKALI METAL BOROHYDRIDE SALTS

In an ionic crystal there is a balance between the steric, repulsive, and electrostatic, attractive forces. These must influence the environment of every ion. These potential surfaces may be studied through the dynamics of a probe embedded within the crystal. The greater the symmetry of the lattice and the ion, used as a probe, the simpler the problem of analysis will become. The regular nature of the alkalic metal borohydride lattices, and the high symmetry of the borohydride ion, make them an ideal case for investigation. Their simplicity enables them to be treated by the models previously proposed; yet the symmetry of the borohydride ion is sufficiently non spherical to be influenced by the potential surfaces within the crystal. This study should be directly complimentary to the study of ammonium ions incorporated in several alkali metal halide lattices (see Section VI).

The alkali metal borohydrides have also been studied by other investigators. Their work, which was confined to heat capacity, crystal diffraction, and infrared measurements, is summarised as a preliminary to this study. Following this the experimental methods of preparing the salts used are described, together with the experiments which were conducted on them. Finally the results are presented and discussed.

1. Previous Studies.

1.1   Because the borohydrides are isoelectronic with the ammonium halides, several heat capacity studies covering the whole series of salts, typically from 15° to 300^OK, have been made (see Table IVi).   In all the salts, except the lithium (11), a λ point (variously called;   a gradual, continuous, smeared, rotational, second-order, and ammonium chloride type transition) occurs below room temperature.   This type of transition was first observed in the borohydrides by Johnston (1953), in the sodium salt.   Stockmayer (1953) interpreted the transition in terms of the ordering of the borohydride tetrahedra in the two equivalent sites.   The entropy change measured at the λ point by Johnston was partially explained by a crystal lattice change, occuring at the λ point, (observed by Abrahams (1954) see later).   However the excess entropy change, c.a. 1.2 cal $deg^{-1}mole^{-1}$(36), is sufficiently close to Rln 2, (the predicted entropy change in this type of order-disorder transition is, Rln 2 = 1.38 cal $deg^{-1}mole^{-1}$) considering the experimental difficulties, to warrant the assignment of the λ point to an order-disorder transition.   The Stockmayer model for the ordered, low temperature, phase of sodium borohydride is shown in Fig. IVi (measurements in the infrared have confirmed this structure, see later).   Measurements on the heat capacity curve below the point enabled Stockmayer to predict the fundamental librational mode at about $350cm^{-1}$, for the ordered phase.

The heat capacity measurements in the region 15 to 100^OK were fitted to an Eistein model, of lattice specific heats, the characteristic temperature, T_E, was found to be 500^OK.   This is

Table IVi.

Transition temperatures of the alkali metal borohydrides

	transition temperature $^{\circ}K$	references
$LiBH_4$	–	Hallet (1953)
$NaBH_4$	190	Abrahams (1954)
	189.9	Johnston (1953)
KBH_4	76	Stephenson (1955)
	77.16	Furakawa (1964)
$RbBH_4$	44	Stephenson (1955)
$CsBH_4$	27	Stephenson (1955)

equivalent to an Eistein oscillator frequency of about $350cm^{-1}$.

Provided that the librational motion of the borohydride is the major

contributing factor to the lattice specific heat this oscillator

frequency can be equated with the fundamental libratory frequency.

The λ point transitions observed by Stevenson (1955) for the

remaining borohydrides were interpreted by him in an exactly analogous

manner.   Infrared studies, discussed below, indicate that the

borohydrides of the heavier alkali metals retain their crystal

structure below the λ point, remaining cubic.

More recently Smith (1974) has attempted to fit a more refined

heat capacity model to the observed data for the sodium and potassium

borohydrides.   The hindered rotational levels of the ion in its

environment were computed and could be fitted to the observed heat

capacity data.   In the case of the sodium salt a good fit to all the

data points was obtained, and this gave an estimated librational

frequency of $240cm^{-1}$ (high temperature phase).   In the case of the

potassium salt the fit to available data was less good; the estimated

librational frequency was $244cm^{-1}$.

1.2   At room temperature all the alkali metal borohydride

salts, except for the lithium salt, have a simple rock salt lattice.

Sodate (1947) first showed that sodium borohydride conformed to this

structure, but was unable to locate the protons.   Abrahams (1954)

confirmed the early result and extended it to the remainder of the

series.   As could be expected the cell parameter increases with

increasing cationic size (see Table IVii).   Abrahams was unable

to refine any proton positions from his studies at room temperature.

Table IVii.   151.

Unit Cell Parameters of alkali metal borohydrides

	Unit cell type	dimensions $\overset{o}{A}$	temperature ^oK	references
$LiBH_4$	Orthorhombic	a 6.81 b 4.43 c 7.17		Harris (1947)
$NaBH_4$	Cubic	a 6.1635	298	Abrahams(1954)
		a 6.157	293	Ford (1954)
	tetragonal body centred	a 4.354 c 5.907	78	Abrahams(1954)
		a 4.353 c 5.909	90	Ford (1954)
KBH_4	Cubic	a 6.7272	298	Abrahams(1954)
		a 6.722	293	Ford (1954)
		a 6.636	90	
$RbBH_4$	Cubic	a 7.029	298	Abrahams(1954)
$CsBH_4$	Cubic	a 7.419	298	

Fig. IV.i

152.

The crystal structure of sodium borohydride in its low
temperature phase.

crystal parameters (Å)

	body centred	face centred
a	4.354	6.157
b	4.354	6.157
c	5.907	5.907

face centred
coordinates

body centred coordinates

⊖ , sodium ions
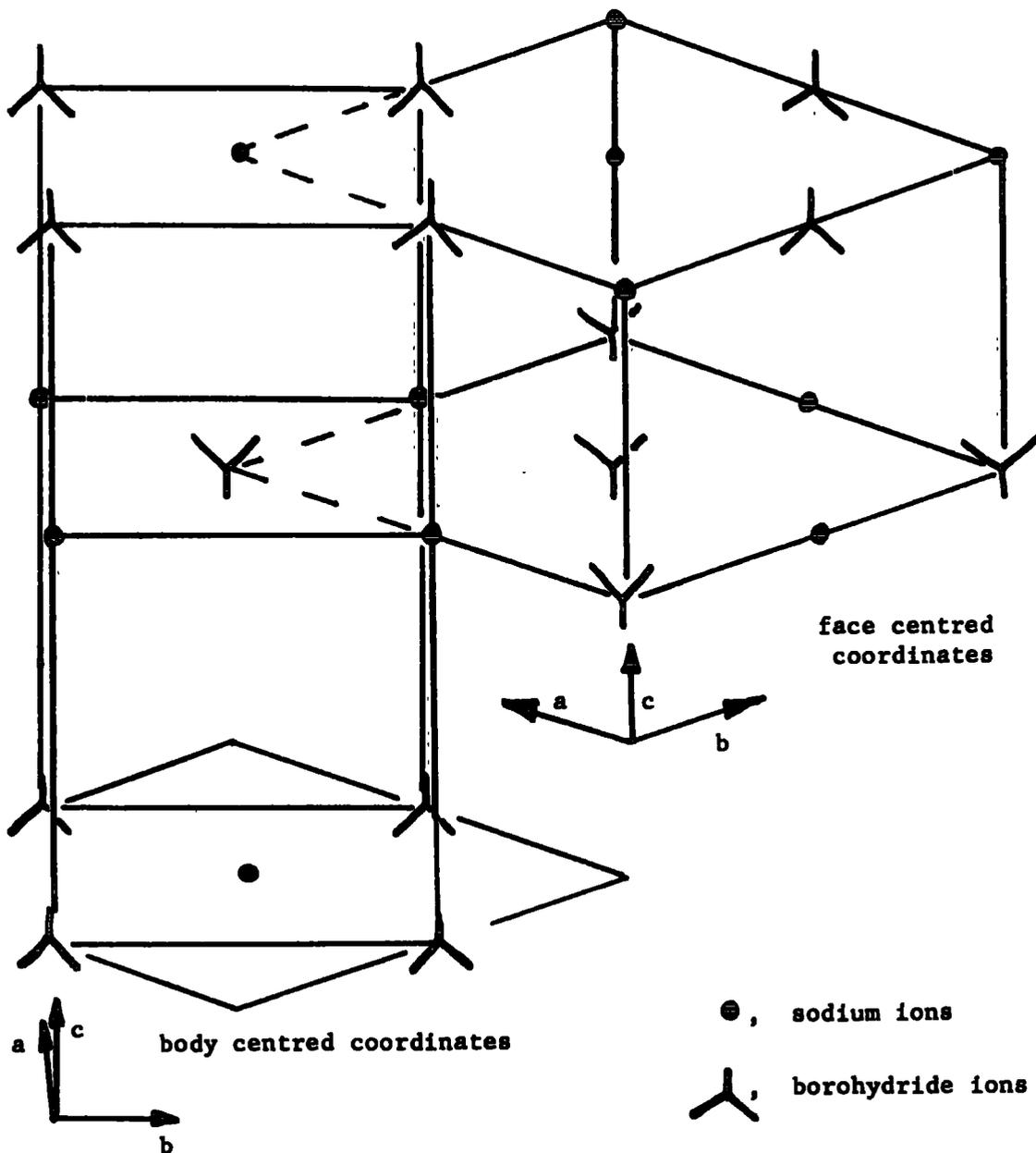
⅄ , borohydride ions

Data collected on the low temperature phase of the sodium salt showed it to have a tetragonal unit cell, consistant with the model proposed by Stockmayer (1953) (see Fig. IVi).   Peterson (1965) made the latest attempt to locate the borohydride protons by diffraction. Using neutron diffraction data from potassium borohydride he was able to determin a B-H bondlength of $1.26\overset{o}{A}$.   The data was most consistant with a disordered model, "half hydrogens" being located along body diagonals (in 32-fold positions).

The crystal structure of the lithium salt was studied by Harris (1947).   It was thought that the data showed considerable proton scattering.   The structure was given as an orthorhombic unit cell, and D_{2h}^{16} (Pcmn) space group; with a roughly tetrahedral environment of both ions.   The original note was not followed by a more detailed paper and there have been no confirmatory structures published.

1.3   The use of nuclear magnetic resonance techniques (N.M.R.) in investigating the solid state borohydrides started with Ogg (1954) who showed that the room temperature structure of the borohydride ion in sodium borohydride was tetrahedral.   Ford (1955) has made a study of the second moments of the proton resonance band.   Finally Tung Tsang (1969) has used a pulse technique to study the spin-lattice relaxation process.

In all substances there are two processes that allow those nuclii which are in a high energy spin state to relax back into a lower energy state.   These are the spin-lattice and spin-spin processes; where the relaxation is caused by interaction of the spin system with any other nuclei (the spin-lattice relaxation), or interaction

within the system itself (spin-spin relaxation). The processes
are characterised by times which are representative of the decay
rates of the signal via the two routes, by convention T_1 is the
spin-lattice relaxation time and T_2 is the spin-spin relaxation time.
Any signal is relaxed by both processes but should one pathway be
extremely efficient, i.e. of short characteristic time, then relaxation
will take place mainly via that route. In a molecular system both
T_1 and T_2 can be considered to have contributions from within the
molecule, intramolecular, and from the remainder of the molecules,
intermolecular. In relaxation studies, before values for one
particular relaxation process can be obtained, account must be taken
of all the other processes.

In a solid where reorientation of a molecular entity is prevented
by a barrier, of height Vo, the instantaneous number of molecules which
can surmount the barrier will be proportional to

$$exp \ (-Vo/kT)$$

As could be expected reorientation will have a profound effect on
relaxation. In the case of spin-spin relaxation the largest effect
is seen in the intramolecular component (10). As the reorientation
becomes closer to, and finally more frequent than, the Larmor precession
frequency the intramolecular relaxation becomes averaged out in time.
Meanwhile intermolecular T_2 values are little affected. In the case
of spin-lattice relaxation the cause of the relaxation are transitions
between the librational levels of the molecule in the well. Transitions
from the ground state librational level to a level close to or above

Table IViii.

Activation Energies of the Alkali metal borohydrides, obtained from N.M.R. data

Borohydride	Activation Energy from N.M.R. Kcal/mole	
	(1)	(2)
Li		4.7 and 3.8
Na cubic phase		2.7
Na tetragonal phase	2.4	3.5
K	3.8	3.55
Rb	3.9	
Cs		

Ref. (1) Ford (1955)

(2) Tung Tsang (1969)

the barrier top are most effective at relaxing the signal (38).
Assuming a temperature dependant distribution of the energy of the
librating molecule, estimates of Vo can be obtained from studies of
the relaxation variations with temperature. The activation energies
obtained will represent the average energy possessed by a molecule when
it undergoes reorientation.

The work done by Ford (1955) was a second moment analysis of the
band shape of the proton resonance signal in the Alkali metal borohydrides
at different temperatures. Such resonances are generally, in crystals
like the borohydrides, (or ammonium salts) broadened by the intramolecular
spin-spin process. An earlier study of the ammonium salts by
Gutowsky (1950) provided the relationship between the intramolecular
spin-spin relaxation time and the barrier height, Vo. Unfortunately
Ford made no study of spin-lattice relaxation times, although these
must have made some contribution to his line width. The results he
obtained for the activation energies are given in Table IViii.

The study of the change in T_1 by Tung Tsang (1969) over a
different temperature range than Ford was more thorough. Corrections
were made to allow for the spin-spin relaxation process, some values
being taken from Ford's paper. The results Tung Tsang obtained for
the activation energies are also shown in Table IViii. These values
would be expected to be a better approximation to Vo than Ford's values,
however, they may be weighted in favour of transitions between low
lying librational states which will yield a low value for Vo. On
passing to the low temperature phase of the sodium borohydride an
increase in the activation energy to reorientation was observed.

(The increase in the energy was about 30%, which might be compared with a unit cell volume change of 4%). Although the crystal structure of the sodium salt at low temperatures will give rise to two different barriers to reorientation of any borohydride ion this effect was not observed in the N.M.R. study.

This was significant since in the lithium borohydride a very broad minimum was observed in the proton spin-lattice relaxation times. This was interpreted as two different relaxation times associated with borohydride ions in different crystal symmetries. Harvey (1971)$_b$ does not agree with this interpretation, he has studied the lithium salt by infrared absorption. He suggested that Tung Tsang's results could be explained by crystallographically non-equivalent protons on any one borohydride ion. The different relaxation times are produced by the large number of non equivalent ways of reorienting the borohydride ion. Tung Tsang's observations were supported by the work of Niemela (1970) on the lithium borodeuteride which also shows a broad minimum. The Li^7 resonance work by Ossman (1967) indicates a tetragonal arrangement of Deutrons about lithium in the lithium borodeuteride.

1.4 The alkali metal borohydrides have been studied by infrared spectroscopy both as pure crystals and also as mixed crystals, with the alkali metal halides. A detailed study of the sodium salt was undertaken by Schutte (1960) to determine if the Stockmayer model of the low temperature phase was correct. A tetrahedral molecule (XY_4) has four modes of vibration (of species A, E, F_1 and F_2) of which only

the triply degenerate F_2 modes are infrared active (16).   The local symmetry of a crystal has a profound effect on the molecular ions in it, under favourable circumstances the local site symmetry will remove the degeneracy of molecular vibrational modes.   This occurs where the site symmetry is lower than the symmetry of the molecule.   In the high temperature phase of sodium borohydride the environment of any borohydride ion is of octahedral symmetry.   The symmetry of an octahedron (represented by its symmetry elements; E, $8C_3$, $3C_2$, $6C_4$, $6C_2'$, i, $8S_6$, $3\sigma_h$, $6S_4$, $6\sigma_d$) is of a higher order than that of a tetrahedron (represented by its symmetry elements; E, $8C_3$, $3C_2$, $6S_4$, $6\sigma_d$) all of the symmetry elements of the tetrahedron are contained within the symmetry elements of the octahedron.   The vibrational degeneracies of the tetrahedral borohydride ion remain.   This is also the case when the ion is a substitutional defect in an alkali metal halide crystal (5).   However below the λ point of the sodium salt the proposed crystal structure of Stockmayer has a space group D_{2d}^9 ($I\bar{4}m2$).   The borohydride now has a site symmetry of D_{2d} (represented by its symmetry elements; E, $2S_4$, C_2, $2C_2'$, $2\sigma_d$) which is of lower symmetry than the tetrahedron and does not contain all of its symmetry elements.   This enabled Schutte to predict the removal of certain degeneracies, the observation of these splittings confirmed Stockmayer's model for the low temperature phase of sodium borohydride.

This form of analysis was also applied to potassium borohydride by Harvey (1971)a.   In this compound the crystal structure below the λ point was unknown.   Since the spectrum was unchanged by passing below the λ point the crystal structure was essentially unchanged.

Harvey has assigned the λ point transition to the ordering of the borohydrides, it was suggested that the space group of the low temperature phase was Td^2 ($F\bar{4}3m$) (the borohydride site symmetry is tetrahedral). Harvey also observed a band at $1153cm^{-1}$ in the low temperature phase of the sodium salt. This band was assigned to the transition $v,3lib.$ (transition from the ground state to the triply excited librational level). This excitation should be infrared active (see Table IVviii) and in the harmonic approximation ($v,3lib$ = $3v, lib$) it provides a value of the librational fundamental as $384cm^{-1}$.

The infrared spectrum of lithium borohydride was first obtained by Price (1949), Schutte (1961) attempted to explain some discrepancies, but the problem was reinvestigated recently by Harvey (1971)b. Using Harris' (1947) crystal data Harvey predicted infrared activities and degeneracies. The results were consistant with a borohydride site symmetry of C_s; however Harris' space group, D_{2h}^{16}(Pcmn), has only one set of four C_s sites, which requires the supporting lithium ions to have a site symmetry of C_1. It is thus possible to predict the species of the infrared absorptions due to lattice vibrations (see Table IVvii) such predictions are inconsistant with Harvey's, and with his spectra.

2. Experimental Procedures

2.1 The sodium and potassium borohydrides, B" enriched, were prepared in two stages from boric oxide. The preparation of the sodium salt will be described, that of the potassium salt was exactly analogous. Isotopically enriched boric oxide (Isotopic distribution

"B 95%) was obtained from "20th Century Electronics".   This was

reacted with methanol after the method of Schlestinger (1953)a, the

Azeotrope $B(CH_3O)_3:CH_3OH$ was prepared and then destroyed.   Boric Oxide,

2 grams (0.028 moles), was carefully added to dry methanol, 200mls

(0.203 moles), a few drops of concentrated sulphuric acid were also

added.   The temperature of the reaction mixture was slowly raised,

fractionation was achieved on a 7" vigreux coloum.   The azeotrope was

collected over the boiling range 52-64°C; a second fractionation

concentrated the azeotrope, which was recollected over the range 52-60°C.

Addition of anhydrous lithium chloride destroyed the azeotrope and

the products separated into two layers.   The lower layer was a

lithium chloride/methanol mixture, and the upper layer was the methyl

borate, used in the next stage.

$$"B_2O_3 + 8CH_3OH \longrightarrow 2[(CH_3O)_3"B]CH_3OH + 3H_2O \qquad (i)$$

$$[(CH_3O)_3"B]CH_3OH + LiCl \longrightarrow "B(CH_3O)_3 + LiCl:CH_3OH \quad (ii)$$
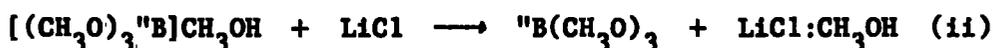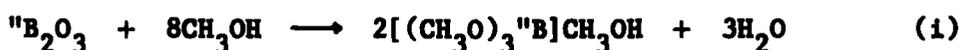
The methyl borate thus prepared was reacted with sodium hydride,

to produce the borohydride, in a reaction after Schlesinger (1953)b.

A three necked flask was fitted with an efficient stirrer, a dropping

funnel, and an acetone/CO_2 condenser.   The flask was immersed in an

oil heating bath.   When the flask had been purged with dry nitrogen

finely powdered sodium hydride, 10grams (0.416 moles), was added.

Whilst stirring the powder the flask was heated to 120°C.   Methyl

borate, 4.38 grams (0.104moles, calculated from equation (iii) below)

was slowly added, and the temperature maintained between 120-150°C. After addition of the methyl borate was complete the temperature was raised to 250°C for thirty minutes.   The flask and contents were allowed to cool, stirring was continued throughout.   The sodium borohydride was extracted from the solid mixture of borohydride and methoxide by dry isopropylamine.   The isopropylamine solution was filtered and the amine solvent removed by distillation, finally under reduced pressure.   The sample produced was 96% pure.   (Analysed by titration of borohydride ion against iodine).

$$4NaH \ + \ (CH_3O)_3{}''B \longrightarrow Na''BH_4 \ + \ 3NaOCH_3 \qquad (iii)$$

Only the sodium and potassium salts were prepared from ''B enriched sources, the rubidium and caesium borohydrides were prepared from a method after Banus (1954).   The preparation of the rubidium salt will be described that of the caesium salt was exactly analogous.

Rubidium hydroxide, 1.03grams (0.010 moles), was dissolved in methanol;   addition of a small amount of water was necessary in order to obtain complete solution.   This solution was filtered and cooled to about 0°C, by an ice/water bath.   Sodium borohydride, 0.38grams (0.009 moles) calculated from equation (iv) below), was dissolved in methanol and similarly cooled to 0°C.   The two solutions were mixed, drop by drop, with stirring.   The rubidium borohydride was precipitated from solution and filtered off.   The solid was pumped dry and was 95% pure.

$$NaBH_4 \ + \ RbOH \longrightarrow RbBH_4 \ + \ NaOH \qquad (iv)$$

The lithium borohydride was obtained from British Drug

Houses, with a purity of 99.5% and was used without further purification.

2.2   The samples were all studied as polycrystalline powders.

Initially the neutron scattering spectra were obtained from the

borohydride salts which were enriched in B". This was to reduce

the amount of neutron absorption by B^{10}. (natural isotopic distribution

is 80.4%B", 19.6% B^{10}). However after taking the spectra of both the

sodium and the potassium B" enriched salts it was decided to use

and unenriched sample of the sodium salt. The inelastic neutron

spectrum of this sample was identical with that of the enriched

sample. Use of unenriched samples of the other salts led to marked

absorption of neutrons, especially in the low energy transfer region,

which caused distortion of the quasi-elastic peak.

All of the samples were contained in silica "cans", which

consisted of two thin silica (c.a. 0.2mm) discs sealed around the

edge except for a small region where a ground glass socket was fused

on (see Fig. IViib). The separation between the discs was of the order

of 0.3 to 0.4mm. At these separations filling the 'can' with a

compound was difficult. The cans were filled and sealed in a

nitrogen dry box. Sealing was by a picene (black wax) film between

ground glass joints; or if the sample environment was to be

evacuated, by a picene film onto a brass plug containing a simple

pressure release device (see Fig. IViib). The whole of the series

of the alkali metal borohydrides were run on the up scattering

spectrometer at Harwell (see Section II) at, or above, ambient

Fig. IV.11.a

163.

The absorption background of the infrared spectrophotometer

(R.I.I.C. FS720)

cm.

Silica "can" for
neutron
spectroscopy

Isolation cell
for I.R.
spectroscopy
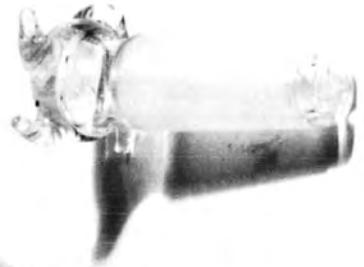
Table IViv. Table showing the experimental conditions under which the spectra were taken at Harwell.

	Li		Na			K		Rb		Cs	
% Scatterer	10	14	12	12	12	12	12	13	11	11	11
Up Scattering											
Temperature °K	295	295	295		295	314	348	295	295		
Incident neutron wavelength Å	4.26	4.77	4.18		4.22	4.15	4.15	4.22	4.22		
B" enrichment	NO	YES	NO		YES	YES	YES	NO	NO		
Can type and window thickness mm.	Si 0.2	Si 0.5	Si 0.2		Si 0.5	Si 0.5	Si 0.5	Si 0.2	Si 0.5		
Comparison Blank	Si 0.2	Si 0.5	Si 0.2		Si 0.5	Si 0.5	Si 0.5	Si 0.2	Si 0.5		
Down Scattering											
Temperature °K	77	295	197	77					295	197	77
Monochromator and plane	Al 1.1.1.,3.1.1.	Al 3.1.1.	Al 3.1.1.	Al 3.1.1.					Al 3.1.1.	Al 3.1.1.	Al 3.1.1.
Infrared Spectra											
Gain setting db.	13.2		31.5			12.0		39.7		51.6	

temperature (294°K).   The spectra of the lithium, sodium, and

caesium salts were also obtained on the down-scattering spectrometer

at Harwell (see Section II).   The experimental details are summarised

in Table IV.iv.   Some additional elastic region studies were made at

Aldermaston on the graphite monochromated-chopper spectrometer.

2.3   A complimentary study of the borohydrides was undertaken in

the far infrared.   The infrared absorption spectra were obtained in the

region 50 to 400cm^{-1} on the Fourier transform spectrometer (see

Section II).   In all cases the compounds were run as finely divided

powders mulled with Nujol.   They were mulled in a nitrogen dry box,

and the mull contained in an isolation cell to prevent hydrolysis by

atmospheric water.   The concentration of the mull was adjusted for

each compound so that the most intense band did not dominate the spectrum.

This could only be judged after experience with several mulls.

All the borohydrides spectra were taken at ambient (293°K) temperature,

and the lithium, sodium and caesium salts were also run at liquid

nitrogen temperature.   Experimental details are shown, for the best

spectra, in Table IViv.

Because of the use of polythene in the construction of the machine

the background in the infrared is not flat.   The background spectrum

of the instrument is illustrated in Fig. IViia.

3.   The alkali metal borohydride spectra

3.1   Transitions from the occupied lattice vibration states, down

toward the ground state, are what would be expected to be seen in any

neutron inelastic up scattering spectrum.   In a sodium chloride type

lattice the main transitions will be from the longitudinal optic
(LO) level, the transverse optic (TO) level, the longitudinal
acoustic (LA) level, and the transverse acoustic (TA) level. In the
case of the alkali metal borohydrides a fifth level, the librational
state (lib), is involved. The optic and acoustic vibrational states
are a property of the crystal lattice, in that they are a description
of the relative motions of all the ions. The librational state of
a borohydride ion is characteristic of that ion, not all the
borohydride ions; it is determined by the relative positions of the
neighbouring ions. The vibrational and librational states are
descriptions of the motions of ions in crystals, their nature is
determined by the crystal lattice type and their value by the
interatomic forces in the lattice. Because the librational state is
of higher energy than the lattice vibrational states, in these compounds,
the bands in the up scattering spectrum would be expected to be
representative of the cascade of transitions from the librational state
down to the less highly excited vibrational states. This is shown
schematically in Fig. IViii.; where the nomenclature for the
transitions is also shown.

It is upon this scheme that the up scattering inelastic neutron
spectra are interpreted. The essential features of the alkali metal
borohydride spectra are summarised, and assignments given, in Tables
IVxi, xiii. From these spectra estimates of the crystal lattice
vibrational levels are obtained, these are given in Table IVix. The
bands and the general features of the inelastic region are then
discussed. In the following section the Quasi-elastic broadening

Fig. IV.iii

168.

De-excitation transitions between the crystal levels
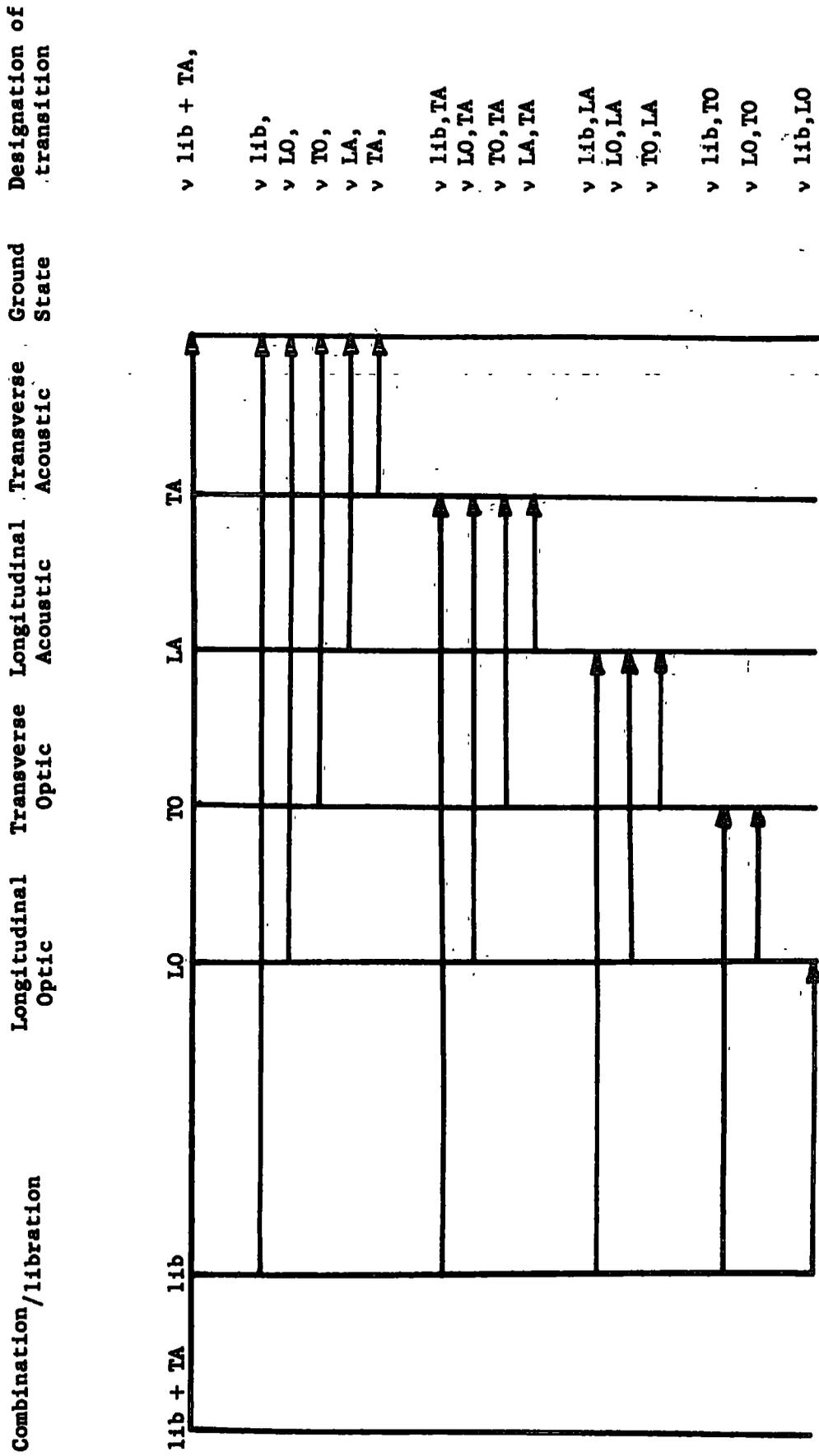
Table IVv. Table giving the irreducible representations of the lattice vibrations of the Alkali metal Borohydrides.

Sample	Crystal Structure	No. of moles to the Bravais cell Z	Ion type	Site group	Site species containing translation	Factor group	Factor species	Irreducible represent. of lattice vibrations		Infrared active species of Factor group	Raman active species of Factor group
								acoustic	optic		
Alkali Metal Borohydride -above transition temperature	O_h^5 F_{m3m}	1	BH_4 Metal	O_h O_h	F_{1u} F_{1u}	O_h O_h	F_{1u} F_{1u}	F_{1u}	F_{1u}	F_{1u}	
Alkali Metal Borohydride below transition temperature	T_d^2 $F\bar{4}3m$	1	BH_4 Metal	T_d T_d	F_2 F_2	T_d T_d	F_2 F_2	F_2	F_2	F_2	F_2
Sodium Borohydride below transition temperature	D_{2d}^9 $I\bar{4}m2$	1	BH_4 Na	D_{2d} D_{2d}	B_2, E B_2, E	D_{2d} D_{2d}	B_2, E B_2, E	$B_2 + E$	$B_2 + E$	B_2, E	B_2, E
Lithium Borohydride	D_{2h}^{16} P_{cmn}	4	BH_4 Li	C_s C_1^*	A', A'' A_u	D_{2h} D_{2h}	A_g, B_{2g}, B_{1u} B_{3u} A_u, B_{1u}, B_{2u} B_{3u}	$B_{1u} + B_{2u} + B_{3u}$	$2A_g + B_{1g} + 2B_{2g}$ $+ B_{3g} + 4A_u +$ $+ 4B_{1u} + 3B_{2u}$ $+ 4B_{3u}$	B_{1u}, B_{2u} B_{3u}	A_g, B_{1g} B_{2g}, B_{3g}

* Harvey has given the Li site symmetry as C_s and ∴ obtains 7 optically active lattice modes (I.R.)

However there is only one set of 4 C_s sites in D_{2h}^{16} and these are occupied by BH_4^- ions ∴ the site symmetry of the Li ions is C_i which gives

11 optically active lattice modes (I.R.).

Table IVvi. Table showing the effects of correlation splitting on the degenerate librations, in the Borohydrides at different temperatures.

Sample	Crystal Structure	No. of moles per Bravais cell Z	Site group	Site species containing rotation	Factor group	Factor Species	Irreducible Represent. of the lattice librations (with Correlation splitting)	Irreducible Represent. of the lattice librations (without Correl. splitting)	Infrared active species in Factor group	Raman active species in Factor group
Alkali Metal Borohydride above transition temperature	O_h^5 F_{m3m}	1	O_h	F_{1g}	O_h	F_{1g}	F_{1g}	F_{1g}		
Alkali Metal Borohydride below transition temperature	T_d^2 * $F_{\bar{4}3m}$	1	T_d	F_1	T_d	F_1	F_1	F_1	E	
Sodium Borohydride below transition temperature	D_{2d}^9 $I_{\bar{4}m2}$	1	D_{2d}	A_2, E	D_{2d}	A_2, E	$A_2 + E$	$A_2 + E$	E	
Lithium Borohydride	D_{2h}^{16} P_{cmn}	4	C_s	A', A''	D_{2h}	A_g, B_{2g}, B_{1u} B_{3u} B_{1g}, B_{2g}, A_u B_{2u}	$A_g + 2B_{1g} + B_{2g} + 2B_{3g} + 2A_u + B_{1u} + 2B_{2u} + B_{3u}$	$A' + A''$	B_{1u}, B_{2u} B_{3u}	A_g, B_{1g} B_{2g}, B_{3g}

* This structure is hypothesised by Harvey in the case of KBH_4

Table IVviii.

Table showing the Irreducible representations of the Combinations and overtones of the librational mode.

System and Site Symmetry	Fundament and Overtones	Character of Fundamentals	Irreducible Representation of Overtone State	Infrared activity shown by	Raman activity shown by	Previous observ.
Metal BH_4 above λ_{pt}						
O_h	ν_{lib}	F_{1g}				
	$2\nu_{lib}$	$(F_{1g})^2$	$A_{1g} + E_g + F_{2g}$		$A_{1g}\ E_g\ F_{2g}$	
	$3\nu_{lib}$	$(F_{1g})^3$	$A_{2g} + 2F_{1g} + F_{2g}$		F_{2g}	
Metal BH_4 below λ_{pt}						
Td site	ν_{lib}	F_1				
	$2\nu_{lib}$	$(F_1)^2$	$A_1 + E$		$A_1,\ E$	
	$3\nu_{lib}$	$(F_1)^3$	$A_1 + E$		$A_1,\ E$	
$NaBH_4$ below λ_{pt}						
D_{2d} site	ν_{lib}	$A_2 + E$				
	$2\nu_{lib}$	$(A_2)^2$	A_1		A_1	
		$(E)^2$	$A_1 + B_1 + B_2$	B_2	A_1, B_1, B_2	
		$A_2.E$				
	$3\nu_{lib}$	$(A_2)^3$	A_2			
		$(E)^3$	$2E$	E	E	1
		$(A_2)^2 E$	E	E	E	
		$(E)^2 A_2$	$2E$	E	E	

Ref. 1   Harvey (1970)a.

Table IVvii.   Table showing the Irreducible Representations of the Combinations of the lattice modes

Fundamentals Combined	Characters of the Fundamentals	Irreducible Representations of the Combined State	Infrared activity shown by	Raman activity shown by	Observed in our I.R. spectra
ν_{TA}	F_{1u}				
ν_{LA}					
ν_{TO}	F_{1u}				
ν_{LO}					
ν_{Lib}	F_{1g}				
$\nu_{TA} + \nu_{TA}$	$(F_{1u})^2$	$A_{1g} + E_g + F_{2g}$		A_{1g}, E_g, F_{2g}	
$+ \nu_{LA}$	$(F_{1u})^2$	$A_{1g} + E_g + F_{2g}$		A_{1g}, E_g, F_{2g}	
$+ \nu_{TO}$	$F_{1u} \cdot F_{1u}$	$A_{1g} + E_g + F_{1g} + F_{2g}$		A_{1g}, E_g, F_{2g}	
$+ \nu_{LO}$	$F_{1u} \cdot F_{1u}$	$A_{1g} + E_g + F_{1g} + F_{2g}$		A_{1g}, E_g, F_{2g}	
$+ \nu_{Lib}$	$F_{1u} \cdot F_{1g}$	$A_{1u} + L_u + F_{1u} + F_{2u}$	F_{1u}		*
$\nu_{LA} + \nu_{LA}$	$(F_{1u})^2$	$A_{1g} + E_g + F_{2g}$		A_{1g}, E_g, F_{2g}	
$+ \nu_{TO}$	$F_{1u} \cdot F_{1u}$	$A_{1g} + E_g + F_{1g} + F_{2g}$		A_{1g}, E_g, F_{2g}	
$+ \nu_{LO}$	$F_{1u} \cdot F_{1u}$	$A_{1g} + E_g + F_{1g} + F_{2g}$		A_{1g}, E_g, F_{2g}	
$+ \nu_{Lib}$	$F_{1u} \cdot F_{1g}$	$A_{1u} + E_u + F_{1u} + F_{2u}$	F_{1u}		
$\nu_{TO} + \nu_{TO}$	$(F_{1u})^2$	$A_{1g} + E_g + F_{2g}$		A_{1g}, E_g, F_{2g}	
$+ \nu_{LO}$	$(F_{1u})^2$	$A_{1g} + E_g + F_{2g}$		A_{1g}, E_g, F_{2g}	
$+ \nu_{Lib}$	$F_{1u} \cdot F_{1g}$	$A_{1u} + E_u + F_{1u} + F_{2u}$	F_{1u}		*
$\nu_{LO} + \nu_{LO}$	$(F_{1u})^2$	$A_{1g} + E_g + F_{2g}$		A_{1g}, E_g, F_{2g}	
$+ \nu_{Lib}$	$F_{1u} \cdot F_{1g}$	$A_{1u} + E_u + F_{1u} + F_{2u}$	F_{1u}		*

obtained in the spectra of the sodium and potassium are presented,

Tables IVxvii, xviii, and discussed.   Then the effect of the crystalline

phase change of sodium borohydride is considered.   A down scattering

spectrum close to the   point of the sodium salt, which shows a

spectrum intermediate between the two phases, is presented.   Finally

the spectra of lithium borohydride are discussed, two well separated

librational transitions are assigned.   Typical spectra obtained by

neutron up scattering, and infrared absorption, are shown in

Figs. IVv to ix.   The down scattering spectra are shown in Figs. IVx,

xi.   A lattice vibrational analysis is conducted, by the correlation

method, and the irreducible representations of the lattice states

are given in Table IVv, vi.   The irreducible representation of the

combinations of the states, in Table IVvii, and the higher librational

states of the borohydride ion are given in Table IVviii.   (The

predicted infrared and Raman activities are also shown in these Tables).

3.2.1   Spectra of the Inelastic region: results

The spectra of up scattered neutrons from the borohydride salts

showed a series of weak peaks, growing in intensity, up to the strongest

band, v_{1ib} (for nomenclature see Fig. IViii).   Several of these peaks

group quite closely to this librational transition, and many were

of comparable intensity.   The inelastic down scattering spectra at

ambient temperatures showed the $v,_{1ib}$ as a very broad scattering

feature at low incident energy.   A few very weak bands were super-

imposed upon this transition.   At lower temperatures the breadth of

the $v,_{1ib}$ scattering feature was suppressed and a distinct $v,_{1ib}$

transition was very much in evidence.   The infrared absorption spectra

were dominated by an intense absorption around $170 cm^{-1}$, and the assigned bands usually appeared as weak inflections at the sides of this absorption.

3.2.2 Spectra of the Inelastic region: discussion

All the spectra can, for the purpose of discussion be split into their component parts. These will comprise: (i) the lattice mode transitions and combination (ii) the broad librational scattering feature present in both up and down scattered spectra, (iii) the librational transitions at low temperatures.

3.2.2.1 Transitions between the lattice vibrational states.

This type of transition is observed in all spectra; in the neutron up scattering spectra de-excitations involving transitions between the lattice states are observed, whilst in down scattering and infrared absorption spectra excitations to combination states are observed. The adoption of the scheme shown in Fig. IViii allowed the energy of the lattice states to be determined from the four most intense bands closest to the torsional scattering. The scheme could then be used to predict values for the other transitions which give bands at lower energy transfer. The up scattering spectra show that most of the transitions between crystal vibrational states are active, see Figs. IVv, vi and also shows that accidental degeneracy is quite common. Some of the transitions do not appear to be always active, this is probably a facet of their expected position in the spectrum. Bands occurring in a high scattering region may be hidden by other features. The bands do not demonstrate any significant

Table IVix.

Table of the energies of the crystal levels, estimated
from the up scattering spectra

Level assignment	Na Energy cm^{-1}	Q $Å^{-1}$	K Energy cm^{-1}	Q $Å^{-1}$	Rb Energy cm^{-1}	Q $Å^{-1}$	Cs Energy cm^{-1}	Q $Å^{-1}$
TA	52	3.37	80	3.10	80	2.86	69	2.94
LA	139	2.72	126	2.76	99	2.71	126	2.51
TO	168	2.43	143	2.62	151	2.28	145	2.33
LO	214	2.0	159	2.49	195	1.89	157	2.0
11b	313	3.71	305	3.55	273	3.42	272	3.42

Notes.

Q $Å^{-1}$ The values of Q given are those of the main neutron group, in the up scattering spectra, which was used to estimate the energy of the level.

Energy cm^{-1}; relative to the ground state.

Table IVx.

Table of predicted transitions between the levels given in

Table IVix as would be observed in an up scattering expt.

| Transition assignment | Predicted values (cm^{-1}) for transitions from Table IVix. | | | |
	Na	K	Rb	Cs
ν,lib	313	305	273	272
νLO,	211	159	195	157
νTO,	168	143	151	145
νLA,	139	126	99	126
νTA,	52	80	80	69
νlib,TA	261	225	193	203
νLO,TA	159	79	116	88
νTO,TA	116	63	71	76
νLA,TA	87	26	19	57
νlib,LA	174	179	174	146
νLO,LA	72	33	96	31
νTO,LA	29	17	52	19
νlib,TO	145	162	122	127
νLO,TO	43	16	44	12
νlib,LO	99	146	78	115
νlib+TA	365	385	353	341
νlib+LA	452	431	372	398
νlib+TO			424	417
νlib+LO				429

Table IVxi.   A comparison of the predictions of Table IVx and the observed results from neutron up scattering θ = 45°

Notes.

w, weak
m, medium
s, strong

NaBH₄

assignment	predicted	observed
vTO,LA	29	25 w
vLO,TO	43	
vTA,	52	55 w
vLO,LA	72	72 w
vLA,TA	87	
vllb,LO	99	99 w
vTO,TA	116	113 w
vLA,	139	140 w
vllb,TO	145	
vLO,TA	159	
vTO,	168	175 w
vllb,LA	174	
vLO,	211	
vllb,TA	251	262 m
vllb,	313	313 s

KBH₄

assignment	predicted	observed
vLO,TO	16	
vTO,LA	17	
vLA,TA	26	
vLO,LA	33	
vTO,TA	63	73 w
vLO,TA	79	98 w
vTA,	80	113 w
vLA,	126	
vTO,	143	146 m
vllb,LO	146	
vLO,	159	162 m
vllb,TC	162	
vllb,LA	179	180 w
vllb,TA	225	226 w
vllb	305	305 s
vllb+LA,	431	427 w

RbBH₄

assignment	predicted	observed
vLA,TA	19	
vLO,TO	44	44 w
vTO,LA	52	
vTO,TA	71	
vllb,LO	78	78 w
vTA,	80	
vLO,LA	96	
vLA,	99	
vLO,TA	116	121 w
vllb,TO	122	
vTO,	151	
vllb,LA	174	174 m
vllb,TA	193	193 w
vLO,	195	
vllb,	273	273 s
vllb+TA,	353	310 m

CaBH₄

assignment	predicted	observed
vLO,TO	12	
vTO,LA	19	
vLO,LA	31	
vLA,TA	57	
vTA,	69	78 w
vTO,TA	76	
vLO,TA	88	90 w
vllb,LO	115	115 w
vLA,	126	127 w
vllb,TO	127	
vTO,	145	
vllb,LA	146	148 m
vLO,	157	
vllb,TA	203	204 m
vllb,	272	272 s
vllb+TA,	341	308 w
vllb+llb,	544	540 w

Table IVxii.

Table showing predicted positions of bands in the down

scattering spectra, from Table IVix.

Level from which transition occurs	Thermal, Boltzman, Population of the level w.r.t. the Ground state : at $^{\circ}$K *			Transition Assignment	Predicted frequency (cm^{-1}) from Table IVix.	
	294	197	77		NaBH$_4$	CsBH$_4$
Ground state	1	1	1	ν,LO	211	157
				ν,lib	313	272
				ν,lib +TA	365	341
				ν,lib +LA	452	398
				ν,lib +TO	481	417
				ν,lib +LO	524	513
				ν,lib +lib	626	544
TA	0.88	0.83	0.61	νTA,lib	261	203
				νTA,lib+TA	313	272
				νTA,lib+LA	400	329
LA	0.65	0.53	0.19	νLA,lib	174	146
				νLA,lib+TA	226	215
				νLA,lib+LA	313	272

* Energies of the states used in this calculation are taken from the observations on the down scattering spectra, not based on estimates given in Table IVix. These values are representative, they will vary as the energy of the state changes.

Table IVxiii.

Table comparing predicted and observed band positions in neutron down scattering spectra.

Transition Assignment	NaBH$_4$ 294°K		CsBH$_4$ 294°K		197°K		77°K	
	predict	observe	predict	observe	predict*	observe	predict*	observe
νLA,lib	174		146					
ν,LO	211	194$_m$						
νLA,lib+TA	226		215					
νTA,lib	261	256$_w$	203			225$_w$ sh		
ν,lib	313	-	272	-				
νTA,lib+TA	313		272			272$_s$		287$_{vs}$
νLA,lib+LA	313	282$_w$	272	257$_w$				
ν,lib+TA	365		341	292$_{vw}$		324$_m$ sh		334$_{vw}$ sh
ν,lib+LA	452	417$_m$	398					
ν,lib+TO	481		417					
ν,lib+LO	524	513$_w$	429			427$_w$		457$_m$
ν,lib+lib	626		544					570$_m$

* Predictions based on Table IVxii would not be expected to bear any relation to spectra below ambient temperatures.

Notes. w, weak; m, medium; s, strong; v, very; sh, shoulder.

Table IVxiv.

Table comparing predicted results and observed values in the absorption infra-red spectra of the borohydrides, at 21°C

Transition Assignment	Predictions based upon Energy levels of Table IVxii frequency of transitions in cm^{-1}							
	NaBH$_4$		KBH$_4$		RbBH$_4$		CsBH$_4$	
	predict	observe	predict	observe	predict	observe	predict	observe
vLO,lib	102		146		78		115	
vTO,lib	145	150$_w$	162	150$_w$	122	112$_w$	127	115?$_w$
v,TO	168		143		151	145$_w$	145	
vLA,lib	174		179	240$_w$	174		146	
v,LO	211	210?$_w$	159		195	190$_w$	157	
vTA,lib	261	230?$_w$	225	270$_w$	195	270$_w$	203	240$_w$
v,lib+TA	365		385		353		341	
v,lib+LA	452		431		372		398	
v,lib+TO	481		448		424		417	
v,lib+LO	524		464		468		429	

w = weak   ? peak doubtful, slight inflection on a steep gradient.
m = medium
s = strong

Note. To preserve the order of the LH. column. the order of "predicted" results may deviate from the strictly consecutive.

dispersion.   The values for the energies of the lattice vibrational

states (see Table IVix) probably represent an average zone edge value,

certainly they cannot represent zone centre values, (at Q = o,

zone centre, the energies of the acoustic states are zero).

This does not apply to the case of the infrared absorptions for

ν,TO and ν,LO.   These are the only two transitions which can be

excited directly by photons.   (Although ν,LO is forbidden its

presence is usually observed for polycrystalline samples since the

incident radiation is not parallel to the transverse modes of all the

crystallites.(3))   Unfortunately ν,LO is usually weak and could

not be differentiated by its intensity, alone, from a combination mode.

It is usually true that the most intense infrared absorption is

ν,TO;   but crystal size can affect this conclusion drastically.   If

a crystal is sufficiently small, with respect to the incident wave

length of radiation, a propagating mode of vibration, involving the

surface of the crystallite only can be established.   Such modes have

been extensively studied by Ruppin (1970).   He has shown that the

surface mode gives easily the most intense absorption, and that the

bulk modes of the crystal ν,TO and ν,LO are not in general visible.

The surface absorption is intermediate in value between the values of

the bulk modes;   its actual position being dependent upon crystal

size and the refractive index of the surrounding medium.   Since our

crystals were prepared by rapid precipitation from ice-cold organic

solvents it is possible that they are very small.   Because of the

difficulty in assigning this absorption the values were omitted from

Table IVxiv but are given in Table IVxv.   The values shown in

Table IVxv do not compare favourably with the expected variation of ν,TO

Table IVxv.

Table giving the position of the maximum absorption in the infrared for borohydrides.

Salt	Position of max. absorption cm^{-1}
$NaBH_4$	175
KBH_4	172
$RbBH_4$	170
$CsBH_4$	161

from salt to salt (since in the TO vibrational state the ions beat
against each other the positions of their absorptions are expected
to be related to the reduced mass of the ions). Those values obtained
for vTO, from the neutron spectra hardly fit the reduced mass
approximation better. (The value of vTO, for potassium borohydride
is completely anomalous). The values for the energies of the
crystal vibrational states at the zone edge might be usefully compared
with the values obtained for ND_4Cl (low temperature phase, IV) (4).
The values, estimated from Brockhouse's (1969) paper are; for acoustic
modes $106cm^{-1}$, optic modes about $140cm^{-1}$ and librational mode about
$277cm^{-1}$. (The crystal structure is not the same as for the
borohydrides). These should be compared with an average acoustic
value of $96cm^{-1}$ an average optic value of $166cm^{-1}$ and a librational
average of $291cm^{-1}$; which are taken from the borohydride results as a
whole.

The width of the infrared absorption bands show marked differences
between one another. Generally the width of a band, which is purely
a transition between two states, is related to the lifetime of the
two states. In a state of short lifetime the vibration is relaxed
and the signal suffers a decrease in intensity and an increase of width.
Although all the infrared absorptions are broad those of the potassium
salt at $270cm^{-1}$, the rubidium salt at $270cm^{-1}$ and the caesium salt at
$240cm^{-1}$ are especially so. These have all been assigned to
transitions involving the TA vibrational state. Since these bands
are so broad their lifetime, in comparison with other vibrational states,
is short. The intensities of the lattice transition bands occurring
close to the librational transition inthe up scattering spectra are

artificially enhanced by superimposition upon a broad inelastic scattering feature. This superimposition is more clearly appreciated from down scattering spectra.

3.2.2.2 The broad inelastic librational scattering feature.

In both up scattered and down scattered spectra a broad feature is obvious, at ambient temperatures. It is most easily seen in the down scattering spectra and reaches its maximum value at $v_{,lib}$. Superimposition of lattice bands complicate its general appearance. Previously such features have been observed in scattering from ammonium salts (24), and also from bisulphide salts (7); and are associated with a rapid reorientation of the librating molecular ion. Interpretation of these features by elementary theory has proved difficult (24), and authors have tended to treat the more tractable quasi-elastic problem (9). Larsson (1973) has however provided the basic theory for this phenomenon, and a model for this reorientational process was also suggested. (This was discussed in section I). From our data we should be able to obtain estimates of Larsson's function F_{11}^{lib} (given in Section I). This function, F_{11}^{lib}, is related to the barrier to reorientation. (F_{11}^{lib} takes two extreme values $F_{11}^{lib} = 0$ for an absence of barrier and $F_{11}^{lib} = 1$ for a very high barrier). By combining the up and down scattering spectra an estimate of the width (full width, half height) of the broad feature was determined for the sodium and caesium salts. The values obtained, for the sodium salt $F_{11}^{lib} \sim 0.44$ and for the caesium salt $F_{11}^{lib} \sim 0.25$, indicate several points of interest. Firstly reorientation of the borohydride ion in sodium borohydride is more difficult than in caesium, that the

barrier is fairly intermediate between the free rotation and the deep well cases, and finally that the length of time spent librating in any one orientation will be of the order of 10^{-12} sec.   Reorientations between successive wells must take place on a time scale equal to, or shorter than, the interaction of a neutron and proton ($\sim 10^{-14}$ sec.). The data obtained does not allow of a more detailed analysis; and it is hoped to repeat the experiment on a down scattering spectrometer, going to much lower incident neutron energy.   The I.N.4. neutron scattering spectrometer, (at I.L.L., Grenoble) when used in the down scattering mode may be best for such an experiment.   Extension of this work would involve a more detailed study of the temperature variation of the broad feature; it is unlikely that up scattering spectra would be of any use since the definition of the band shape is important.

3.2.2.3 The Librational transitions

The librational transition (v_{1ib})gives the most intense band of the up scattered spectrum, and the down scattering spectrum ($v,_{1ib}$). The transition is very evident in any low temperature down scattering spectra.   At 197°K the width of the $v,_{1ib}$ band can be measured properly (full width at half height = $56cm^{-1}$) and that at 77°K is the narrower of the two (F.W.H.H = $34cm^{-1}$).   This behaviour may be due to the short lifetime of any librational state which will lower and widen the band.   However Larssons model (20) for the reorientation indicates another method of broadening the line.   The thermal motions of the ions, the instantaneous positions of which determine the librational potential well, are of larger amplitude at higher temperatures.   This provides a wider distribution of barrier

heights, than at lower temperatures, and so determines the width.

This explanation is consistant with the other observations.

Firstly the breadth of the broad librational scattering is reduced

gradually as the temperature is lowered.   This is as a result of

the restricted thermal motions of the neighbouring ions.   Secondly

the position of the transition moves to higher frequencies, as a

result of the overall contraction of the crystal with lowering of the

temperature.   We are essentially observing the growing importance

of the librational time (t_o discussed in section I 2.3.3) with the drop

in crystal temperature.   As was indicated above, this band is the

result of the ensemble average of the potential wells of all the

borohydride ions; and the values of these barriers can be obtained

from equations III.1.xiv,xix   which were discussed previously.   The

application of these equations is justified by the observation of a

band assigned to the v, 2lib transition.   This is assigned in the

down scattering spectrum at 77°K, Table IVxiii.   The transition occurs

at twice the value for v,lib; whilst the exactness of the observation

may be fortuitous it does show that the harmonic approximation can be

applied to this case.   The values obtained for the barrier heights

are given in Table IVxvi.   As can be appreciated from the table the

uncertainty in the value of the transition, when observed in both up

and down scattering spectra, produces as much variation in the value

of the barrier height, Vo, as do the different equations.   Overall a

barrier height of about 4 Kcals mole^{-1} is indicated (slightly less for

crystals with large unit cells and slightly more for compact crystals).

This, however, is not an effective measure of the barrier which exists

when a borohydride ion reorientates.   There is no data published which

Table IVxvi.

Table showing the values obtained for the barriers to reorientation of a librating borohydride ion.

Sample	Temperat. °K	ν_{lib}, up scattered results cm^{-1}	ν,lib down scattered results cm^{-1}	Results of the applications of the equations below * Vo in Kcals mole^{-1} (a)		Results of the applications of the equations below * Vo in Kcals mole^{-1} (b)	
				(1)	(2)	(1)	(2)
NaBH$_4$	294	313	282	4.41,	3.58	4.87,	3.99
KBH$_4$	294	305		4.19		4.64	
RbBH$_4$	294	273		3.36		3.76	
	294	272		3.33		3.73	
CsBH$_4$	197		272		3.33		3.73
	77		287		3.71		4.13

(1) from up scattering results

(2) " down scattering results

* value of Inertia of BH$_4$ ion is 7.08 x 10^{-40}g cm^2

(a) The deep well approximation, Eyring, Walter and Kimball

(b) Das's solution for the Mathieu equation (Discussed in section III)

is directly comparable to these results. However Durig and Rush have studied phosphonium halides and Venkataraman has published work on the ammonium halides (see Section VI). The crystal structures of these compounds are all very similar, distorted caesium chloride type with ordered tetrahedra. Typically the results obtained gave values for Vo of about 7.5 Kcals mole^{-1} for the Phosphonium salts, and about 4.0 Kcals mole^{-1} for the ammonium salts. In these cases however the barrier has been described as electrostatic in nature and there is more variation in the value of Vo from salt to salt.

The values for the barrier to reorientation, Vo obtained by Smith (1974) for the sodium and potassium salts (see previous section) cannot meaningfully be compared with those presented in Table IVxvi. His results, 2.98 Kcals mole^{-1} for the sodium salt and 3.44Kcals mole^{-1} for the potassium salt, are significantly different from those presented here. This stems from the different techniques used. Smith assumed that the ion could only reorientate by passing over the barrier Vo. The spectra presented here show that reorientation and libration occur together. The data used by Smith to fit to his model were bulk measurements and will represent an averaged value of the reorientational and librational barriers. As is the case Smith's value for Vo should be lower than the one presented here, it is comparable to results obtained from N.M.R. studies (33).

The possibility of reorientation via a quantum tunnelling effect was considered. The barriers obtained in Table IVxvi, Vo, were regarded as static and application was made of Das's work (discussed in Section I). The value of the transition between any two adjacent librational sub states was determined (for a fourfold barrier there are

three librational sub levels caused by tunnelling for every major librational level).   This splitting was estimated at about $10^{-3}cm^{-1}$, for the typical Vo value of 4 Kcals mole^{-1}.   It is unlikely that tunnell splitting made any significant contribution to the observed spectra.

3.3.1   Spectra taken in the Elastic Region: results

The spectrum of elastically and quasi-elastically scattered neutrons was accessible only by up scattering experiments.   Because of absorption of neutrons by ^{10}B the B" isotope enriched salts of sodium and potassium were studied.   At ambient temperatures with low resolution, in the results obtained for the potassium salt, no quasi-elastic peak was observable and the elastic features were similar to the resolution function of the machine.   When the temperature was raised some quasi-elastic scattering became evident, but the elastic peak could not be separated, overall the total width appeared to increase (shown in Table IVxii).   At better resolution, the results obtained for the sodium salt, the elastic and quasi-elastic features were usually easily separable.   The elastic peak width was left unchanged by raising the temperature (shown in Table IVxiii), whereas the height of the quasi-elastic peak was obviously increasing with temperature (Table IVxviii (a)).

3.3.2   Spectra taken in the elastic region: discussion

Since the resolution of the up scattering spectrometer used to study the potassium salt was poor, '6H' at Harwell was used (see Section II), the elastic and quasi-elastic contributions to the total peak in this

Table IVxvii

A comparison of the full widths at half height of the

elastic *peaks of KBH$_4$ at different temperatures.

Scattering vector		Full widths at half heights. K"BH$_4$		
o	Q^2 $\overset{o}{A}^{-2}$	Vanadium $x10^{-2}$meV	313°K $x10^{-2}$meV	348°K $x10^{-2}$meV
18	0.224	61.2	55.3	54.2
27	0.499	64.8	56.2	54.9
36	0.874	64.8	57.3	58.3
45	1.340	64.8	60.8	61.5
54	1.886	60.0	68.1	75.7
63	2.499	63.6	77.4	83.7
72	3.162	67.2	75.2	106.0
81	3.861	69.6	79.7	108.0
90	4.577	69.6	84.2	127.0

* Data collected at Harwell on the '6H' up scattering
spectrometer are present here. The contributions to the
peak width from purely elastic and quasi-elastic could not
be effectively separated.

Table IV xviii

Table comparing the Full widths at half heights of the elastic *peaks, separated from the quasi-elastic background, of $NaB''H_4$ at various temperature.

Scattering Vector Q^2 $\overset{\circ}{A}^{-2}$		Full width at half height V $\quad$ $NaB''H_4$			
		10^{-2} meV	10^{-2} meV	10^{-2} meV	10^{-2} meV
20	0.266	34.57	34.97		36.81
30	0.590	34.57	36.81	34.97	34.97
40	1.055	34.57	34.97	34.97	36.81
50	1.574	36.45	38.66	38.66	36.81
60	2.203	38.32	42.34	38.66	40.50
70	2.899	43.06	44.18	44.18	40.50
80	3.641	43.99	51.54	47.86	42.34
90	4.406	43.99	40.45	47.86	42.34

* Data collected at Aldermaston on the 'G.M.C.' up scattering spectrometer.

The results are given in this format for comparison with Table IVxvii. They are reproducible to within 2.0×10^{-2} meV.

Table IVxviii(a).

Table comparing measured and deconvolved quasi-elastic peak widths, at various temperatures

Scatt. Angle	Full width at half height of the Quasi-elastic peak, and the representative function.						
	Vanadium	NaB"H$_4$					
		295°K		333°K		377°K	
	Gausian 10^{-2}meV	Voigt 10^{-2}meV	Loren'. 10^{-2}meV	Voigt 10^{-2}meV	Loren'. 10^{-2}meV	Voigt 10^{-2}meV	Loren'. 10^{-2}meV
20	34.6					70	53
30	34.6			107	95	99	85
40	34.6	138	126	103	91	99	85
50	36.4	123	111	107	93	96	82
60	38.3	116	102	110	95.5	99	82.5
70	43.1	120	102.5	123	106	109	91
80	44.0	131	114.5	133	117	107	88
90	44.0	129	112	131	114.5	105	85

Note (i) the 'Voigt' is the measured full width at half height of the quasi-elastic peak.

(ii) 'Loren' is the value of the full width at half height of a Lorentzian function which when convolved with the appropriate Gaussian full width gives the value of the Voigt full width.

region could not be separated. The width of the peak observed,
appears to broaden because of the presence of an unresolved quasi-elastic
contribution. Scattering from the sodium salt was clearly separated
into the two components. The elastic peak, which is simply an addition
to the quasi-elastic peak, is the result of the proton being confined
to more on the surface of a sphere, as its motion is averaged out over
time. The quasi-elastic peak is composed of two contributing parts.
These are the rotational and librational-quasi-elastic components.
In the observed spectrum both the quasi-elastic and the superimposed
elastic peaks are convolved with the machines resolution function,
this resolution function is effectively given by the elastic peak data
obtained for vanadium. The measurement of the full widths at half
heights of the sodium salt spectra were taken by hand, and are found
to be reproducible to within about 2.0×10^{-2} meV (see Table IVxviii).
Within this limitation the results show that the width of the elastic
peak does not vary appreciably with either temperature or momentum
transfer, and reflects the resolution of the spectrometer at that
scattering angle.

The analysis of the quasi-elastic peak widths was also conducted
by hand. The width measured was the full width at half height and
represents the width of a Voigt function. (Voigt functions are the
result of convolutions of Gaussians with Lorentzians). At ambient
temperatures and low values of momentum transfer the quasi-elastic
peak width was difficult to measure. The Voigt curves were
deconvolved by generating several trial Voigt curves from the known
resolution function, a Gaussian and and estimated Lorentzian function
the final Lorentzian value being interpolated. The results are

shown in Table IVxviii(a).

The width of the deconvoluted Lorentzian function is not expected to show any variation as the value of the momentum transfer changes, but only as the sample temperature changes. The results given in Table IVxviii(a) show little variation of Lorentzian width with Q (compare (19, 32, 9)). The temperature variation would be expected to reflect the change from a fixed librator to a more freely rotating system (20). The results obtained show that at any one Q value the width decreases with temperature, which suggests that the rotational contribution, already predominant at room temperature is increasing. This is equivalent to the situation in Section I 2.3.3 case (C). Values of t_1 can be estimated from Table IVxviii(a). These t_1 values are 7.5, 8.2 and 10.3 (10^{-12} sec) for temperatures of $295°$, $333°$ and $373°K$ respectively. (The logarithm of the t_1 appear to be directly related to temperature). These values are similar to the values reported for other reorientating molecular systems (9, 19, 32) and are also of the same order of magnitude suggested by the F_{11}^{lib} measurements (see previously).

Although this is probably the correct explanation of the observations, it is important to state that the errors in measuring widths are likely to make less contribution to estimated widths as the temperature rises. This is because the quasi-elastic peak becomes more intense as the temperature rises. The estimated half height is thus more accurate and leads to a corresponding increase in the accuracy of the full width measurement. These spectra should be repeated, collecting significantly more data. This is especially true for the ambient temperature spectra.

3.4.1 Spectra of sodium borohydride at low temperatures: results

The down scattering spectrum of sodium borohydride at 77°K was obtained from ca. 220cm^{-1} (lowest incident neutron energy), the results are given in Table IVxix. Only two peaks, one with a low energy shoulder, were observed. There was no broad inelastic scattering feature. The neutron down scattering spectrum was also taken at the intermediate temperature of ca. 197°K. This was more complex, showing a broad scattering feature with some superimposed peaks, these peaks were very broad (see Table IVxix). The infrared absorption spectrum taken at 77°K was little different from that at 294°K.

3.4.2 Spectra of sodium borohydride: discussion

At 190°K the sodium salt undergoes a phase transition (17) from face centred cubic to body centred tetragonal. This phase change and the reduction in the thermal motions of the ions in the lattice are responsible for the spectral changes observed. The absence of any broad scattering feature in the down scattering spectrum at 77°K is a reflection of the increased residence time of the borohydride unit in a librational state. This is consistent with the low temperature observations on the caesium salt (which is still face centred cubic at 77°K). Two librational states are predicted for the low temperature phase of sodium borohydride, A_2 and E in character (see Table IVvi). Both peaks, at 246 and 339cm^{-1}, and also the main peak with shoulder, at 308(sh) and 339cm^{-1}, could be assigned to transitions involving these states. (v,libA$_2$ and v,libE). The two librational states are caused by the relative contraction, of the unit cell of sodium borohydride, by only a small amount along the c axis (a 4% difference of the c

Table IVxix.

Table comparing the spectral results of the two phases of sodium borohydride.

NaBH₄ Disordered Phase					Assign.	Ordered Phase		
294°K Infra-red This study cm⁻¹	Previously cm⁻¹	294°K neutron scattering up =45° cm⁻¹	down cm⁻¹	197°K down cm⁻¹		77°K Infra-red This cm⁻¹	80°K Prev. cm⁻¹	77°K neutron down scatt. cm⁻¹
	(1)						(1)	
		25						
		55						
		72						
		99						
		113						
150	161	140				145		
210?		175	194				172	
230?		262	256	225$_b$		225		
		313	282	303$_b$	ν, OB_2			246
			417					
			513		$\nu, libA_2$			308$_{sh}$
					$\nu, libE$		(350$_{(2)}$)	339
							384	

notes.

ν, OB_2 = transition to an optic mode of B_2 character, etc. for $\nu, libA_2$ etc.

b = broad
sh = shoulder
? = possibly not observed

ref. (1) Harvey (1971) (2) Stockmayer (1953)

N.B. For the assignments of the bands observed in the disordered phase see relevant tables. For explanation of the assignments see text.

axis relative to the a or b axes). The main peak and its shoulder,
at 308(sh) and 339cm^{-1} are assigned to the librational transitions.
Calculations (discussed in section III) show that the barrier to
reorientation of a borohydride ion about an S_4 axis, parallel to
either a or b directions in the unit cell, is greater than the barrier
to reorientation about an S_4 axis, parallel to the c direction.
Therefore the shoulder at 308cm^{-1} is the transition ν, lib_{A_2}
(this involves the libration about the c crystal axis) and the band
at 339cm^{-1} is the transition ν, lib_E (this involves the librations about
the a or b crystal axis). The E mode, being doubly degenerate, would
be expected to have about twice the intensity of the A_2 mode, the
measured intensity ratio A2 : E : 1:1.57. (there was difficulty in
estimating a background to take the intensity measurement from
and since the cross-section for the two events is not strictly equal,
the ratio obtained is reasonable). The values obtained for the
fundamental transitions ν, lib_{A_2} and ν, lib_E may be compared with the
estimates given by Stockmayer (1953) and Harvey (1971)(a), see
Table IVxix. Stockmayers estimate of 350cm^{-1} is in reasonable
agreement, considering he used thermodynamic data. His results
represent an average of the two fundamentals. Harvey's estimate, 384cm^{-1},
is somewhat high, especially since it is estimated from a transition
assigned to $\nu, 3lib$ (see Table IVviii). In the harmonic approximation
our results indicate $\nu, 3lib_E$ of 1017cm^{-1}, and $\nu, 3lib_{A2}$ of 924, which
are over 100cm^{-1} removed from Harveys assigned band. Considering that
our spectra show no evidence of $\nu, 2lib$ or $\nu, 3lib$ it is likely that
Harvey's assignment of the band at 1153cm^{-1} is wrong. The values

of the fundamentals (308 and $339cm^{-1}$) provide the barrier heights

to their particular wells.   The barriers (Vo) are 4.27 and 5.13Kcals

$mole^{-1}$ respectively (for the deep well approximation eq

and 4.72 and 5.67 Kcals $mole^{-1}$ (for Das's solution of the matheiux

equation: eq III.1.xix).   The lower barrier is comparable with

that obtained for the high temperature phase since the relevent unit

cell dimensions are similar (below λ pt a = b = 6.157$\overset{o}{A}$, above

λ pt a = b = c = 6.164$\overset{o}{A}$).   The high barrier, result of the

contraction along the c axis, is about 20% higher than the low

barrier.

The low energy band in the spectra, $246cm^{-1}$, is likely to be the

excitation of an optic mode.   In the low temperature phase of sodium

borohydride the optic modes have different character B_2 and E,

see Table IVv.   Both modes are infrared active, however there is no

appreciable difference between the ambient temperature infrared and

that taken at $77^{o}K$.   This is a further indication that the

infrared spectrum is dominated by surface modes.   In the ambient

temperature phase v,LO was observed at $194cm^{-1}$ and as the temperature

falls and the unit cell becomes more compact the energy of the LO

vibrational state would be expected to increase.   The band at

$246cm^{-1}$ is assigned to the transition from the ground state to the

optic mode of B_2 characters.   The sharp features seen in the spectrum

at $77^{o}K$ do not remain above the λ point.

At $197^{o}K$, just above the λ point, the spectrum shows a very

broad scattering feature.   This may be a broad scattering feature

similar to that observed in the ambient spectra or it could be the

envelope of unresolved bands.   As was done with the ambient spectra

an estimate of the position and width of the broad scattering feature

was obtained.   (This was to provide a value of F_{11}^{lib}, discussed in

Section I, eq. I2.3.3(xxi)).   The value of F_{11}^{lib} obtained

($F_{11}^{lib} \sim$ 0.35) is not in line with expectations.   At ambient

temperatures $F_{11}^{lib} \sim$ 0.44 and should increase at lower temperatures.

It is most likely that the broad feature results from a failure to

resolve several bands.   All of these bands are broad and flat topped,

thus their position is not well defined.   The two most prominent bands,

at 225 and 303cm^{-1}, may represent transitions from the ground state

to the longitudinal optic and librational states (v,LO and v,lib).

They could be as readily assigned to the high or the low temperature

phase of the salt.   It is probable that the solid is not in one phase

wholly, but exists as a mixture of crystals in different phases all

of which contribute to the spectrum.   It might be possible to estimate

from the spectrum the percentage of each phase present.   This was not

attempted with these samples since the main transitions do not change

in value significantly with the change of phase.

3.5.1 Lithium borohydride: results

The ambient temperature inelastic up scattering spectrum of lithium

borohydride, in its general appearance, was very similar to the other

alkali metal borohydrides.   The bands were superimposed on a region

of high scattering, Table IVxx.   The down scattering spectrum, at

77°K, showed no broad scattering, Table IVxx.   The infrared spectrum

was completely atypical of results from the other borohydrides.

Absorption was strong over the region covered from 100cm^{-1};   the peaks

observed, at 77°K, were broad and of slight intensity above this background.

Table IVxx.

Table showing the observed bands in the LiBH$_4$ spectra, cm^{-1};

at different temperatures.

LiBH$_4$				Neutron up scatt. assignment	Prediction of band positions from Fig. IViv
Inelastic neutron		Infrared absorption			
up-scatt. 294°K cm^{-1}	down scatt. 77°K cm^{-1}	this study 77°K cm^{-1}	previous work 80°K(1) cm^{-1}		cm^{-1}
50				νlib1,A1	50
90	70			νlib1,A2	90
148	157	156	162.5	νlib1,A3	148
		170$_{sh}$	175.5		
193	204			νlib1,	193
242	256	235$_b$	232	νlib2,A1	233
273	287	275	274	νlib2,A2	273
	335	315$_b$	324	νlib2,A3	331
		390	391		
376	412		(418)*	νlib2,	376
464					

Notes. sh = shoulder   **Ref.** (1) Harvey (1971)(b)
b = broad

* estimated from ν,311b transition at 1254cm^{-1}

scattering angle of 45°.

3.5.2 Lithium borohydride: discussion

Lithium borohydride is the only alkali metal borohydride with
a non-cubic crystal structure at ambient temperature.   Given by
Harris (1947) its lattice structure is D_{2h}^{16} (Pcmn);   the lattice
vibrational states are given for this structure in Table IVv.
These are not in agreement with Harvey's (1971)(b) analysis.   He
assumed a lithium ion site symmetry of C_s;   however the D_{2h}^{16} space
group possesses only four C_s sites, which we have taken to be occupied
by borohydride ions.   The site symmetry of lithium ions adopted in
this study is C_i.   (which is the only other site symmetry in D_{2h}^{16}
with four equivalent positions).   The irreducible representations
of the lattice librational states are shown in Table IVxi, and are in
agreement with Harvey (1971)(b).   Infrared spectra of the internal
molecular vibrations of the borohydride ion show no correlation field
splitting (15).   If correlation field splitting is ignored only the
site symmetry is important in determining the librational states
of an ion.   (Table IVvi also shows the libration of irreducible
representations in the absence of correlation field splitting).   Two
states are predicted, of character A' and A" respectively.   Transitions
involving these two states are assigned to the bands at 204 and 412cm^{-1}
(down scattering), which are very strong in all neutron spectra but
absent from the infrared spectra.   The relative intensities of the two
bands in the up and down scattering spectra remain constant at 1:1.
This similarity of intensity indicates that both bands are fundamentals,
rather than a fundamental and its first overtone.   The expected
occupancy of the states of a fundamental and its first overtone

(ν,lib and ν,2lib) would be I ν,lib: I ν,2lib: 1: 0.41 (using

ν,lib = 204cm^{-1} and ν,2lib 412, and using a Boltzman distribution

of states.

This estimate is a lower bound to the contribution made by

ν, 2lib.. Since the displacement of protons in the first overtone .

is larger than that for the fundamental. If the band is associated

with the first overtone it would demand that the proton displacement

in this mode be over twice that in the fundamental mode. The

cross-section for anovertone transition is lower than for the

fundamental (see Section I). The values of the potential barriers

are shown in table IVxxi. The uncertainty in the value of the

transition produces more variation in the value of the barrier than

the different equations used to obtain the values. The two barriers

are probably well represented by values of about 1.9 Kcals mole^{-1} for

the shallower well and 7.3 Kcals mole^{-1} for the deeper well.

The breadth of the librational bands, even at 77°K is large

(full width, half height of about 64cm^{-1}; which could be compared to

that of the ν,lib band in CsBH$_4$, 77°K, 34cm^{-1}).   It would not be

difficult to rationalise the width of these two librational transitions

as being broad inelastic features. It has been seen that such a broad

inelastic feature exists in the ambient up scattering spectra of the

other alkali metal borohydrides. The N.M.R. data (37) indicates only

one proton resonance (which is equivalent to rapid reorientation on the

N.M.R. time scale of 10^{-8}sec). It is likely that the ambient

temperature up scattering spectrum has another feature which is hidden

by the librational transitions. Unfortunately since the sample

contained B^{10} nothing could be gleaned from the quasi-elastic region.

Table IVxxi.

Table showing the barriers to reorientation of a librating

borohydride ion in lithium borohydride

Librational State	vlib, Up Scattering cm^{-1}	v,lib down Scattering cm^{-1}	Results of the application of the equations below *	
			(a) Kcal mole^{-1}	(b) Kcal mole^{-1}
vlib 1	193	204	1.68, 1.84	1.96, 2.18
vlib 2	376	412	6.35, 7.64	6.90, 8.24

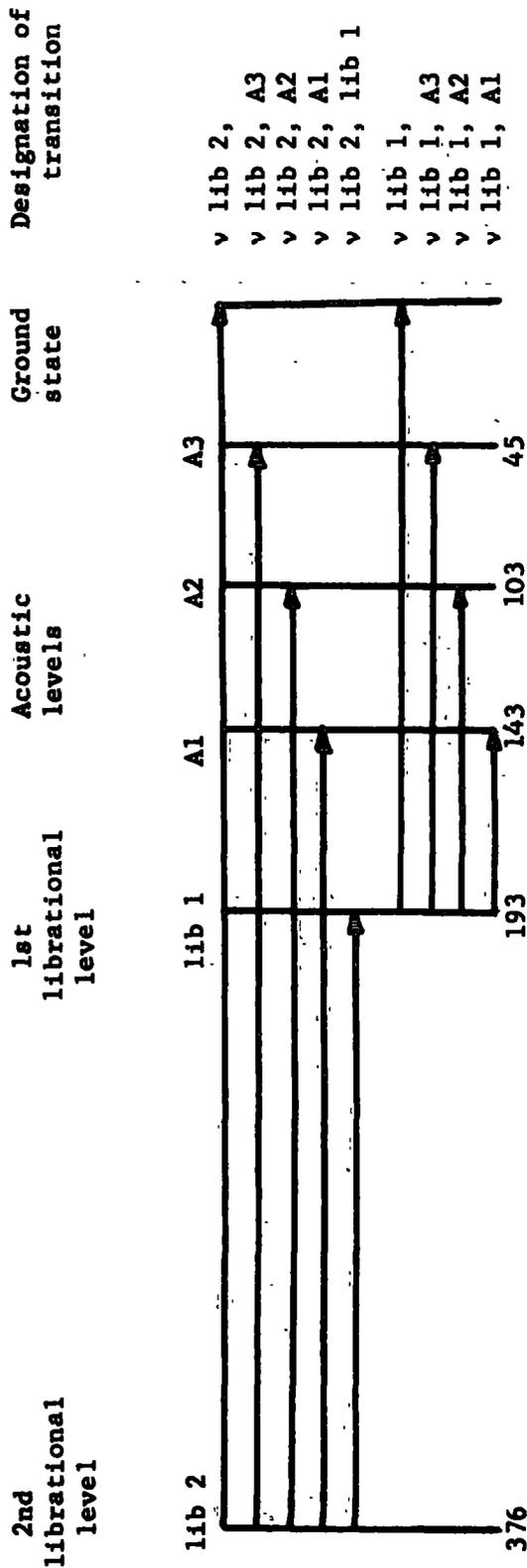* value of inertia of a BH_4 ion is 7.08×10^{-40} gm.cm.^{2}

(a) Deep well potential, Erying, Walter and Kimbal

(b) Solution of Matheiu equation by Das. (See Section III)

Most of the other bands observed in the inelastic spectra have corresponding absorptions in the infrared region. As was previously shown, for the main alkali metal borohydrides, the number of transitions between lattice states can be very large; and may follow a complex pattern. The presence of two distinct librational modes and a more complex crystal structure in lithium borohydride multiplies the opportunities for such transitions. However all of the bands can be explained in terms of the previously used cascade model. The levels required are the two librational states and three lattice vibrational states (see Fig. IVix and Table IVxx). Transitions between these levels explain the observed up scattering spectrum, and reasonable agreement is found for the down scattering events. The vibrational states which these levels represent probably correspond to the three accoustic modes of the crystal; which have B_{1u}, B_{2u}, and B_{3u} character (see Table IVv). The values are shown in Fig. IViv. It is not clear why the optic modes themselves are not strongly active even in the infrared spectrum. Infrared absorption over the whole region from $600cm^{-1}$(14) to $100cm^{-1}$ is strong and it may be that the optic modes are responsible for this.

The spectra observed are explicable in terms of the expected site symmetry of the borohydride ion. It is unnecessary to postulate, as Tung Tsang (1969) has, two crystallographically different borohydride sites. The change in the proton relaxation times T_1 observed by Tung Tsang (1969), see earlier, is probably a reflection of the two librational states of the borohydride ion. The T_1 relaxation process is governed by the transitions from the ground state to higher librational states (38). The observed relaxation times are an average

Fig. IV.iv

205.

De-excitation transitions suggested for lithium borohydride

| 2nd librational level	1st librational level	Acoustic levels			Ground state	Designation of transition

(approximate energy of the levels, cm^{-1})

of the relaxation caused by transitions to the A' librational states and also to the A" librational states. As the temperature is lowered from ambient the relative importance of the two types of transition, in relaxing the signal, should change. At low temperatures in the shallower potential well transitions can still occur to states close to the barrier top. (These transitions are most efficient at relaxing the signal (38)). Whilst transitions of similar energy occuring in the deeper potential well will not involve states close to its barrier top. This type of mechanism would explain the apparent decrease in activation energy as the temperature falls. (A similar state of observations should hold for sodium borohydride below its λ point, however the two wells are so very much alike that their change with temperature is probably not appreciable in N.M.R. results).

Fig. IV.v

207.
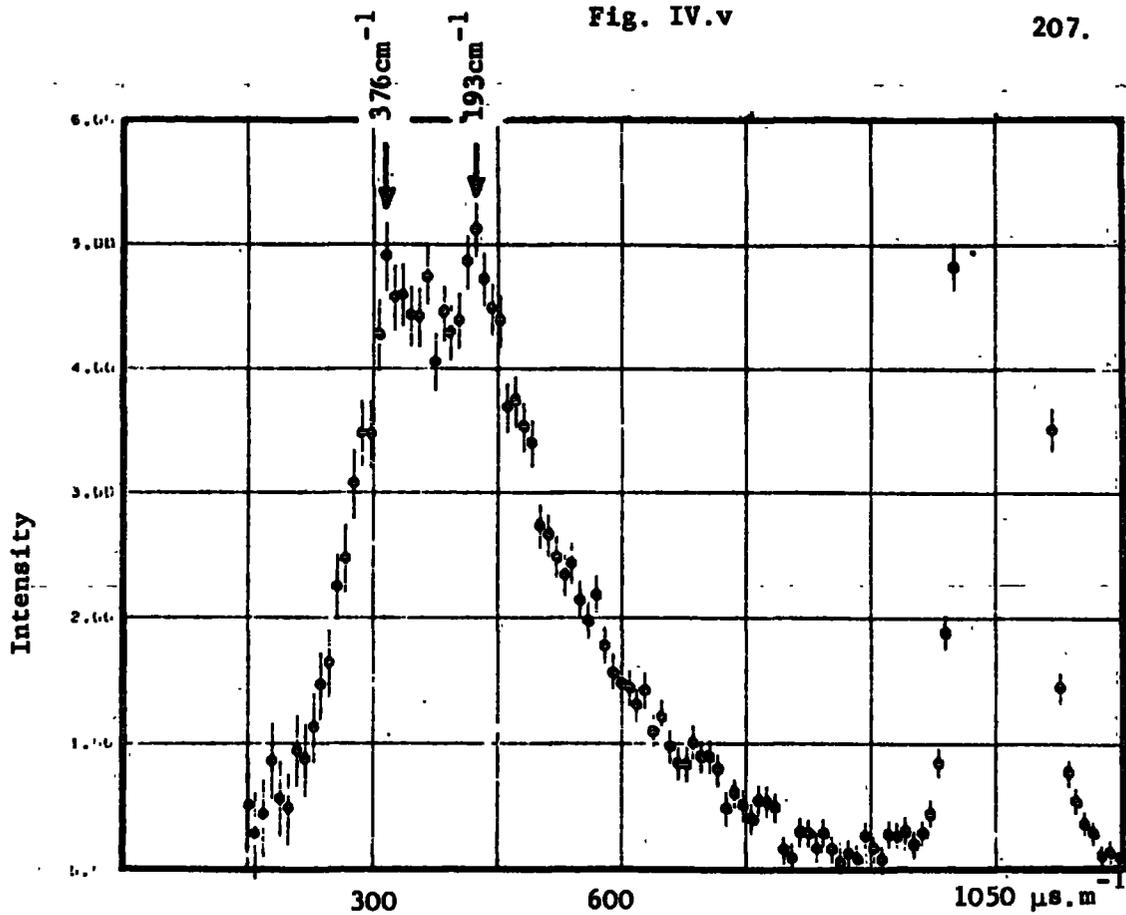
Inelastic up scattering spectrum of LiBH$_4$ θ = 45°
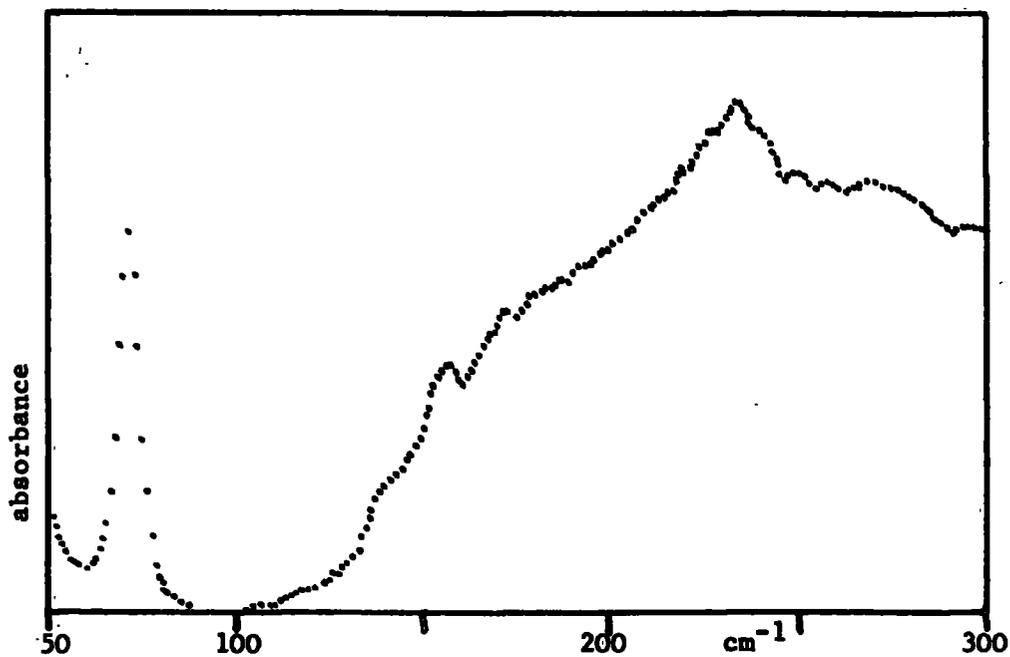
Infrared absorption spectrum of LiBH$_4$

Fig. IV.vi

208.
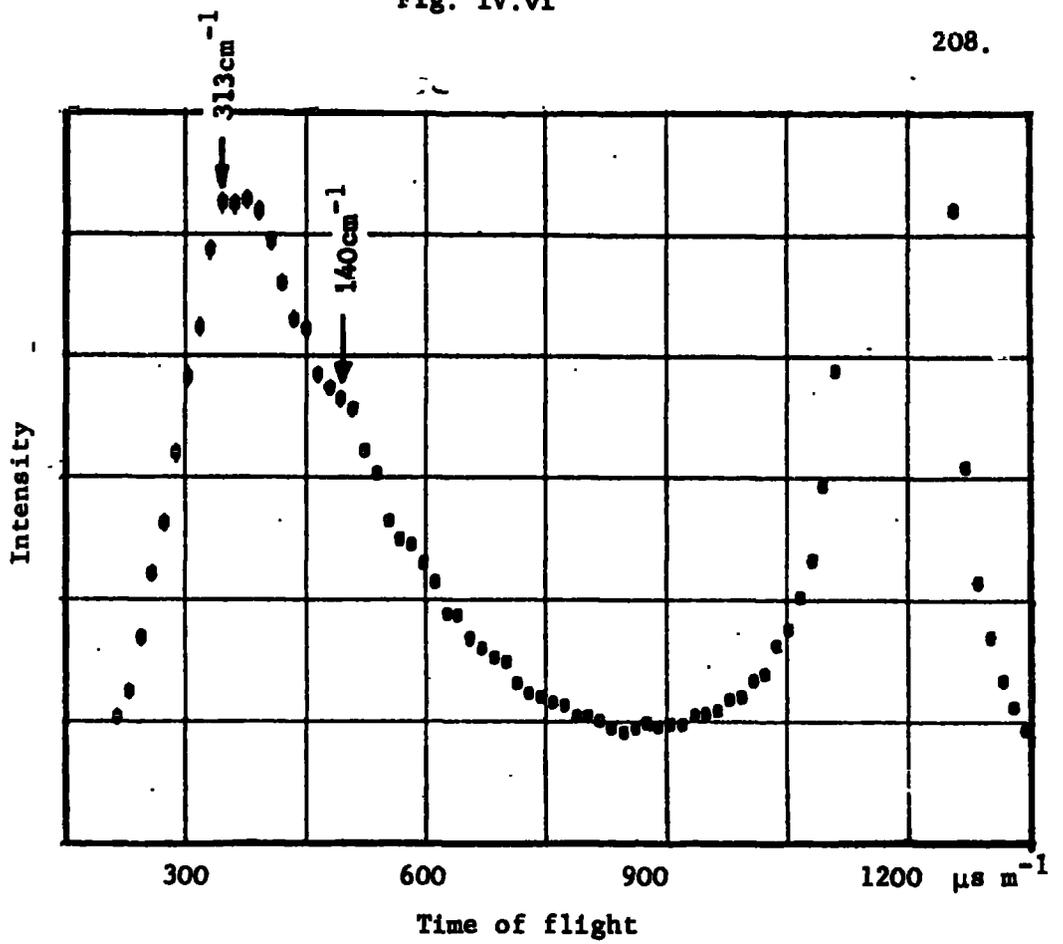
Inelastic up scattering spectrum of NaBH$_4$, $\theta = 45°$
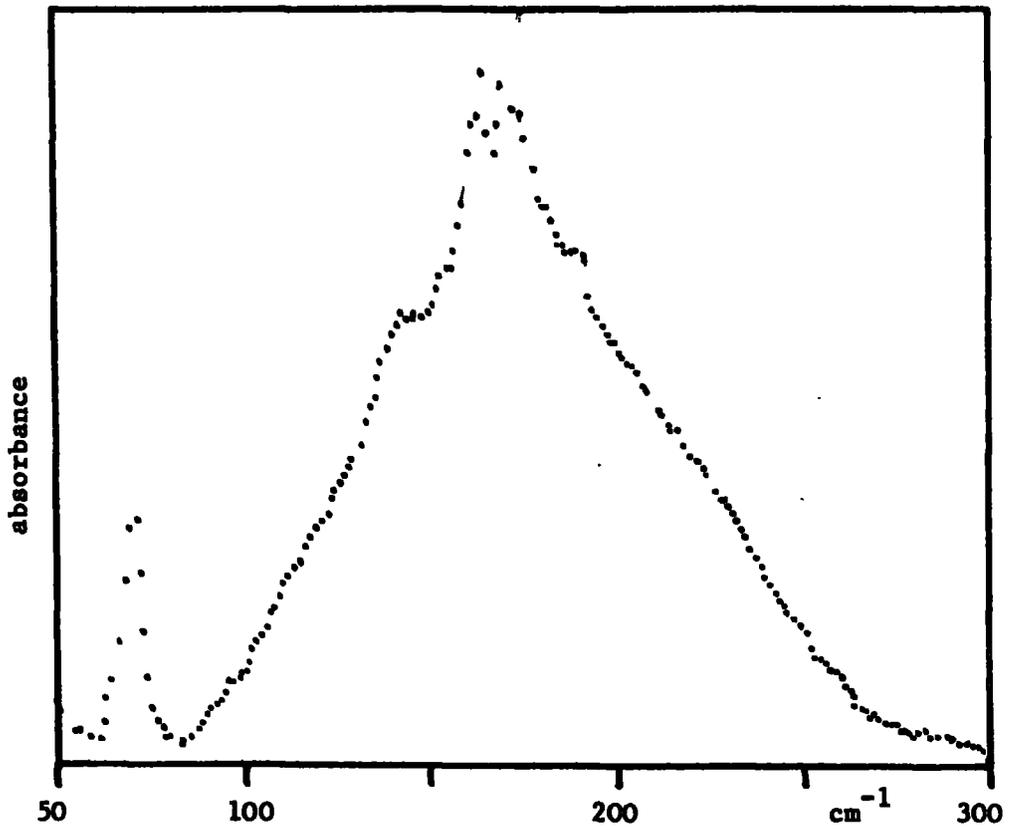
Infrared absorption spectrum of NaBH$_4$

Fig. IV.vii

209.
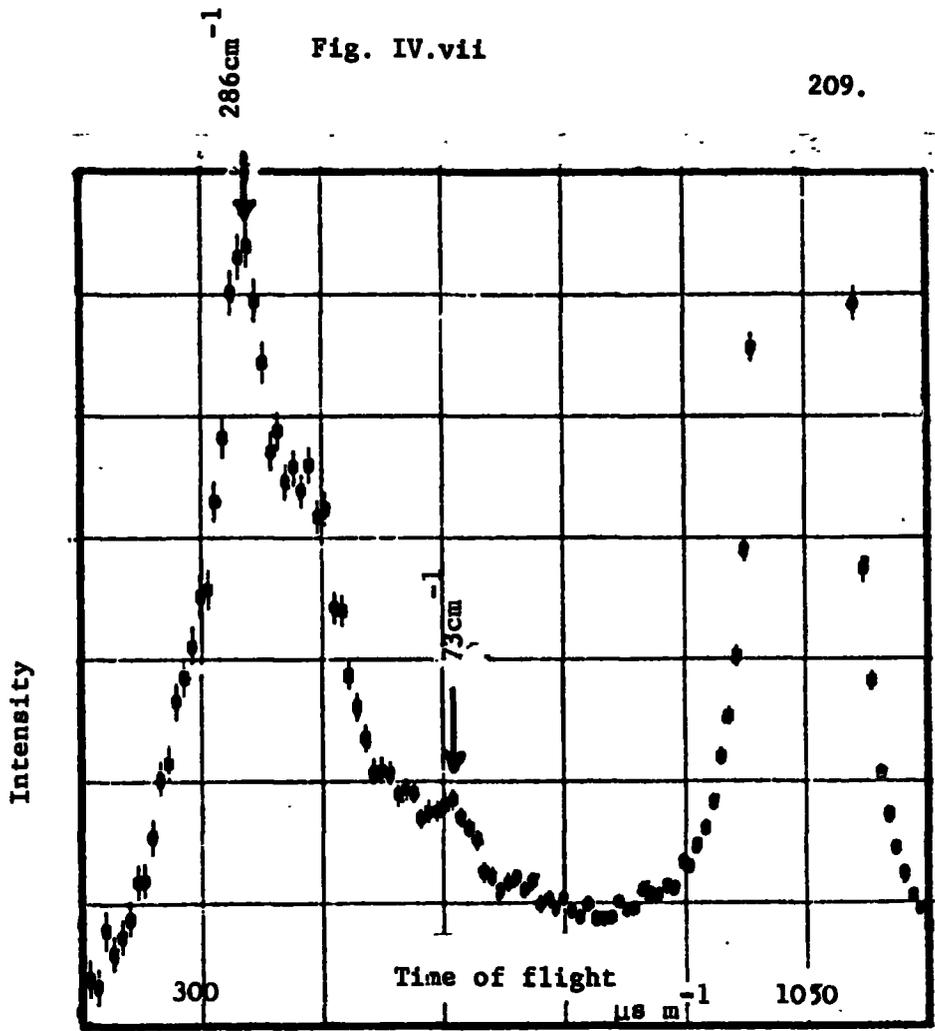
Inelastic up scattering spectrum of KBH$_4$, θ = 45°
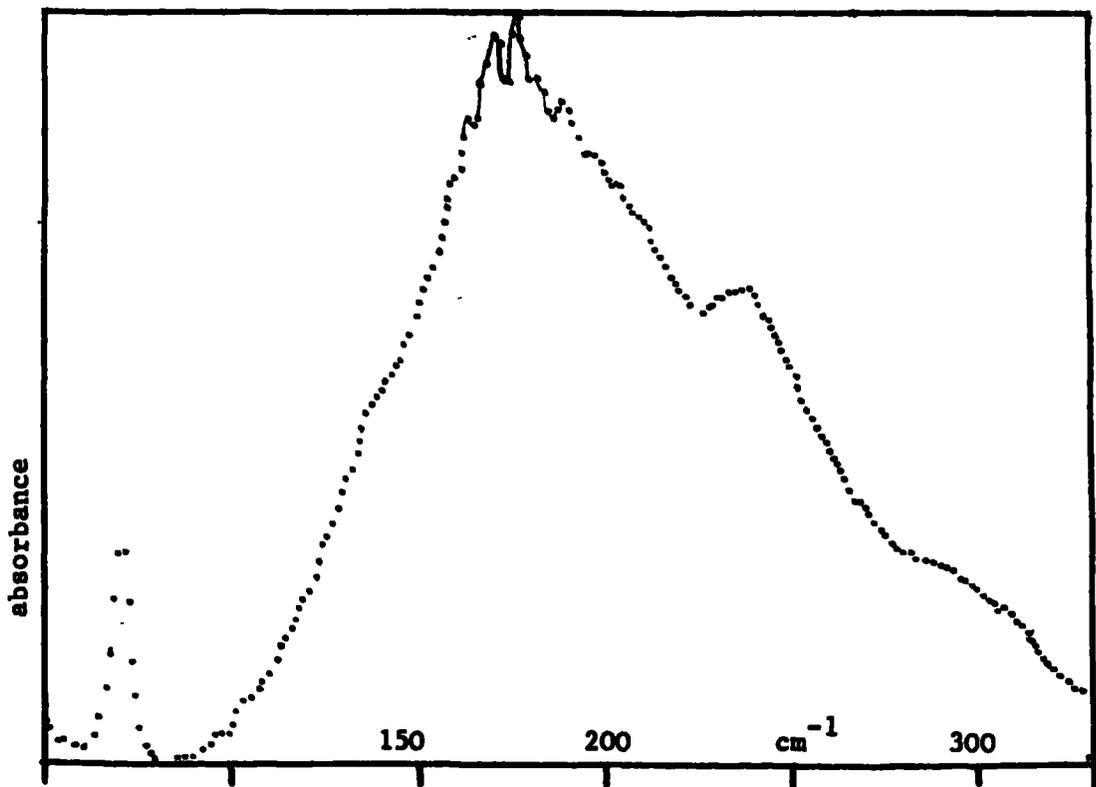
Infrared absorption spectrum of KBH$_4$

Fig. IV.viii

210.

273cm^{-1}

174 cm^{-1}

Intensity

Time of flight

300

1050 µs m^{-1}

Inelastic up scattering spectrum of RbBH$_4$ θ = 45°

Absorbance

100   200   cm^{-1} 300
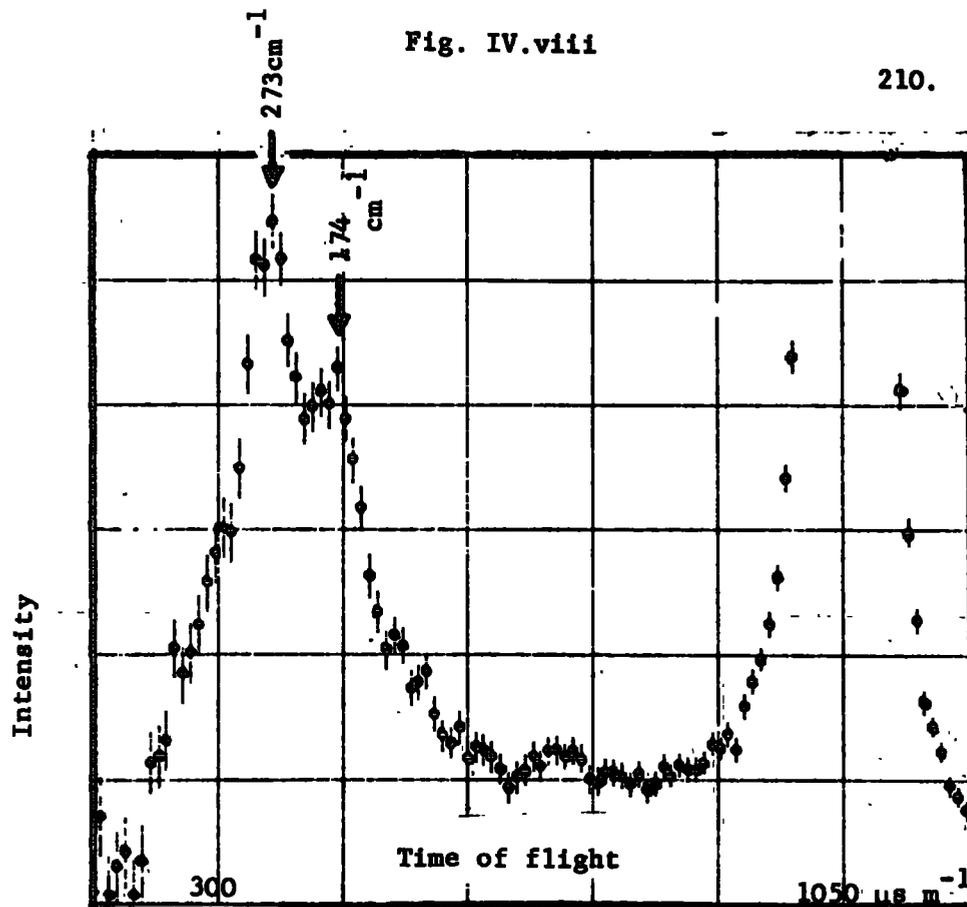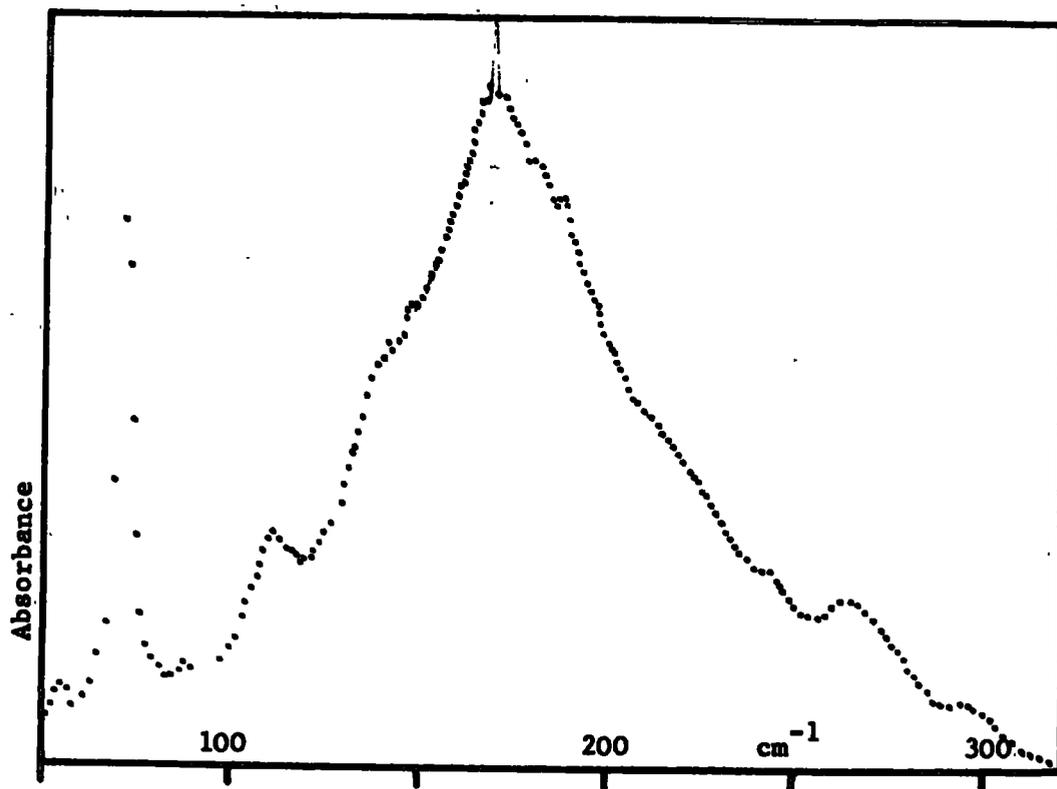
Infrared absorption spectrum of RbBH$_4$

Fig. IV.ix   211.
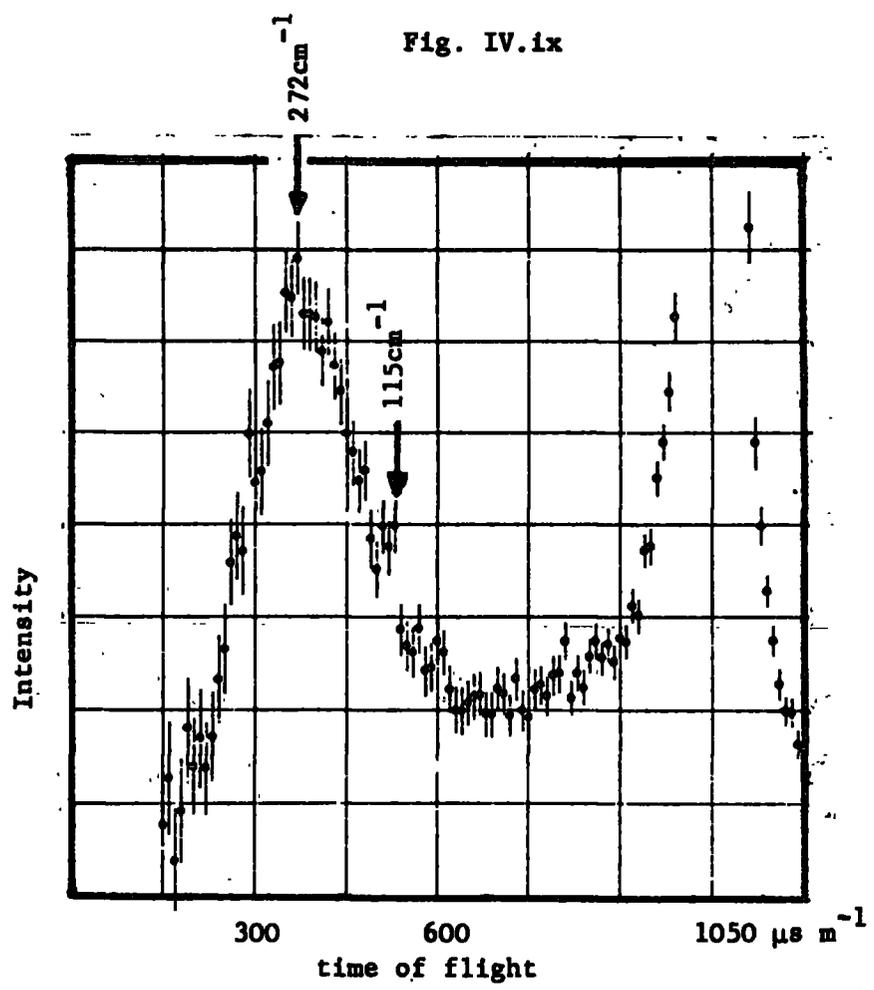
Inelastic up scattering spectrum of CsBH$_4$ $\theta = 45°$
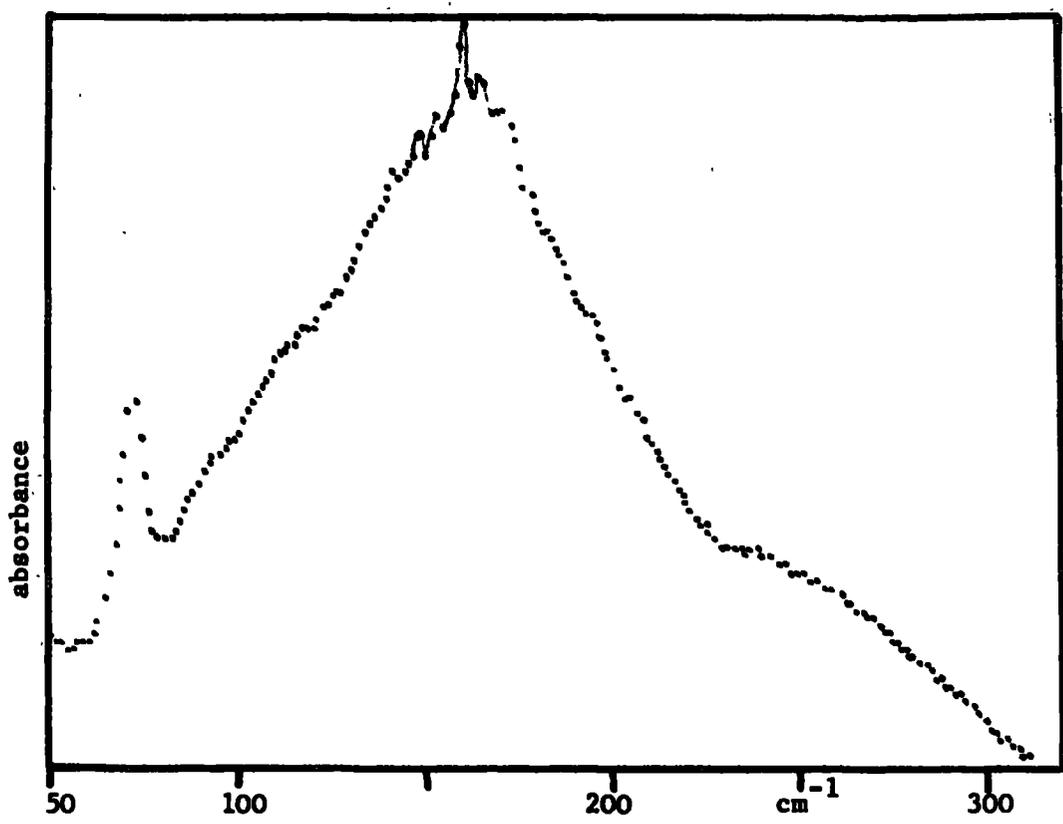
Infrared absorption spectrum of CsBH$_4$

Fig. IV.x

212.

Inelastic down scattering spectra of CsBH$_4$

Incident neutron energy.

Fig. IV.xi

213.
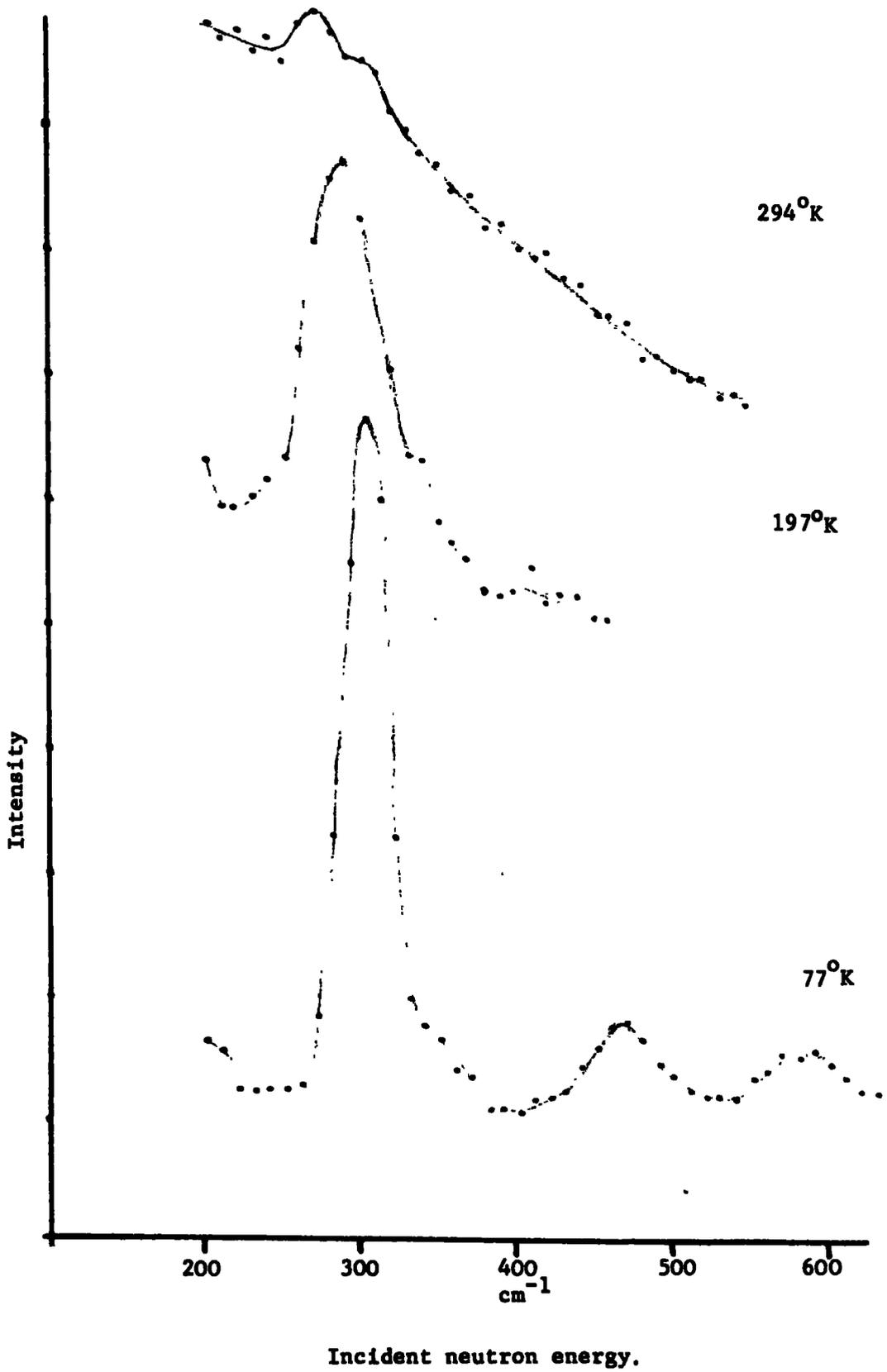
Inelastic down scattering spectrum of

NaBH$_4$, below the λ point, 77°K

Incident neutron energy
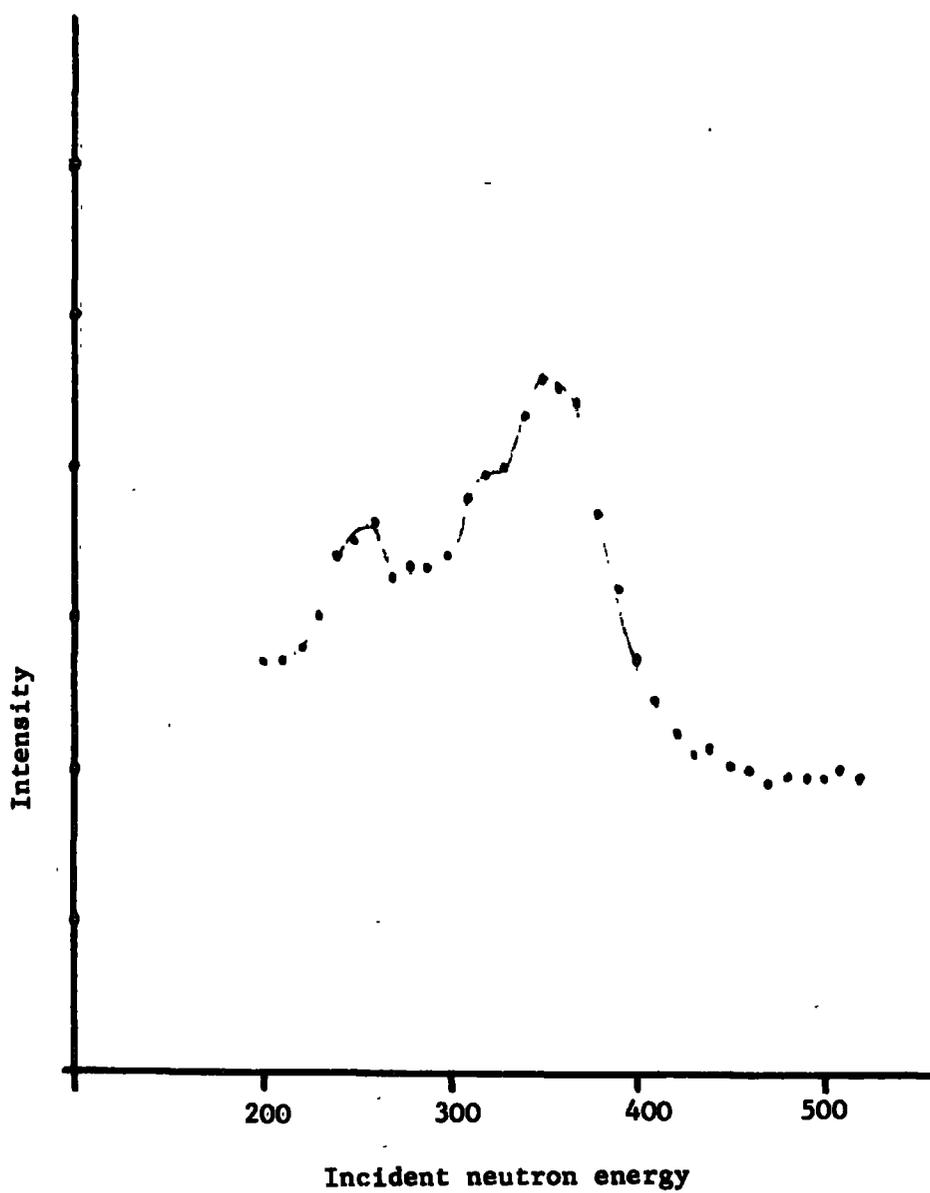
REFERENCES

1. Abrahams, S.C.   J. Chem. Phys. 22, 434, (1954).

2. Banus, M.D.   J. Am. Chem. Soc., 76, 3948 (1954).

3. Berreman, D.W.   Phys. Rev., 130, 2193, (1963).

4. Brockhouse,   Phys. Letters. 29A, 694, (1969).

5. Coker, H.E.   J. Chem. Phys., 48, 2713 (1968).

6. Ford, P.T.   Acta Cryst., 7, 604, (1954).

7. Ford, P.T.   Discus. Faraday Soc., 19, 230, (1955).

8. Furukawa, G.T. J. Nat. B. Standards 68A, 651, (1964).

9. de Graaf, L.A.   I.N.S. Proceedings, Grenoble.   247, (1972).

10. Gutowsky,   J. Chem. Phys., 18, 162, (1950).

11. Hallet, N.C.   J. Am. Chem. Soc., 75, 1496, (1953).

12. Harris, P.M.   J. Am. Chem. Soc. 69, 1231, (1947).

13. Harvey, K.B. (a)   Can. J. Chem. 49, 3272, (1971).

14. Harvey, K.B. (b)   Can. J. Chem. 49, 3282, (1971).

15. Harvey, K.B. (c)   J. Chem. Phys. 55, 4390, (1971).

16. Hertzberg, G.   "Molecular Spectra Vol II" Van Nostrand (1945).

17. Johnston, H.C.   J. Am. Chem. Soc., 75, 1467, (1953).

18. Ketelaar, J.A.   Spectrochim. Acta., 17, 1240, (1961).

19. Kim, H.J., Solid State Comm., 8, 889, (1970).

20. Larsson, K.E.   J. Chem. Phys., 59, 4612 (1973).

21. Niemela,   An. Univ. Turku., 1A, 132, (1970).

22. Ogg, R.A. J. Chem. Phys., 22, 1933, (1954).

23. Ossman, G.W.   J. Chem. Phys., 47, 5452 (1967).

24. Pavlevsky, H.   J. Phys. Chem. Solids., 24, 617 (1963).

25. Peterson, E.R.   Diss. Abst., 25B, 5588 (1965).

26. Price, W.C.   J. Chem. Phys., 17, 1044, (1949).

27. Ruppin, R. Rep. Prog. in Phys., $\underline{33}$, 149, (1970).

28. Schlesinger, H.I. (a) J. Am. Chem. Soc. $\underline{75}$, 213, (1953).

29. Schlesinger, H.I. (b) J. Am. Chem. Soc. $\underline{75}$, 205, (1953).

30. Schutte, C.J.H. Spect. Acta., $\underline{16}$, (1960).

31. Schutte, C.J.H. Nature. $\underline{189}$, 745, (1961).

32. Skolt, K. J. Chem. Phys., $\underline{49}$, 2443 (1968).

33. Smith, D. J. Chem. Phys., $\underline{60}$, 958, (1974).

34. Soldate, A.M. J. Am. Chem. Soc., $\underline{69}$, 987, (1947).

35. Stephenson, C.C. J. Chem. Phys., $\underline{23}$, 1960, (1955).

36. Stockmayer, W.H. J. Chem. Phys., $\underline{21}$, 1311, (1953).

37. Tung Tsang. J. Chem. Phys., $\underline{50}$, 3498, (1969).

38. Wallach, D. J. Chem. Phys., $\underline{52}$, 2534, (1970).

CHAPTER V

THE MOLECULAR BOROHYDRIDES

As the dynamics of a probe are determined by its environment, the study of the molecular borohydrides is complementary to the study of the crystalline borohydrides. The molecular borohydrides of aluminium and zirconium can be regarded as aggregates of borohydride ions and metal ions. The intramolecular dynamics of these molecules will be discussed in terms of the motions of these components. However the molecular nature of these compounds introduces features which contrast with the dynamics of calcium borohydride, which is strictly an aggregation of ions. Further it will be seen that the concept of a borohydride unit is not always useful. The dynamics of systems like the octahydrotriborate anion cannot be discussed in this manner.

The individual compounds are discussed in turn, firstly the ionic calcium borohydride then the molecular borohydrides of aluminium and zirconium and finally the octahydrotriborate anion. A review of previous work on these compounds is given. Then the experimental work is presented and the results interpreted. Finally the results as a whole are discussed.

1. Previous Work.

Unfortunately the molecular borohydrides, borohydrides of the alkaline earth metals, and higher boron hydrides do not form so useful

Table VI.

Comparison of the atomic properties of some relevent metals

Li	Be	
+1 0.6	+2 0.31	
0.97	1.47	
0.08	0.03	
Na	**Mg**	**Al**
+1 0.95	+2 0.65	+3 0.5
1.01	1.23	1.47
0.2	0.1	0.07
K	**Ca**	**Zr**
+1 1.33	+2 0.99	+4 0.8
0.91	1.04	1.22
0.9	0.6	-

(1) Alred-Rochow calculation,   (2) H ≡ 1.0,   (3) F ≡ 1.0.

Scheme.

Element

normal Ionic   Ionic (1)
charge   Radius

Electronegativity(2)

Polarisability (3)

a group for study as do the alkali metal borohydrides. These
compounds are all well known in the literature and their chemical
properties are determined (45). Some aspects of their physical
properties are not known at all, and for those that are there are
variations in detail.

1.1 Calcium borohydride Ca(BH$_4$)$_2$

There are no reports in the literature of any, but chemical,
properties of this compound. Table VI. shows a comparison of the
properties of calcium with other metals of interest. It is obvious
that the calcium atom has more in common with metals forming ionic
borohydrides than those which form molecular borohydrides. Indeed
compared to the borohydrides of beryllium and magnesium, calcium
borohydride has been described as more ionic. (46). The reported
chemical properties support this view; high melting point (320°C)
593°K and low solubility in tetrahydrofuran. Unfortunately its
structure in the crystalline form is unknown and crystal effects are
known to be very important in the beryllium compound (36).

1.2 Aluminium borohydride Al(BH$_4$)$_3$

This compound is molecular, it is a low melting point liquid
(209°K) with appreciable vapour pressure at ambient temperatures, (46).
The models most often used to represent the molecule are those
suggested by Longuet-Higgins (1946). These involve coplanar
aluminium and boron atoms, with two possible proton configurations which
lead to D$_3$ or D$_{3h}$ symmetry (see Fig. VI). Beach (1940), using electron
diffraction, showed the coplanarity of the heavy atoms. However

Fig. V.i

220.

Configurations of the aluminium borohydride molecule

(The central aluminium atom is omitted)

D_{3h} symmetry
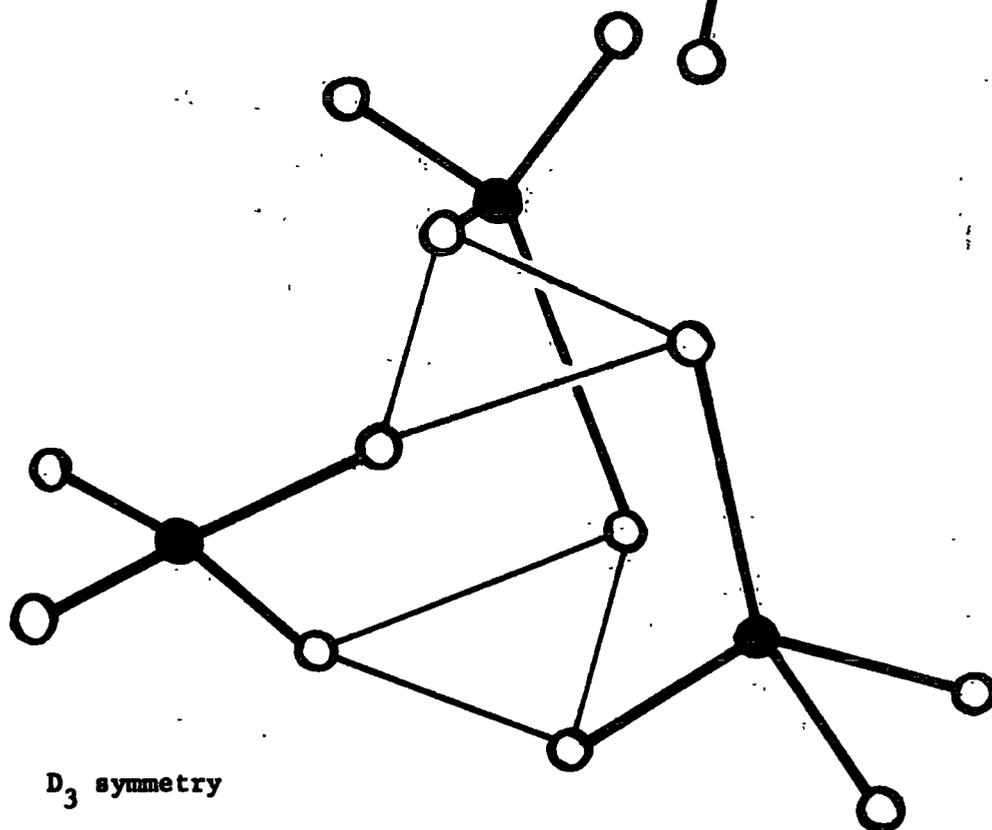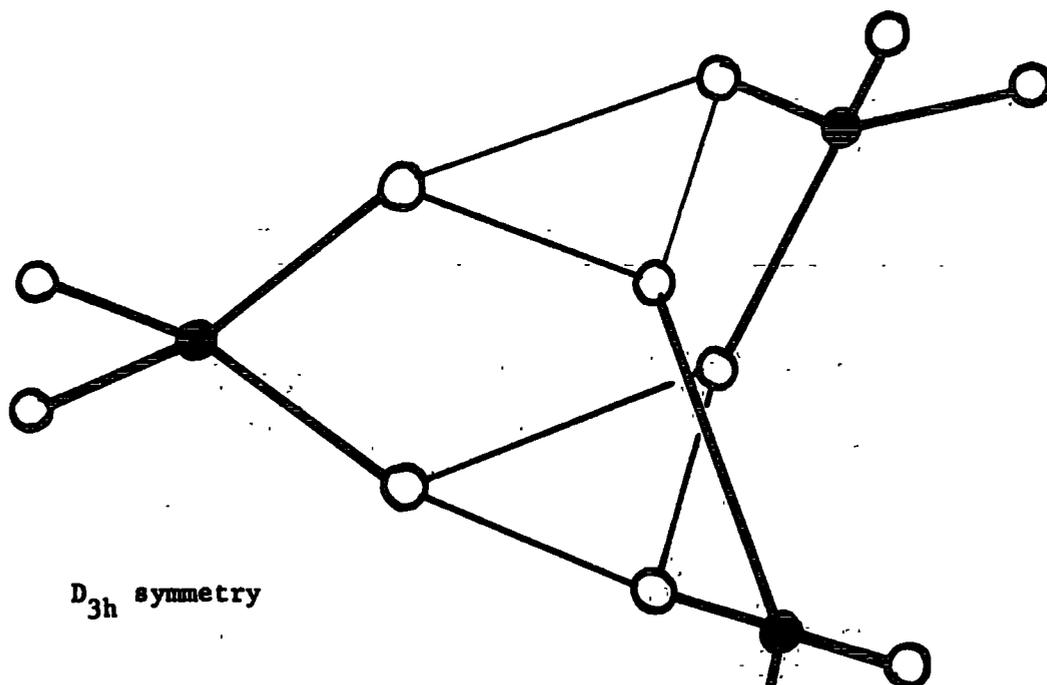
D_3 symmetry

this study and the early spectroscopic work, Price (1949) infrared,
and Emery (1960) Raman, were unable to distinguish between the two
symmetries. Almeningen (1968) collected electron diffraction data
most consistent with a D_{3h} symmetry. Coe (1972) undertook a very
extensive survey of the infrared, Raman, and proton N.M.R. spectra;
of the solid, liquid, and vapour. Infrared and Raman spectra should
be a most sensitive probe for molecular symmetry, since their
selection rules are dependent upon molecular symmetry. The results
obtained by Coe indicated a D_{3h} symmetry with little if any D_3
character. Crystal structure studies, by X-rays, conducted by
Semenenko (1972) showed that his data was consistent with a D_{3h} model.
There was a transition point at $195^{\circ}K$ which corresponded to a crystal
phase change, from alpha to Beta phases, molecular symmetry was however
conserved. The space group of the low temperature α phase was not
reported (the unit cell was hexagonal a = 7.5, c = 9.05Å). The β
phase was orthorhombic (a = 7.5, b = 12.1, c = 8.94 Å), and had
D_2^4 ($P_{21'21'21}$) space group. Levison (1970) has attempted to correlate
the geometry of aluminium borohydride D_{3h} or D_3 with a suitable
electronic structure. The computed molecular energy of the two
symmetries indicated that the structure should be determined by nuclear
repulsions, as is the case in many conformers. (e.g. ref. 2). The
geometry of D_{3h} symmetry was found to be the most stable (by ca 212
Kcals mole^{-1}).

1.3 Zirconium borohydride $Zr(BH_4)_4$

Zirconium borohydride has only been studied relatively recently,
however it has proved much more amenable to analysis than the aluminium

Fig. V.ii

222.

Configuration of zirconium borohydride.

(The central zirconium atom is omitted)
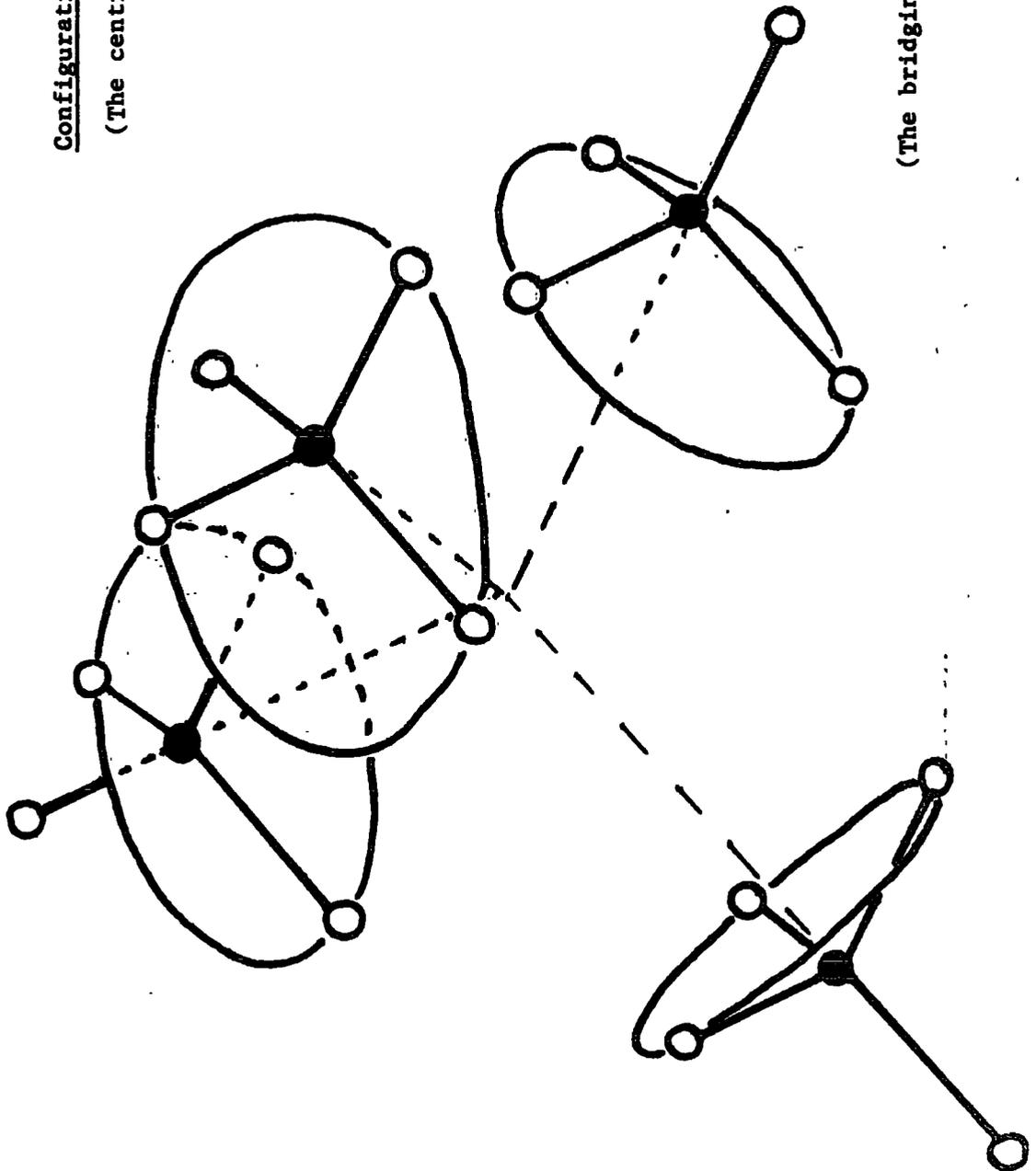
(The bridging protons are somewhere on the circles).

borohydride. The compound is molecular it is a liquid at just above ambient temperatures (M.P. = 302°K). X-ray results collected by Bird (1967) show the molecule to be of tetrahedral symmetry with only one terminal proton per boron atom. This suggested a triple proton bridge structure (see Fig. Vii). Electron diffraction data, Plato (1971), showed that this structure was present in the vapour phase. This work was confirmed by the Raman spectrum obtained by Smith (1971) and the infrared spectrum obtained by Davies (1973). The strict tetrahedral symmetry was sufficient to explain all observed modes and the spectra were consistent with a triple proton bridge. The crystal structure of zirconium borohydride, at 113°K, is T_d ($P\overline{4}3m$) with one molecule to the unit cell. There have been no thermodynamic data published.

1.4 Octahydrotriborate anion $B_3H_8^-$

Little work on this stable anion has been undertaken, mostly it has been concerned with its structure. Lipscomb (1959) suggested the structure shown in Fig. Viii. This was confirmed by the work of Peters (1960) from x-ray crystallographic data (conducted on diamoniate tetraborane $[(H_3N)_2BH_2^+][B_3H_8^-]$ at 173°K). The molecular ion has C_{2v} symmetry and appears to retain it in a number of compounds (20). The crystal structure of the tetramethyl ammonium salt is unreported, and no data on the $B_3H_8^-$ salts are available.

1.5 Fluxional behaviour of the molecular compounds

For the molecular borohydrides the concept of a stable proton configuration is unlikely to be valid. This conclusion is the result

Fig. V.iii

224.

The structure of the octahydrotriborate anion, and its carbon heterocycle analogue

1,3 dioxolane

, boron

, oxygen

octahydrotriborate anion

, hydrogen

; carbon

C$_{2v}$ symmetry
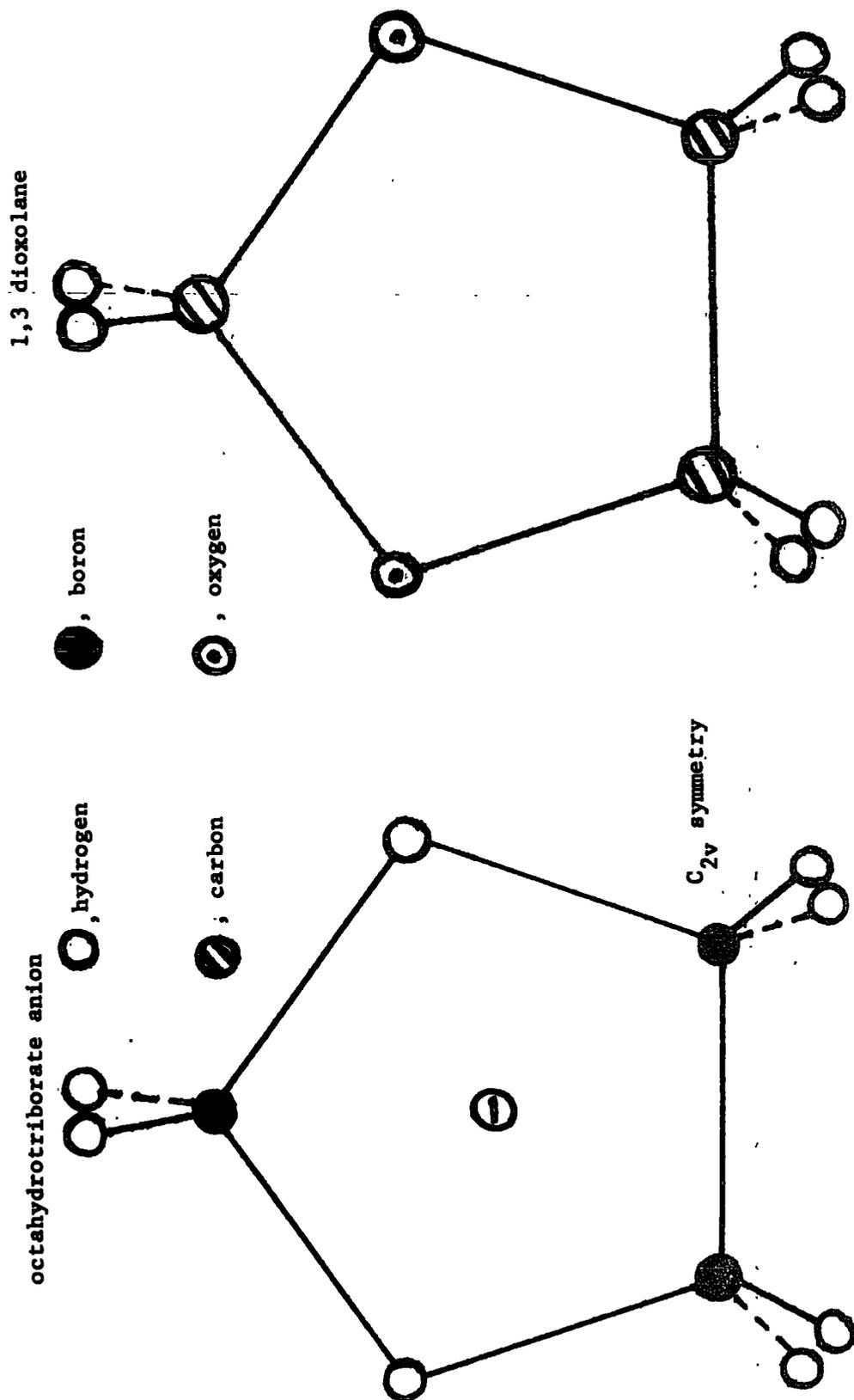
of much work on these compounds by proton N.M.R. studies. In a stable molecular configuration of protons, different resonances would be expected for protons in different chemical environments. This however is not observed in the spectra. (In this section ^{11}B is used specifically to discuss results, however the remarks concerning quadrupolar relaxation apply to both ^{10}B and ^{11}B). The main feature of the proton N.M.R. spectra is a quartet (of relative intensities 1:1:1:1). This was first observed by Ogg (1955) for aluminium borohydride. This proton signal is the result of all protons being chemically equivalent and coupled to ^{11}B, which has four spin states. (The protons are also coupled to aluminium, and this has to be removed to observe the proton-boron coupling). When the temperature of the sample is lowered the quartet structure coalesces slowly. These observations are confirmed by Maybury (1967) and Coe (1972), and were also observed for the zirconium and hafnium borohydrides by Marks (1972)b. Marks' study is the most thorough and probably offers the best explanation of the spectra.

The ^{11}B nucleus has a quadrupole which allows it to couple to fluctuations occuring in its immediate environment. The collapse of the quartet proton spectrum to a singlet can be explained as a temperature variation in the spin-lattice (T_1) relaxation time of the ^{11}B nucleus. At ambient temperatures the spin lattice relaxation is an inefficient process and the ^{11}B spin states ($I = \frac{3}{2}, \frac{1}{2}, -\frac{1}{2}, -\frac{3}{2}$) couple with the proton resonance. At lower temperatures the relaxation time is shorter and the individual ^{11}B spin states no longer have an appreciable life-time. The protons have no spin states to couple with and the proton signal collapses. The efficiency of

the spin lattice relaxation is governed by the two reorientation processes which are occurring in the molecule. The intramolecular reorientation of the individual borohydride units, and the reorientation of the molecule as a whole. At ambient temperatures, or in non viscous media, both reorientation rates are too fast to allow the boron quadrupole time to couple with the fluctuations. Marks (1972)b has shown by a detailed temperature and solvent study that the whole body molecular reorientation is the most important factor in deciding the T_1 relaxation times for boron nuclei in zirconium borohydride. Ogg (1955), who had not taken account of the boron spin lattice relaxation, suggested that the temperature variation of the proton signal in aluminium borohydride was due to a slowing in the intra-molecular reorientation. Without the detailed solvent study reported for zirconium borohydride, it is difficult to be certain, but it is likely that molecular reorientation will account for most of the temperature variation in the proton resonance relaxation of the molecular borohydrides.

Apart from the molecular borohydrides, other boron hydrides show anomalous proton N.M.R. spectra. The proton spectrum of the $B_3H_8^-$ ion, despite its structure (see Fig. Viii) shows three equivalent borons and eight equivalent protons (39). Again as the temperature is lowered the ^{11}B quadrupole relaxation decouples the proton resonance. Only when this molecule is involved in bonding, e.g. in $[(C_5H_5)_3P]_2CuB_3H_8$, has the intramolecular reorientation rate been slow enough to enable the contributing resonances to be resolved.

The routes available for intramolecular reorientation in these molecules have been speculated on (29, and its refs). In the molecular borohydrides the existence of known examples of double and triple hydrogen bridges suggests intermediates with such structures. Thus Marks (1972)b proposes that the reorientation in aluminium borohydride might go through a triply bridged intermediate and that the zirconium borohydride should reorientate through a doubly bridged intermediate. The reorientation pathway in the $B_3H_8^-$ ion was first suggested by Lipscomb (1959) as a pseudorotation of the ring which at no stage involves the breaking of a bond without simultaneous creation of another. An alternative to these chemical pathways of reorientation was suggested by Ogg (1955). This involves quantum tunnelling of the protons through the potential barriers; such a process would leave the electronic environment unchanged. Tunnelling would be expected to give rise to other effects, splitting of molecular vibrational bands, no such affects have been observed.

Behaviour involving intramolecular reorientation between equivalent structures, which have equal Gibbs free energy of formation, is well known (11). Molecules which exhibit this behaviour have been termed Fluxional by von Doering (1963), and are normally associated with delocalised electron systems (eg. π-allyl donation of electrons to a metal, or the metalocenes). It is obvious from the proton N.M.R. that all of the molecular borohydrides studied are fluxional in nature. (The ordered ionic borohydrides might be considered as the limiting case where molecular bonds are formally absent, but the initial configuration is equivalent to the final configuration). Attempts

have been made to study this reorientation process by proton N.M.R. techniques, as was described earlier. Unfortunately these studies are usually limited by the insolubility of the compounds in suitable solvents, and their extreme reactivity. Marks (1972)a measured the free energy barrier to reorientation in a complex uranium tetrahydroborate, as about 5 kcals $mole^{-1}$. Bushweller (1971) measured the barrier in a copper(I) B_3H_8 complex as a 10 kcal $mole^{-1}$. (The metal B_3H_8 salts are known to be involved in hydrogen bridging through the metal (19)). Even in these cases, which are especially suitable to proton N.M.R. study, the Arrhenius activation energy for the reorientation process could not be given. This was because of the unknown effect of the boron relaxation process on the half widths of the proton lines, and also the unknown temperature dependence of the proton and boron chemical shifts. It is unlikely that proton N.M.R. will be successful in studying the simpler borohydrides or ionic B_3H_8 since these are amongst the most rapidly fluxioning molecules known (12).

2. Experimental.

2.1 Preparation of calcium borohydride

The metathetic reactions of the borohydrides have been described by Wallbridge (1970). One such reaction was used to prepare calcium borohydride. Anhydrous calcium was prepared by reacting powdered calcium chloride with excess thionyl chloride, according to equation (i).

$$CaCl_2:H_2O + SOCl_2 \longrightarrow CaCl_2 + SO_2 + 2HCl \qquad (i)$$

The reaction, vigorous at first, was allowed to proceed until evolution of hydrogen chloride ceased. The excess thionyl chloride was decanted off and the solid was pumped dry. Sodium borohydride and the calcium chloride were mixed, in the molar ratio of 2:1 respectively. Some tetrahydrofuran (T.H.F.) was added to make a slurry of the reagents. The reaction mixture was heated under reflux for forty eight hours and reacted according to equation (ii)

$$CaCl_2 + 2NaBH_4 \xrightarrow{\text{T.H.F.}} Ca(BH_4)_2:2T.H.F. + 2NaCl \qquad (ii)$$

More T.H.F. was added and the hot solution was decanted from the starting material and by-products. On cooling, crystals separated from the mother liquor. These were the well characterised calcium borohydride; T.H.F. solvate. The solvate was separated off and destroyed by heating to $100^\circ - 115^\circ C$ under a hard vacuum. The calcium borohydride prepared in this manner was better than 98% pure. (Analysed by titration of borohydride against iodine).

2.2 Preparation of zirconium borohydride

The zirconium borohydride was prepared by a method after Reid (1957) where zirconium chloride is reacted with lithium borohydride according to equation (iii).

$$ZrCl_4 + 4LiBH_4 \longrightarrow Zr(BH_4)_4 + 4LiCl \qquad (iii)$$

In a nitrogen atmosphere finely powdered zirconium chloride was mixed with a greater than four molar excess of lithium borohydride

(see equation (iii)). The reaction was done 'dry' and an efficient stirrer was necessary. After about thirty minutes stirring the powder became 'wet' and the mixture warmed. The flask was cooled and placed on a vacuum line and evacuated. The zirconium borohydride was distilled into a liq. nitrogen trap.

2.3 The samples of Aluminium borohydride used in this study were kindly provided by Professor M. Wallbridge. These were ready sealed in silica 'cans'. The tetramethyl ammonium octahydrotriborate salt and the corresponding iodide were obtained from Strem Chemicals Inc. Massachussets and British Drug Houses Ltd. The salts were checked for spectroscopic impurity's and the iodide had to be recrystallised several times from water. These compounds were used without further purification.

2.4 Spectral observations.

The samples were studied as solids, all but the aluminium borohydride were polycrystalline solids at ambient temperatures. Isotopic enrichment of the B^{11} content was not necessary, although in all neutron spectra, absorption was appreciable. As with the alkali metal borohydrides the elastic and quasi-elastic regions were heavily distorted.

The samples of calcium borohydride and the tetramethyl ammonium salts were contained in silica cans similar to the alkali metal borohydrides (Q.V.). The aluminium and zirconium borohydrides were put onto a vacuum line and distilled, under reduced pressure, into a modified silica can; adapted to take liquids and low melting solids.

Fig. V.iv

231.

Aluminium Cell, to protect reactive samples

thin aluminium top

rubber sealing ring

recess for sample

securing bolts
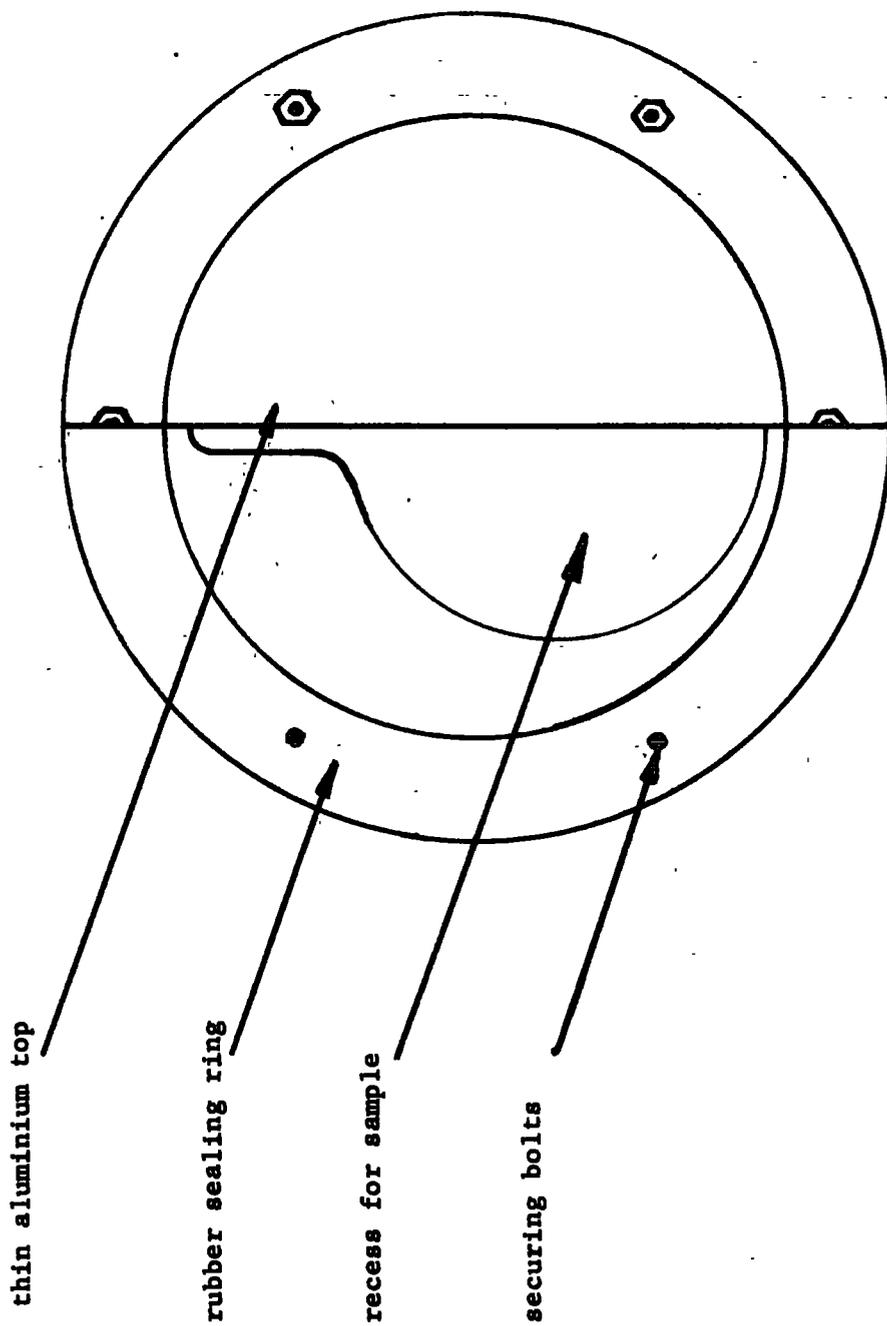
These 'liquid cans' were made by sealing two thick silica discs
(ca. 0.5mm) around the edge except for a small region. At this point
a long stemmed cone was fused, and slightly drawn out (to facilitate
sealing later). Across the face of the 'liquid can' some dimples
were made;   these strengthened the can. Cans prepared in this way
were capable of withstanding at least one atmosphere pressure, applied
internally or externally. The separation of the discs was greater
than in the cans produced for solids, being between 0.5 to 1.0mm.
When the compound had been distilled into the can and frozen down to
liquid nitrogen temperature, the neck was sealed off as close to the
body as possible. Because of the possibility of damage to the fragile
silica can and the extreme reactivity of the contents the can itself
was contained in a closely fitting aluminium cell. (The material
used was an aluminium magnesium alloy). A rubber sealing ring prevented
atmospheric exposure and was easily shielded by cadmium from the
neutron beam (Fig. Viv).

The calcium borohydride, the tetramethyl ammonium salts and the
aluminium borohydride were all run on the up scattering spectrometer
at Harwell (see Section II). Although the spectra were usually taken
at ambient temperatures ($294^{\circ}K$) the aluminium borohydride was cooled
to $183^{\circ}K$ to ensure it was below its melting point. The aluminium
borohydride and the tetramethyl ammonium salts were also run on the
down scattering spectrometer at Harwell (see Section II) as was
zirconium borohydride. The down scattering spectra were all collected
at liquid nitrogen temperatures ($77^{\circ}K$). Some experimental details are
summarised in Table Vii.

Table Vii.

Table shewing experimental parameters

	$Ca(BH_4)_2$	$Al(BH_4)_3$	$Zr(BH_4)_4$	$B_3H_8^-$
Extra can protection	NO	YES	YES	NO
Up scattering				
Temperature $^\circ K$	294	183	294	294
Incident neutron wavelength Å	4.27	4.20		4.20
Can material window thickness	Si .2	Si .5	Si .5	Si .2
Blark comparison window thickness	Si .2	Si+Al .5	Si+Al .5	Si .2
Down scattering				
Temperature $^\circ K$		77°	77°	77°
Monochromator and scattering plane		Al 3.1.1. 5.1.1	Al 3.1.1	Al 3.1.1
Infrared gain db.	43.4			9.05

A complimentary study of the calcium and tetramethyl ammonium, optical, spectra was also undertaken, in the near and far infra-red region. The region from 50 to 400cm^{-1} was covered by the Fourier transform spectrometer (see Section II). The samples were prepared in an exactly analogous manner to the alkali metal borohydrides. Spectra were recorded at both ambient (293°K) and liquid nitrogen (77°K) temperatures. Experimental details for the best spectra are given in Table Vii.

3. Calcium borohydride

3.1 Results obtained.

The up scattering spectrum of calcium borohydride was obtained at 294°K; the results are shown in Table Viii and Figure Vv. Down scattering spectra were not taken. The results show a broad scattering inelastic feature with weak bands superimposed upon this, there are no intense bands. Absorption by ^{10}B was apparent and distorted the elastic and quasi-elastic regions.

The infrared spectra were recorded at both ambient and liquid nitrogen temperature; the results are summarised in Table Viii, see Figure Vvi. A very broad absorption was observed with no prominent peaks above this.

3.2 Discussion of results

There are no intense bands in the spectrum of calcium borohydride which could be associated with molecules. The spectrum obtained is similar to the alkali metal borohydrides. A broad scattering feature is typical of rapid reorientation, and the weak bands superimposed upon

Table Viii.

Calcium Borohydride spectra.

Neutron up scattering $\theta = 45^{\circ}$ $T = 294^{\circ}K$ cm^{-1}	Infrared absorption at	
	$294^{\circ}K$ cm^{-1}	$77^{\circ}K$ cm^{-1}
51_w		
65_w		
96_m		
122_w		
157_w	140_{wsh}	140_{msh}
194_w	190_{bs}	215_{bs}
244_w		285_{bs}
332_m	330_{wb}	320_{bs}
435_w		

Notes. w = weak
m = medium
s = strong
b = broad
sh = shoulder

Fig. V.v

Inelastic neutron scattering spectrum of Ca(BH₄)₂ at ambient temperature

$\theta = 45^o$

Fig. V.vi

237.
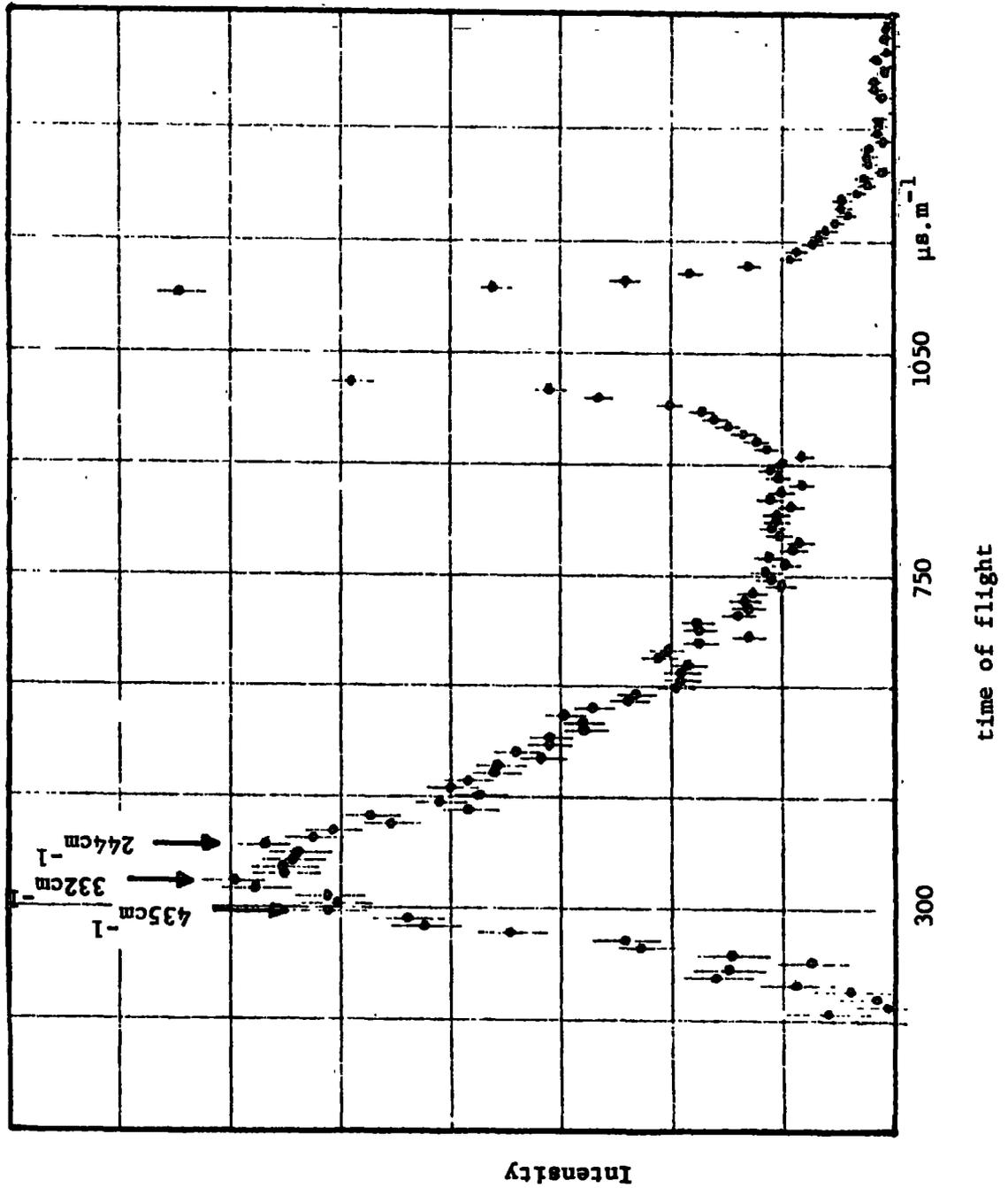
Infrared absorption spectrum of Ca(BH$_4$)$_2$
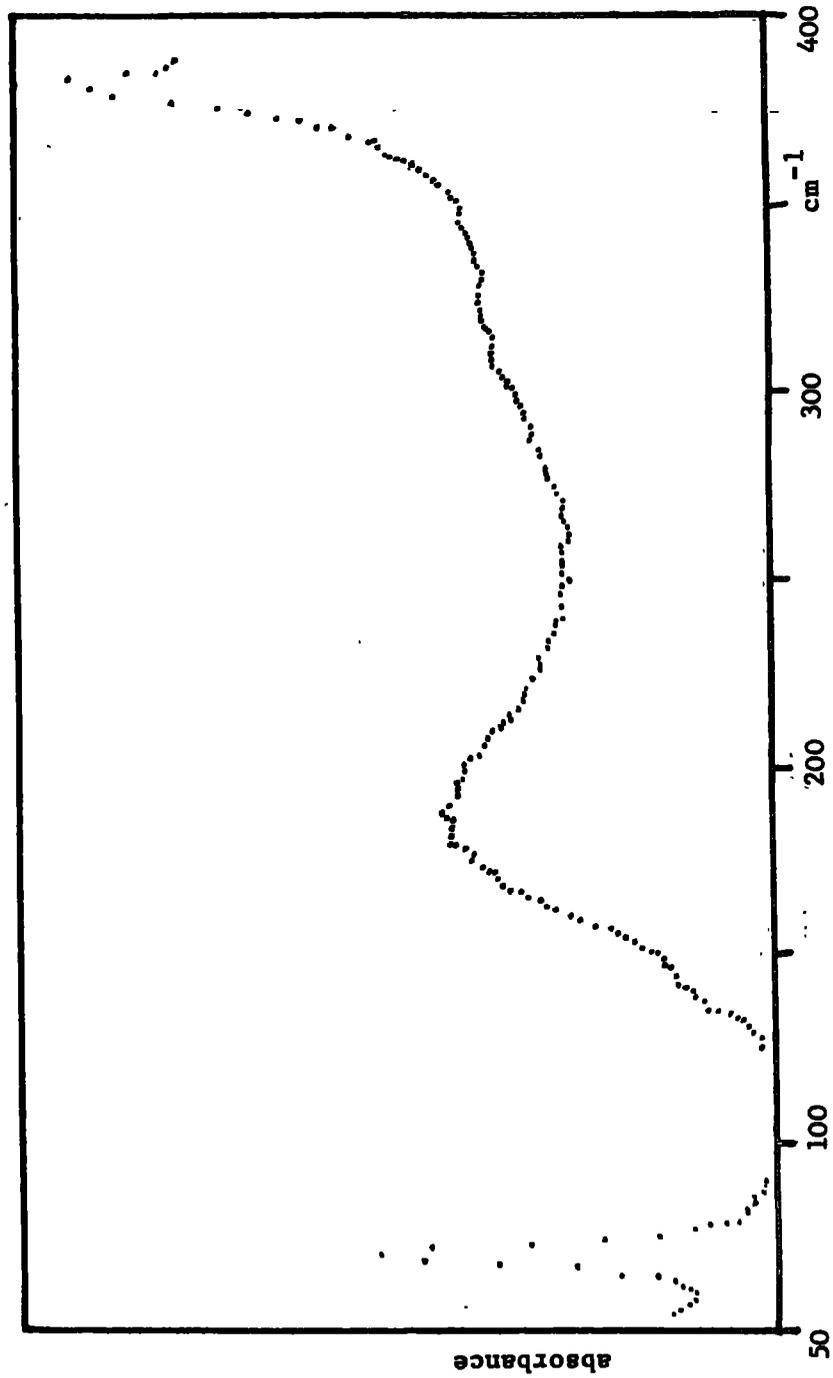
this was also observed in the other ionic borohydrides.
Interpretation of these weak bands must wait upon a detailed crystal
study of calcium borohydrides, though the bands are probably
transitions from higher lattice vibrational states to those of lower
energy. Only one band can be picked out as possibly a fundamental
lattice transition. This is the peak at $332cm^{-1}$.

This band is most probably associated with the transition from
the first librational state down to the ground state (νlib,). This
transition occurs in a region similar to that of the other ionic
borohydrides, typically about $290cm^{-1}$. If the band at $332cm^{-1}$ is a
single librational band and not an unresolved multiplet, it is
possible to make some comments on the site symmetry of the borohydride
ions. For reasons of valence there are two borohydride ions to every
metal ion. Since only one librational mode is observed these two
ions must not only be equal, crystallographically, but they must also
be in highly symmetric sites. (The effects of a non symmetric site,
upon the inelastic neutron spectrum, is shown by the case of lithium
borohydride, see Figure IV.v). The borohydride ion must be on a
site of tetrahedral, or higher, symmetry.

The librational peak is broad, as for the other ionic borohydrides.
This broad inelastic feature is caused by rapid reorientation, of the
borohydride ion, between libratory periods. This broad scattering
can be characterised by $F_{||}^{lib}$ of Larrsen (1973), which was discussed in
section I, and it depends on the position of the maximum of the
feature and its full width at half height. This provides a crude
but useful index to the depth of the well, at reorientation; $F_{||}^{lib}$

was measured as 0.61. (The limits are $F_{||}^{lib} \sim 0$, for a very shallow well, and $F_{||}^{lib} \sim 1$, for a very deep well). The value of $F_{||}^{lib}$ obtained is of an intermediate nature but indicates that reorientation is more difficult than in the case of the sodium borohydride (for the sodium salt. $F_{||}^{lib} \sim 0.44$).

The infrared spectra which were recorded showed broad absorption over the far infrared region and were not unlike the lithium borohydride spectrum in its general appearance. There were no bands which might be assigned from their intensity alone and without crystal data it is unlikely that any bands can be assigned. It is probable that between $294^{O}K$ and $77^{O}K$ the calcium borohydride undergoes a phase change: bands not present at $294^{O}K$ are observed at $77^{O}K$, see Table Viii.

It may be concluded that calcium borohydride probably has a crystal structure. of high symmetry and that it appears, from its spectra, to be intermediate between the sodium and lithium salts in ionic nature.

4. Aluminium borohydrides

4.1 Results obtained.

The up scattering neutron spectrum of aluminium borohydride was obtained at $183^{O}K$ and the results are given in Table Vv. see Figure Vvii. Several well defined bands were observed. The down scattering spectrum was also taken, at $77^{O}K$, from $220cm^{-1}$ incident neutron energy see Figure Vvii. Up to about $350cm^{-1}$ the up and down scattering spectra overlapped significantly, and can be seen to be consistent with each other. Other bands not accessible to the up scattering spectrometer were

Table Vlv.

The normal modes of vibration of $Al(BH_4)_3$, of symmetry D_{3h}.

Description	Mode Symmetry Species	No.	Assigned to bands Coe (1973) cm^{-1}
Terminal BH stretches			
symmetric	A_1'	ν_1	2471
symmetric	E'	ν_{16}	2469
asymmetric	A_2'	ν_8	2544
asymmetric	E'	ν_{15}	
Bridge BH stretches			
symmetric	A_1'	ν_2	2059
symmetric	E'	ν_{17}	2059
asymmetric	A_2''	ν_{11}	2026
asymmetric	E''	ν_{24}	2030
Bridge Al-H stretches			
symmetric	A_1'	ν_3	1511
symmetric	E'	ν_{18}	1420
asymmetric	A_2''	ν_{12}	1531 †-
asymmetric	E''	ν_{25}	1565

† this band is possibly displaced by Fermi resonance.

Description	Mode symmetry Species	No.	Value assigned This work cm^{-1}	Coe(1973) cm^{-1}
BENDS				
BH₂ deformation	A_1'	ν_4	-	1113
	E'	ν_{19}	-	1104
BH₂(terminal)twist	A_1''	ν_7	793	1155
	E''	ν_{26}	833	
BH₂(bridge) twist	A_1''	ν_6	793	1146
	E''	ν_{27}	833	
BH₂(terminal)rock in plane	A_2'	ν_9	723	967
	E'	ν_{20}	763	
BH₂(terminal) wag out of plane	A_2''	ν_{13}	833	779
	E''	ν_{28}	883	723
SKELETAL MODES				
Al-B stretch symmetric	A_1'	ν_5	-	495
assymetric	E'	ν_{21}	-	596
AlB₃ bend out of plane	A_2''	ν_{14}	-	229
in plane	E'	ν_{22}	329	325
BH₂(Bridge) wag *	A_2'	ν_{10}	241	232
	E'	ν_{23}	256	255

* also called BH₂(bridge) bend in I.R. texts.

A modes are all in phase modes
E "   " out of phase modes

Table Vv.

Observed bands, and their assignments, in the spectra of Al(BH$_4$)$_3$

Neutron up $\theta = 45°$ 183°K cm^{-1}	Study down 77°K cm^{-1}	Infrared (10) 18°K cm^{-1}	Raman (10) 18°K cm^{-1}	Assignments See Table Viv.
15 w			20 m	
		--	34 w	
			61 s	
			66 m	
81 w			83 s	
95 w			95 m	lattice modes
			105 m	
			112 m	
125 w			120 m	
138 m			136 m	
162 m			146 m	
		205 w	201 vw	
			230 vw	
213 w		216 w		
		229 w		ν 14
	241 vw	232 †		ν 10
254 m	256 s	254 vw	256 w	ν 23
	308 m			ν 23 + 61 = 315
325 w	329 wsh	324 w	327 w	ν 22
	723 w	–	723 w	ν 9
	763 vw	–	–	ν 20
	793 w	779 m	–	ν 6, ν 7
	833 wb	–	–	ν 26, ν 27, ν 13
	883 w	–	–	ν 28

Notes. w = weak   †, band infered from a combination
        m = medium   mode in IR
        s = strong
        v = very   (ν_{10} = 232 cm^{-1})

Fig. V vii   242.

Inelastic up scattering spectrum of Al(BH$_4$)$_3$ at 183°K, θ = 45°

Inelastic down scattering spectrum of Al(BH$_4$)$_3$ at 77°K

observed at higher incident energies in the down scattering spectrum.
Scattering at all incident energies was low, due probably to absorption
by boron, which lead to poor statistics for the observed bands.
Several attempts were made to obtain better data over the regions
220 to 400cm^{-1} and 700 to 1000cm^{-1} but were only marginally successful
in the latter case.   However all spectra taken show reproducibility
despite intensity variations in the region 700 to 1000cm^{-1}.   A
broad scattering feature appeared to be present in the up scattering
spectrum, beneath the molecular bands.

4.2 Discussion of results.

The discussion of the aluminium borohydride spectrum divides
itself naturally into three sections.   A low energy region accessible
only to the up scattering technique, an intermediate region covered
by both up and down scattering, and a high energy region accessible
only through the down scattering technique.   The assignments of the
bands was greatly aided by previous spectroscopic studies (41, 16)
especially that of Coe (1973), whose vibrational notation is used
(see Table Viv).

In the lowest energy region of the spectrum, below the lowest
molecular mode, are expected the lattice modes of the aluminium
borohydride crystal.   There is no published data on the factor group
of the alpha phase of aluminium borohydride (43).   It was thus not
possible to predict the number, or type, of these lattice modes.   A
large number of Raman bands were observed in this region and have all
been attributed to lattice vibrations (10). (Coe has suggested that the
unit cell must contain at least four molecules, to account for all these

bands). A limited number of these bands were observed in the up

scattering spectrum, and they were generally weak. Crystal data

will be necessary before any assignments can be made. It is useful

at this point to discuss the broad scattering feature which underlies

the whole up scattering spectrum, (see Fig. Vviii). In previous

compounds this feature could be clearly associated with the reorientation,

and libration of individual borohydride ions. In this case however,

whilst it probably is associated with intra molecular reorientation of

the borohydride units, it may also be associated with whole body

reorientations of the molecule. (Although the whole body motion would

be expected at very low frequency indeed). This feature is

tentatively assigned to intramolecular borohydride reorientation libration.

This is because the highest scattering occurs in the region associated

with the molecular modes v_{23}, v_{10} (see later). Extreme amplitudes

of motion in these modes would lead to intramolecular reorientation of

the borohydride units. (This is discussed later, under barriers to

rotation). Because of the molecular modes superimposed upon the

broad feature the parameters which are used to characterise it (see

Section I 2.3.3) are difficult to obtain. The value obtained for $F_{||}^{lib}$

is about 0.80 (where $F_{||}^{lib} \sim o$, very shallow well and $F_{||}^{lib} \sim 1$, very

deep well). This value of $F_{||}^{lib}$ indicates that the librational well

is quite deep, more so than for the ionic borohydrides, and yet this

does not prevent rapid reorientation on the neutron scattering time

scale.

In the region from 200 to 400cm^{-1} the skeletal modes of the molecule

are expected, v_5, v_{21}, v_{14} and v_{22}. These involve, primarily, motions

of the aluminium and boron atoms. Also expected in this region

Fig. V.viii

245.

The molecular bends of Al(BH$_4$)$_3$ in terms of the principal axes of a borohydride ion

twist

rock

wag

Al
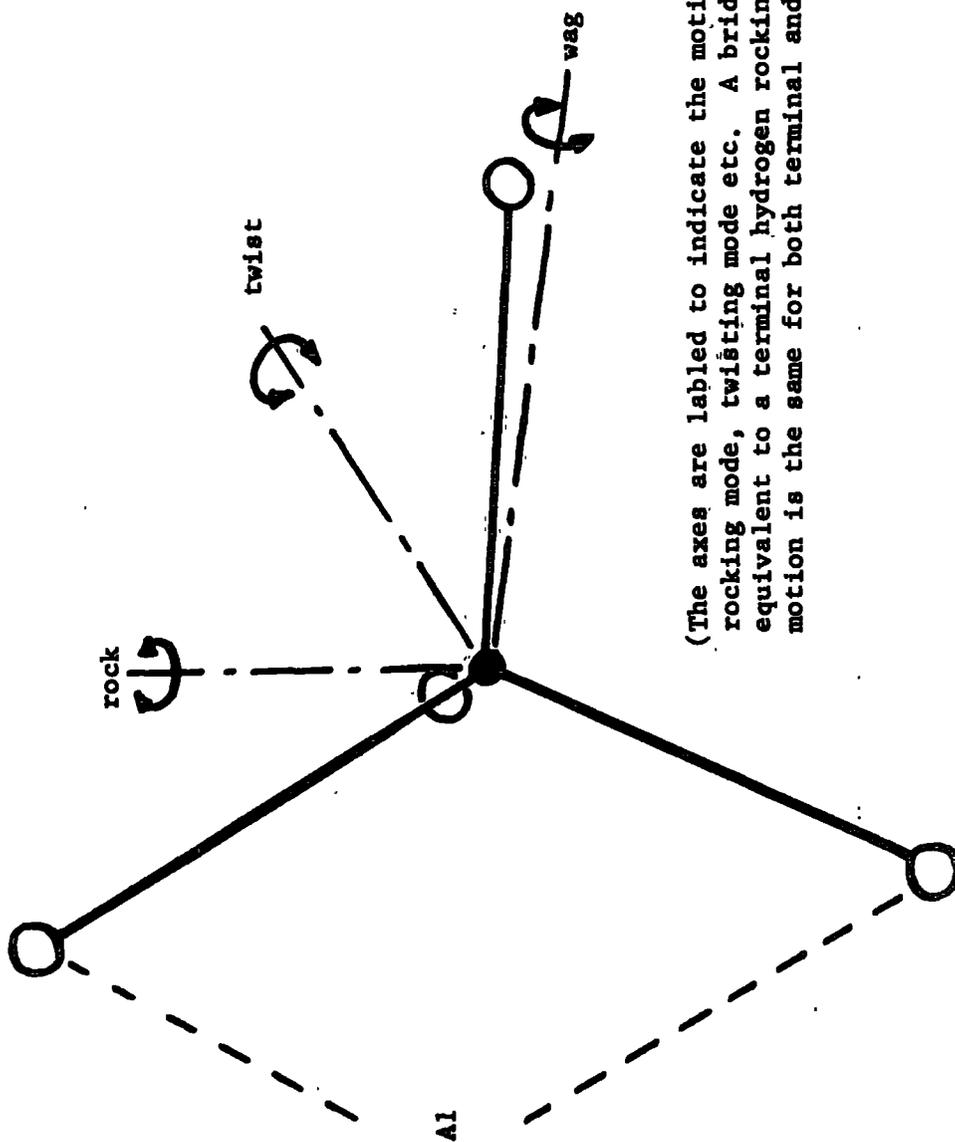
(The axes are labled to indicate the motion of the terminal hydrogens in their rocking mode, twisting mode etc. A bridging hydrogen wagging motion is equivalent to a terminal hydrogen rocking motion; the axis for twisting motion is the same for both terminal and bridging hydrogens).

are the wagging motions of the bridge protons (also termed bridge bends in I.R. literature), ν_{10}, ν_{23}. (This motion is equivalent to the rock of the terminal protons (see Fig. Vviii)). The most intense bands in this region will involve numbers of protons in large amplitude motions. The doubly degenerate, out of phase, bridge proton wagging mode ν_{23} (character E') involves all six bridging protons and would be expected to show the most pronounced scattering. The intense band at $256cm^{-1}$ is assigned to this mode, see Table Vv. The corresponding in phase motion, ν_{10}, also involves all the bridging protons, but this is only singly degenerate. It would be expected at lower energies. The shoulder at $241cm^{-1}$ is assigned to this band, Table Vv. (The assignment of ν_{23} is in agreement with the infrared and Raman study (10)). There are two other bands observed in this region of the spectrum, at 308 and $329cm^{-1}$. The shoulder at $329cm^{-1}$ may be assigned immediately: it corresponds closely to an optical band assigned to ν_{22}. This mode is the in plane aluminium-boron vibration (of character E'), however it has been shown that the protons are heavily involved in this mode. The mode ν_{14} which is the corresponding in phase motion (character A_2'') was not observed. (Coe has shown that proton involvement is less in this mode). The remaining band at $308cm^{-1}$ is not easily assigned. It does not correspond to any optical band reported, but is quite intense. It cannot be assigned to ν_{14}, since this would make an A mode more intense than the corresponding E mode, ν_{22}. The band is assigned to a combination band; probably involving, ν_{23} see Table Vv. It is obvious from this region of the spectrum that the proton motions generally are not heavily involved with the skeletal modes of the molecule.

The other region of the spectrum where the fundamental vibrations of the protons are expected is above $600 cm^{-1}$. It is in this region that the terminal proton wags (v_{13}, v_{28}), and rocks (v_9, v_{20}); and the terminal and bridging twists $(v_7, v_6, v_{26}, v_{27})$ are anticipated. These modes involve the terminal protons moving about an axis passing through the boron atom (see Fig. Vviii). Only in the case of the twisting motion do the bridging protons have their modes at similar energies. The bridging protons' wag were assigned to the low energy bands, previously discussed. Whilst the bridging protons' rock is contained within the asymmetric aluminium-hydrogen stretching modes, at higher energies. Previously these fundamentals have been assigned in the regions, 600 to $1400 cm^{-1}$ by Price (1949), 950 to $1400 cm^{-1}$ by Emery (1960) and 700 to $1100 cm^{-1}$ by Coe (1973). It is obvious from the spectra taken for this study that these authors have been too optimistic about the range of values these essentially similar vibrations take. The wags, rocks, and twists described in Table Viv derive their existence from the rotational degrees of freedom of a borohydride moiety. In a highly symmetric environment, e.g. the alkali metal borohydrides, the librational motion about any principal axis is degenerate with the other two. This natural degeneracy is removed when the borohydride is introduced into the aluminium borohydride molecule. The wags, rocks, and twists can still be described in terms of librations about the principal axis of rotation of a borohydride unit, (this is illustrated in figure Vviii), but the extent to which the terminal protons are different from the bridging protons will be dependent upon the strength of the aluminium-

hydrogen bond. In a weak Al-H bond the bridging proton vibrations would not have a fundamental frequency too different from the terminal proton vibrations.

When more than one borohydride unit is incorporated into a molecule, as with aluminium borohydride, the units would be expected to be coupled to some extent in their librations. This coupling gives rise to the two character species associated with the librations in aluminium borohydride. The singly degenerate in phase motion of all three borohydride units (of A character), and the doubly degenerate out of phase motions (of E character). If the coupling between motions is strong there will be a large separation in the frequencies of vibration of the two modes. When there is no coupling between units the motions become degenerate.

Although the spectra obtained over the region 700 to 900cm^{-1} are not good some obvious conclusions can be drawn. That the twists, wags and rocks of the terminal protons, along with the twists of the bridging protons, are all grouped closely together. That the coupling between the in phase (A) and out of phase (E) modes is not large. The band assignments for the region are given in Table Vv. These assignments were difficult to make and should be regarded as tentative. The main difficulty was the poor intensity of the individual bands. These assignments are based on the following principles. When the borohydride unit is incorporated within an aluminium borohydride molecule its description as a borohydride unit is modified but not lost. There is thus expected to be a high degree of coupling between the terminal proton motions and bridging proton motions. The bridge proton wag , described as a bend in I.R. literature, is associated with the terminal

proton rock, see Fig. Vviii.   The bridge proton rock (described

entirely as the asymmetric aluminium hydrogen stretching in the I.R.

literature) is related to the terminal proton wag.   The bridge and

terminal proton twists are obviously related, see Fig. Vviii and are

expected to be in close agreement with each other.   From these ideas

and knowing that A modes are lower in energy than the corresponding E

modes an order can be predicted for these vibrations.   The lowest

energy bands would be expected to be related to the terminal rocking

modes, v_9, v_{20}.   The highest energy bands would be expected to be

related to the terminal wagging modes v_{13}, v_{28} (and compares well with

the diborane molecule).   The in phase twisting modes v_6 and v_7, would

be expected to be almost degenerate;   as would the corresponding out of

phase modes v_{26}, v_{27}.   The twisting modes are assumed to lie between

the terminal rocks and the terminal wags, this order was used to make

the assignments of Table Vv.   Some of the assignments can be used to

obtain barriers to intramolecular reorientation (see later).   Only

two bands occur in this region of the optical spectrum, which may be

compared with neutron peaks;   these are at 723 and $779cm^{-1}$ respectively(10).

This region was difficult to interpret and many alternative assignments

were discussed by Coe.   As opposed to the assignments given in

Table Vv, Coe has chosen the terminal proton wags of lowest energy and

terminal proton rocks of highest energy.   The preferred assignments

for the two bands at 723 and $779cm^{-1}$ puts the A_2'' (v_{13}) mode at

higher energy than the corresponding E" mode v_{28}.   If these assignments

were correct the relevent bands should have been observed above $900cm^{-1}$

in our spectra.   It may be concluded that the dipole change associated

with these vibrations is negligible, and they produce no infrared

absorptions.

The data collected for this study may contradict Coes'
conclusions concerning the molecular symmetry of aluminium
borohydride.   He argued, from the absence of bands in certain
regions of the infrared and Raman spectra, that the symmetry of
aluminium borohydride was D_{3h}.   The region of most importance in
this respect was from 700 to 2000cm^{-1} and involved some of the
librational modes discussed.   The spectrum represented here casts
doubt on some of Coes' assignments in this region of the spectrum and
indicates the difficulty of observing these molecular modes in the
infrared.   Since there are no selection rules in neutron spectroscopy
the assignments presented here can be no aid in determining a molecular
symmetry.

Other molecular modes which are moderate or strong features of
the optical spectra are not observed in the spectra shown here.   These
modes include deformations of the borohydride moiety and all proton
vibrations.   The amplitude of proton motion associated with these
modes is expected to be lower than for librations.

5.   Zirconium borohydride.

5.1   Results obtained.

The neutron down scattering spectrum of zirconium borohydride was
obtained at 77°K, and covered the range from 125 to 1000cm^{-1}, incident
energy.   The results are summarised in Table Vvi, see Figure Vix.
The scattering from the sample was moderate and increased markedly beyond
about 1000cm^{-1}.   Several regions of the spectrum had to be re-run
because of difficulties with a noisy counter system.   The data
presented are a combination of these regions.

Table Vvi.

Assignments of the bands on the spectrum of $Zr(BH_4)_4$

Neutron down scattering 77°K cm^{-1}	Infrared (vapour) Davies (1973) cm^{-1}	Raman (liquid) Smith (1971) cm^{-1}	Assignments See Table Vvii.
	213 m	216 s	ν 23
227 s			ν 21
318 w			519-227 = 292
376 w			600-227 = 373
519 s	507 s	510 vw	ν 24
			ν 5 †
		549 vs	ν 4
600 s			ν 15
640 w sh			ν 15 + ν A
800 w			600+227 = 827

†; favoured assignment

ν A; the acoustic lattice mode, not observed

(only down scattering spectrum taken)

Table Vvii.

Normal modes of vibration of $Zr(BH_4)_3$ and their correlation

to site and Factor Groups

Description	Symmetry species				
	A_1	A_2	E	F_1	F_2
BH stretch terminal	ν_1				ν_{16}
BH stretch symm. bridge assymm.	ν_2		ν_6	ν_{11}	ν_{17} ν_{18}
ZrH stretch symm. bridge assymm.	ν_3		ν_7	ν_{12}	ν_{19} ν_{20}
Bridge deformation			ν_8	ν_{13}	ν_{21}
BH_3 rock			ν_9	ν_{14}	ν_{22}
BH_3 libration		ν_5		ν_{15}	
Skeletal modes	ν_4		ν_{10}		ν_{23} ν_{24}
Molecular Group Td	A_1	A_2	E	F_1	F_2
Site Group Td	A_1	A_2	E	F_1	F_2
Factor Group Td	A_1	A_2	E	F_1	F_2
Infrared active					*
Raman active	*		*		*

Fig. V.ix

253.

Inelastic neutron down scattering spectrum of $Zr(BH_4)_4$, at 77^oK

neutron energy transfer

Intensity
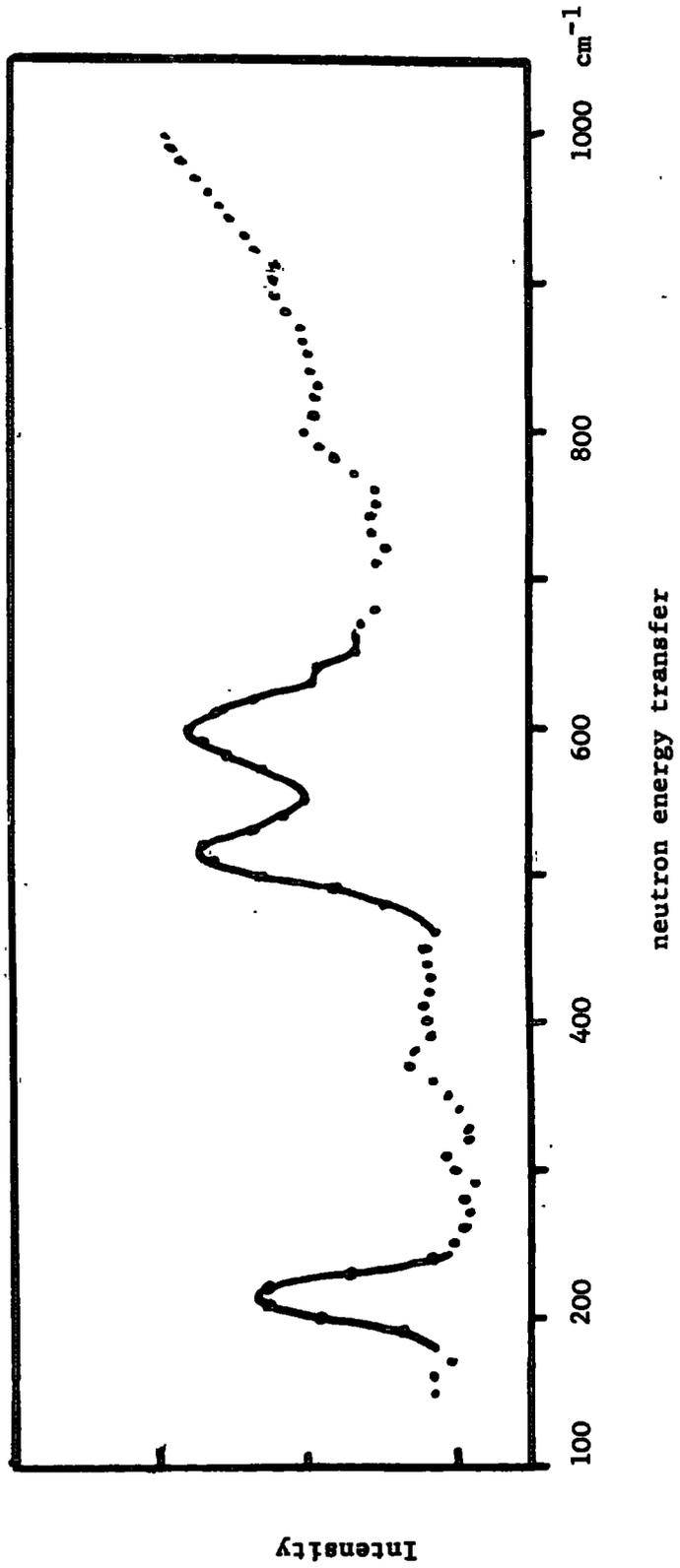
5.2 Discussion of results.

The bands observed, see Fig. Vix, can be assigned to molecular fundamentals and their combinations, see Table Vvi. Zirconium borohydride is a tetrahedral molecule and its infrared and Raman spectra are consistent with strict tetrahedral symmetry (12, 44). The irreducible representations of the normal modes of vibration of zirconium borohydride are given in Table Vvii. At 113^OK zirconium borohydride crystallises with the Td (P$\bar{4}$3m) space group (7); with one molecule to the unit cell, the factor group has only the symmetry elements of the molecular point group. There is no correlation field splitting; one lattice acoustic mode, of character F_2, and one lattice librational mode, of character F_1 , are predicted.

The assignments presented in Table Vvi were aided by the optical study conducted by Davies (1973). Vibrational bands were observed at 227, 519 and 600cm^{-1} in the neutron down scattering spectrum. The band at 227cm^{-1} is close to bands which are active in both infrared (12) and Raman (44) these are of F_2 character. Low frequency modes involving bending motions of the hydrogen bridges are expected in this region, and skeletal modes are also found here. The two possible assignments are thus v_{23} or v_{21}, unfortunately the data presented here do not go low enough to choose between them, definitively. (The perdeutero studies on this band were confused by Fermi resonance (12)). The skeletal modes, of which v_{23} is one, involve primarily the motion of the boron atoms with respect to the zirconium atom, and might be compared with similar modes in aluminium borohydride. In this case the proton motions were not heavily coupled to those of the boron.

For this reason the band at 227cm^{-1} is assigned to ν_{21}. The other two bands will be considered together.

The libration of the borohydride units about the boron-zirconium axes involves the coupled motion of them all. Such a system of oscillators leads to four modes of libration: one singly degenerate mode (of A_2 character) representing the in phase motion of the borohydride units, and three degenerate modes (making a mode of F_1 character) representing the out of phase motions. In the molecular borohydrides studied the coupling between the borohydride units has been low (10,12). The A_2 and F_1 modes might thus be expected to be almost degenerate, although the A_1 mode will be of lower value if any coupling is present. The two bands, at 519 and 600cm^{-1}, can be assigned to these modes; 519cm^{-1} to ν_5 (A_1 character) and 600cm^{-1} to ν_{15} (F_2 character). There can be no doubt about the band at 600cm^{-1}, since this should be optically inactive and no bands are observed in the optical spectra of this region (12, 44). Unfortunately the intensity ratio of the two bands does not match the prediction. The triply degenerate mode ν_{15} should be about three times as intense as the singly degenerate ν_5 mode, assuming equal proton displacements in the two modes. There are also two optical bands which may be associated with the band at 519cm^{-1}. These are the bands at 510 and 549cm^{-1} (44) which have been assigned to the skeletal vibrations, ν_{24} and ν_4 respectively, (12). The skeletal modes are not thought to be significantly coupled to the proton motions (as in the previous assignment). The bands at 519 and 600cm^{-1} are thus assigned to the ν_5 and ν_{15} modes respectively. (From these bands the barriers to

reorientation may be estimated, see later). The regions of the spectrum containing the bands 519 and $600cm^{-1}$ were run, with the noisy counter, and without, respectively. This will have disturbed the intensities of the two peaks.

The remaining bands are all weak and are assigned as combination and difference bands, see Table Vvi. Reasonable agreement between the predicted and observed frequencies was difficult to obtain and may reflect the use of the wrong combinations. The combination mode at $640cm^{-1}$ is assigned to combination of the intramolecular librational mode v_{15} with the acoustic lattice mode. This gives a value of $40cm^{-1}$ for the acoustic lattice mode, which corresponds to what might be expected considering the mass of the zirconium borohydride (atomic weight of 151). All of these combination bands are strictly active in either infrared or Raman. Observing these bands in the optical spectra may be very difficult as their intensity in the neutron spectrum is low.

6. The Octahydrotriborate anion

6.1 Results obtained

The up scattering spectra of tetramethyl ammonium iodide (T.M.A.) and tetramethyl ammonium octahydrotriborate (O.H.T.B.) were obtained concurrently at $294^{o}K$; the results are shown in Table Vviii see Figure Vx. Several very intense bands at low energy transfer were observed as well as a group of bands at around $350cm^{-1}$. The down scattering spectrum of T.M.A. and O.H.T.B., obtained at $77^{o}K$, was complex. The results are also given in Table Vviii, see Figure Vxi. (Much

Table Vviii   Assignments of the bands in the spectra of tetramethyl ammonium, Iodide-and B_3H_8 salt.

B_3H_8				$N(CH_3)_4$ (I)				$N(CH_3)_4$ in $N(CH_3)_4MnCl_3$		1,3Dioxolane		Band assignments for	
neutron work up 294°K cm^{-1}	work down 77°K cm^{-1}	Infrared 293°K cm^{-1}	Infrared 77°K cm^{-1}	neutron up 294°K cm^{-1}	work down 77°K cm^{-1}	Infrared this study 293°K cm^{-1}	Infrared previous (8) cm^{-1}	Neutron (22) 296°K cm^{-1}	Infrared (22) cm^{-1}	Infrared (4) cm^{-1}	Raman (4) cm^{-1}	$N(CH_3)_4$ I See Tables Vlz,x.	B_3H_8 See Tables Vz,xi
27 w				27+ w								ν Eu,11b	νL 1
45 w				38+ w								ν A2u,11b	νL 2
59 ssh		100 m		83 vs	163 w	80 vs	74 vs					ν 11b,	νL 3
				92 vs		90 s	91 vs					ν Eu,	
106 ssh		140 w		151 w		140 vw						ν A2u,	νL 4
143 msh		165 w											νL 5
220 msh	231 m			279msh	262 s			327	369			ν 4	νL 6
296 vs	294 vs			337 s	350 vs	345 w	341 vw	415	457			ν 12	ν 27
413wsh	356 m			444msh	448 s	458 m	453 w					ν 19	ν 26
	443 m	435 mb	425 / 445			475 w	470 vw						
	540 w	540 w,sh	535		540 w					680 w	658	ν 19+ν Eu,	ν 26,27+νL 4
					610 m					723 w	671	ν 19+ν A2u,	ν 24
		720 w			700 w							ν 19+ν 4	ν 25
		775 w											ν 17
		915msh				919	916 m			921 s		2ν 19	
		945 s				945	944 vs					ν 18	ν 18
		10.0 s					951 vs						

Note. All up scattering bands measured at θ = 45° except for those labelled + which are from θ = 36°.

νL are lattice modes, the numbering is entirely arbitrary.   * This band is also strongly Raman active.

transitions involving modes labelled ν 11b, concern whole body librations of the $N(CH_3)_4$ ion in the crystal.

Table VIx.   258.

Irreducible Representations of the lattice modes of tetramethyl
ammonium iodide.

Crystal Structure $D_{4h}^{7}(P_{4/nmm})$	Tetramethyl Ammonium ion $N(CH_3)_4^{+}$	Iodide ion I^{-}
Site Group	D_{2d}	C_{4v}
Site species containing translation	B_2, E	A_1, E
rotation	A_2, E	-
Factor Group	D_{4h}	D_{4h}
Factor species of translation correlated	B_{2g}, A_{2u}, E_g, E_u	A_{1g}, A_{2u}, E_g, E_u
of rotation correlation	A_{2g}, B_{2u}, E_g, E_u	
Irreducible representations of the lattice modes		
Acoustic	$A_2 + E_u$	
Optic	$A_{1g}+B_{2g}+A_{2u}+2E_g+E_u$	
Libration	$A_{2g}+B_{2u}+E_g+E_u$	
Infrared active species in D_{4h} Factor Group	A_{2u}, E_u	

Table Vx.   259.

Normal mode assignments for $N(CH_3)^+$ ion and their correlation to site and Factor groups.

Description	Symmetry species				
	A_1	A_2	E	F_1	F_2
CH_3 non symmetric stretch			ν_5	ν_9	ν_{13}
CH_3 symmetric stretch	ν_1				ν_{14}
CH_3 non symmetric deformation			ν_6	ν_{10}	ν_{15}
CH_3 symmetric deformation	ν_2				ν_{16}
CH_3 rock			ν_7	ν_{11}	ν_{17}
CH_3 libration (twist)		ν_4		ν_{12}	
Skeletal modes	ν_3		ν_8		ν_{18} ν_{19}

Molecular Group T_d — Site Group D_{2d} — Factor Group D_{4h} correlation diagram

Molecular Group T_d: A_1 † , A_2 , E † , F_1 , F_2 *†

Site Group D_{2d}: A_1 † , A_2 , B_1 † , B_2 *† , E *†

Factor Group D_{4h}: A_{1g} † , A_{2g} † , B_{1g} † , B_{2g} † , E_g , A_{1u} , A_{2u} *† , B_{1u} , B_{2u} , E_u *†

Notes   * , indicates Infrared activity
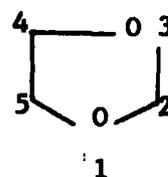
† , indicates raman activity.

Table Vxi. 260.

Normal mode Vibrations of the $B_3H_8^-$ ion (4)

Mode ν	Description	Symmetry Species	Motion of terminal protons at position
1	BH$_t$	A_1	4,5
2	stretch	B_1	
3		A_2	4,5
4		B_2^2	
5		A_1^1	2
6		B_1^1	
7	BH$_{t_2}$ scissors	A_1	2
8		A_1^1	4,5
9		B_2^1	4,5
10	BH$_{t_2}$ wag	A_1	4,5
11		B_2	2
12		B_2^2	4,5
13	twist	A_2	2
14		A_2^2	4,5
15		B_1^2	4,5
16	rock	A_2^2	4,5
17		B_1^2	2
18		B_1^1	4,5
19	ring stretching	A_1^1	
20		A_1^1	
21		B_2^1	
22		B_2^2	
23	(breathing)	A_1^2	
24	Ring deformation	A_1^1	
25	in plane	B_2^1	
26	out of plane	A_2	
27		B_1^2	

Molecule ion
$B_3H_8^-$

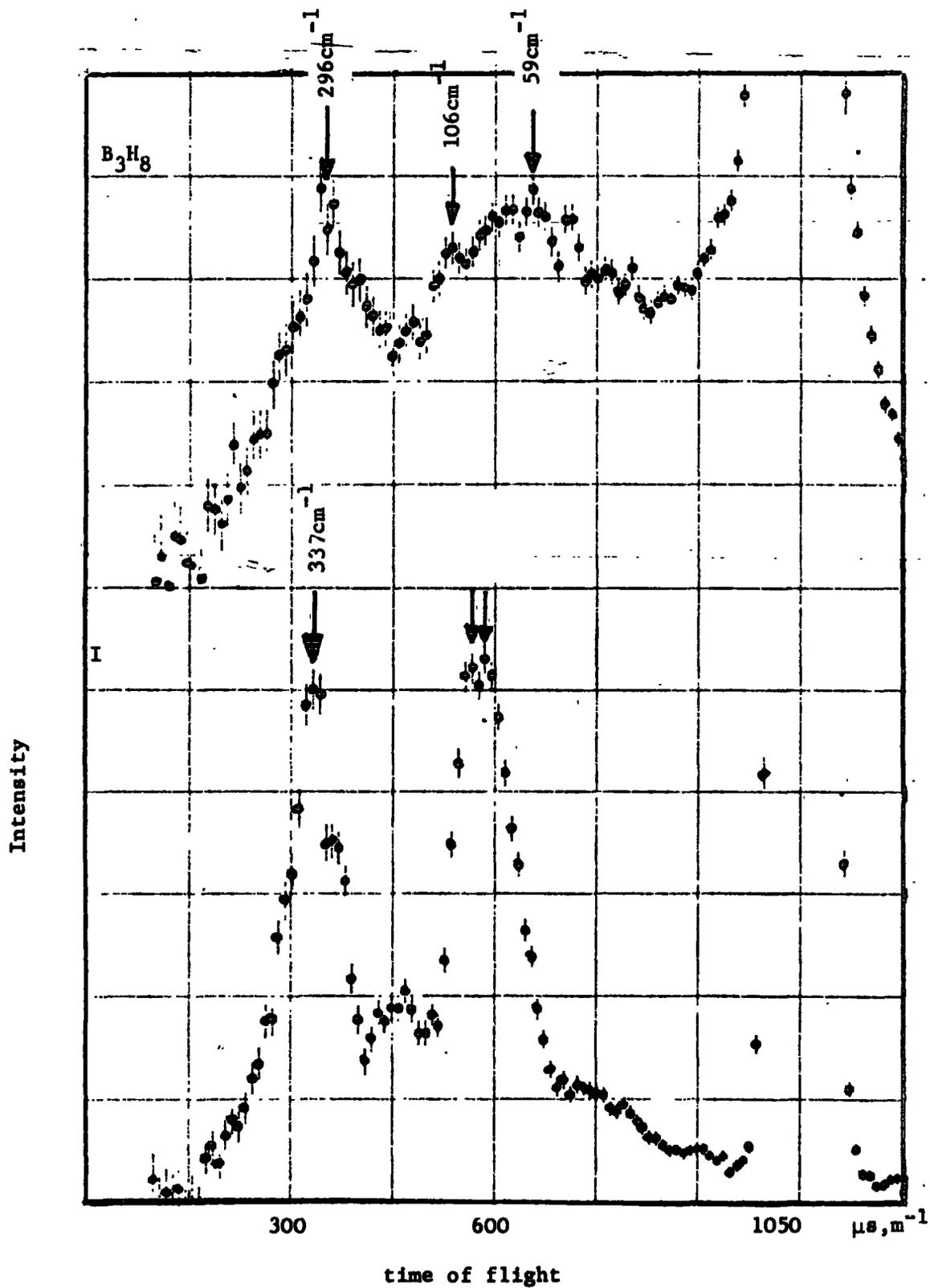
Model molecule used
1,3 dioxolane
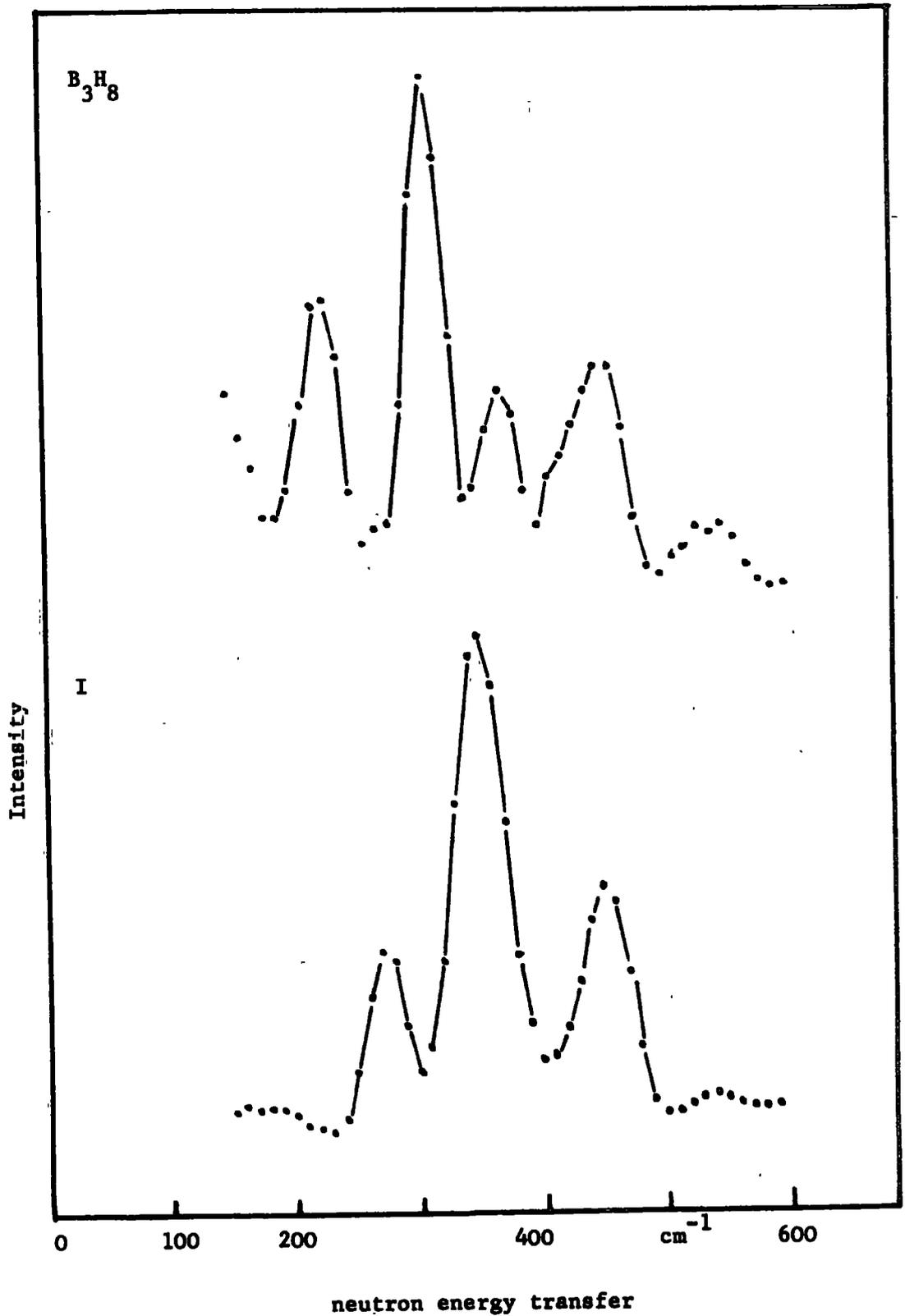

Notes.   A species are symmetric
B "   " assymmetric

A_2 species are Raman active only,
all other species are Raman and
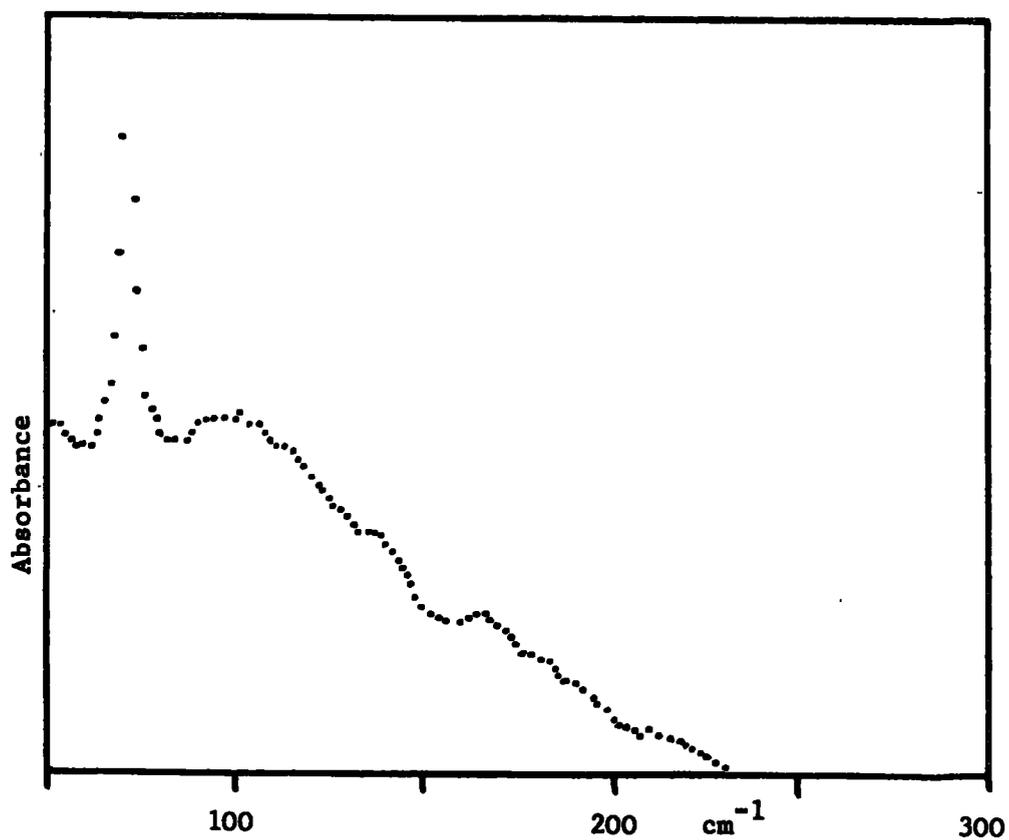Infrared active.

Subscript t refers to the terminal protons.

Fig. V.x

261.

Inelastic neutron up scattering spectra of B_3H_8 $N(CH_3)_4$ and

I $N(CH_3)_4$, $\theta = 45°$

time of flight

Fig. V.xi

262.

Inelastic neutron down scattering spectra of
$B_3H_8 N(CH_3)_4$ and $I N(CH_3)_4$, at 77^OK

Fig. V.xii

263.

Infrared absorption spectrum of $B_3H_8 N(CH_3)_4$

Fig. V.xiii

264.

Infrared absorption spectrum of I N(CH$_3$)$_4$

a : thick mull

b : thin mull
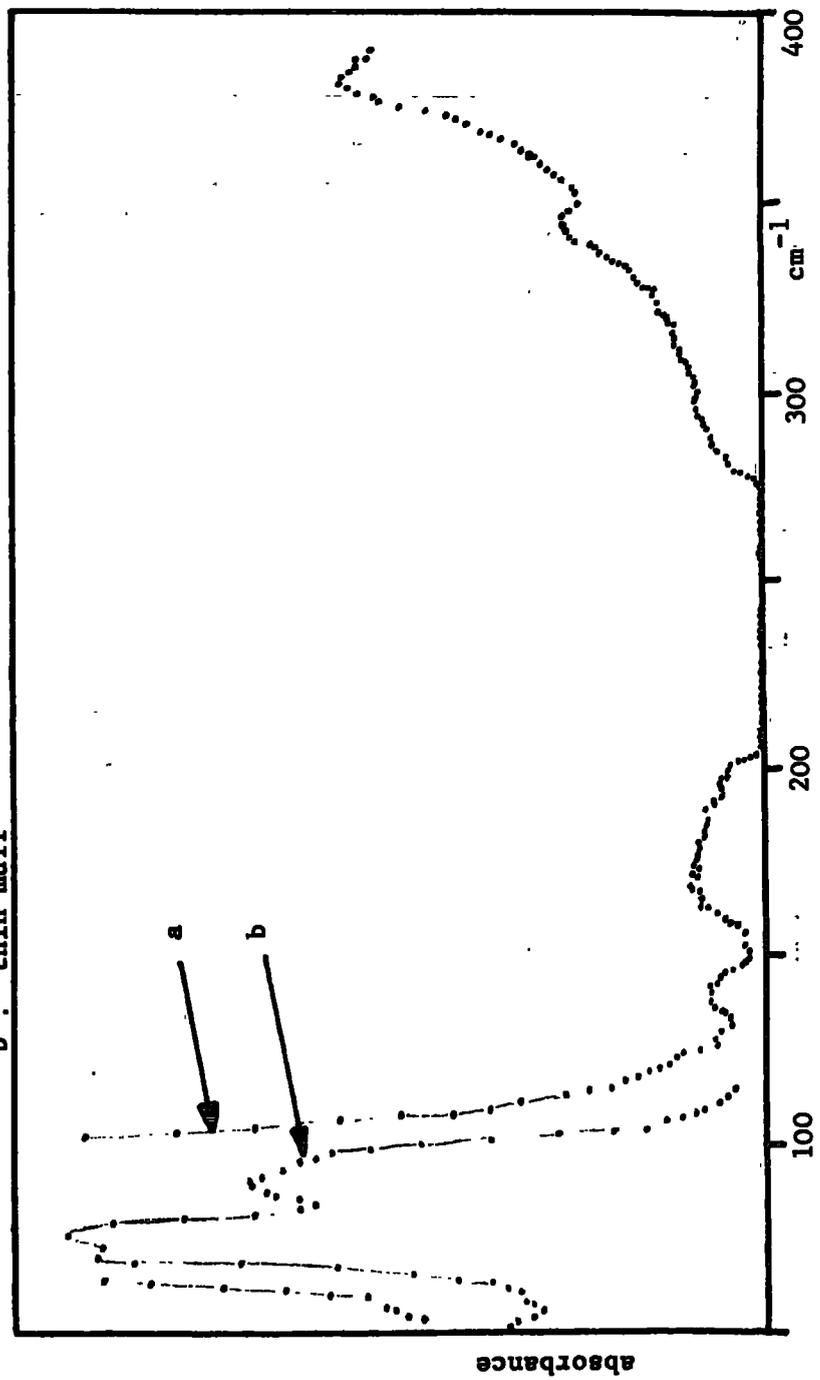
sharper bands were observed at the lower temperature). Compared with T.M.A. the scattering from O.H.T.B. was low, this may have been due to B^{10} absorption which was an obvious feature of the up scattering spectrum.

Infrared spectra in the near and far regions were obtained for both salts (see Figures Vxii and xiii). The Raman spectrum of O.H.T.B. was also taken.

6.2 Discussion of results

The spectra observed are best discussed in terms of the two contributing molecular ions. The tetramethyl ammonium ion was present in both samples but the octahydroborate anion was only present in one (O.H.T.B.)

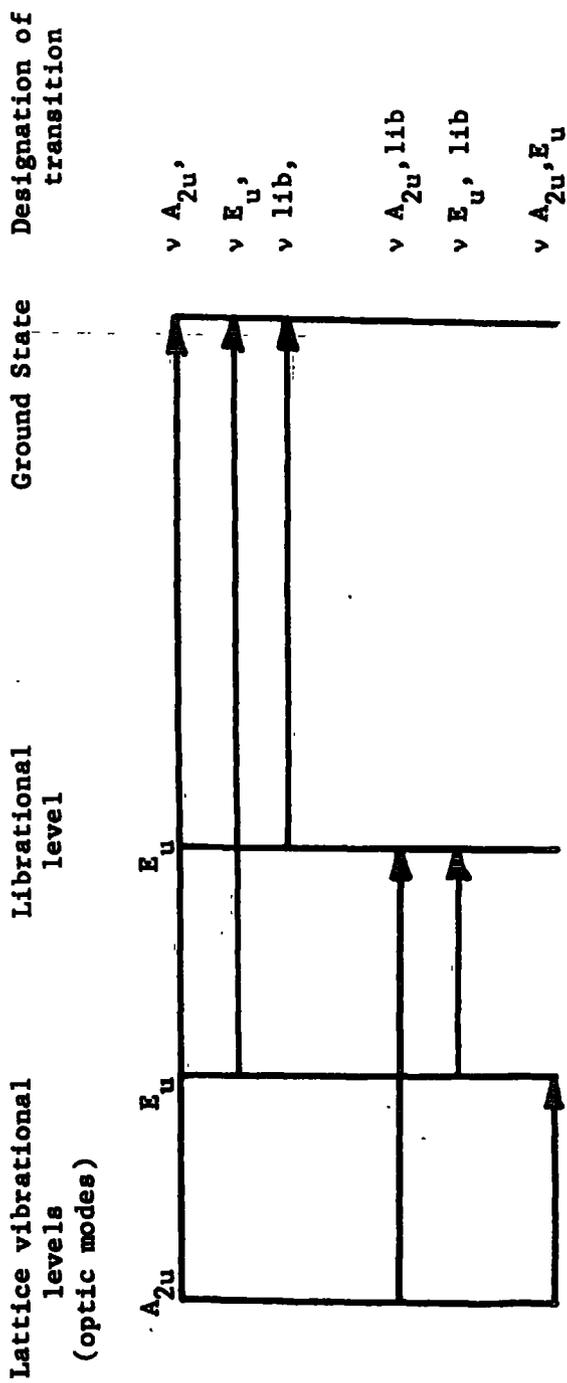### 6.2.1 The scattering from the tetramethyl ammonium cation.

This ion has tetrahedral symmetry (8) and its infrared spectrum should normally show no librational modes. The neutron spectra would be expected to show these modes strongly. These modes can be studied in isolation in the spectra of tetramethyl ammonium iodide (T.M.A.) T.M.A. has a D_{4h}^7 (P4/nmm) crystal structure, the irreducible representations of the lattice modes of T.M.A. are given in Table Vix. The irreducible representations of the intramolecular normal modes of vibration, and their correlations to the crystal field, are given in Table Vx. Following Bottger (1965) the mode notation of Young (1947) is used. (Table Vx also gives an approximate description of the modes).

The infrared bands at 458 and 475cm^{-1} are due to the skeletal vibration ν_{19}. This mode, of character F_2, is split by the crystal field to give the two bands, of character A_{2u} and E_u. In the neutron spectra these two bands are unresolved and are assigned to the peak at 448cm^{-1}. The main scattering feature of both up and down scattered spectra is the band at 350cm^{-1}, this is coincident with a very weak infrared band at 345cm^{-1}. These bands are due to the out of phase methyl librational mode, ν_{12}, which is of F_1 character in the molecular point group. In the crystal this mode is infrared active, of character E_u. This has been wrongly assigned by Bottger (1965) to the ν_8 mode, (of character E in the molecular point group, this mode is still inactive in the crystal field). The in phase methyl librational motion mode ν_4, of character A_2, would be expected at lower energy than ν_{12} but not too different in value. The peak at 262cm^{-1} in the down scattering spectrum is assigned to this mode, there are no corresponding absorptions in the infrared. (A_2 species are infrared inactive in both molecular and crystal symmetry groups). As expected this mode ν_4 gives less intense scattering than ν_{12} (Figure Vxi).

The remaining bands are low energy lattice modes observed in the up scattering and far infrared spectra, and the molecular combination bands observed in the down scattering spectrum. The two intense bands at 80 and 90cm^{-1} are assigned to the lattice vibrational and librational modes, both are of E_u character. The lattice vibrational transition involving the optic mode of A_2 character was weakly observed in the infrared, at 140cm^{-1}. This

Fig. V.xiv

267.

De-excitation transitions between some of the lattice states of

I N(CH$_3$)$_4$

Lattice vibrational levels (optic modes)	Librational level	Ground State	Designation of transition

ν A$_{2u}$'

ν E$_u$'

ν lib,

ν A$_{2u}$, lib

ν E$_u$, lib

ν A$_{2u}$, E$_u$

E$_u$

E$_u$

A$_{2u}$

allowed the construction of a scheme of transitions involving the optical modes (see Figure Vxiv). This is highly speculative but allows the assignment of some weak bands at very low energy in the up scattering spectrum. The bands observed above $500cm^{-1}$ can be assigned to a suitable combination of molecular and lattice modes (see Table Vviii). The bands at $540cm^{-1}$ and $610cm^{-1}$ are formally infrared inactive, from the assignments given. These bands are not observed in the infrared. The band at $700cm^{-1}$ should be infrared active but was not observed. (The intense neutron feature at $350cm^{-1}$ is very weak in the infrared).

6.2.2 Scattering from the Octahydrotriborate anion

This anion was not studied in isolation but may be treated as isolated by accounting for the molecular modes of the tetramethyl ammonium cation. Only two bands occur in the neutron scattering spectrum of the tetramethyl ammonium octahydroborate salt O.H.T.B., which are associated with the molecular modes of the octahydroborate anion ($B_3H_8^-$ ion). There are the bands at $443cm^{-1}$ and $540cm^{-1}$, see Table Vviii and Fig. Vxi. Unfortunately no vibrational spectroscopy has been reported for the B_3H_8 ion and no readily acceptable set of normal vibrations is available. The anion is of C_{2v} symmetry (38, 20) and could be described in terms of an analogous carbon heterocycle. One such molecule is 1,3dioxolane, see Figure Viii. This almost planar molecule is described in terms of a C_{2v} symmetry (4) and has been studied by Barker (1959). The normal modes of vibration of this compound, and their approximate descriptions, are given in Table Vxi; they are used in the assignments of the B_3H_8 spectrum.

The normal modes involving B-H stretches, BH_2 scissoring, and ring stretches will be in the region above $1000cm^{-1}$. The twists, wags, and rocks of the terminal protons are usually assigned above $700cm^{-1}$ (10). The only modes likely to be active in the region of the observations are the ring bends. These are the in plane ring bends v_{24}, v_{25} of characters A_1 and B_2; also the out of plane ring bends v_{26}, v_{27} of characters A_2 and B_1. The out of plane modes v_{26}, 27 are anticipated at lower energy than the in plane modes $v_{24,25}$. (In 1,3dioxolane $v_{24,25}$ were ca $660cm^{-1}$ and $v_{26},27$ were thought to be below $420cm^{-1}$(4)). The strong neutron band at $443cm^{-1}$ is assigned to unresolved molecular transitions involving v_{26} and v_{27}. This band was also found to be the only feature of the Raman spectrum of the B_3H_8 salt. (The band was very strong). This discounts the possibility that the band is due to the tetramethyl ammonium v_{13} mode, which appears at $444cm^{-1}$ in the T.M.A. down scattering spectrum. (The most intense Raman feature of T.M.A. in this region would be expected to be v_3, of A_1 character, which was observed by Edsall (1937) at $752cm^{-1}$). The neutron band observed can be associated with the broad infrared band at $435cm^{-1}$. This infrared absorption is split upon going to lower temperatures, 77^oK (see Table Vviii). In the two modes v_{26}, v_{27} the majority of the motion will be imparted to the protons, with the relatively heavy boron atoms remaining fixed. Under these circumstances the symmetric mode A_2, v_{26}, will take on a character not unlike a bridge proton wag. Whilst the asymmetric B_1 mode could be described as a bridge proton twist. The difference in energy of these modes and the corresponding terminal modes, which are

observed above $900cm^{-1}$; indicate the extent to which the B_3H_8 anion

is a molecule and not a loose combination of a borohydride ion and a

B_2H_4 unit. The range of measurement was too restricted to observe

other B_3H_8 anion modes in the neutron spectra; however all modes are

infrared active and some of these are assigned in Table Vviii.

(These bands have similar values to the bands observed in

1,3dioxolane). The peak at $540cm^{-1}$ is obviously a combination mode,

as no other fundamentals remain to be assigned in this region.

Combination of the $443cm^{-1}$ band and the lattice mode observed at

$106cm^{-1}$ (designated v_{L4} in Table Vviii) would yield a suitable

value, $549cm^{-1}$. This band is infrared active, observed at $540cm^{-1}$.

The lattice modes, which are assigned below the lowest internal

fundamental of the tetramethyl ammonium ion, are confused. The

broad absorption in the infrared spectra are reflected as broad

scattering in the up scattering spectrum. Unfortunately no crystal

data are vailable on O.H.T.B. and the origin of the bands remains

unknown. This breadth of scattering may be of the same type as was

observed for the ionic borohydrides, but it is more intense and occurs

closer in to the elastic peak. This type of feature is completely

absent from the T.M.A. spectrum, see Figure Vx. A similar type of

behaviour was observed in the tetramethyl ammonium manganese chloride

spectra by Lassier (1973). In the high temperature phase the T.M.A.

ions were considered to be rapidly reorientating, which should give

rise to a weak shoulder in the quasi-elastic region. In the low

temperature phase an intense broad scattering feature was observed

at $32cm^{-1}$ which was assigned to a librationary motion of the whole

T.M.A. ion, with occasional reorientation. It may be that the

crystal structure of O.H.T.B. will be less hindering to the $N(CH_3)_4$

ion, than is the case for the T.M.A. salt itself. An alternative

explanation involves a series of unresolved lattice modes. These

problems however cannot be adequately tackled without source data on

the crystalline state of O.H.T.B.

7. Barriers to reorientation

The intramolecular reorientation in the compounds studied, which

gives rise to the fluxional behaviour observed in the proton N.M.R.,

can be regarded as rotational in nature. All of the structurally

inequivalent protons can be brought into equivalence, by rotation of

an integral internal segment, the borohydride unit, about some axis.

It has been suggested by several authors that vibrational modes, if

of sufficient amplitude, provide a mechanism for permutation of atoms

in a molecule (23,34,36). It can readily be appreciated that some of

the normal modes observed in the spectra presented here would permute

atoms (e.g. v_{15} and v_5 in zirconium borohydride will permute all

bridging protons between their equivalent positions). Although in

ionic compounds the borohydride ions can be treated as independent

oscillators, the extent to which this approximation holds in a molecule

must be limited. Splitting of the modes into 'in' and 'out of' phase

motions have been observed in the aluminium and zirconium borohydrides.

Grant (1968) has shown that in compounds like neopentane the methyl

groups couple to each other through the anharmonic component of the

potential well (18,19,26) (see Section III). In the case of aluminium

and zirconium borohydrides an estimate of this anharmonicity can be

Table Vxii

Calculated Barriers to intramolecular reorientation, and reorientation in crystals.

Compound	Vibrational mode	Description	Observed frequency cm^{-1}	Equation used	Number of wells n	Number of Coupled O sill N	Barriers to intramolecular reori'. γ Kcal mole^{-1}	Coupling potential V_1 Kcal mole^{-1}	Coupled rotors V_0 $(=\frac{V}{N})$ kcalmole^{-1}	Uncoupled rotors V_0 Kcal mole^{-1}
Ca(BH$_4$)$_2$	ν 11b$_3$	libration in the crystal	332	(a) (b)	4(c)					4.96 5.45
Al(BH$_4$)$_3$	ν 25 * ν 12 *	bridge + rock	1565 1531	(a)	2	3	422.6	6.33	140.9	
	ν 27 ν 6	bridge + twist	833 793	(a)	2	3	113.3	3.95	37.8	
	ν 23 ν 10	bridge + wag	256 241	(a)	2	3	10.48	0.44	3.49	
Zr(BH$_4$)$_4$	ν 15 ν 5	bridge twist	600 519	(a)	3	4	19.77	1.81	4.94	

Notes.

(a) deep well approximation
(b) Das's formulation
(c) crystal structure unknown

For the derivation and discussion of the equations used see Section III

* values taken from Coe (1973)

† see Fig. Vvii.

obtained. This is the V_1 of Table Vxii (The formula used to

obtain the intramolecular barriers are discussed in section III).

The values obtained for the barriers are given in Table Vxii. The

V values represent the barrier to reorientation of all the borohydride

units which are coupled (N). Dividing by this number yields the

average barrier to reorientation V_o(19).

In the case of calcium borohydride the system is not molecular

and the two borohydride units are uncoupled. The reorientational barrier

is comparable with those obtained for the alkali metal borohydrides.

Its value is higher, as might be expected from its high $F_{||}^{11b}$. As with

the other ionic borohydrides this value V_o does not represent the

barrier at reorientation.

The barriers calculated for the case of aluminium borohydride are

reasonable, and have simple physical explanations. The highest

barrier involves the rocking motion of the bridging protons, see

Fig. Vviii. (This is usually given as the aluminium-hydrogen

asymmetric stretching mode in I.R. literature). That this barrier

is high can be considered as a property of an intermediate configuration

which might result from the extreme amplitude of this motion. At

this intermediate stage all the borohydride units would be bonded to

the aluminium through only one hydrogen bridge. This is energetically

very unfavourable and leads to the high barrier. Similarly at the

intermediate stage of the twisting vibration, see Fig. Vviii, all

of the bridging protons lie in the aluminium-boron plane. This is

the position of maximum nuclear repulsion. It has been calculated

that this nuclear repulsion is the dominant term in specifying the

molecular configuration of aluminium borohydride (24). Finally
there is the intermediate stage for the wagging vibration of the
bridging protons (usually called the bridge bend in I.R. texts). In
this mode the bridge protons would be displaced to one side and a
terminal proton will be brought in; to make all three protons
equidistant from the aluminium atom. This is a chemically realistic
state (29). Any of the three bridging bonds can be broken; there
is a one in three chance that a terminal and bridging proton will have
been exchanged. It is obvious that these intermediates forma series;
from an electronically unacceptable intermediate stage, through a
highly repulsive intermediate, to a low energy intermediate. The
barrier which hinders the exchange of terminal and bridging protons
in aluminium borohydride is associated with the bridge wage, it is
about 3.5 Kcal mole^{-1} (in the deep well approximation). This barrier
is consistent with the proton N.M.R. data, which indicates equivalence
of all protons. It can be seen from Table Vxii that the coupling
between the borohydride units is very low. The V_1 term, which is a
measure of the coupling, is no more than 4% of the total barrier, V,
for any vibration.

The barriers obtained for the zirconium borohydride can be
rationalised in a similar manner. In this case the barrier to
reorientation V_o given in Table Vxii, is the barrier to rotation about
the zirconium-boron axis. It is given at 4.94 Kcals mole^{-1}. There
are several points of interest in this case. Firstly the value for
the total barrier V is less than the equivalent barrier in aluminium
borohydride. Also that the coupling between the motion of the
borohydride units is larger. The value of V_1 is equal to 9.1% of

the barrier V. Although the number of borohydride units around the zirconium atom is four, compared with three in aluminium borohydride, the metal boron distances in the two compounds are similar (Zr-B is about 2.34Å (7,40) and Al-B is about 2.14Å (1)). It may be concluded that the congestion about the zirconium atom is severe, and leads to intermeshing of the borohydride units. This intermeshing, in a cog like manner, explains the higher degree of coupling observed.

The vibration which allows the exchange of terminal and bridging protons is probably a zirconium-hydrogen asymmetric stretching frequency. This would lead to an intermediate which has a double proton bridge from boron to zirconium (29). Unfortunately a complete vibrational analysis of this compound has not been published and the nature of the motions involved in its vibrational modes is unclear. The mode v_{21}, described by Davies (1973) as a bridge deformation, may be the mode required. This mode involves significant proton motion and was assigned to the band at $227cm^{-1}$, Table Vvi. In the deep well approximation for independent rotors (discussed in Section III) this band is associated with a barrier, V_o, of 1.03 Kcal $mole^{-1}$. (Because of the tentative nature of the association of this band with terminal-bridge exchange the calculation was omitted from Table Vxii). This value for the reorientational barrier ($V = N.V_o$; 4 x 1.03 Kcals $mole^{-1}$) $V = 4.12$ Kcals $mole^{-1}$, is low, but is consistent with N.M.R. work. The proton N.M.R. work conducted on zirconium borohydride has shown that intramolecular reorientation should be more hindered than the whole body reorientation of the molecule in the liquid (29). This whole body reorientational barrier was determined at about 3.1 Kcal $mole^{-1}$.

The modes which exchange the bridging and terminal protons in the B_3H_8 anion are pseudo rotational in nature (25). These vibrational modes are usually observed in the region below about $100cm^{-1}$ (21), and were not observed in the spectra presented here. They would be expected to lead to very low barriers to intramolecular reorientation.

REFERENCES

1. Almeuningen, A.   Acta Chem. Scand. 22, 328, (1968).

2. Armstrong, D.R.   J. Chem. Soc. A, 1044, (1969).

3. Bailey, N.A.   J. Inorg. and Nuc. Chem. 32, 3116, (1970).

4. Barker, S.A.   J. Chem. Soc.   802, (1959).

5. Beall, H.   J. Am. Chem. Soc.   92, 3484 (1970).

6. Beach, J.Y.   J. Am. Chem. Soc.   62, 3440, (1940).

7. Bird, P.M.   Chem. Comm.   403, (1967).

8. Bottger, G.L.   Spectrochim. Acta.   21A, 1701, (1965).

9. Bushweller, C.H.   J. Am. Chem. Soc.   93, 2145, (1971).

10. Coe, D.A.   Spectrochim. Acta.   29A, 1789, (1973).

11. Cotton, F.A.   Acc. Chem. Res.   1, 257, (1968).

12. Davies, N.   J. Chem. Soc. (Dalton), 162, (1973).

13. Von Doering, E.   Angew. Chem. (Internat.) 2, 115, (1963).

14. Durig, J.R.   J. Chem. Phys.   49, 675, (1968).

15. Edsall, J.T.   J. Chem. Phys.   5, 225, (1937).

16. Emery, A.R.   Spectrochim. Acta 16, 1455, (1960).

17. Grace, M.   J. Am. Chem. Soc.   93, 2145, (1971).

18. Grant, D.M.   J. Chem. Phys.   52, 4424, (1970).

19. Grant, D.M.   Phys. Rev. Letters.   20, 983, (1968).

20. Klanberg, F.   Chem. Comm.   1293, (1967).

21. Laane, J. "Vibrational Spectra and Structure"   Dekker (1972).

22. Lassier, B.   Journal de Phys (Paris) 34, 473, (1973).

23. Lehr, A.D.   J. Phys. Chem.   67, 389, (1963).

24. Levison, K.A.   Rev. Roum. Chim.   15, 153, (1970).

25. Lipscomb, W.N. Advan. Inorg. and Radiochem. 1, 117, (1959).

26. Livingston, R.C. J. Chem. Phys. 58, 1438, (1973).

27. Longuet,Higgins, H.C. J. Chem. Soc., 139, (1946).

28. Marks, T.J. (a) Chem. Comm. 1019, (1972).

29. Marks, T.J. (b) J. Am. Chem. Soc. 94, 1542, (1972).

30. Marks, T.J. (c) Inorg. Chem. 11, 2540, (1972).

31. Marynick, D.S. Inorg. Chem. 11, 820, (1972).

32. Marynick, D.S. J. Chem. Soc. (A) 1160, (1970).

33. Mayburg, C.P. Inorg. Chem. 6, 1286, (1967).

34. Muetterties, E.L. Inorg. Chem. 4, 769, (1965).

35. Muetterties, E.L. Acc. Chem. Res. 3, 267, (1970).

36. Nibler, J.W. J. Am. Chem. Soc., 94, 3349, (1972).

37. Ogg, R.A. Discussion Faraday Soc. 19, 246, (1955).

38. Peters, C.R. J. Am. Chem. Soc. 82, 5758, (1960).

39. Phillips, W.D. J. Am. Chem. Soc. 81, 4496, (1959).

40. Plato, V. Inorg. Chem. 10, 590, (1971).

41. Price, W.C. J. Chem. Phys., 17, 1044, (1949).

42. Reid, W.E. J. Electro. Chem. Soc., 104, 21, (1957).

43. Semenenko, K.N. Zh. Struckt. Khim. 13, 540, (1972).

44. Smith, B.E. Inorg. and Nuc. Chem. Letters, 7, 857, (1971).

45. Young, C.W. J. Am. Chem. Soc., 69, 1410, (1947).

46. Wallbridge, M.G.H. Prog. Inorg. Chem. 11, 99, (1970).

CHAPTER VI

THE INCORPORATION OF THE AMMONIUM ION IN

LATTICES OF THE ALKALI HALIDES.

Since the early theoretical work by Pauling (1930) and

Frenkel (1946) the ammonium halides have been extensively studied.

Many of these studies have had the object of determining the

rotational dynamics of the ammonium ions, and the extent to which

these are influenced by the presence of other ammonium ion neighbours

(22, 42).   Unfortunately the ammonium halides undergo many phase

changes as the temperature varies (42).   This makes it difficult

to study the temperature variation of the dynamics in these salts.

Also, unlike the borohydrides, the crystal structures of the pure

ammonium halides are not highly symmetric.   It was with the object

of overcoming these difficulties that the ammonium ion was incorporated

into the alkali metal halide lattices.   These lattices maintain

their highly symmetric structure despite temperature variation.

The crystal dynamics of a lattice containing defects are discussed;

with specific reference to the ammonium ion in the alkali halide

crystals.   Following this the experimental methods of preparing

the mixed crystals are described, and also the studies which were

conducted on them.   Finally the results obtained are presented and

discussed.

1. **The Dynamics of a lattice containing Molecular Substitutional defects.**

The dynamics of a pure lattice were touched upon previously in Section IV. In this section the effects of a molecular substitutional defect in a diatomic lattice is considered. Beginning with the simplest case, the monatomic substitutional mass defect; this is easily extended to cover the molecular mass defect. Throughout the discussion it is assumed that the defect experiences the same force constants as would the substituted atom. (Force constant changes are sometimes required to improve the fit of the predictions to experimental observation (38). Generally if the force constant increases for a defect then it has the same effect as lightening the defect mass).

1.1 A light monatomic mass defect

1.1.1 Substituted into a monatomic lattice.

The solutions to the dynamical equations of a three dimensional monatomic lattice fall into one band. These are the acoustic modes. In substituting a light defect the vibrational frequency of the defect in the lattice will be higher than for the substituted atom. The solutions, representing the frequency of the defects will move out of the band to higher values.

1.1.2 Substituted into a diatomic lattice.

In a diatomic lattice, of two ions with different masses, the problem is more complex. The dynamical equations of the pure lattice show two sets of solutions, the acoustic and optic modes; due to the

presence of the two masses. Usually there is a frequency gap between the two sets of solutions which corresponds to forbidden frequencies for the lattice. This is termed the 'Gap'. The motions of the two masses, with respect to each other, are different for the two bands. Consider a pure lattice of two masses M_h and M_l, the heavy and light ions respectively. Model calculations by Mazur (1956) have shown how these motions can be used to understand the effects of a light defect atom. The defect atom is denoted by m, and is lighter than either M_h or M_l.

At the zone edge of an acoustic branch the M_h atoms only are vibrating, π out of phase with each other; the M_l atoms are situated at nodes. Substituting m for M_h will move the solutions of the dynamical equations representing the motion of the defect to higher frequency. (This is similar to the case for the monatomic lattice). Modes of the same symmetry in the optic band will also be forced to higher frequency. This is because of the mutual repulsion between modes of the same symmetry (37). At the zone edge of an optic branch the M_l atoms are moving π out of phase with each other, and the M_h atoms are situated at the nodes. Substitution of a m atom for M_l will again lead to the solutions for the defect atom being found at higher frequency. In this case above the optic branch. However the mode in the acoustic band, which has the same symmetry, is not moved out of the band.

The modes produced by promoting a solution out of the optic band is a vibration which is too high in frequency to be propogated

Table VII.   Principal spectral properties of the pure alkali halide lattices

| Pure Compound	Estimates of (1) Gap cm^{-1}	ω_{max} cm^{-1}	Temperature °K	Reference	Observed Optic mode cm^{-1}	(2) Longitud. Optic mode cm^{-1}	References
NaCl	104-127	261	80	Ranino (1970)a	170.1	270	Hass (1960)
Br		210	295	Reid (1970)	135.3	211	Jones (1961)
I	77-84	174	100	Cowley (1963)	116.6	184	"
KCl		214	80	Ranino (1970)a	149.0	221	Hass (1960)
			115	Copley (1969)			Jones (1961)
Br	94-100	167	90	Cowley (1963)	115.3	167	"
I	70-97	144	95	Polling (1966)	108.3	151	
RbCl	100-107	170	30	Ranino (1970)b	126.9	190	"
Br		134	80	Rolandson (1971)a	96.7	139	"
I		100	80	Ranino (1970)c	81.6	112	"
CsCl	87-94	164	78	Ahmad (1972)	105.0	174	"
Br		110	80	Rolandson (1971)b	79.3	132	"
I					65.8	104	"

Notes.   (1) Gap, forbidden band between acoustic and optic modes.

ω_{max},   maximum frequency which the lattice can propagate.

These are estimated from the frequency distribution functions published by the authors.

(2) Calculated from Lydanne Sachs Teller relationship.

Fig. VI.i

283.

Eigen vector diagrams of infrared active impurity modes,
in a diatomic linear chain.

Localised mode

Gap mode

Resonant mode
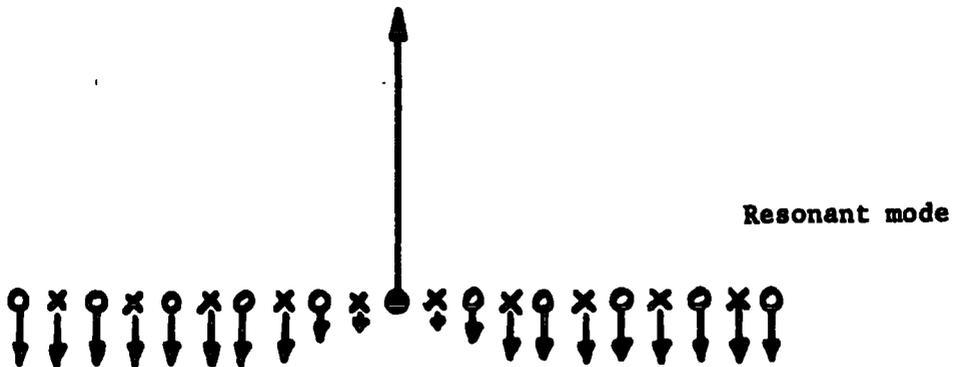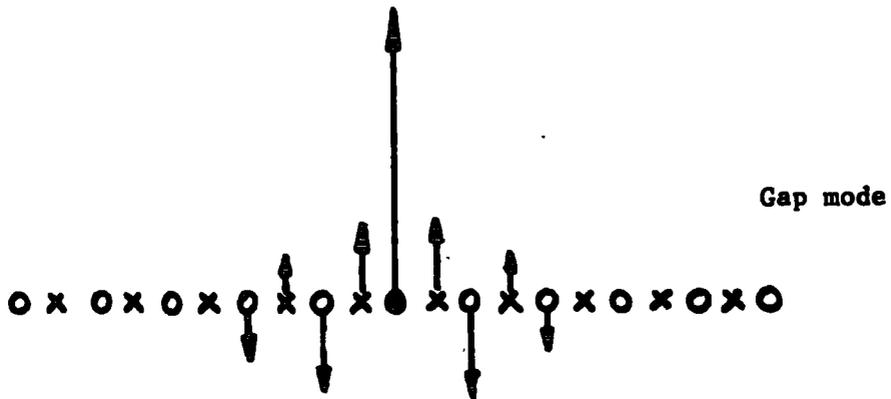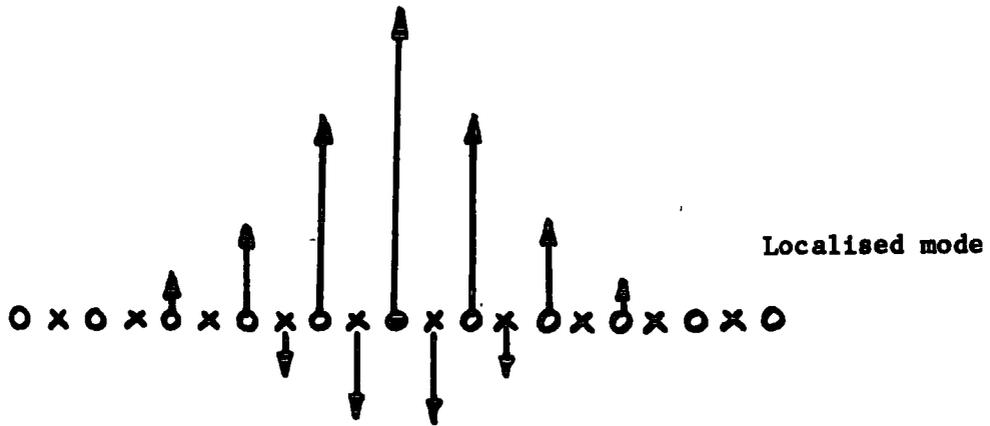
after Renk (1967)

by the whole lattice.   Such modes are above the maximum

propogating frequency of the lattice, ω_{max}.   This maximum frequency

is the frequency of the highest mode in the optic branch of the pure

crystal.   Motions of the impurity atom which are transferred to its

neighbouring atoms are heavily damped.   Vibrations in this mode will

involve primarily motion of the impurity atom.   The mode is

therefore localised in space, and is termed a localised mode. (See

Fig. VIi).   Modes localised in space are also produced when a

solution is promoted out of the acoustic branch into the forbidden

frequency gap.   These are usually termed gap modes in the literature

(see Fig. VIi).   In some pure alkali halides there is no forbidden

frequency gap, see Table VIi.   Defect modes promoted from the

acoustic branch of these salts will appear in the optic branch.   Any

impurity mode which has a frequency within either the acoustic or

the optic branches will resonate with the lattice at that frequency.

These modes are termed resonance (see Fig. VIi) modes.   In this thesis

it is unimportant whether a mode promoted from the acoustic branch is

strictly a gap mode, or a resonance mode.   For the purpose of

consistency all defect modes promoted out of the acoustic branch will

be termed gap modes.

1.2 A light polyatomic defect substituted into a diatomic lattice.

Previously, substitution of a defect left the mixed lattice with

the same number of atoms as the pure lattice.   In the case of

polyatomic ion substitution more atoms are added and the lattice has

extra degrees of freedom.   A more complex dynamical equation is

required to describe the system and apart from some solutions
being moved, extra solutions are expected.   This problem was
treated by Wagner (1963) and (1964).   The polyatomic·defect,
represented by a point at its centre of mass, is treated as a mass
defect.   The equations are then further modified by coupling
between the lattice and molecular systems.   The set of solutions
to these equations, which represent the frequencies of the lattice
modes, include the molecular vibrational frequencies.   (Since
the interatomic bonding in a polyatomic ion is much stronger than
the inter-ionic interactions the molecular vibrations should not be
shifted greatly from the free ion values).   These solutions to
high frequency are in addition to the high frequency modes promoted
out of the optic and acoustic bands.   One further set of modes is
also expected, the librational modes.   For non spherically
symmetric ions as many as three modes would be expected, associated
with the different moments of inertia.   In a lattice where the
molecular axes are distributed among the equivalent crystal symmetry
directions, the molecule may take on the statistical appearance of
a sphere (45).   There are some results which are in accordance with
this suggestion (23).   Any molecular modes whose frequencies fall
within the optic or acoustic bands from resonance modes (20).

1.3 Modifications to the molecular vibrational spectrum by
     substitution into a lattice.

When a molecular entity is condensed into the crystalline
state its spectrum is affected.   Even in pure crystals the molecular
spectrum is modified by its environment.   This was partially

discussed in section IV. The largest influence comes from the ion's immediate environment, site group effects. The larger environment of the unit cell in a pure crystal can cause further modification, Factor group effects, but these may be so weak as to be absent (13). In a substitutionally defective crystal there can be no Factor group effects (this follows from the definition of a solid solution as opposed to a mixture of crystallites). It is with the object of changing the site group effects, and to sharpen bands that molecular ions are usually incorporated into other crystals. Under suitable conditions the site environment will remove degeneracy of molecular modes and make other modes active (see Section IV). However the band shapes and fine structure around bands in the molecular vibration region cannot always be successfully explained by site group effects (41, 20).

Such effects can be explained in other ways. These are, concentration effects, and combination modes. Van der Elsken (1964) has shown that, unless very weak solutions of the incorporated ion are used, infrared active satalite bands are produced. These arise from coupling of the intramolecular modes in clusters of the defects. It results in in-phase and out of phase modes for these bands. This does not explain all structure and can be produced by using low concentrations.

A satisfactory explanation has been provided by Metselaar (1966). (This follows from similar explanations of ultra violet spectra, Timusk (1964). In the high frequency region of a strongly active molecular vibrational band fine structure is often observed. This

can be interpreted as a combination of the molecular mode with the band spectrum of the lattice modes (21, 23). In the case of incorporated nitrate ions, in alkali halide lattices, the main features of the bands of the lattice modes were observed. These were on the high energy side of the intense nitrate stretching mode at 1388cm^{-1} (v_3, character E'), also observed were the localised modes caused by the nitrate ion acting as a mass defect (21). This combination with the frequency distribution spectrum of the lattice covered the region up to about 1600cm^{-1}. Its overall shape fitted the published lattice frequency spectrum of the pure host. The extra peaks observed occurred in the region of the host lattice gap, and also slightly above ω_{max} of the pure host.

2. Spectral modifications expected for the incorporation of ammonium ions in alkali halide lattices.

In the neutron inelastic scattering spectrum of a lattice all modes would be expected to be active (see Section I), incorporation of a defect will merely change the values of the modes. Infrared absorption spectroscopy, however, is fundamentally changed by incorporated defects (37). The strict translational symmetry of a pure lattice imposes a selection rule for the interaction of light with lattice modes. (This selection rule demands the conservation of wave vector). When defects are introduced into the lattice the translational symmetry is lost and the selection rule relaxes. In any mixed crystal all modes are formally infrared and Raman active although there may still be some modes which interact preferentially with light due to symmetry considerations (37).

Table VIii.

Table showing the modes predicted in a mixed
ammonium alkali halide crystal

Pure Host	Heaviest of Host atoms	Localised Modes predicted:		
		in the Gap	above ω_{max}	as a libration
NaCl	Cl		*	*
Br	Br		*	*
I	I		*	*
KCl	K	*	*	*
Br	Br		*	*
I	I		*	*
RbCl	Rb	*	*	*
Br	Rb	*	*	*
I	I		*	*
CsCl	Cs	*	*	*
Br	Cs	*	*	*
I	Cs	*	*	*

Note. NH_4^+ always displaces the metal ion, and is
a light impurity.

2.1 Low frequency region.

The ammonium ion substituted into the alkali metal halides is always a light impurity; it is lighter than any alkali metal, save lithium.   Provided the ion interacts with the lattice via the same force constants as the displaced metal, predictions can be based upon the model of Mazur (1956) discussed earlier.

These predictions can be illustrated by consideration of the potassium chloride and potassium bromide salts.   The ammonium ion substitutes for the potassium ion in both salts.   In potassium chloride the light defect, the ammonium ion, is substituted for the heavier ion of the pure host lattice.   Thus, apart from the librational mode, a gap mode and a localised mode are predicted. However, in the case of potassium bromide the potassium ion is the lighter ion of the pure host lattice.   Thus, apart from the librational mode, only a localised mode is predicted.   The modes predicted for the substitution of ammonium ion defects into alkali halide lattices are given in Table VIii.   Smith (1972) has reported some neutron inelastic work conducted on the potassium (ammonium) chloride crystal lattice.   He has shown that two localised modes occur, a translational and a librational mode.   The translational localised mode could be explained by considering force constant changes of about 20 to 25%.   The librational mode was at higher frequency.

2.2 Molecular vibration region.

It might be anticipated that the region to high frequency of a

strong molecular band would show combination with the lattice
modes. Such behaviour would be directly analogous to the nitrate
and nitrite observations (21, 23). In this environment only two
molecular vibrations are infrared active, v_3 and v_4 of character F_2
the band at ca. $1400cm^{-1}$ (v_4) lies in the least cluttered region
of the spectrum. An extensive study of the vibrational region
of the infrared spectrum of ammonium ions incorporated into alkali
halides was undertaken by Vedder (1958). He covered the two regions
1300 to $1650cm^{-1}$ and 2500 to $3900cm^{-1}$. Spectra were obtained at
different temperatures, as low as $4^{\circ}K$. The results he obtained
are reproduced in Table VIiii. It is obvious from his results that
the expected behaviour is not occurring, even the broad general
features are absent. It was suggested that a satellite band, at
$1458cm^{-1}$, to the main ammonium bending mode, at $1403cm^{-1}$, was a
combination. The combination proposed was with a libratory mode;
involving libration about the C_3 symmetry axis. Vedder did not
appear to appreciate the possible explanation in terms of
combinations of the lattice and molecular modes (discussed earlier).
However this does not necessarily invalidate his interpretation.
The assigned band is only $55cm^{-1}$ from the fundamental intramolecular
band with which it is combined. Although the band may be
associated with the expected gap mode, promoted from the acoustic
branch, its value is low. (In the case of KCl there is no gap,
see Table VII). Further, no localised mode, promoted from the optic
branch was observed. Such a mode might be expected to accompany
any gap mode.

Table VIiii.

Results reported by Vedder (1958) for the I.R. spectrum
of K-NH$_4$Cl in the 1400cm^{-1} region at 5°K.

K-NH$_4$Cl	
Infrared absorption maxima (cm^{-1})	
Dilute solution	Concentrated Solution
	1536 b
	1495 b
1470 b	1470 b
1457 b	1458 b *
1438	1438
1424.8	1424.8
1413.5	1413.2
1404.8 vs	
1401.8 vs	
1396.5	
1385	1384.5

*   band assigned to a combination of libration
    and molecular bending. Vedder (1961)

3. <u>Experimental</u>

The mixed crystals were prepared by a simple procedure, after the starting materials had been purified. The best grade of starting materials was obtained, for some of the alkali halides this was 'optran' standard, from B.D.H. Other salts were obtained as 'Analar' quality. (Only in the case of rubidium salts and ammonium iodide were crystals of less purity used). The starting materials were checked for spectroscopic impurity, over the range 4000 to 250cm^{-1}, using thick nujol mulls. Most of the salts were used without further purification. In the case of all rubidium salts and some caesium and ammonium salts recrystallisation was necessary. The salts were recrystallised from water (distilled water was used throughout the preparation), recovering 90 to 95% of the solute. Even with the rubidium salts two recrystallisations were adequate.

The preparation of the mixed salts was conducted after a method due to Fock (1897). A large weight of the host crystal, about 80gm, and a small quantity of the appropriate ammonium salt were taken up into solution with water. This was done slowly at ambient temperature, so that a very concentrated solution was obtained. The solution was placed in a refridgerator maintained at about -5°C. Crystals of the mixed salt slowly precipitated over a few hours; and no more than 10% of the solute was recovered. (Although in the case of the expensive rubidium salts larger quantities were precipitated).

The mixed crystals were separated from the mother liquor and dried at the pump; final drying was done in an oven maintained at

65°C.   Spectroscopically dry samples were used in all the
experiments.   Samples of the dry salts were analysed for total
nitrogen content by the standard Kjeldahl method.   It was possible
to check the consistency of the precipitated crystals in the
potassium(ammonium)salts.   In this sytem large conglomerates of
crystallites formed, up to 1.5cm high, and often 2 by 2cm square.
Samples taken from the base and from the top gave the same
analytical figures.   Only about 2.5% (by mole) of the host lattice
was substituted for, by the relevent ammonium halide.

At this concentration about 75% of the ammonium ions will have
only metal ions as their nearest cationic neighbours, and about 20%
will have one other ammonium ion as a neighbour.   The remaining 5%
are in groups of three or four (2).   This was achieved by slowly
increasing the weight of ammonium salt in the initial solution
whilst keeping the host at constant concentration.   As reported by
Vedder (1958) the concentrations of the original solution, necessary to
achieve the required solid solution concentration, varied widely
from salt to salt.   Experimental difficulties were found with all the
iodides due to the tendency of the iodide ion to oxidise.   (The
I $^-$ going to I_3^- ion).   These preparations were conducted under
nitrogen to limit the oxidation.   Inability to control the %
incorporation of ammonium ions into caesium salts is probably due
to too rapid a precipitation rate.

3.1   For the purpose of all neutron scattering experiments
the dry salts were contained in aluminium foil satchets.   These
satchets were easily formed from 0.002" aluminium foil shaped into

Table VIiv.

Table of experimental details for the spectra of ammonium incorporated into alkali halide lattices

Sample	K-NH$_4$			Rb-NH$_4$	Cs-NH$_4$		
	Cl	Br	I	Cl	Cl	Br	I
% by mole NH$_4^+$ incorp.	2.61	2.14	4.45	2.41	2.40	6.17	0.61
Up scattering							
Can material	Al	Al	Al	Al	Al	Al	Al
wt. of compound gm	39.59	40.63	14.94	10.48	8.46	15.50	10.08
Thickness cm	1.3	1.2	0.45	0.35	0.30	0.35	0.25
Area cm^2	32.5	32.5	33.0	22.5	35.0	32.5	30.0
Background (Host in Al)	KCl	KBr	KI	RbCl	CsCl	CsBr	CsI
wt. of Host gm	40.0	47.77	14.98	10.74	8.42	15.54	10.15
Thickness cm	1.2	1.2	0.40	0.30	0.25	0.35	0.20
Area cm^2	32.4	32.5	30.0	22.5	35.0	30.0	30.0
Down scattering							
Monochromater	Al	Al	Al	Al		Al	
plane	3.1.1.	3.1.1.	3.1.1.	1.1.1/3.11		3.1.1.	
Infrared spectrum							
db gain	24.9	12.5					26.5

a square pocket about 5cm by 5cm.   Initially, because scattering
from the samples was expected to be low, very thick (up to 13mm)
samples were used.   This was later found to be unnecessary.
Satisfactory scattering was obtained from about 12gms of the mixed
salt, which gave sample thicknesses of about 3mm, when rolled flat.
The aluminium satchets were not air tight and all samples were
stored in vacuum dessicators above phosphorus pentoxide.   The
up scattering spectra were taken on the 6H spectrometer at Harwell
(see Section II).   The down scattering spectra were obtained on the
beryllium filter spectrometer at Harwell (see Section II).   A sample
of the pure host lattice was run as a background to the relevent
incorporated salt.   This background was subtracted from the spectra
of the mixed salts to obtain the extra scattering due to the
ammonium ions.   All relevent experimental details are given in
Table VIiv.

3.2   The infrared absorption spectra of some of the pure, and
mixed, salts were obtained in the far infrared region.   The far
infrared Fourier transform spectrometer was used (see Section II)
and the samples were prepared as has been previously described (see
Section IV).   The experimental details for the best spectra are
given in Table VIiv.

4. Results.

The infrared results are presented first, these are shown
in Table VIv, and illustrated in Fig. VIii,iii.   These results are
discussed together.   Secondly the results of the inelastic neutron

scattering spectra are presented, these are given in Tables VIvi,
VIvii, and shown in Fig. VIiv to x.   The tables are given in the
best manner to facilitate comparison with the ideas of Mazur
(discussed previously).   These results are discussed in three
sections.   The first is devoted to the overall number of extra modes,
and how it compares with predictions.   In the second the observed
bands are assigned.   Finally the reorientational processes at
work in the crystal are discussed.

4.1 The infrared spectra

The study of the infrared region from 50 to 450cm^{-1} was made,
to observe the expected localised modes (discussed earlier).   The
results given in Table VIv are for potassium chloride, host lattice,
only;   analogous results were obtained for the caesium iodide and
sodium chloride host lattices.   It is obvious that the
incorporation of ammonium ions into the host lattice has not given
rise to any extra absorptions, over this region.   It has made no
observable changes to the host lattice at all.   The reasons for this
involve the limitations of the apparatus and the temperature
dependence of the localised mode.   The apparatus used was incapable
of maintaining temperatures lower than about 77°K (see Section II).
This is a relatively high temperature to search for localised modes.

The localised mode couples to the lattice vibrations.   This
coupling is through anharmonic terms of the potential used in the
lattice dynamical equations.   The coupling produces extra bands,
at the sides of the main localised mode.   These side bands grow as

Table VIv.

Infrared absorptions of the mixed crystal potassium
ammonium chloride and the host lattice.

KCl		K-NH$_4$Cl	
observed bands		observed bands	
293°K cm^{-1}	77°K cm^{-1}	293°K cm^{-1}	77°K cm^{-1}
142 msh	145 msh	138 ssh	149 msh
148 vs	156 vs	148 vs	153 vs
153 msh	162 ssh	158 s	
205 vw	190 vwsh		
213 w	220 w	213 m	220 w
230 vwb	240 vwb	234 vwb	235 vwb

Notes.

    s, strong

    m, medium

    w, weak

    v, very

    b, broad

Fig. VI.ii

298.

Infrared absorption spectrum of potassium (ammonium) chloride

Fig. VI.iii

299.
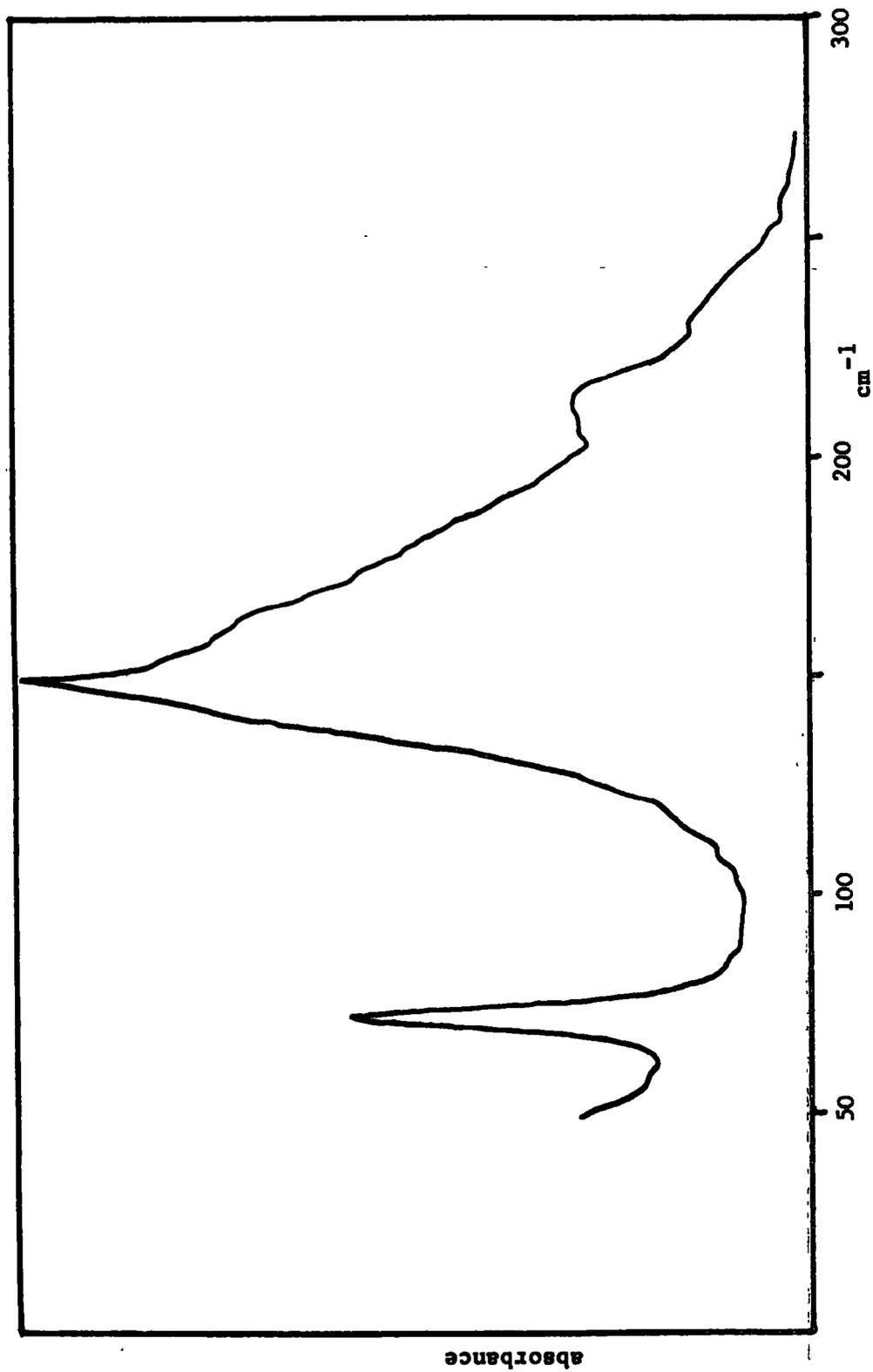
Infrared absorption spectrum of potassium chloride
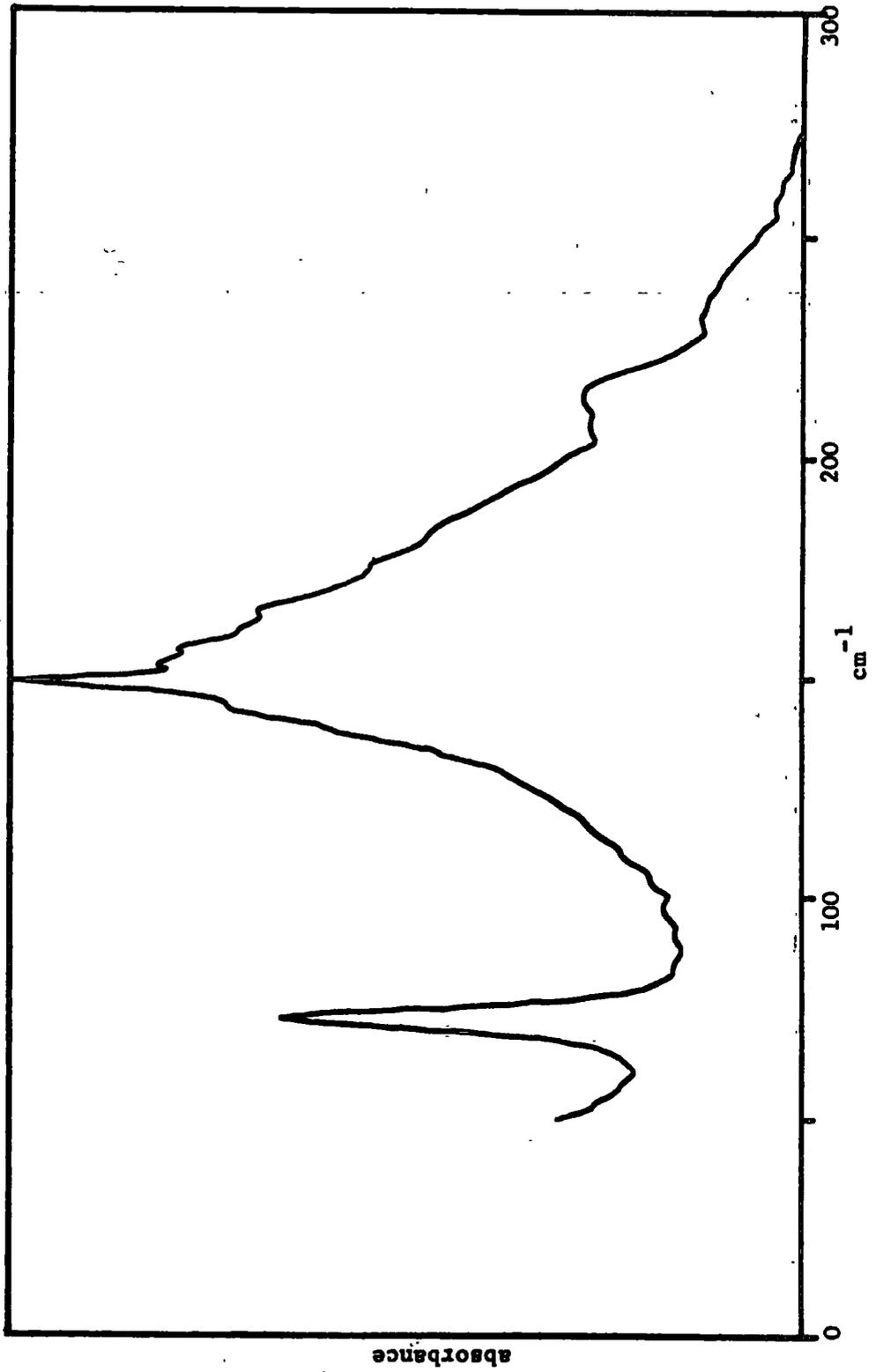
the temperature rises, gaining intensity at the expense of the main mode (16). Further, experimental difficulties can hinder the observation of the localised mode. Except at very low temperatures the lattice vibrations of the host crystal may swamp the local mode (36). It is probable that the sample temperature was too high to observe these modes.

4.2 The inelastic neutron scattering spectra.

Up scattering spectra were taken of caesium (ammonium) chloride, bromide, and iodide at ambient temperature; and also of potassium (ammonium) bromide at ambient temperature and at $176^\circ K$. Down scattering spectra were taken, all at $77^\circ K$, of the potassium (ammonium) chloride, bromide and iodide; and also of rubidium (ammonium) chloride and caesium (ammonium) bromide. Insufficient time was available on the instruments to study all the compounds available. Instead the above representative selection was covered.

4.2.1 Substitution of ammonium ions for the light ions of a lattice, K-NH$_4$Br and K-NH$_4$I.

As shown in Table VIvi there are only two localised modes expected in these salts:. The translational localised mode of the ammonium ion and its librational mode. The spectra of potassium (ammonium) bromide, given in Table VIvi see Fig. VIiv, clearly show only two intense modes. These are at 228 and 305cm^{-1}. Both of these bands are above the maximum propogating frequency of the pure host lattice (ω_{max}) (4). If ω_{max} is a reasonable approximation to the limit of the propogating frequencies in the

Table VIvi

Table showing the extra scattering from ammonium

(Substituted for the lighter host atom)

KBr			KI	Assignment
neutron scattering			neutron down	
up $\theta = 45^{\circ}$ T = 294°K cm^{-1}	up $\theta = 45^{\circ}$ T = 176°K cm^{-1}	down T = 77°K cm^{-1}	T = 77°K cm^{-1}	
15 vw				
43 vw	43 w			
	82 w			
110 w				
141 m	149 m			
	(167)		(144)	
217 vs	194 vs	228 vs	208 vs	translation
259 s	275 s sh	305 s	257 s	libration

Notes. (   ); this represents the maximum frequency that the crystal can propagate. See Table VIi.

w = weak
m = medium   v = very
s = strong
sh = shoulder

mixed crystal, then the observed modes are localised. It has been
suggested that this is the case (38), their assignment is discussed
later. The extra scattering intensity which occurs as peaks in
the in-band region of the host lattice probably represents the
weak involvement of the ammonium ions with certain lattice modes.
Since the infrared absorptions of both the pure hosts and the mixed
salts are coincident, it is unlikely that the bands are the product
of a bad background correction. The weak intensity of the bands
argues against their being unexpected gap or resonance modes.

The values of the lattice modes at specific points, of high
symmetry, on the Brillouin zone boundary have been published
(References are given in Table VIi). The extra scattering observed
in the spectra presented here can be matched with some of these
modes. In potassium bromide the peaks at 43, 110, and $141 cm^{-1}$ may
be matched to the $[0,0,1]$, ν,TA; $[\frac{1}{2},\frac{1}{2},\frac{1}{2}]$ ν,TO; and $[\frac{1}{2},\frac{1}{2},\frac{1}{2}]$ ν,LO
lattice vibrations respectively. Such assignments are tentative,
and are not shown in Table VIvi .

4.2.2 Substitution of ammonium ions for the heavy ions of the lattice, K-NH$_4$Cl Rb-NH$_4$Cl Cs-NH$_4$Hal.

As shown in Table VIvii two localised modes and one gap mode,
promoted from the acoustic branch, are predicted for this case. One
of the localised modes being the librational mode of the ammonium ion.
The results obtained for the caesium(ammonium) chloride clearly show
two strong bands. The gap mode at $129 cm^{-1}$ and a localised mode at
$316 cm^{-1}$. A moderately intense band occurs at $158 cm^{-1}$ (see Fig. VIvii).

Table VIvii

Table showing the extra scattering from ammonium.

(Substituted for the heavier host ion)

Previous work KC1 (1) cm⁻¹	KC1 Neutron down 77°K cm⁻¹	RbCl Neutron down 77°K cm⁻¹	CsCl Up scatt. θ = 45° 294°K cm⁻¹	CsBr Up scatt. θ = 45° 294°K cm⁻¹	CsBr Neutron down 77°K cm⁻¹	CsI Up scatt θ = .45° 294°K cm⁻¹	Mode Assignm.
			42 w	42 w			
			51 w				
			87 w	96 vw			
				(110)			
			129 s	135 s	≤ 140		Gap
			158 m				
	(214)	(170)	(164)				
			233 w	196 w			
227 s	257 s	228m					translat.
337 w	343 s	353m	316 s	306 s	348vs		libration

Notes. (   ); the bracketed figures are the maximum frequency
              which can be propagated by the pure host lattice
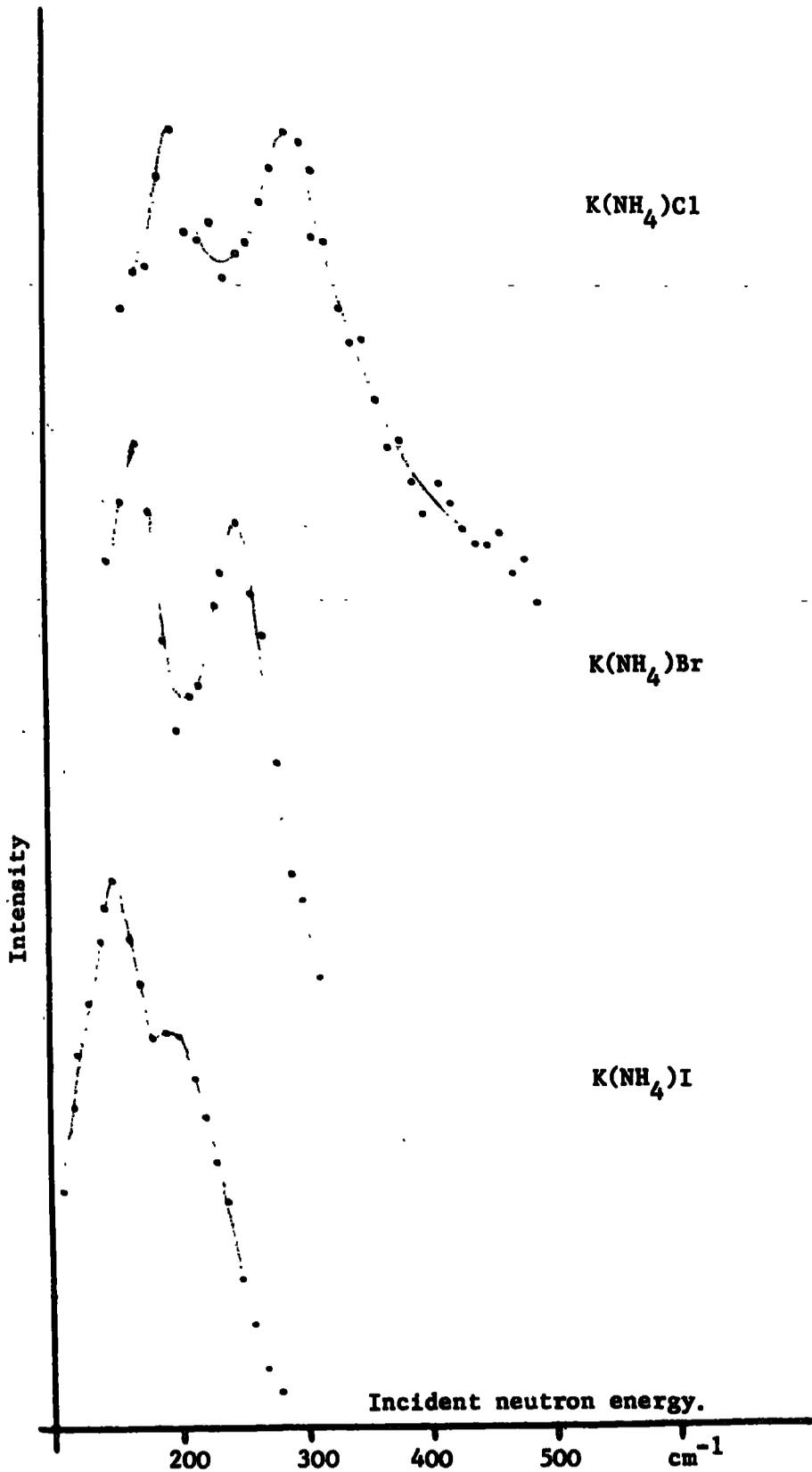
              see Table VIi.

w = weak   ref: (1) Smith (1972)
m = medium
s = strong
v = very

This is close to ω_{max} for the caesium chloride lattice, 164cm^{-1} (1), and is probably the other localised mode expected.   Similarly the spectrum of caesium(ammonium) bromide shows two intense bands at 135 and 306cm^{-1}.   These bands are both above ω_{max} for caesium bromide, 110cm^{-1} (33).   The band at 135cm^{-1} is assigned to the two unresolved translational modes, the gap mode and the localised mode.   The band at 306cm^{-1} is the other localised mode, the localised modes are discussed later.   The caesium(ammonium)iodide sample had a very low concentration of incorporated ammonium ions, see Table VIiv. There were no bands observed in the spectrum of this sample.
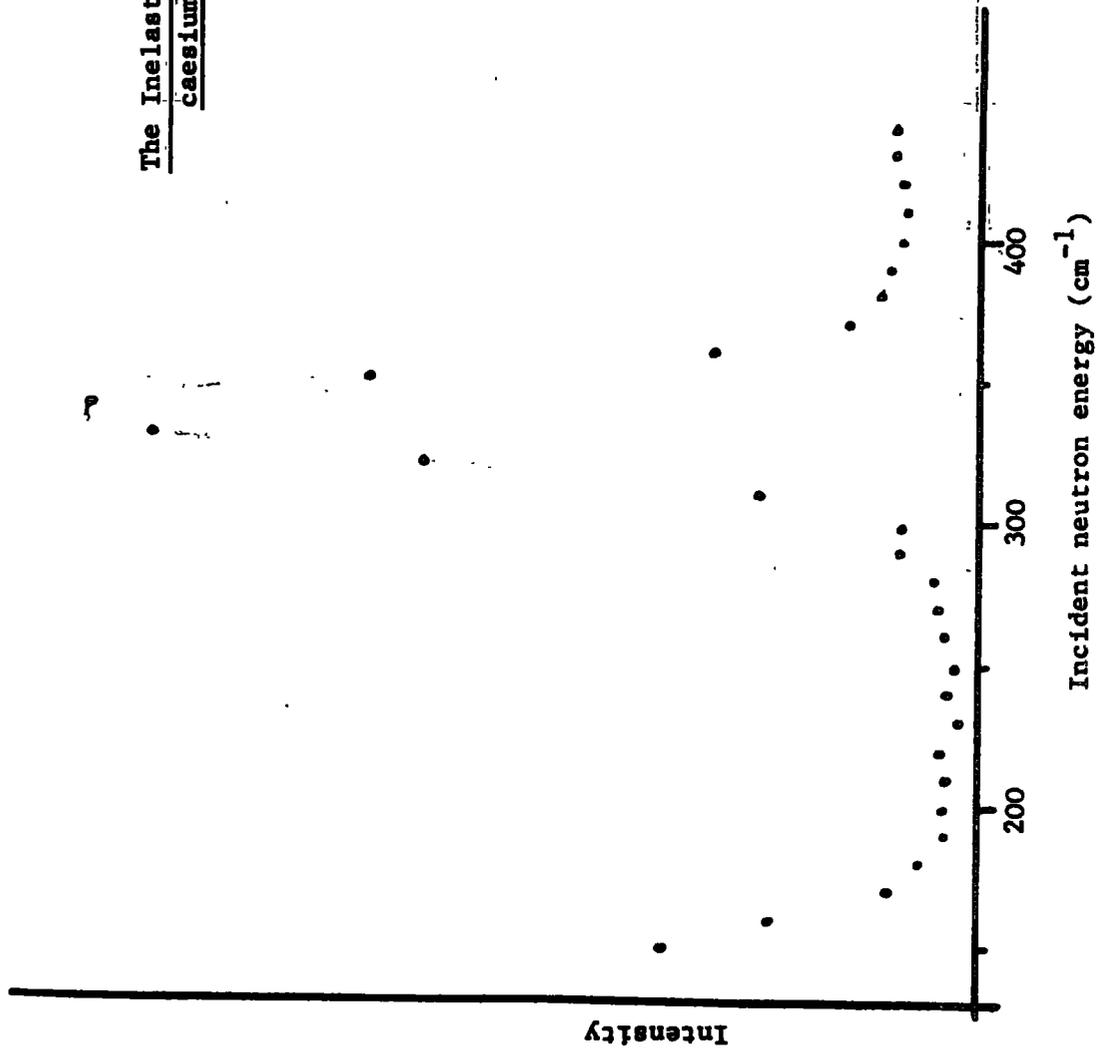
The spectra of the potassium(ammonium) chloride and rubidium (ammonium) chloride clearly show two localised modes (see Table VIvii and Fig. VIiv).   These bands are well above ω_{max} for the host lattice, unfortunately no low energy spectra are available for these compounds. The assignment of these modes is discussed later.   In the up scattering spectra, of the caesium halide mixed crystals, several weak features were observed apart from the strong bands;   this is similar to the up scattering spectra of the potassium mixed salts.   Again these are assigned to a slight involvement of the ammonium ion in these modes.

The weak bands at 42, 51, and 87cm^{-1} in the spectrum of caesium (ammonium) chloride may be matched to the [0,1,1] ν,TA; [1,0,0] ν,TA; and [1,0,0] ν,LA zone edge lattice modes of the host, respectively. Whilst the bands at 42, and 96cm^{-1} in the spectrum of caesium(ammonium) bromide may be matched with the [1,1,0] ν,TA; and [1,0,0] ν,LO Brillouin zone edge values of caesium bromide.   In conclusion it can be said that the predictive ideas of Mazur (1956) are in accord with the gross outlines of the results presented here.

Fig. VI.iv

305.

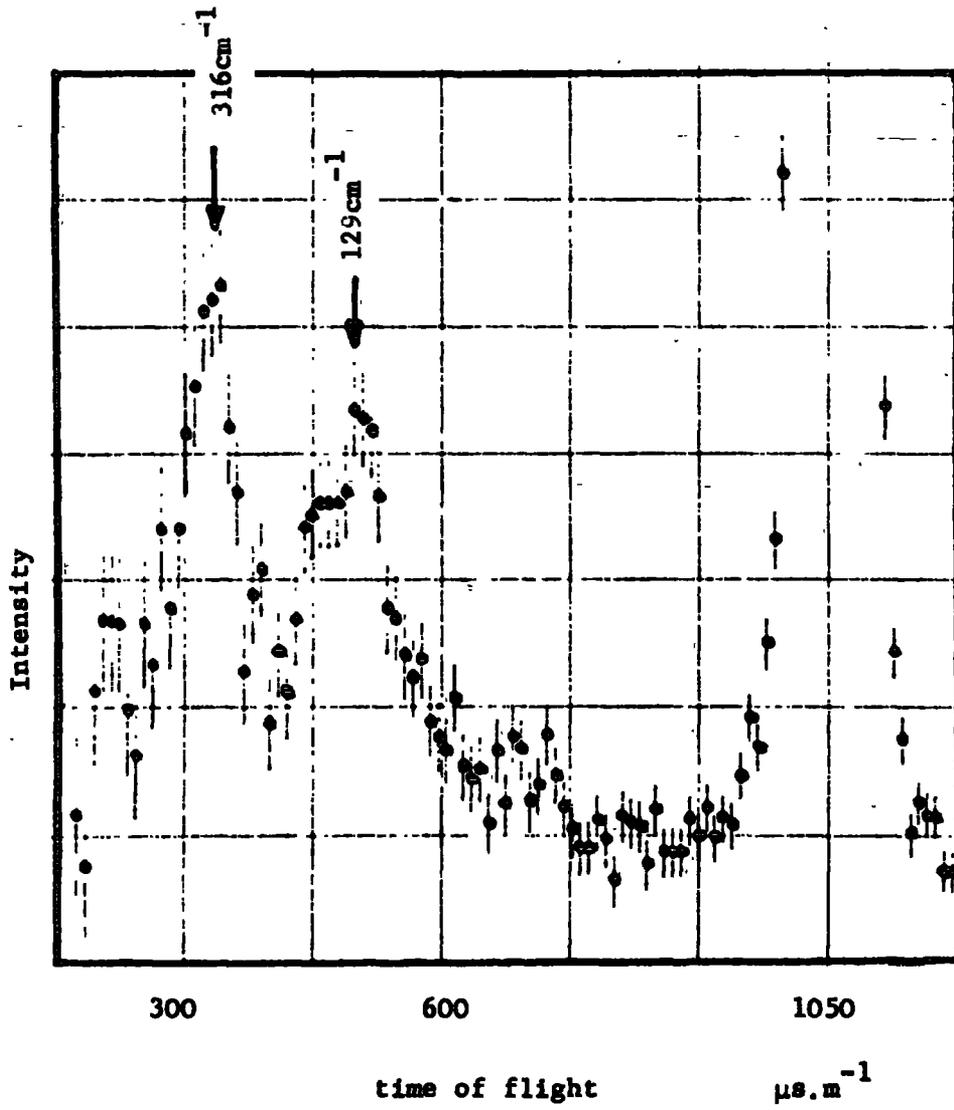Inelastic down scattering spectra of the potassium
(ammonium) halides at $77^{\circ}K$

K(NH$_4$)Cl

K(NH$_4$)Br

K(NH$_4$)I

Incident neutron energy.

200   300   400   500   cm^{-1}

Fig. VI.v

306.

The Inelastic down scattering spectrum of
caesium (ammonium) bromide at 77°K.

Intensity

Incident neutron energy (cm^{-1})

200 300 400

Fig. VI.vi

307.

Inelastic up scattering spectrum of caesium
(ammonium) bromide θ = 45°
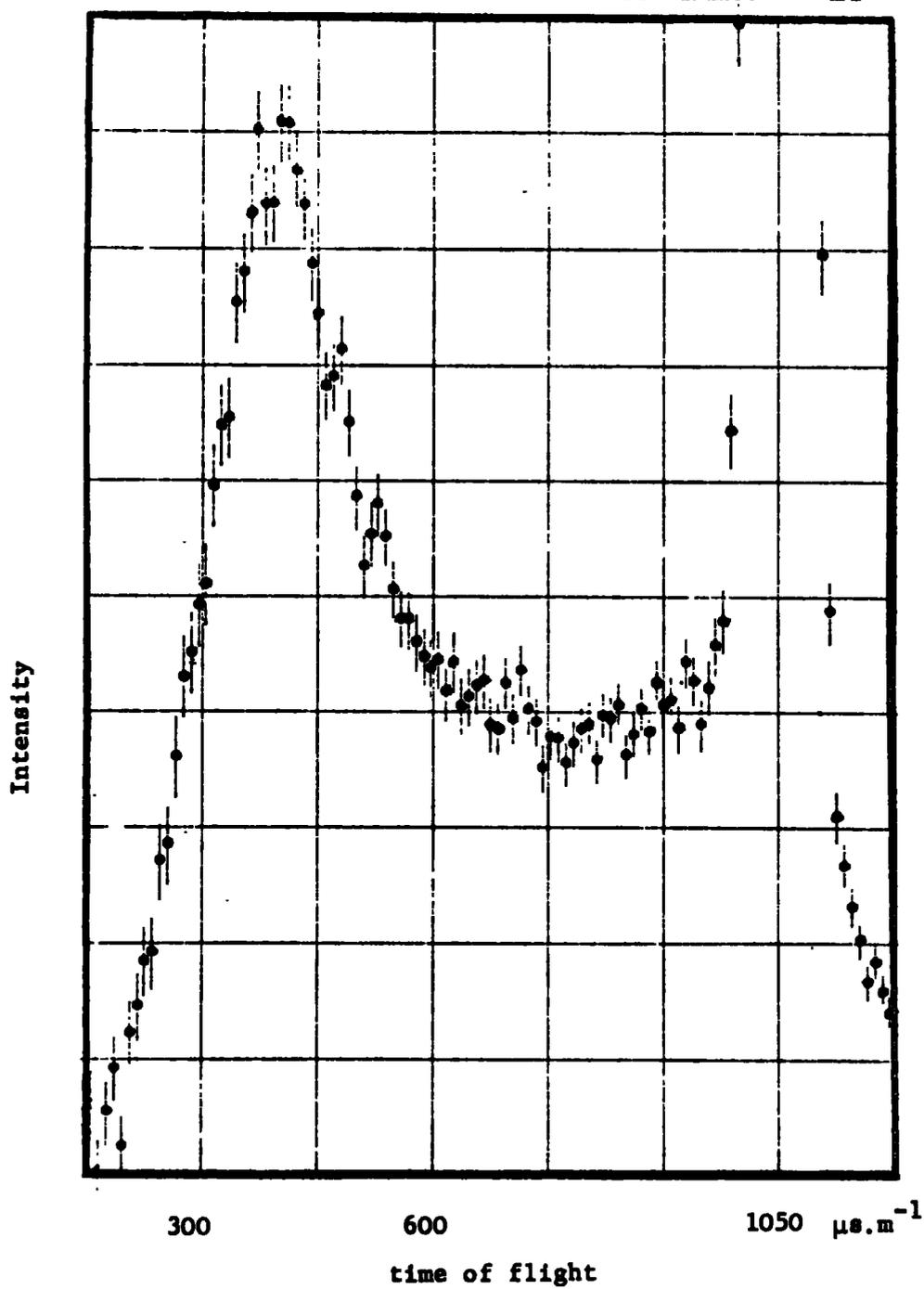
Fig. VI.vii

308.

Inelastic up scattering spectrum of caesium
(ammonium) chloride   θ = 45°

Fig. VI.viii

309.
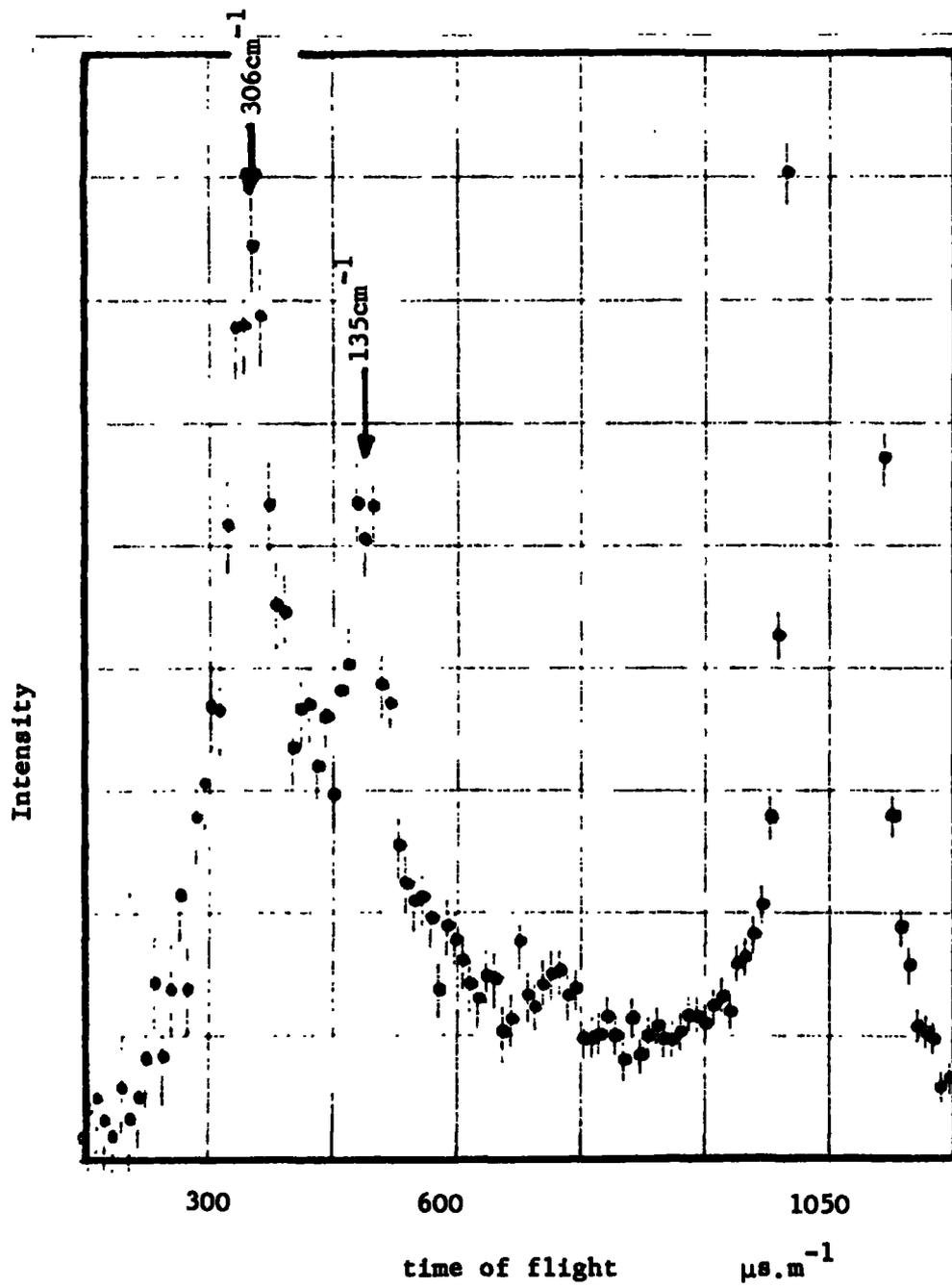
Inelastic up scattering spectrum of pottassium
(ammonium) bromide at 176°K $\theta = 45^{\circ}$

300   600   1050 $\mu s.m^{-1}$

time of flight

Fig. VI.ix

310.
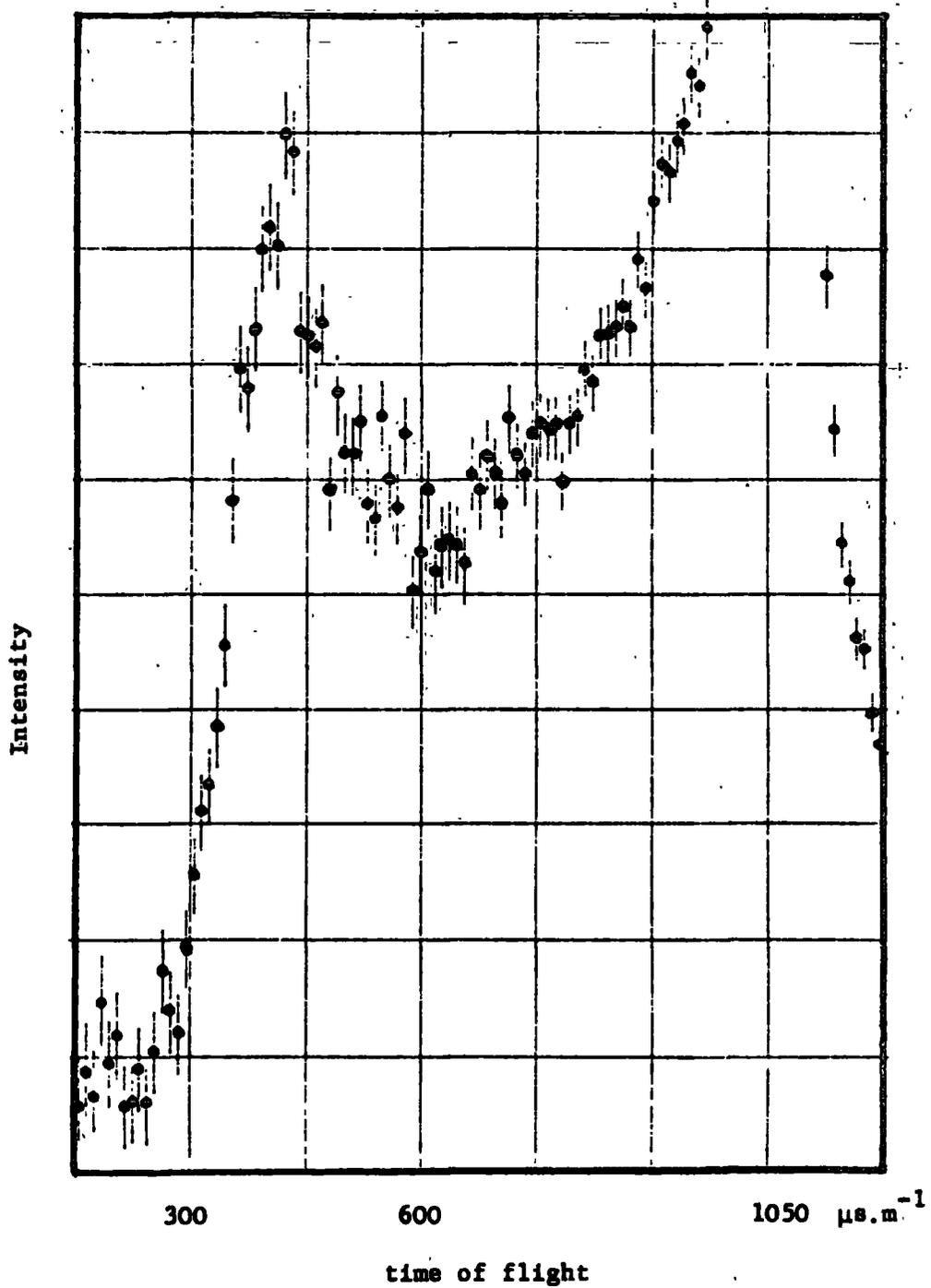
Inelastic up scattering spectrum of potassium
(ammonium) bromide at $294^{O}K$ $\theta = 45^{O}$

4.2.3 Assignment of the libratory and translatory modes.

In all sets of data where the two localised modes were observed, either band could be assigned to the translational or librational vibration. Smith (1972) working on the potassium(ammonium) chloride salt assigned his bands by conducting a similar experiment on a deuterated sample. His results for the non-deuterated mixed salt are in agreement with those presented here, see Table VIvii. In the deuterated analogue only one mode was observed, and Smith assigned this to the librational mode. (It was displaced from the non deuterated librational band by the factor $\sqrt{2}$). This system of assignments however makes the translational mode the most intense scattering feature of the spectra. This is true for both up and down scattering results. Reichhardt (ref. 38, under discussion) has pointed out that the magnitude of the one-phonon cross section for the librational mode of an ammonium ion, in an alkali halide lattice, would be expected to be larger than that for its translational mode. The intensity of a neutron band is directly related to the displacement of the scattering atom (see section I); using the simple harmonic approximation this displacement can be estimated. In the first excited librational state proton displacement is about three times greater than in the first excited translational state. Further, the most intense features of the inelastic neutron spectra of the pure ammonium halides are the librational peaks (42, 24). However it is not possible to rationalise a displacement of a translational mode by a factor of $\sqrt{2}$, upon deuteration. The expected displacement of a translational mode in these systems, is about 1.08, to lower frequencies. It is for this reason that the assignment of the bands presented here follows Smith (1972).

The intense band at about $310 cm^{-1}$ in the ambient up scattering spectra of the caesium(ammonium) salts is assigned as a librational mode. A localised mode is also expected in this region and the two bands may lie so close together as to be unresolved, even by the beryllium filter technique (see Section II). It is unlikely that the band at lower energy, about $130 cm^{-1}$, (assigned previously as a gap mode) is the librational mode. The librational frequency of the incorporated ammonium ion in caesium salts would be expected to be approximately the same as that of the pure ammonium halides. The pure ammonium halides have a caesium chloride type phase, and the librational frequencies are $389 cm^{-1}$ (ordered, ammonium chloride), $345 cm^{-1}$ (disordered, ammonium chloride), $303 cm^{-1}$ (disordered, ammonium bromide), and $324 cm^{-1}$ (ammonium iodide) (42, 22 and refs within).

4.3 Reorientational motion of the ammonium ions in the mixed crystals.

The ambient temperature neutron up scattering spectra of the pure ammonium halides show evidence of reorientation (22 and ref.). Up scattering spectra of several ammonium salts, taken by Palevsky (1963), showed very broad inelastic librational scattering. The ammonium ions in some of these salts were successfully treated in terms of three dimensional free rotors. It is not unexpected to find evidence of reorientation in the spectra of the incorporated salts. However the absence of phase changes in the incorporated ammonium salts will greatly simplify the problem. The complementary study of the isomorphous, isoelectronic alkali metal borohydride salts is also useful. In the borohydrides reorientation of the polyatomic anion showed itself

in the broadening of the librational scattering observed;
quasi-elastic broadening was also observed.

In the spectra of the potassium(ammonium) bromide these features were present to a different extent. This salt should be representative of all the face centred cubic incorporated salts. The up scattering spectra taken at different temperatures show two different reorientational processes. At low temperature a feature at very low energy transfer broadens out the quasi-elastic energy gain region (see Fig. VIviii). This shoulder loses intensity at higher energy transfers. This shoulder is much larger than would be expected from a mere quasi-elastic broadening, due to rapid reorientation. The quasi-elastic peak observed in sodium borohydride (see Section IV) is much narrower than this feature. At high temperature a broad librational scattering feature is present in the inelastic region of the spectrum. (This can be directly compared with the up scattering ambient spectra of the alkali metal borohydrides(see Section IV)). Such a feature should decay away in intensity to lower energy transfer. The plateau which is actually observed may be regarded as the sum of the broad inelastic feature and the broad quasi-elastic shoulder. These two features - the broad quasi-elastic shoulder and the broad librational scattering - can be explained in terms of the possible reorientational processes of an ammonium ion in a face centred cubic lattice.

In a face centred cubic arrangement of ions electrostatic minimum potential sites exist when anyone of the tetrahedral arms points directly at any nearest neighbour ion. (This is discussed in Section III).

In the case of ammonium ions incorporated into an alkali metal halide salt this is when a proton is pointed at a halide ion. This has been called the single approach model (26). This single approach defines a C_3 axis of symmetry, from the four available in an ammonium ion. Further, the electrostatic barrier to reorientation about such an axis is very low (see Section III). Free rotation of the ammonium ion about this C_3 axis would lead to a broad shoulder in the quasi-elastic region of the spectrum (43). This is because the rotor is restricted to one axis (degree of freedom). Calculations conducted by Lassier (1973) also show that such a feature is observed even if weak hindering of reorientation is present. Previous authors have used this single approach model to explain data on ammonium salts. Plum (1953) and Levy (1953) have both used it to explain their studies on the low temperature modifications of ammonium bromide and iodide. (The structure of these were isomorphic with sodium chloride). Vedder (1961) has used the single approach model to explain his infrared study.

Unfortunately, calculations indicate that steric repulsion is more significant in determining the orientations of the ammonium ion, in these crystals, than electrostatic attraction (see Section III). The orientations dictated by the steric potential do not lead to a unique axis of reorientation. (Reorientation about any of the three S_4 axis of the ammonium ion are possible). This could not lead to the type of spectrum observed at low temperature for this salt. The conclusion which must be reached is that the formation of Hydrogen bonds is important in this system. (Hydrogen bonding was only considered qualitatively in section III). Formation of strong Hydrogen bonds would lead to the required properties for the incorporated salt.

It is consistent to suggest that as the temperature is raised reorientations between all of the possible single approach situations will occur. There are a total of 24 such positions (six equivalent wells for any one of four equivalent protons to fall into). This can be described as a reorientation of the C_3 axis, to a new site. Such a movement involves all the ammonium protons and is not easily described in terms of the symmetry elements of a tetrahedron. A broad librational scattering feature would be expected from this reorientation as in the borohydrides. Reorientations of this nature involve more than one axis of rotation (degrees of freedom). The librational band would be expected at all temperatures, up to at least ambient. This band represents the frustrated attempts to reorientate the C_3 axis, it will lose its identity as a librational mode completely when the energy of the ammonium ion is greater than the depth of the well. (At very low temperatures, about $10^{\circ}K$, a second librational broadening should be observed which represents frustrated reorientation about a given C_3 axis). As was shown by the borohydride spectra, ambient experiments using down scattering techniques will have difficulty in defining the librational mode as a band associated with the reorientation of the C_3 axis. This will explain why Smith (1972) had to go to low temperatures to conduct his observations. The general conclusion which can be drawn from the up scattering spectra of the potassium(ammonium) bromide is that two types of reorientation are possible in these crystals, and dependent upon temperature, make more or less contribution to the scattering. It is probably safe to generalise this observation to what will be expected from the other

Fig. VI.x

316.

78°K

Intensity

10   meV   100
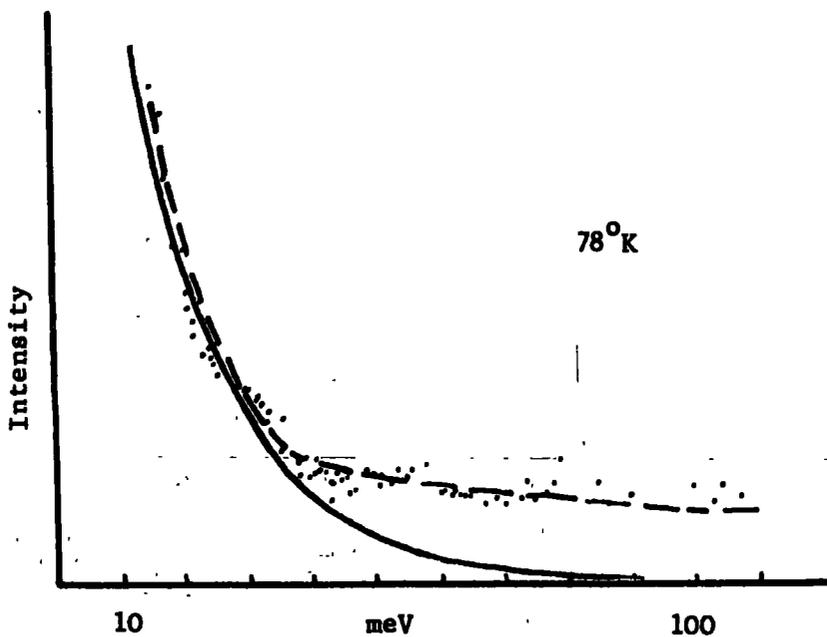
<u>Scattering from potassium(ammonium) iodide reproduced from</u>

<u>Mikke (1965.)</u>

297°K

Intensity

10   meV   100
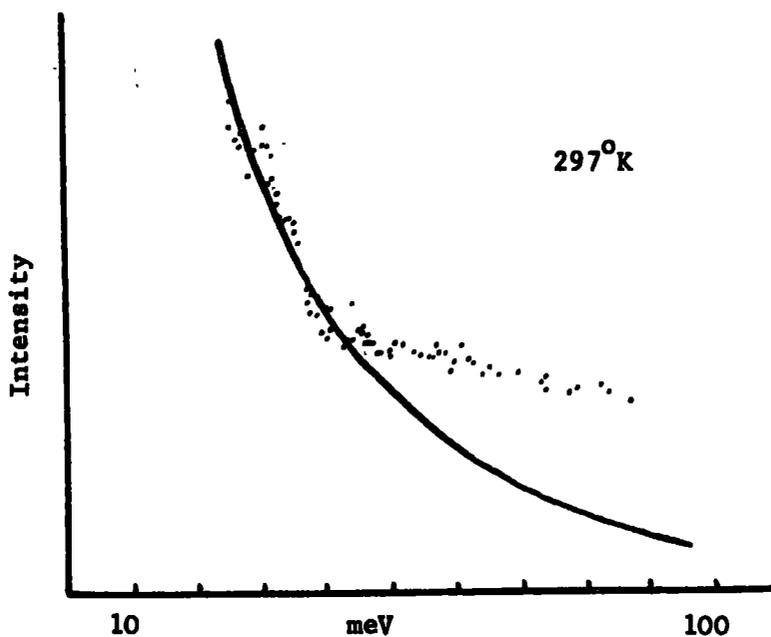
——————— theoretical curve for three axes of rotation

— — —   "   "   mixture of three axes and one
                                         unique axis.

face centred cubic incorporated salts. Some support for these
general observations is given by Mikke (1965), he has also studied
the mixed crystals described here. Unfortunately no librational
peaks were observed, even at low temperature. A down scattering
spectrometer was used, measuring the scattered intensity as a
function of incident energy. The results were interpreted in
terms of simple rotation of the incorporated ion. The data was
consistent with the occurrence of two types of reorientation, and the
reorientational processes discussed above were the ones suggested.
Some of his spectra, reproduced from Mikke (1965) are shown in
Fig. VIx. It is obvious that further detailed experiments will be
required on these mixed systems to elucidate the lattice motions of
the ammonium ion.

The lattice structure of the caesium(ammonium) halides is
different from those discussed above. Being body centred cubic,
a minimum in the electrostatic potential can be achieved by pointing
the ammonium protons to the corners of the cube (see Section III).
This could be described as the four approach model; there are eight
equivalent positions. Reorientations between equivalent positions
by rotation about a C_3 axis of the ammonium ion is more hindered than
reorientation about an S_4 symmetry axis of the ion (see Section III).
Apart from the low lying gap mode these salts have spectra similar to
the borohydrides at low temperatures (see Section IV).

As with ammonium ions incorporated into sodium chloride type
lattices, calculations conducted for the caesium chloride type lattices
indicate the importance of steric repulsion, in determining molecular
orientation (see Section III). The possibility of hydrogen bonding

in these systems is obvious and has been supported by the

observations on the incorporation of ammonium ions into sodium

chloride type lattices.   In the case of caesium chloride type lattices

there is the possibility of forming four hydrogen bonds simultaneously.

It might be expected that this would lead to a large increase in the

reorientational barrier in caesium chloride type lattices, as compared

with sodium chloride type lattices.   However such hydrogen-bonds

will be longer than those in the corresponding sodium chloride type

lattice.   This is indicated by the lower repulsion barrier in

caesium chloride type lattices than in sodium chloride type lattices.

Such that, although four hydrogen bonds are formed they may not be

as strong as those which might be formed in the sodium chloride type

lattices.

5. Barriers to reorientation

The results shown in Tables VIvi, VIvii can be used to obtain

estimates of the barrier to reorientation. The values of the

librational modes are substituted into equations III 1.1(xiv),

(xix) and (xxi) (previously discussed in section III), and values

of V_o are obtained. These barriers are given in Table VIviii.

As previously they represent the average barrier to the ammonium ion

reorientation. The barriers in the case of sodium chloride lattices

were treated as fourfold. It is not obvious which value to use in

this case. Four was chosen because it reflects the symmetry of the

reorientations with which the mode is associated. For lattices'

of the caesium chloride type the choice was obviously fourfold.

The results shown in Table VIviii may be divided into two sets:

The values for the sodium chloride lattice type and those values for

the caesium chloride lattice type. All four protons on the ammonium

ion are enabled to reside in potential minima only in the case of

caesium chloride type lattices. The barriers obtained for the

caesium chloride type host lattice may be compared with the data of

Venkataraman (1966). He obtained results for the caesium chloride

phase of the pure ammonium halides. The barriers to a twofold and

a fourfold reorientation of the ammonium ion were, 5.08 Kcal mole^{-1}

(ordered, caesium chloride lattice type at 100°K, and 4.38 Kcal mole^{-1}

(disordered, caesium chloride lattice type at 300°K). In ammonium

bromide the barrier was 3.67 Kcal mole^{-1} (disordered, caesium chloride

lattice type at 300°K). (No results for the caesium chloride phase

of ammonium iodide were presented). These results are significantly

Table VIviii.

Table showing the barrier to reorientation Vo
obtained for the incorporated salts

Sample	Temp °K	Scattering results		V_o (Kcal mole) *			
		vlib, up cm⁻¹	vlib down cm⁻¹	(a) up	down	(b) up	down
K-NH₄							
Cl	77		343		3.58		4.24
Br	294 / 176	259 / 275		2.05 / 2.31		2.51 / 2.89	
	77		305		2.85		3.45
I	77		257		2.02		2.49
Rb-NH₄							
Cl	77		353		3.81		4.63
Cs-NH₄							
Cl	294	316		3.04		3.51	
Br	294 / 77	306	348	2.85	3.72	3.30	4.20
I							

* Moment of inertia for NH_4^+ = 4.79×10^{-40} gm cm^2

(a) Using the deep well approximation

see Section III.

(b) Using the formula of Das.

different from those presented in Table VIviii. The differences

must in part be explained by the smaller lattice parameter of the

pure ammonium salts. (The ammonium chloride lattice parameter is

3.875Å, at 300°K (6) the ammonium bromide parameter is 4.06Å, at

300°K (6); whilst for caesium chloride and bromide it is 4.121Å,

and 4.296Å, respectively (6)). Another contributing factor is the

presence of neighbouring polyatomic ions. At such short separations

the ammonium ions must influence each other's motions. The ordering

of the caesium chloride lattice, which occurs at 243°K (42), shows

the importance of neighbouring ammonium ions. In this phase the

barrier to reorientation has increased by 14%, to 5.08 Kcal mole^{-1},

whilst the lattice parameter has decreased by only 0.8% (6). It may

be concluded that the replacement of the neighbouring ammonium ions

by the simple alkali metal ions lowers the librationary barrier, V_o,

significantly.

REFERENCES

1.   Ahmad, A.A.Z. Phys. Rev. B6, 3956 (1972).

2.   Behringer, R.E. J. Chem. Phys., 29, 537 (1958).

3.   Copley, J.R.D. Phys. Rev., 182, 965, (1969).

4.   Cowley, R.A. Phys. Rev. 131, 1030, (1963).

5.   Dolling, G. Phys. Rev., 147, 577 (1966).

6.   Donnay, J.D.H. "Crystal data" U.S. Dept. Commerce (1973).

7.   Durig, J.R. J. Chem. Phys., 49, 666, (1968).

8.   Durig, J.R. J. Chem. Phys. 51, 4449 (1969).

9.   Durig, J.R. J. Chem. Phys., 52, 5542 (1970).

10.   Van der Elsken,J. J. Chem. Phys., 41, 3451 (1964).

11.   Fock,   Z. Kryst. 28, 337 (1897).

12.   Frankel, J. "Kinetic theory of Liquids" Dover (1946).

13.   Harvey, K.B. J. Chem. Phys. 55, 4390 (1971).

14.   Hass, M. Phys. Rev., 119, 633 (1960).

15.   Jones, G.O. Proc. Roy. Soc., 261, 10 (1961).

16.   Klein, M.V. "The Physics of Colour Centres".

17.   Lassier, B. J. Phys. (Paris) 34, 473 (1973).

18.   Levy, H.A. J. Am. Chem. Soc. 75, 1536, (1952).

18a. Maradndin, A.A. Rep. Prog. Phys. 28, 331 (1965).

19.   Mazur, P. J. Wash. Acad. Sci. 46, 2 (1956).

20   Metselaar, R. Phys. Rev. Letters. 16, 349 (1966)

21.   Metselaar, R. Phys. Rev., 165, 359 (1968).

22.   Mikke, K. Proc. I.N.S. (Vienna) II, 383 (1965).

23.   Narayanamurti, V. Phys Rev., 148, 481 (1966).

24.   Palevsky, H. J. Phys. Chem. Solids 24, 617 (1963).

25.   Pauling, L.   Phys. Rev., 36, 430 (1930).

26.   Phun, R.C.   J. Chem. Phys., 21, 366 (1953).

27.   Ranino, G. (a)   Phy. Rev., B2, 2098 (1970).

28.   Ranino, G. (b)   J. Phys. C3, 1013 (1970).

29.   Ranino, G. (c)   Phys. Stat. Solidi 40, 749 (1970).

30.   Reid, J.S.   Phys. Rev., B1, 1833 (1970).

31.   Renk, K.F.   Z. Phys. 201, 445 (1967).

32.   Rolandson, S. (a)   J. Phys. C4, 958 (1971).

33.   Rolandson, S. (b)   Phys. Rev., B4, 4617 (1971).

34.   Rush, J.J.   J. Chem. Phys., 44, 1722, (1966).

35.   Rush, J.J.   J. Chem. Phys., 51, 2947 (1969).

36.   Seivers, A.J.   Phys. Letters 14, 271 (1965).

37.   Seivers, A.J.   "Far Infrared Spectroscopy" Wiley (1971).

38.   Smith, H.G.   Pro. I.N.S. (Grenoble) 103, (1972).

39   Timustz, T.   Phy. Rev. Letters 13, 373 (1964).

40.   Vedder, W. "The Infrared absorption spectrum of the ammonium
         ion in lattices of the NaCl type". Amsterdam Univ. (1958).

41.   Vedder, W.   J. Chem. Phys. 35, 1560 (1961).

42.   Venkataraman, G.   J. Phys. Chem. Solids. 27, 1103, (1966).

43.   Waddington, T.C.   Private communication.

44.   Wagner, M.   Phys. Rev., 131, 2520 (1963).

45.   Wagner, M.   Phys. Rev., A133, 750 (1964).